9-14-2015

Ascending CNS Progression of EAE: Linkage of Events at the Choroid Plexus and Spinal Cord

Bandana Shrestha
shrestha.bee@gmail.com

Ascending CNS Progression of EAE: Linkage of Events at the Choroid Plexus and Spinal Cord

Bandana Shrestha
University of Connecticut (2015)

Dysfunction of the blood brain barrier (BBB), the specialized complex of cells situated at the central nervous system (CNS) microvasculature has been associated with numerous neuroinflammatory disorders like multiple sclerosis (MS) and its animal model, experimental autoimmune encephalomyelitis (EAE). BBB known to restrict passage of soluble and cellular elements between the blood and CNS is breached. The mechanism by which auto-reactive T cells cross the normally "impermeable" BBB, invade the initially naive CNS, and cause neuroinflammation, remains unclear. Recent studies suggest an initial route by which these cells first gain entry from circulating blood through the choroid plexus (CP). The permeable fenestrated capillaries of CP allow these sentinal T cells into the cerebrospinal fluid (CSF) across the surrounding tight junction expressing choroidal epithelium also known as the blood-CSF-barrier (BCSFB). Once into the CSF, these cells travel to the subarachnoid space (SAS) that surrounds the CNS parenchyma. Here, T cells are known to encounter their cognate antigen and set off a cytokine storm that propagates inflammation. The effects are first observed within the SAS in the meningeal vessels followed by activation of parenchymal inflammation. However, several critical questions in this scenario remain. First, how do these T cells cross the epithelium of the CP to enter the CSF? Does this involve changes in the tight junctional integrity between adjacent epithelial cells to allow leukocyte diapedesis? Second, once they enter the CSF, do these cells select a segment within the SAS to ignite the inflammatory sequence? Given the ascending inflammation within spinal cord segments in developing EAE (caudal to rostral), regional blood vessels in meninges and parenchyma might display unique vulnerabilities depending upon the

segment of the spinal column in which they reside. Third, what links the inflammatory signals in the SAS to neuroinflammation in the parenchyma? Results obtained from this work show evidence towards the hypothesis that the ascending course of EAE is due to initial penetration of sentinal T cells through a structurally compromised CP choroidal epithelium, followed by a spinal segment-dependent relay of inflammatory signals between meningeal and parenchymal vessels.

Ascending CNS Progression of EAE: Linkage of Events at the Choroid Plexus and Spinal Cord

Bandana Shrestha
B.S. Mcneese State University, 2009

A Dissertation

Submitted in Partial Fulfillment of the

Requirements for the Degree of

Doctor of Philosophy

at the

University of Connecticut

[2015]

APPROVAL PAGE

Doctor of Philosophy Dissertation

Ascending CNS Progression of EAE: Linkage of Events at the Choroid Plexus and Spinal Cord

Presented by
Bandana Shrestha, B.S.

Major Advisor

_____

Joel S. Pachter, PhD.

Associate Advisor

_____

Robert E. Cone, PhD.

Associate Advisor

_____

James Watras. PhD.

Associate Advisor

_____

Stephen J.Crocker. PhD.

University of Connecticut
[2015]

Table of Contents

Appendix (co-authored publications)

1. Ge S, **Shrestha B**, Paul D, Keating C, Cone R, Guglielmotti A, Pachter JS. The CCL2 synthesis inhibitor bindarit targets cells of the neurovascular unit, and suppresses experimental autoimmune encephalomyelitis. (Journal of Neuroinflammation, July 2012)
2. Demarest TG, Murugesan N, **Shrestha B**, Pachter JS. Rapid expression profiling of brain microvascular endothelial cells by immuno-laser capture microdissection coupled to TaqMan(®) low density array. (Journal of Neuroscience methods, Mar 2012.)
3. Murugesan N, Paul D, Lemire Y, **Shrestha B**, Ge S, Pachter JS. Active induction of experimental autoimmune encephalomyelitis by MOG35-55 peptide immunization is associated with differential responses in separate compartments of the choroid plexus. (Fluids and barriers of the Central Nervous System, Mar 2014)

Publications and contributions to Thesis project:

1. **Chapter II: Choroid Plexus in evolving EAE:** This work focuses on the regulation of the Blood-Cerebrospinal Fluid barrier at the level of the Choroid Plexus (CP), in terms of tight junctions within the epithelial layer of the CP and the functional assessment of permeability associated with it during evolving EAE induced by immunization with myelin oligodendrocyte glycoprotein (MOG) peptide$_{35-55}$ along with adjuvants. This study sheds light on how the leukocytes navigate across the tight junctions of the choroidal epithelial layer into circulating Cerebrospinal Fluid (CSF) leading to anatomical changes within this intricate system. Understanding the changes in the tight junctions between the epithelial cells of the CP has provided valuable information about the regulation of BCSFB via possible trans epithelial migration of infiltrating immune cells. BCSFB breach has also been assessed functionally by permeability studies, thus co-relating the breakdown of tight junctions with possible increase in the "leakiness" of the barrier.

2. **Chapter III: Spinal cord in evolving EAE:** Once the immune cells enter the CSF from the choroid plexus during evolving EAE, do they select a segment within the SAS to ignite the inflammatory sequence? This work provides the possibility that regional blood vessels in the meninges and parenchyma might display unique vulnerabilities depending upon the segment of the spinal column in which they reside. These differences could aid in preferential accumulation and infiltration of inflammatory cells within the lumbar segment followed by ascending progression in disease pathology. This work has attempted to address these issues using 3D confocal microscopy of spinal cord segments, whole spinal cord images and a systematic and detailed segmental transcriptomic analysis of inflammatory gene expression patterns of spinal cord meningeal and parenchymal venules.

3. **Chapter IV: CCL2 sources in evolving EAE:** This report uses two qRT-PCR-based approaches to clarify the relative contributions of the parenchymal and vascular compartments to CNS CCL2 gene expression during evolution of EAE induced by immunization with myelin oligodendrocyte glycoprotein (MOG) peptide$_{35-55}$ along with adjuvants. One approach used a crude separation of CNS parenchymal and microvessel fractions, based on a common preparative method from homogenized CNS tissue. The other employed the laser capture microdissection (LCM), to more precisely retrieve separate BMEC, astrocyte and other parenchymal cell types. Additionally, we assessed CCL2 expression levels following MOG immunization as well as after injection of these adjuvants alone, to highlight the effects due to MOG immunoreactivity.

- **Appendix-Attached paper 1**: This work focuses on the CCL2 synthesis inhibitor bindarit and it effects on the cells of the neurovascular unit effectively suppressing experimental autoimmune encephalomyelitis. Bindarit repressed CCL2 expression in cultured murine astrocytes, microglia and BMEC, and antagonized upregulated expression of CCL2 in both brain and spinal cord *in vivo* following LPS administration. Bindarit also significantly modified the course and severity of clinical EAE, diminished the incidence and onset of disease, and evidenced signs of disease reversal.

- **Appendix-Attached paper 2:** This work allowed us to perfect an experimental technique coupling Laser Capture Microdissection (LCM) with Taqman Low Density Arrays (TLDA) plates using expression profiling of brain microvascular endothelial cells. We were able to report, for the first time, the feasibility of direct cDNA synthesis without RNA isolation in

mircoarrays. This set the ground work for our following publications using the technique to show the differential CP epithelial and endothelial expression profile and CP regulation during EAE.

- **Appendix-Attached paper 3:** This work was instrumental to establish the feasibility of LCM on separate compartments of the intricate system of choroid plexus structure and coupling it with TLDA analysis. This work put down the ground works, building upon which, CP epithelial cells were isolated using LCM and probed for tight junctions expression. This led to experiments towards understanding how these tight junctions were regulated and BSCFB was maintained during evolving inflammation in EAE.

List of figures:

CHAPTER I: Introduction

MS and its comprehensive animal model, EAE are widely considered as chronic immune mediated demyelinating diseases of the CNS (1-5). Breakdown of the BBB and leukocyte extravasation have been associated with the pathology of these diseases (6, 7). Little is known however about the initial trigger that activates the healthy, naïve immune system and the resting vasculature of the CNS within which BBB resides. The spark that initiates the sequence of events leading to targeted demyelination and subsequent neurodegeneration has been speculative (8, 9). Reports have highlighted important initial inflammatory events that occur before the breakdown of the BBB and provide possible leads to the earlier steps necessary for disease (10-13). These studies suggest that the molecular changes at the level of the BBB are downstream effects of earlier reported events such as entry of inflammatory T cells via routes other than the BBB. Evidences point to the CP, cells primarily known to produce CSF (14, 15), as a possible site where pioneer T cells infiltrate the CNS in MS/EAE.

CP has garnered attention as a critical player in immune reactions of the CNS (13, 16-18). It is located within the cerebral ventricles and is composed of a highly vascularized stroma encapsulated by a "tight" layer of epithelial cells decorated with tight junctions (TJ) (19, 20). CP stromal capillaries are fenestrated and permit hydrophilic molecules typically excluded by the BBB (21). This leaky nature of the CP endothelium is known to allow extravasation of T cells engaged in immunosurveillance. Reboldi et al.(22) reported that CCL20, produced by choroidal epithelial cells, attracts T_H17 cells bearing the cognate receptor CCR6, in circulation within the capillaries, across the endothelium. However these cells need to cross the blood-CSF barrier (BCSFB)(6, 23) formed by a tighter epithelium juxtaposed with the "leaky" capillaries in order to get into the CSF. The CCL20 chemokine gradient doesn't explain how these cells get past the

epithelial layer. Reports of adhesion molecules being present in the apical surface of the epithelial cells rather than the basolateral side further fuels the question of how do T cells get past the BCSFB (18). Works included within the scope of this thesis contributes to bridge this gap in knowledge and answer unresolved critical questions lingering in the field.

Is there breach of the BCSFB? Significance of this work lies in understanding how the leukocytes navigate across the tight junctions of the choroidal epithelial layer. There has been very limited work in terms of understanding the tight junction regulation of the CP epithelial layer during naïve as well as pathological scenarios(18, 24, 25). Having established the importance of the CP, it is as important to understand the anatomical changes within this intricate system. Understanding the changes in the tight junctions between the epithelial cells of the CP has provided valuable information about the regulation of BCSFB via possible trans epithelial migration of infiltrating immune cells. BCSFB breach has also been assessed functionally by permeability studies, thus co-relating the breakdown of tight junctions with possible increase in the "leakiness" of the barrier.

In association, the SAS, which is connected to the CP via CSF, is reported to be another important compartment that supports earlier inflammatory events (10-12). It is within the SAS, the initial inflammatory T cells are known to encounter their cognate antigen. T cells are reactivated within the SAS by MHC class II expressing macrophages and DCs presenting myelin epitopes (26). Reactivated T cells are then known to produce inflammatory cytokines that set off an inflammatory cascade. The effects are first observed within the SAS in the meningeal vessels followed by activation of parenchymal inflammation(27). Parenchymal vascular changes in terms of expression of adhesion molecules and production of cytokines activate the BBB and allow leukocytes to permeate this normally restrictive BBB (28, 29).

Once across this barrier and into the CNS parenchyma, these cells then release soluble factors that initiates destruction of myelinated axons and damage to neurons (4). However, there are several critical questions within this scheme of events. This work aimed at providing some answers that will stipulate a holistic picture of immune pathology in EAE.

What links the inflammatory signals in the spinal cord SAS to neuroinflammation in the parenchyma? Studies have shown that the inflammatory cascade begins in the SAS long before it is observed in the parenchyma during developing EAE (10, 11, 13). Meningeal vessels within the SAS are shown to accumulate immune cells and to allow extravasation earlier than the underlying parenchymal vessels. Why do infiltrating T cells prefer meningeal to parenchymal vessels to begin infiltration? Is there differential regulation of inflammation within the two vascular regions and what links them? A detailed immune profile of regional vascular endothelium within the meninges and underlying parenchyma provided a key in answering these questions. Major immune players such as adhesion molecules, cytokines, chemokines, statins, interleukins, T cells activation markers, co-stimulatory molecules, transcription factors and apoptotic markers were probed to provide a complete immune profile during developing EAE.

Does heterogeneity within the spinal cord segments lead to ascending EAE? Ascending progression of spinal cord pathology and clinical disease observed in many EAE models has remained enigmatic (5). The reasons behind the progression of inflammation from the caudal/lumbar segment to the rostral/cervical segment are yet to be explained. Once the immune cells enter the CSF from the choroid plexus, do they select a segment within the SAS to ignite the inflammatory sequence? Our work has shed light on the possibility that regional blood vessels in the meninges and parenchyma might display unique vulnerabilities depending upon the segment of the spinal column in which they reside. These differences could aid in preferential

accumulation and infiltration of inflammatory cells within the lumbar segment followed by ascending progression in disease pathology. This work has attempted to address these issues using a systematic and detailed segmental analysis of inflammatory gene expression patterns of spinal cord meningeal and parenchymal venules.

The significance of this work lies in tackling unresolved questions important to understand the nascent alternate routes proposed. i.e. the CP and SAS meningeal venules. First, how do leukocytes navigate across the tight junctions of the tight choroidal epithelial layer and possibly breach the BCSFB during disease onset? Second, what are the immune gene changes within the meningeal and underlying parenchymal vessels in the spinal cord segments that could highlight differences within regional vascular environments and the segmental co-relation between them? Understanding the earliest events in disease pathology will provide uniquely sensitive avenues for therapeutic interventions that could halt or delay the progression of the disease.

This study is novel not just in terms of the unique questions asked but in using new and challenging technical approaches as well. Quantitative 3D analysis of TJ breakdown and permeability assessment was used to highlight aspects of CP morphological and functional changes not resolved before. Previous works in similar accounts (24) have been defined by 2D qualitative analysis in thin sections, which is restricted to visualization of only a small portion of the given specimen. Given the tortuosity of the complex of cells within CP, visualizing TJs embedded within the epithelial cells and the leakage is limited. Focal changes in TJ expression and functional changes in BCSFB breach was quantified effectively using an encompassing 3D approach in thicker sections, providing an enhanced perspective of in vivo changes in tight junctions and permeability within the CP.

Characterization of immune genes between regional and segmental vasculature was done with a novel isolation procedure- Laser Capture Microdissection (LCM). With this work we were able to resolve the differences in meningeal and underlying parenchymal vessels in terms of their immune gene profile. This work encompassed specialized isolation of vascular endothelium from meningeal and parenchymal regions within spinal cord segments. This laboratory has successfully demonstrated that immunohistochemistry-guided laser capture microdissection (immuno-LCM) can precisely acquire designated cell populations in highly purified form from their in situ setting (30-34). These lab reports have shown that immuno-LCM coupled to qRT-PCR enables highly reproducible, quantitative gene expression profiling of captured cells. This level of intricate isolation and profiling has not been done before in comparing meningeal and parenchymal vascular endothelial cells. Tenacious profiling of immune genes within these vascular types has provided cues for the ascending course of EAE, which we hypothesized, is due to spinal segment-dependent relay of inflammatory signals between meningeal and parenchymal vessels.

CHAPTER II: Choroid plexus in evolving EAE

Alterations in tight junction protein and IgG permeability accompany leukocyte extravasation across the choroid plexus during neuroinflammation.

1. Abstract

The choroid plexus (CP) is considered a point of leukocyte entry into the central nervous system (CNS) during normal immune surveillance and developing neuroinflammatory disease. However, structural or functional alterations within the CP that support this migration are much less understood. Quantitative, high-resolution 3D fluorescence imaging was thus used to detail inflammatory responses within the CP following induction of experimental autoimmune encephalomyelitis (EAE) by immunization with myelin oligodendrocyte glycoprotein (MOG) and Complete Freund's Adjuvant/pertussis toxin (MOG-CFA/PTX), or adjuvants alone (CFA-PTX). MOG-CFA/PTX and CFA/PTX produced near comparable effects, the former being consistently more severe. Both treatments resulted in accumulation of serum IgG and leukocytes in the CP stroma, consistent with elevated stromal capillary permeability. They also provoked remarkable distortions in staining pattern of tight junction (TJ) adaptor protein ZO-1 in the choroidal epithelium, with diminished staining but no obvious change in pattern of the associated TJ protein, claudin-2. Only MOG-CFA/PTX triggered visible extravasation of IgG and leukocytes across the choroidal epithelium. Results suggest CFA/PTX primes the CP for neuroinflammation by inducing several structural changes that are exacerbated when co-administered with MOG, and reinforce the CP is a gateway for leukocytes to enter the CNS by accessing the cerebrospinal fluid and meninges.

2. Introduction

The choroid plexus (CP) is a specialized out-pocketing of the roofs of the third, fourth and lateral ventricles, and has long been recognized as the site of production of cerebrospinal fluid (CSF), within which it hangs suspended (14, 19). A highly compartmentalized structure, the CP contains at its core, a tortuous capillary plexus displaying a fenestrated endothelium more permeable than that of capillaries forming the blood-brain barrier (BBB) in the CNS parenchyma (21). This vascular core is surrounded by a layer of choroidal epithelium having a relatively high density of tight junctions (TJs) and limited permeability, providing the CP its classification as part of the blood-CSF-barrier (BCSFB) (6, 23). Located between the capillaries and choroidal epithelium is a confined stromal space.

Since the pioneering work of Helen Cser (35), the CP has been commonly recognized for its role in generating CSF, as most recently reviewed (36). However, a growing number of reports has turned attention to the CP as a site through which T cells might enter an initially uninflamed central nervous system (CNS) to spark neuroinflammatory disease, such as multiple sclerosis (MS) and its animal model experimental autoimmune encephalomyelitis (EAE) (13, 16-18, 22). It has been proposed that once encephalitogenic T cells cross the CP and enter the CSF, they can migrate to the subarachnoid space (SAS) surrounding the brain and spinal cord, and there forge immune synapses with resident dendritic cells. Cytokine bursts stemming from such synapses, in turn, are reasoned to activate the endothelial surfaces of nearby microvessels within the SAS, thereby enabling adhesion and extravasation of leukocytes circulating in the bloodstream (10-12). Interactions between these leukocytes and other dendritic cells in the SAS are thought to follow, ultimately propagating an inflammatory wave along the surface-penetrating microvessels that enter the CNS parenchyma.

This scenario begs the question: Are there changes within CP anatomy and integrity during evolving neuroinflammation that would allow leukocytes to navigate across the TJs of the choroidal epithelium and enter into the CSF? Currently, direct evidence of leukocyte extravasation across the CP into the CNS ventricles, or structural arrangements of the choroidal epithelium that might support this process, is lacking. High-resolution 3D fluorescence imaging, was thus used to highlight aspects of CP morphological and functional changes not previously resolved during progression of EAE.

Specifically, immunization with myelin oligodendrocyte glycoprotein (MOG) peptide$_{35-55}$, along with Complete Freunds Adjuvant (CFA) and pertussis toxin (PTX), was used to induce EAE, and at different time-points qualitative and quantitative assessments were made for two TJ proteins expressed by the CP: claudin-2 (CLN-2) and zonula occludens-1 (ZO-1) (24, 25, 37). CLN-2 belongs to a large family of claudins (> 20 members), integral membrane proteins that perform cell-cell bridging, while ZO-1 is a peripheral membrane scaffolding/adaptor protein that directly or indirectly links claudins (and other integral membrane TJ proteins) to the actin cytoskeleton (38-40). TJ protein changes were further correlated with leakage of serum immunoglobulin G (IgG) – a marker of barrier permeability status (41)– and leukocyte extravasation across the successive CP compartments. As administration of just the adjuvants CFA and PTX can significantly alter gene expression patterns in the CP (42), MOG$_{35-55}$-immunized mice were contrasted with those receiving these adjuvants alone or no treatment.

Results indicate that ZO-1 and CLN-2 immunostaining patterns within the CP choroidal epithelium displayed significant, yet different, changes during evolution of EAE, with the former showing a severely altered morphology, and the latter a gradual decrease in staining intensity. IgG was detectable at a low level in the CP stroma even in naïve animals, appreciably increased

during disease, and later in acute disease was observed to extravasate across the CP choroidal epithelium. A few leukocytes were also detected in the CP stroma of naïve mice. These cells, showed an acute transient accumulation early in EAE, and then seemed to reduce to near pre-disease level. Correlating with this decline, leukocytes could apparently be seen in the process of extravasating across the CP choroidal epithelium and into the ventricles, presenting direct evidence supporting the theory that the CP is the entry site into the CNS for leukocytes in the ontogenesis of neuroinflammation (13).

3. Materials and Methods

3.1 Animals: Female C57BL/6 mice, age 8–10 weeks, were obtained from Charles River Laboratories, Inc. (Wilmington, MA) and used throughout. A total of n = 3 animals/group were used for each treatment and time-point assessed. All animal experimental procedures were performed following Animal Care and Use Guidelines of the University of Connecticut Health Center (Animal Welfare Assurance # A3471-01), and approved under protocol #100346-1214.

3.2 EAE induction: EAE was induced in mice by active immunization with MOG_{35-55} peptide (MEVGWYRSPFSRVVHLYRNGK), of murine origin (W. M. Keck Biotechnology Resource Center, Yale University), as described (43) Briefly, on day 0 (D0), one group of mice was injected subcutaneously with 300 μg of MOG peptide in complete Freund's adjuvant (CFA, DIFCO) into the right and left flank, 100 μl per site. These mice were also injected i.p. with 500 ng pertussis toxin (PTX, List Laboratories, Campbell CA) in PBS on D0 and D2 following the first immunization (referred to as the MOG-CFA/PTX group). Another group of age-matched mice received only CFA and PTX (500 ng) injections on D0 and a second injection of 500 ng PTX on D2 (referred to as the CFA/PTX "control" group). A third group of age-matched mice

was left untreated (referred to as "naïve" mice), and represented "normal" tissue. Only the MOG-CFA/PTX group developed EAE. Mice typically showed development of acute clinical symptoms at ~ D12, followed by ascending paralysis and chronic disease (44). Animals were killed at D0 (naïve), D6, D9 and D15 post-injection (with MOG and/or CFA/PTX). Animals were monitored for clinical disease severity and mean clinical scores were calculated where 0 =normal; 1 = tail limpness; 2 = limp tail and weakness of hind legs; 3=limp tail and complete paralysis of hind legs; 4 = limp tail, complete hind leg and partial front leg paralysis; and 5 = death. The time-points selected for analysis, D6, D9 and D15, represent pre-clinical (score 0), early (score 0-0.5) and acute stages of EAE (score 2-2.5), respectively.

3.3 Tissue preparation and sectioning for 3D analysis: Mice were anesthetized by intraperitoneal injection of Ketamine (80 mg/kg) and Xylazine (10mg/kg) in phosphate-buffered saline, pH 7.4 (PBS). Animals were then transcardially perfused (via the left ventricle) first with Heparin-PBS (10 usp/ml) to eliminate vascular blood content, and then with fixation Buffer (2% paraformaldehyde in 0.1 M phosphate buffer, pH 7.4), as described previously (43) Brains were embedded in OCT cryomatrix compound (Thermo Fisher Scientific, Waltham, MA) prior to sectioning. Cryosections of 20µm thickness were obtained using a Microm HM 505M cryostat (Mikron Instruments; Oakland, NJ) maintained at -25°C, and deposited onto poly-L-lysine coated slides.

3.4 Immunostaining for 3D analysis: Sections were permeabilized with 0.6 % Triton X-100 in PBS for 30 min, and non-specific binding blocked by incubation with Power block® for 10 min in Ultrapure (GIBCO) distilled water (41). The CP capillary endothelium was stained by rat anti-mouse CD31 antibody (BD Pharmingen) at 1:160 dilution, followed by incubation with goat

anti-rat Alexa Fluor® 555 antibody (Life Technologies) at 1:250 dilution. Choroidal epithelial cells were stained using monoclonal pan-cytokeratin-FITC antibody (Sigma) at 1:160 dilution. Rabbit polyclonal antibodies to CLN-2 (Invitrogen) at 1:160 dilution, CLN-3 (Abcam) at 1:100 dilution, ZO-2 (Invitrogen) at 1:100 and ZO-1 (Invitrogen) at 1:160 dilution, followed by Alexa Fluor® 488 goat anti-rabbit IgG (Life Technologies) at 1:250 dilution, were used to stain epithelial TJs. Alexa Fluor® 488 goat anti-mouse IgG F_{ab} fragment (Life Technologies) at 1:160 dilution was used to detect endogenous IgG within the CP. DRAQ5 (Biostatus Ltd., Leicestershire, UK) was used at 1:1000 dilution to stain nuclei. Alexa Fluor® 647 anti-mouse CD45 (Biolegend) at 1:160 dilution was used to stain for leukocytes. Sections were mounted in Mowiol (Sigma-Aldrich).

3.5 Image acquisition and quantitative analysis of TJ proteins, IgG and leukocytes in the CP: Confocal z-stacks (multi-track scan) were acquired using a Zeiss LSM 510 Meta equipped with Zeiss Fluar 40X/1.30, 63X Plan-neofluar/1.25, and 100X Plan-apochromatic/1.4 oil immersion objective lenses. Thereafter, z-stacks were imported into Bitplane Imaris® suite version 7.1 x64 software (Bitplane Inc., South Windsor, CT), as described previously (41).

The CP tissues specifically located in the lateral ventricles were evaluated in all experiments, as complexity and developmental changes of TJ proteins have been reported to show differences among the CP locales in rat (Kratzer et al., 2012). Images of these TJ proteins were first isosurface rendered to obtain a measure of total surface area, and the epithelial nuclei were represented as spots to estimate the number of epithelial cells per image. The total area of TJ protein staining per epithelial cell was calculated as follows:

$$\textbf{Total TJ area/epithelial cell} = \frac{\text{Total surface area of green isosurface}}{\text{No. of epithelial nuclei}}$$

A slightly different method was used for relative 3D quantification of endogenous IgG that had extravasated from the circulation into the CP. Specifically, a volumetric approach was taken as IgG became diffusively distributed throughout the CP by D15 of EAE. Images of extravasated IgG were isosurface rendered, and mean voxel intensities determined. IgG staining along the endothelial lining of the capillaries was specifically masked in order to quantify only the IgG that leaked out of the vasculature. This was done by creating an isosurface of the capillary staining (CD31) and assigning all the included green (IgG) voxel intensities to zero. A mean red voxel intensity value of the capillary isosurface was then obtained. The volume of extravasated IgG per volume of capillaries was calculated as follows:

$$\textbf{Volume of IgG/ Volume of capillaries} = \frac{\text{Total green intensity}}{\text{Total red intensity}}$$

Total green intensity = Mean green intensity X no. of green voxels
Total red intensity = Mean red intensity X no. of red voxels

Leukocyte quantification was performed using the measurement points module of the Imaris® software suite, first representing the $CD45^+$ cells as 'spots' and then counting the total number of spots present in the field of view. The surface area of the capillaries was determined by creating an isosurface of the capillary staining (CD31), and the number of leukocytes per capillary surface area of the CP was calculated as follows:

$$\textbf{Total number of leukocytes/capillary area} = \frac{\text{Total no. of spots} \times 10^4}{\text{Total surface area of the red isosurface}}$$

3.6 LCM and qRT-PCR

Immunohistochemistry-guided LCM was performed as recently detailed (42). In brief, naïve animals were euthanized by gradual CO_2 inhalation. Brains were immediately removed, snap-frozen in dry ice-cooled 2-methylbutane (Acros; Geel, Belgium), and embedded in cryomatrix

compound (Thermo Fisher Scientific, Waltham, MA) for cryosectioning. Coronal sections (7μm) were cut on a Microm HM 505 M cryostat (Mikron Instruments; Oakland, NJ) and affixed to uncoated, pre-cleaned glass slides (Fisher Scientific, Pittsburgh, PA). The CP stromal capillaries were stained using a substrate combination of nitro-blue tetrazolium chloride/5-bromo-4-chloro-3'-indolyphosphate p-toluidine salt (Vector Labs, Burlingame, CA) to detect the endogenous alkaline phosphatase activity in endothelial cells. The choroidal epithelial cells were immunostained with monoclonal pan-cytokeratin-FITC antibody (Sigma). A PixCell IIe laser capture microscope (Life Technologies, Foster City, CA) was used to retrieve CP choroidal epithelial tissue from the lateral ventricles. LCM samples were solubilized in Cell Lysate Buffer (Signosis; Sunnyvale, CA) for direct reverse transcription and relative cDNA levels were quantified by qRT-PCR using an ABI 7900HT Fast Real-Time PCR System (Life Technologies Corp, and normalized to housekeeping gene RPL-19 as described previously (34). Samples were probed for TJ proteins – CLN-1, -2 , -3, -11, occludin and ZO-1 – and the purity of captured LCM material was assessed by epithelial marker (cytokeratin-8) and endothelial marker (CD31) levels.

4. Statistical Analysis

Two CP sections from each animal and a total of three animals were used for each group: naïve, control (CFA/PTX) and EAE (MOG-CFA/PTX). Data from all experiments was initially assessed for normality using a Shapiro-Wilk test. Accordingly, data from ZO-1, IgG and leukocytes determinations was subsequently analyzed by a one-way non-parametric Kruskal-Wallis test followed by Dunn's post-test analysis, while data from CLN-2 determinations were analyzed by a one-way ANOVA followed by Bonferroni post-test. All statistical analyses were performed using GraphPad Prism 5 (GraphPad, La Jolla, CA). Results were considered

significant at $p \leq 0.05$.

5. Results

5.1 Relative expression of genes encoding TJ proteins in the CP

The normal CP choroidal epithelium was first analyzed by laser capture microdissection (LCM) to establish the relative expression of TJ components in this tissue layer of naïve mice (Fig. 1). Prior descriptions by this laboratory (42) have highlighted the ability of LCM to resolve with high purity the choroidal epithelium from the vascularized core. Analysis of LCM-derived choroidal epithelial tissue by qRT-PCR revealed expression of cytokeratin 8 (K8), as well as mRNAs encoding the TJ proteins ZO-1, CLN-1, CLN-2, CLN-3 and CLN-11, which have also been previously identified in the CP *in situ* by immunocytochemistry as well as in cultured choroidal epithelial cells (24, 25, 37, 45). Notably, expression of CD31 – found in all endothelial cells but not choroidal epithelial cells – was barely detectable, reinforcing the high precision of the LCM process. Because of their relatively prominent expression, immunofluorescence studies of ZO-1 and CLN-2 were further pursued to determine whether cytological changes of these CP TJ components were correlated with functional aspects of neuroinflammation during evolving EAE.

5.2 Distribution of TJs proteins, IgG and leukocytes within the CP of naïve mice

Initial studies sought to demonstrate the status of the normal CP in naïve mice (Fig. 2). With respect to ZO-1 and CLN-2 distribution (Fig. 2a and 2b, respectively), strong immunostaining for both these TJ proteins revealed a smooth contour and continuous pattern, delimiting the junctions of all choroidal epithelial cells. A scarce amount of IgG could be detected within the CP stroma of naïve mice (Fig. 2c), along with a few leukocytes (Fig. 2d). The approaches used to

perform relative quantification of ZO-1, CLN-2, IgG and leukocytes in the CP are illustrated in Fig. 3.

5.3 Distribution of ZO-1 in the CP following immunization

Subsequent studies evaluated immunostaining of TJ proteins and IgG at different time-points in both control mice (receiving CFA/PTX) and mice following EAE induction (receiving MOG-CFA/PTX) (Fig. 4a). The staining pattern of ZO-1 was altered in both groups, but the changes varied in scope. In CFA/PTX-treated control mice, immunostaining of ZO-1 was a bit distorted at D6, showing ridge-like irregularities in the contour at some locales that persisted through D15. Treatment with MOG-CFA/PTX to induce EAE resulted in more drastic alterations in ZO-1 staining pattern. Similar ridge-like irregularities were initially obvious along some choroidal epithelial cells at D6, but these became more pronounced through the disease course. By D15, the ZO-1 staining pattern was severely crenulated throughout the choroidal epithelium, giving a palisade appearance. To quantify these changes in TJ staining patterns, total area of ZO-1 staining within the CP epithelium of each image was related to the number of CP epithelial nuclei (Fig. 4b) as shown in Fig. 3. Control mice evidenced no changes in this parameter over the time-points evaluated, while mice with EAE showed a step-wise elevation, with significant changes at D9 and D15 (compared to naïve). As this suggested an increase in individual CP epithelial cell surface area during evolving EAE, inter-nuclei distances were also determined as a surrogate for corresponding volume/cell-size changes. At D15 EAE, mean inter-nuclei distance in CP epithelial cells was nearly three-fold higher than that found in naïve mice, suggesting a significant increase in CP epithelial cell volume during neuroinflammatory disease (see Figure, Supplemental Digital content 1, which shows an increase in CP epithelial inter-nuclei distance). These observations were further supported by a significant increase in perimeter of ZO-1

staining in CP epithelial cells in D15 EAE mice compared to naïve mice (see Figure, Supplemental Digital content 2, which shows an increase in perimeter of ZO-1 staining within the CP epithelium).

5.4 Distribution of CLN-2 in the CP following immunization

The response of CLN-2 was different both qualitatively and quantitatively from that of ZO-1 (Fig. 5a)**.** The immunostaining pattern of CLN-2 did not appear to change in control mice receiving CFA-PTX alone, remaining relatively linear at intercellular borders. There was, however, a slight change in the staining intensity by D15. Likewise, the overall CLN-2 staining pattern remained unaltered following EAE induction with MOG-CFA/PTX, though a steeper reduction in staining intensity was more noticeable in this group, which by D15 revealed sites of sharp discontinuities (arrows). The ratio of total area of CLN-2 immunostaining to number of CP epithelial cell nuclei was calculated as for ZO-1 (Fig. 5b). This parameter did not significantly change in control mice until D15, but was significantly reduced earlier in mice with EAE – showing a decrease at D9 and an even greater decline at D15 of MOG-CFA/PTX treatment as discontinuities became more evident.

Given the strongly disparate responses between ZO-1 and CLN-2, additional studies were carried out to determine whether the different patterns of TJ protein redistribution might be related to these proteins being of peripheral and integral membrane classes, respectively (see Figure, Supplemental Digital Content 3, which shows ZO-2 and CLN-3 staining in the CP from naïve and MOG-CFA/PTX-treated mice). ZO-2, another peripheral membrane TJ protein, demonstrated a response much like that of ZO-1, showing a similarly crenulated pattern while apparently maintaining constant intensity following MOG-CFA/PTX immunization. In contrast,

the response of CLN-3, another integral membrane TJ protein, paralleled that of CLN-2, exhibiting a less intense and discontinuous pattern.

5.5 Distribution of IgG in the CP following immunization

Increased IgG staining was seen in both control mice and in mice following EAE induction, though to different extents (Fig. 6a). It increased in CFA/PTX-treated control mice by D6, and displayed greater elevation through D15. The IgG appeared to be restricted to the CP stroma, as none could be readily seen to infiltrate the choroidal epithelium. These changes in IgG were even more dramatic in mice subjected to EAE by MOG-CFA/PTX treatment. A visible increase in IgG immunostaining was first noted by D6, becoming more extreme by D15. At this later time IgG was clearly seen permeating across the choroidal epithelium. Because IgG staining became extremely diffuse by later stages of EAE, relative IgG leakage within the CP was quantified by relating its total volumetric staining to total volumetric staining of capillaries within each image (Fig. 3). An increase in IgG leakage was established in both control mice and those with EAE, with a greater level (~ three-fold) seen in the latter by D15 (Fig. 6b).

5.6 Distribution of leukocytes in the CP following immunization

CFA/PTX injection alone resulted in increased apprearance of leukocytes in the CP, compared to that seen in naïve mice (Fig. 7a). However, these leukocytes appeared to be in close association with the CP capillaries and/or confined to the stroma. This moderate leukocyte increase was reversed to normal level by D9, where it remained through D15. MOG-CFA/PTX also resulted in an apparent influx of leukocytes in the CP at D6 and D9, which reverted by D15. Notably, at D15 leukocytes could be seen closely associated with the choroidal epithelium, a few apparently caught in the act of extravasating past the epithelial barrier. That these leukocytes

were, in fact, outside of the CP stroma, was revealed by rotation of 3D images, wherein some extravasated leukocytes in the CSF could be seen still tethered to the luminal surface of choroidal epithelium (see Video, Supplemental Digital content 4, which shows leukocytes attached to the CP epithelium). It is important to emphasize here that any leukocytes fully extravasated into the CSF are unlikely to be represented in these images, as the cells would not be retained in the ventricles following tissue sectioning and immunostaining. Quantification showed that the number of leukocytes significantly increased in the CP at D6 following CFA/PTX treatment, and also did so at D6 and D9 after MOG-CFA/PTX, before returning to normal levels (Fig 7b).

6. Discussion

While the appearance and developmental regulation of TJs in the CP have been rigorously investigated over nearly five decades (24, 25, 46-57), much less is understood of the alterations of these junctions and their protein constituents during neuroinflammatory disease and their relation to BCSFB permeability and leukocyte extravasation (58). Hence, high resolution, 3D imaging of the CP was performed in this study to track and quantify such alterations and their functional correlates; i.e., extravasation of IgG and leukocytes, during evolving EAE, and to distinguish MOG-associated changes from those due to adjuvants alone.

Our use of LCM/qRT-PCR to selectively analyze the CP choroidal epithelium confirmed the relative gene expression of major TJ proteins in the particularly MOG-sensitive C57BL/6 mouse, a similar pattern having previously been described in the Sprague-Dawley rat by standard qRT-PCR of total RNA from whole CP tissues (25). These results reinforced emerging LCM technology as a critical tool to probe gene changes in discrete compartments of the CP (42), and focused our attention on TJ proteins ZO-1 and CLN-2 for detailed, 3D image analysis.

Strong and smooth immunostaining of both ZO-1 and CLN-2 was associated with all intercellular junctions of CP epithelial cells in naïve mice, as has been previously reported in these cells from various species (24, 37, 45, 59). However, ZO-1 and CLN-2 showed markedly different responses to MOG immunization or injection of adjuvants. The pattern of ZO-1 immunostaining became moderately distorted after CFA/PTX alone, and more drastically crenulated following MOG immunization. To the best of our knowledge, this is the first description of such alterations in TJ staining *in vivo*. Recent *in vitro* reports have given similar accounts of "ruffled" or "wavy" ZO-1 patterns associated with loosening of epithelial TJs of cultured Caco-2 and MDCK cells following application of nanoparticles or mechanical stretch (60, 61). Together, these observations seemingly highlight a common manifestation of ZO-1 redistribution that accompanies epithelial barrier disruption.. While the basis and physiological significance of the peculiar alteration of ZO-1 appearance noted here remain unknown, Samak et al. (43) noted the comparable disruption in Caco-2 cells to be associated with JNK-2-, c-Src- and MLCK-dependent mechanisms. Interestingly, radical ultrastructural changes in CP epithelial cells, e.g., widening of intercellular clefts, have been reported following experimental traumatic brain injury (62), and the two findings may be related to observations in the current study. The ~ three-fold increase in both the mean inter-nuclei distance and ZO-1 perimeter of CP epithelial cells during EAE is further consistent with a significant increase in cell volume, and points toward an even more gross histopathology associated with EAE than has been previously imagined. Interestingly, while describing distributions of TJ proteins at the CP more than a decade ago, Wolburg et al. (24) did not note any changes in ZO-1 distribution in EAE afflicted mice, and specifically commented on the difficulties of obtaining quantitative results by immunohistochemistry when using conventional confocal microscopy. The advantages afforded

by state-of-the-art high-resolution 3D imaging may thus have uniquely enabled us to uncover and quantify the remarkable ZO-1 responses in the CP choroidal epithelium.

By contrast to the observed effects on ZO-1, changes in CP epithelial CLN-2 following immunization appeared much more subtle. CLN-2 showed no obvious alterations in pattern after CFA/PTX treatment and a minimal decrease in the amount of immunoreactivity. A similar trend was observed following MOG immunization, but with a sharper decrease in immunoreactivity of CLN-2 that ultimately presented a fragmented appearance. Wolburg et al.(24) similarly observed the immunostaining of CLN-2 to be "interrupted" in the CP choroidal epithelium following EAE immunization, but did not resolve whether this was due to MOG or adjuvant effects. Kooij et al.(45) also recently described a comparatively tempered loss of CLN-3 immunostaining in this tissue in mice immunized for EAE, possibly suggesting this type response is common among the different CLN proteins of the CP during neuroinflammation, as opposed to the more peculiar change in pattern evidenced by ZO-1.

That the responses of the two classes of TJ proteins, ZO-1/ZO-2 and CLN-2/CLN-3, were vastly different from each other could reflect their respective positions and roles within the TJ complex. Peripheral membrane ZO proteins, lying internal to CLNs and directly connected to the actin cytoskeleton (38-40), might transduce the disruptive inflammatory signal to their integral membrane CLN protein partners. Inasmuch as the epithelial actin cytoskeleton can become severely disorganized during both PTX treatment and inflammation (63, 64), this could potentially lead to retraction of ZO proteins from its membrane locale and disengagement from CLNs. No longer bound to ZO proteins, CLNs might be susceptible to rearrangement and/or degradation (41, 43). Whatever their cause, the different effects on these two proteins underscores the complexity of actions taking place at the level of the TJ in the CP choroidal

epithelium, and that the response of individual TJ proteins cannot be assumed to be similar. Disparities in responsiveness among various TJ proteins have also been reported in cultured CP choroidal epithelial cells (65). In this case, CLN-2 showed reduced protein level by Western blotting following treatment with protein kinase C activator, phorbol 12-myristate 13-acetate, while levels of CLN-1, ZO-1 and occludin were spared.

In line with the characterization of the fenestrated CP capillaries as normally "leaky" (15, 66, 67), there was some evidence – albeit scarce – of IgG immunostaining and a few leukocytes in the CP stroma of naïve mice. In contrast, while using the same technology as employed here, virtually no IgG or leukocytes were detected around parenchymal CNS microvessels in the naive situation (41, 43). It would thus appear that while CP capillaries in the healthy state are somewhat more permeable than the BBB, their perception as being "highly permeable" (68) and "allowing the free passage of molecules and cells (69)" may merit some reconsideration. This would concur with the description of fenestrated endothelia in airway exchange vessels having permeabilities to plasma proteins that are about the same as found in continuous endothelia (70).

CP capillaries nevertheless seemed to become significantly more leaky in response to CFA/PTX or MOG-CFA/PTX, allowing for extravasation of IgG and leukocytes into the stromal compartment. It is possible that some of the IgG appearing in the stroma might have derived from intrathecal synthesis by B cells. However, the fact that IgG levels continually increased while leukocytes decreased in the CP stroma at later time points argues against B cells being the exclusive or major source of IgG observed, suggesting a significant amount of this protein was serum-derived. The basis for this effect is unclear at this time, as the presence of TJs or other less-restrictive junctional specializations in CP capillaries has not been confirmed (68). Nevertheless, CLN-5, occludin and ZO-1 have been reported in this vascular bed (45, 53) and

could possibly be targets of CFA/PTX or MOG-CFA/PTX action. A previous finding by this laboratory that the chemokine CCL2 is elevated within the CP capillary plexus following CFA/PTX or MOG-CFA/PTX treatment (42) may thus relate to the enhanced IgG leakiness noted here, as this chemokine has been linked to downregulation and/or redistribution of endothelial CLN-5, occludin and ZO-1 in association with increased permeability (43, 71-75). Appearance of IgG leakage across the CP choroidal epithelium was only observed following MOG-CFA/PTX, and may be due to the more severe alterations in TJ proteins that accompany neuroinflammation.

The observation that few leukocytes were present in the CP stromal space in naïve mice is consistent with other recent descriptions (45, 76), and may reflect a limited permeability of normal CP capillaries to blood cellular elements. Specifically, scant $CD3^+$ and $CD4^+$ T cells, and $CD68^+$ cells of myeloid lineage (dendritic cells and macrophages) have been shown to normally reside in this CP compartment (13, 77, 78). Both CFA/PTX and MOG-CFA/PTX produced a transient increase in the CP leukocyte population. The pathway(s) by which leukocytes accumulate in the CP stroma remains uncertain, as previous reports using immunohistochemistry at the light and ultrastructural levels noted expression of adhesion molecules, ICAM-1, VCAM-1 or MAdCAM-1, on the CP choroidal epithelium but not along the CP capillaries in SJL mice with EAE induced by immunization with CFA/PTX and proteolipid protein (79, 80). However, this laboratory recently utilized laser capture microdissection to detect upregulated gene expression of VCAM-1, E-selectin, P-selectin and Smad-3 in the CP capillary bed of C57BL/6 mice following CFA/PTX or MOG-CFA/PTX, with Smad-3 exclusively among these showing super induction during MOG-CFA/PTX-induced EAE (42). Reinforcing the relevance of these gene findings, E- and P-selectin immunoreactivity has also been described in the CP vasculature

of patients with non-neurological disorders (13). Previously noted examples of up-regulated chemokine expression in these microvessels, e.g., CCL2, CCL5 and CCL19 (42) may thus act cooperatively with elevated adhesion molecule expression to drive leukocyte extravasation across the CP capillaries into the stroma. At present, we are unaware of any descriptions of the CP bearing specialized post-capillary venules – the preferred sites of exit of leukocytes from the circulation (81) – but are mindful of the possibility that leukocyte extravasation from the circulation could occur at the transitional regions between the CP capillary plexus and draining venules (13).

Only MOG-CFA/PTX treatment showed clear evidence of leukocyte extravasation across the CP choroidal epithelium – which, for CCR6-bearing Th17 cells, is thought to be mediated, in significant part, by epithelial expression of the chemokine CCL20 (22). That the CD45+ cells observed clinging to the apical side of the CP choroidal epithelium actually represent extravasating leukocytes, is strongly supported by the sequence of images following MOG-CFA/PTX immunization, which showed these cells first appearing in the CP stroma, then in association with the basolateral epithelial surface, and finally attached to the apical epithelial surface facing the CSF. To the best of these authors' knowledge, the scenario shown is the first histological evidence of such directed transit through the entire CP. This finding is also in accord with inability of CFA/PTX treatment, alone, to cause clinical EAE in these mice (42), and directly supports that the rudimentary processes underlying neuroinflammatory diseases such as MS and EAE originate via the trafficking of leukocytes through CP into the CSF (13, 16-18, 22). The prior observation by Schmitt et al.(77), that CFA/PTX, alone, resulted in a subtle but definite increase in the number of myeloid cells in the extraventricular CSF spaces, could suggest that this adjuvant combination promotes modest leukocyte extravasation across the CP

choroidal epithelium but at a level too low to be readily detected even by high-resolution, 3D confocal microscopy. In this regard, histologically capturing leukocytes in the act of extravasating across the CP choroidal epithelium is particularly challenging, as they are, in effect, washed away after entering the CSF.

As with the observed IgG leakage at this site, the more profound perturbations in TJ proteins caused specifically by MOG-CFA/PTX treatment may enable leukocytes accumulating within the CP stroma to more effectively migrate between the choroidal epithelial cells and into the CSF, as depicted schematically in Fig. 8. Alternatively, other factors induced by MOG-CFA/PTX, e.g., chemokines and/or adhesion molecules, may facilitate leukocyte extravasation at this level, which, in turn, alters the integrity of the CP choroidal epithelium leading to the TJ protein manifestations and IgG leakage observed. The fact that the CP stroma showed apparent reduction in the leukocyte population from D9 to D15 may further represent time needed for leukocyte extravasation across the CP choroidal epithelium.

While no absolute cause and effect relationship between the observed TJ alterations and IgG/leukocyte extravasation can be established at this time, it is significant to point out that neither IgG nor leukocytes were seen permeating the CP choroidal epithelium until D15 following MOG-CFA/PTX, while changes in both ZO-1 and CLN-2 were observed earlier (D9). This time frame is thus consistent with the noted structural changes in CP choroidal epithelial TJ proteins having functional consequences that encourage extravasation of IgG and leukocytes.

Collectively, these results reinforce the notion that CFA/PTX instigates a series of molecular and structural changes associated with neuroinflammation that is augmented when this adjuvant combination accompanies MOG immunization. At present, it is unclear whether only one or both adjuvants were responsible for the observed effects, as our objective was to specifically highlight

changes in TJ protein distribution and IgG/leukocyte extravasation stemming from MOG immunization versus collective adjuvant action. CFA and PTX have each been shown to separately disrupt TJs and increase permeability at the BBB in other settings (82, 83). However, PTX was not found to disrupt barrier function in epithelial *Plexus choroideus*-derived monolayer cultures (84), suggesting that CFA might be responsible for the effects noted here or that the two adjuvants cooperate to alter TJs and structural integrity of the CP capillaries and/or choroidal epithelium *in vivo* in support of IgG and leukocyte extravasation.

This laboratory previously reported that CFA/PTX alone elicited significant changes in the expression of numerous immune response associated genes in both CP capillary and choroidal epithelium compartments (42), while MOG-CFA/PTX resulted in super induction of some of these genes as well as stimulated a novel cadre of genes in this same functional category. In the current report we extend these findings to show CFA/PTX further instigates structural changes in the CP that may facilitate the autoimmune response to MOG. Thus, while it has been reported that PTX, in particular, can drive CNS autoimmunity via regulation of TLR4 signaling and opening up the BBB (85, 86), CFA/PTX appears to act more broadly to "raise the floor" of a collective of inflammatory processes in the CP necessary for neuroinflammatory disease, like EAE, to develop. A couple of implications are worth noting here. Attempts to attribute gene or histological changes seen in EAE as being a specific autoimmune response to MOG, might overlook significant contributions by CFA and/or PTX. Also, the fact that CFA/PTX exerts prominent effects in the CP – considered a possible gateway for leukocytes to invade the uninflamed CNS (8, 9, 87) – calls attention to the prospect that other environmental toxins with activities like CFA or PTX might target this brain structure to help trigger cases of CNS autoimmunity (88)

Further clarification of the modes of leukocyte trafficking through the CP should enable more efficient drug targeting to this organ and significantly broaden the prospects to treat neuroinflammatory disease (89, 90).

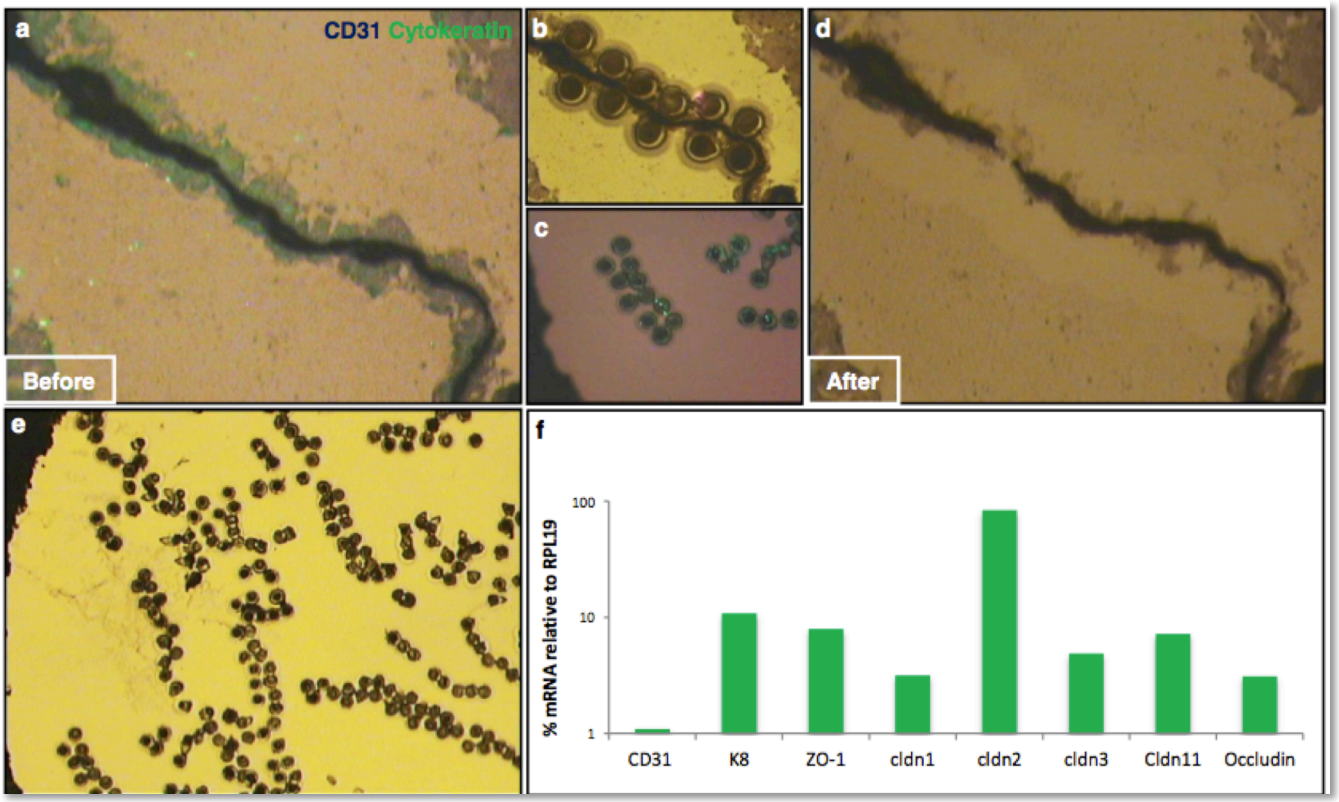

FIGURE 1. LCM analysis of tight junction gene expression in choroidal epithelial cells. The CP of a naïve mouse was double immunostained for LCM analysis. **(a)** CP tissue section *before* LCM retrieval. Capillaries were stained by immunohistochemistry for CD31, employing alkaline phosphatase detection and NBT/BCIP substrate (dark purple); choroidal epithelial cells were stained by immunofluorescence using FITC-conjugated antibody to pan-cytokeratin (green). **(b)** Laser shots showing the retrieval of choroidal epithelial cells and their deposition on the cap **(c)**. **(d)** CP tissue section *after* LCM retrieval of epithelial cells, showing capillaries left behind. **(e)** Collection of LCM shots of epithelial cells on the cap used for gene expression analysis. **(f)** qRT-PCR analysis of LCM-derived CP epithelial tissue, indicating expression of the epithelial marker K8, and several tight junction proteins.

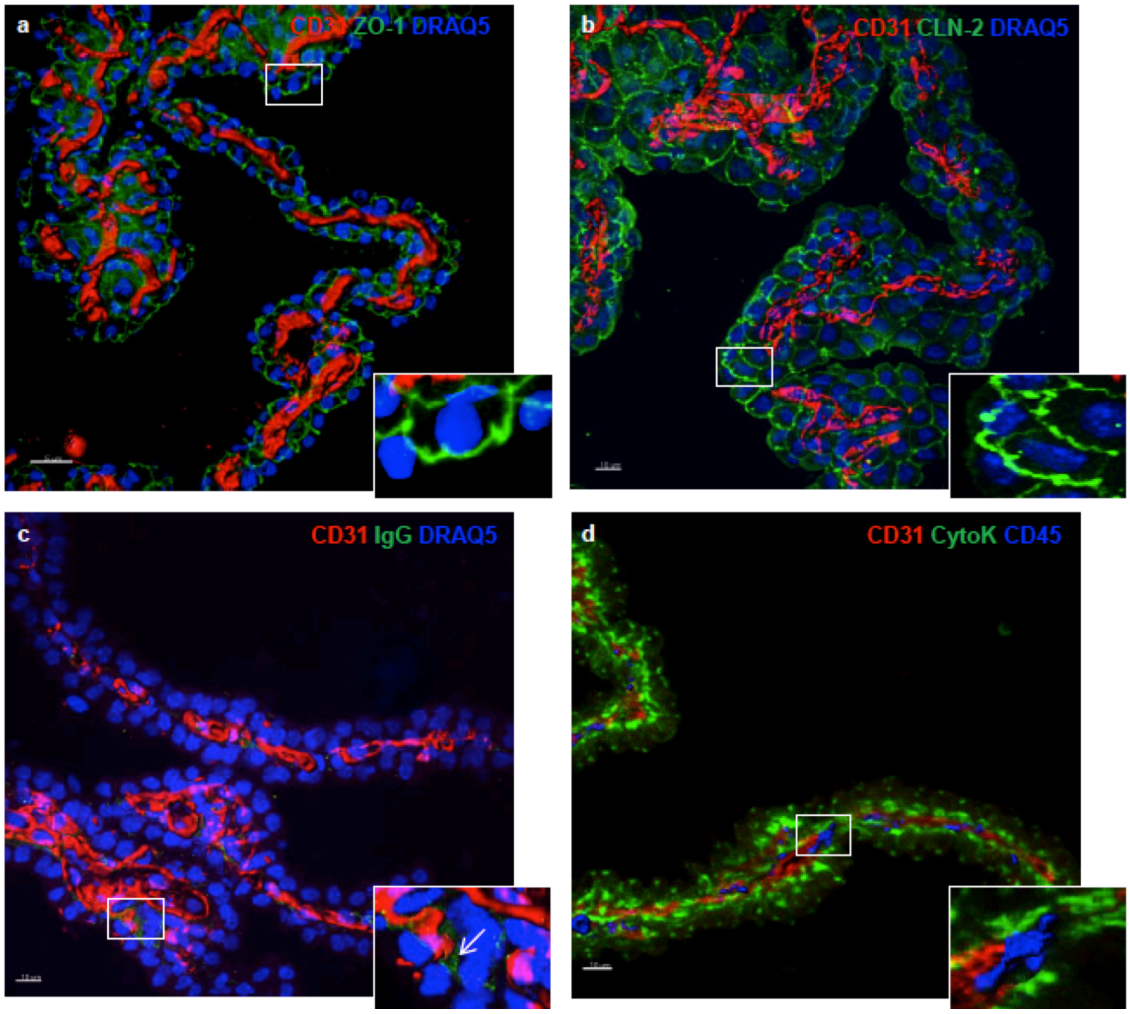

FIGURE 2. Distribution of tight junction proteins, IgG and leukocytes in normal CP tissue. Representative sections of the CP of naïve mice are depicted. Capillaries were immunostained for CD31 (red) in all images, and isosurface rendered in images **(a – c)**. Nuclei of the choroidal epithelial cells were stained with DRAQ5 (blue) in images **(a – c)**. **(a)** ZO-1 immunostaining (green) and **(b)** CLN-2 immunostaining (green) appear uniform and smooth along the inter-epithelial junctions, as highlighted in the insets. **(c)** IgG immunostaining (green) is scant and seen in only focal deposits apparently within the stroma (white arrow, insert). **(d)** Choroidal epithelial cells were immunostained for cytokeratin (green); leukocytes were immunostained for CD45 (blue), and isosurface rendered to highlight their 3D appearance and spatial relation to the different compartments of the choroid plexus. A few leukocytes are clearly present, seemingly associated with capillary network or in the stroma (insert)

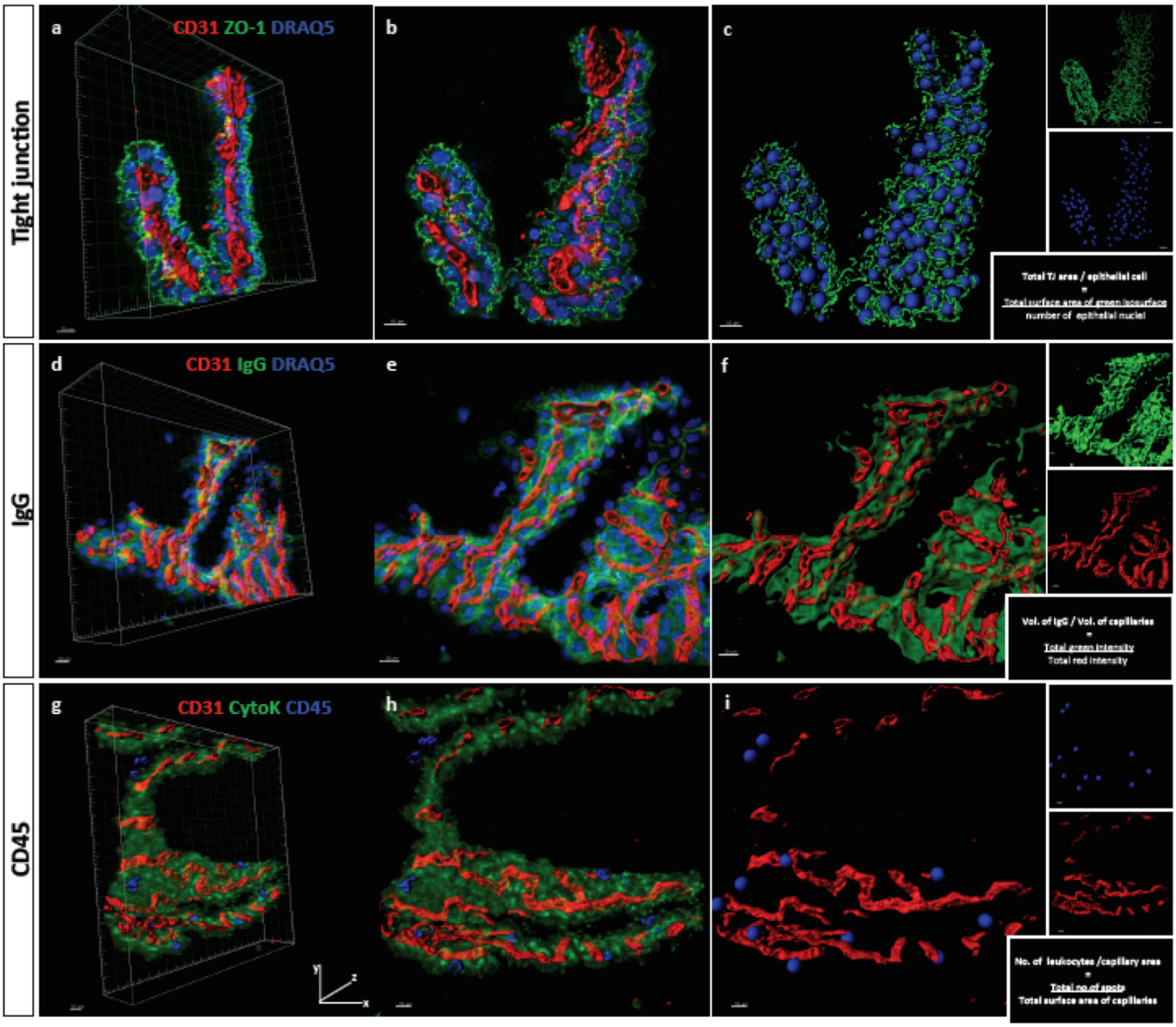

FIGURE 3. 3D quantification of CP tight junction protein, IgG and leukocytes during evolving EAE**.** Representative sections of the CP of mice at D15 EAE are depicted to elaborate the approaches used for quantification of disease-associated changes in CP tight junction protein and IgG leakage. **(a, d, g)** show composite 3D data sets of confocal z-stacks. The 3D frames are presented to display the holistic acquisition of the data. **(b, c)**, **(e, f) and (h-i)** show 2D depictions of the images in **(a)**, **(d) and (g)**, respectively. Such 2D projections of 3D images served as the sources from which quantitative data were obtained. Isosurface rendering was performed to highlight the tortuous nature and 3D disposition of the respective CP compartments. Capillaries were immunostained for CD31 (red) and isosurface rendered throughout. ZO-1, shown as an example of tight junction protein within the choroidal epithelium, was immunostained (green) in **(a – c)**, and isosurface rendered in **(c)**. IgG was also shown immunostained (green) to exemplify serum protein leakage **(d – f)** , and isosurface rendered in **(f)**. Choroidal epithelial nuclei were stained with DRAQ5 (blue) in **(a-f)** while leukocytes were stained for CD45 (blue) in **(g-i);** DRAQ5- and CD45-stained structures were reconstructed as "spheres" in **(c) and (i) respectively**. Inserts in **(c)** show the total ZO-1 staining (top) and nuclei staining (bottom) used to calculate relative amount of tight junction protein/choroidal epithelial cell. Inserts in **(f)** show total IgG staining (top) and capillary staining (bottom) used to calculate relative amount of leaked IgG/capillary mass. Inserts in **(i)** show the total number of leukocytes (top) and total capillary staining (bottom) used to calculate relative number of leukocytes/ capillary surface area.

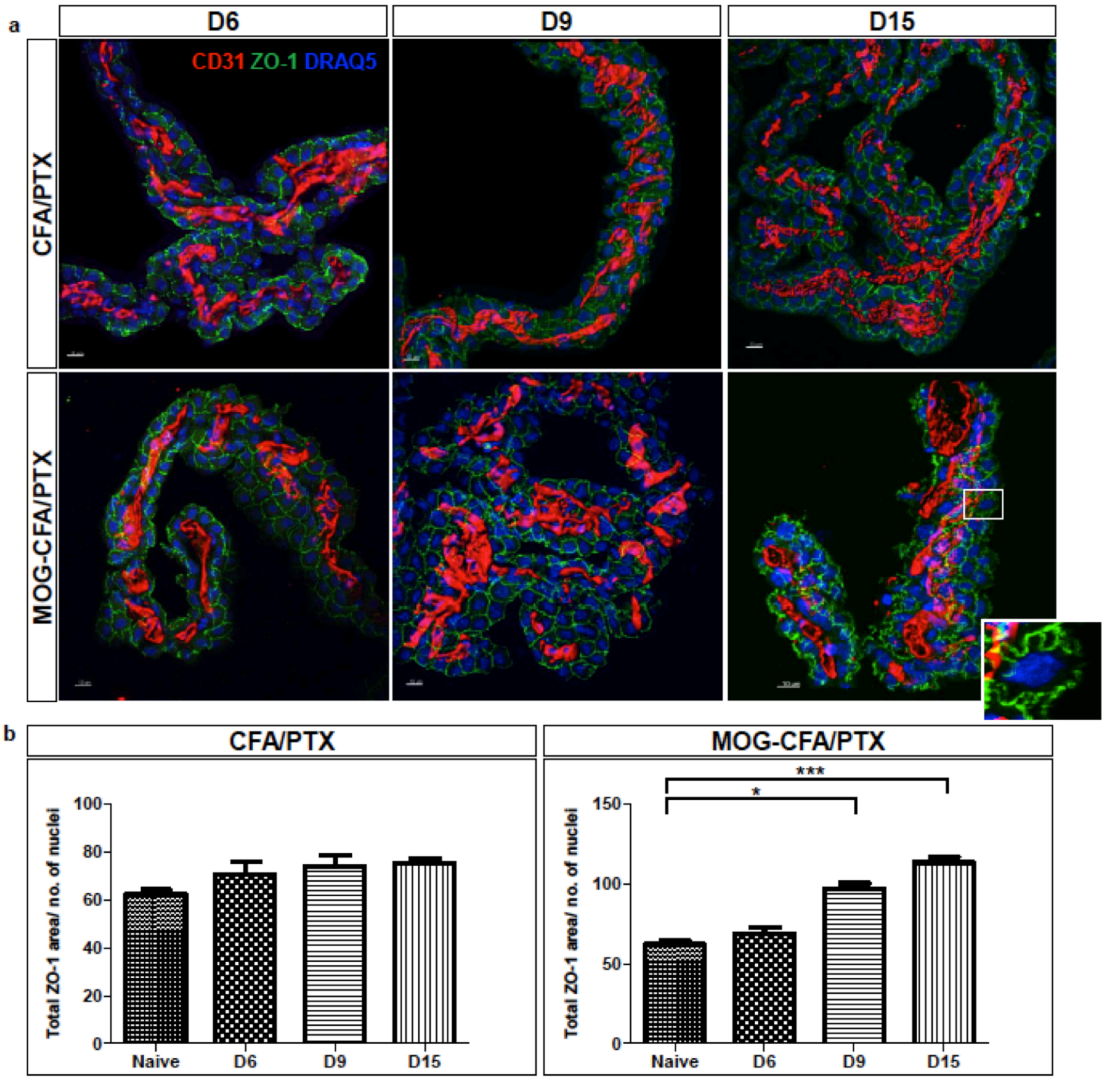

FIGURE 4. ZO-1 distribution in the choroid plexus during evolving EAE. **(A)** Representative sections of the CP were collected at the indicated time-points in control mice (CFA/PTX) or in mice following EAE induction (MOG-CFA/PTX). Capillaries were immunostained for CD31 (red), and isosurface rendered in all images to highlight the swelling of these microvessels during disease. Choroidal epithelial cells were stained with DRAQ5 (blue) to identify their nuclei and immunostained for ZO-1 (green). Insert highlights area of extensive crenulation of ZO-1 immunostaining in mice at D15 EAE. **(B)** 3D quantification and analysis of the changes in total area of ZO-1 per epithelial cell nuclei for both the groups: CFA/PTX and MOG-CFA/PTX. A significant increase in area is seen in D9 and D15 EAE compared to naïve ZO-1 staining, *p<0.05, ***p <0.001

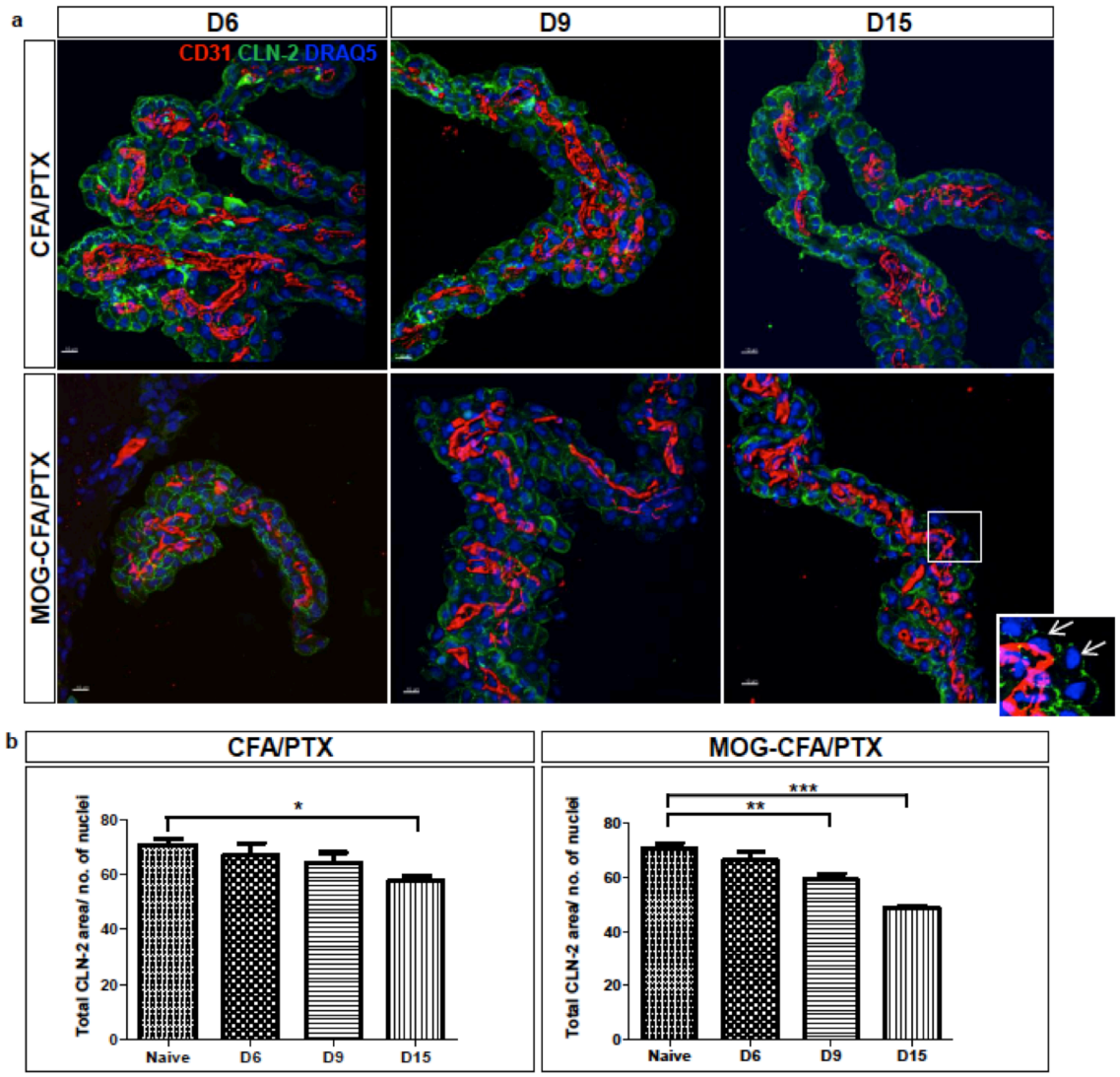

FIGURE 5. CLN-2 distribution in the choroid plexus during evolving EAE. **(A)** Representative sections of the CP were collected at the indicated time-points in control mice (CFA/PTX) or in mice following EAE induction (MOG-CFA/PTX). Capillaries were immunostained for CD31 (red), and isosurface rendered in all images to highlight the swelling of these microvessels during disease. Choroidal epithelial cells were stained with DRAQ5 (blue) to highlight their nuclei and immunostained for CLN-2 (green). White arrows show focal disruptions in CLN-2 staining by D15 EAE. **(B)** 3D quantification and analysis of the changes in total area of CLN-2 per epithelial cell nuclei for both the groups: CFA/PTX and MOG-CFA/PTX. A significant decrease in area corresponding to the loss in focal staining is seen in D9 and D15 EAE compared to naïve CLN-2 staining, **$p<0.01$, ***$p<0.001$. CFA/PTX group showed a significant decrease in area by D15 as well, *$p<0.05$

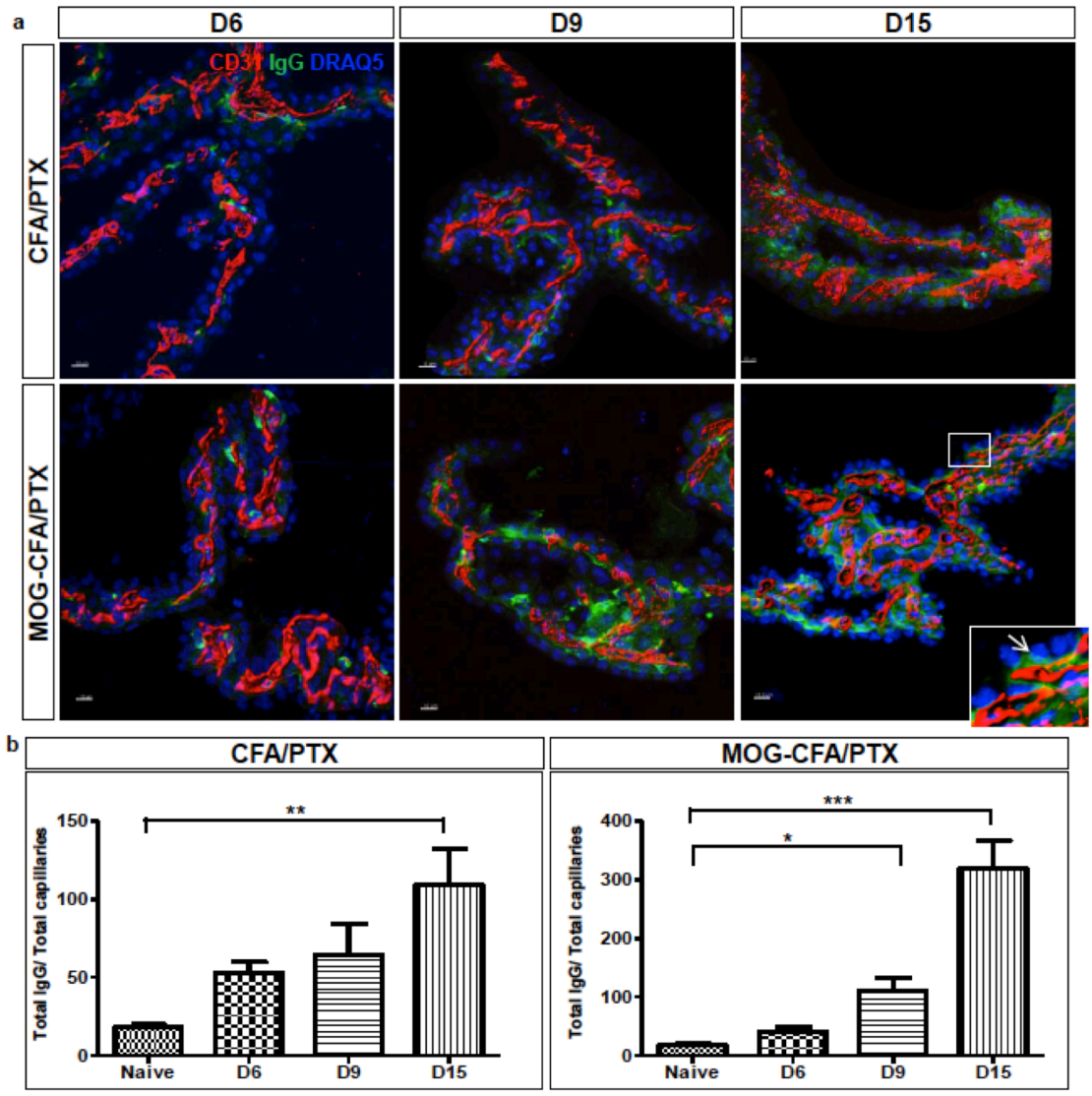

FIGURE 6. IgG distribution in the choroid plexus during evolving EAE. **(A)** Representative sections of the CP were collected at the indicated time-points in control mice (CFA/PTX) or in mice following EAE induction (MOG-CFA/PTX). Capillaries were immunostained for CD31 (red), and isosurface rendered in all images to highlight the swelling of these microvessels during disease. Choroidal epithelial cells were stained with DRAQ5 (blue) to highlight their nuclei, and IgG was immunostained (green). IgG can be seen extravasating across the choroidal epithelium in mice increasing with extending timepoints in CFA/PTX and with increased severity in MOG-CFA/PTX (white arrows, insert). **(B)** 3D quantification and analysis of the changes in total IgG per total capillaries for both the groups: CFA/PTX and MOG-CFA/PTX. A significant increase in extravasating IgG can be seen in D15 Control and, D9 and D15 EAE compared to naïve IgG staining, *p<0.05, **p<0.01 and ***p<0.001

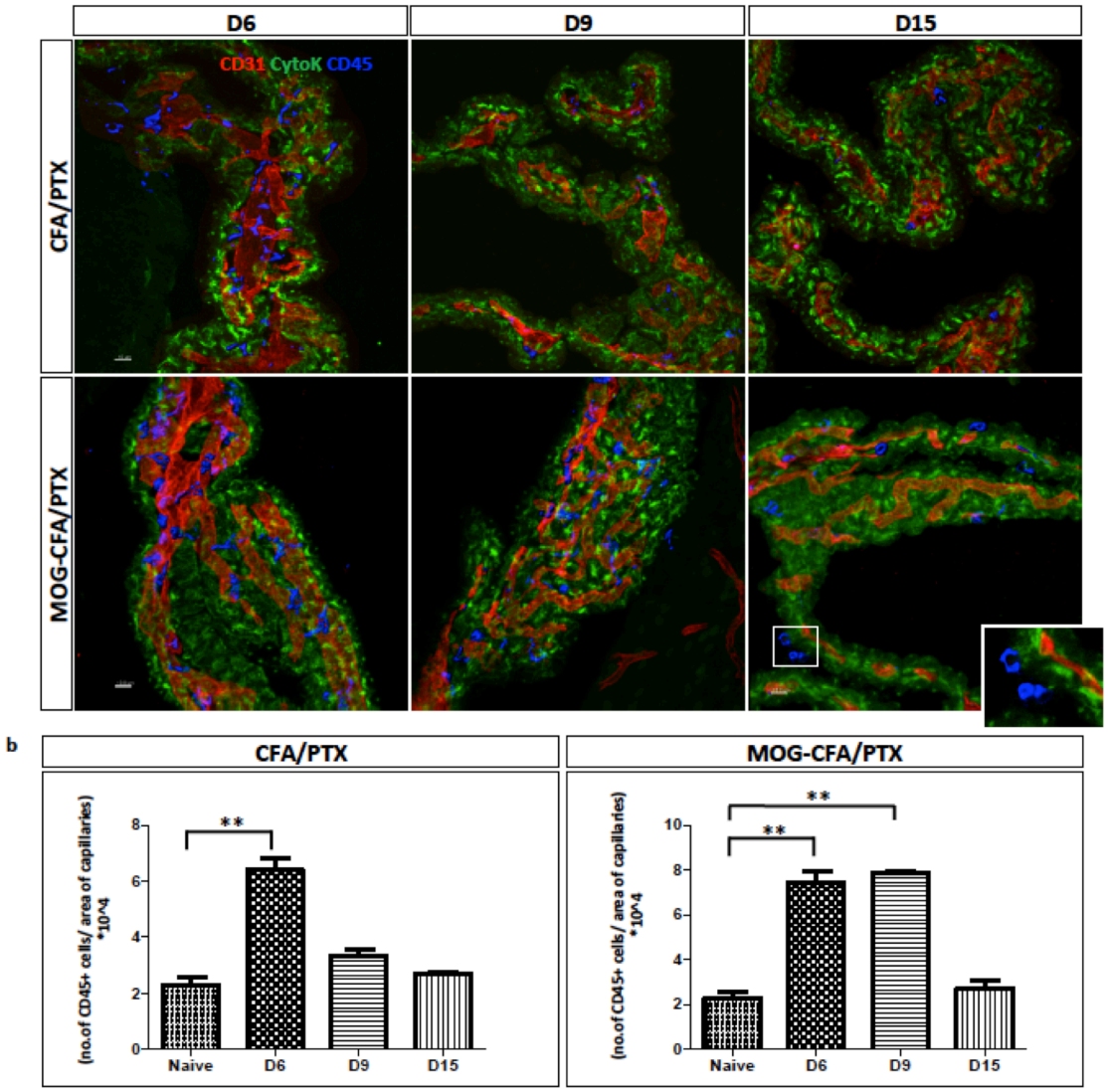

FIGURE 7. Leukocyte extravasation in the choroid plexus during evolving EAE. Representative sections of the CP were collected at the indicated time-points in control mice (CFA/PTX) or in mice following EAE induction (MOG-CFA/PTX). Capillaries were immunostained for CD31 (red). Choroidal epithelial cells were immunostained for cytokeratin (green). Leukocytes were immunostained for CD45 (blue), and isosurface rendered in all images to highlight the 3D appearance of these cells and their spatial relation to the different compartments of the choroid plexus. In control choroid plexus, the number of leukocytes appears to increase at D6 but returns to near naïve level by D9 and D15. The leukocytes in these mice appear to remain associated with the capillaries or stroma. In choroid plexus of mice with EAE, an increase in leukocytes is apparent at D6 and D9, which reverses to naïve level by D15. Insert highlights leukocytes that can be seen associated with the apical surface of the choroidal epithelium, likely extravasating into the CSF at D15 EAE. **(b)** 3D quantification and analysis of the changes in total number of leukocytes per total surface area of capillaries for both the groups: CFA/PTX and MOG-CFA/PTX. A significant increase in accumulation of leukocytes can be seen in D6 Control and, D6 and D9 EAE compared to naïve CD45 staining, *p<0.05, **p<0.01 and ***p<0.001.

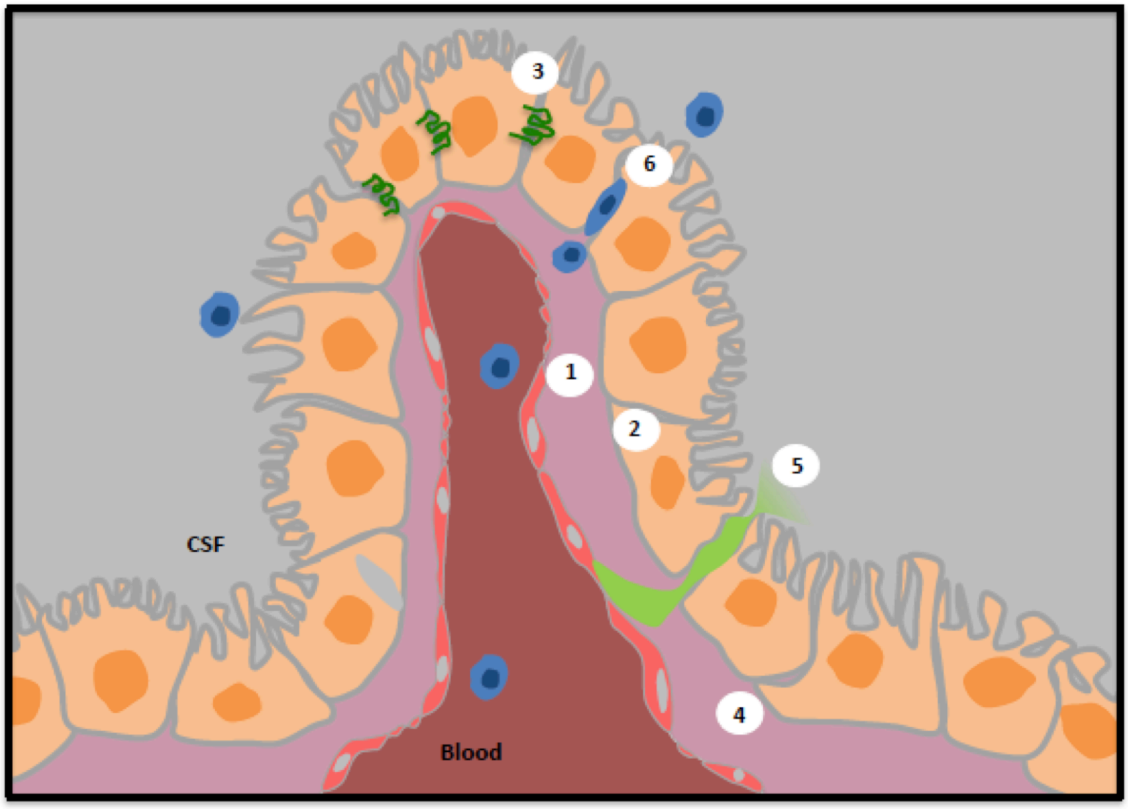

FIGURE 8. Schematic diagram of the Choroid Plexus. "Leaky" fenestrated capillaries **(1)** are surrounded by a "tight" layer of epithelial cells **(2)** that express tight junctions **(3)**, forming the BCSFB. The stroma **(4)** lies in between the two layers. Loss of BCSFB integrity during neuroinflammation is associated with alteration of tight junctions **(3)**, leakage of serum protein IgG **(5)** and extravasation of leukocytes **(6)** across the BCSFB into the CSF. Leukocyte extravasation is depicted as occurring paracellularly; i.e., between choroidal epithelial cells, as it accompanies junctional disruption, though the precise mode has not been established.

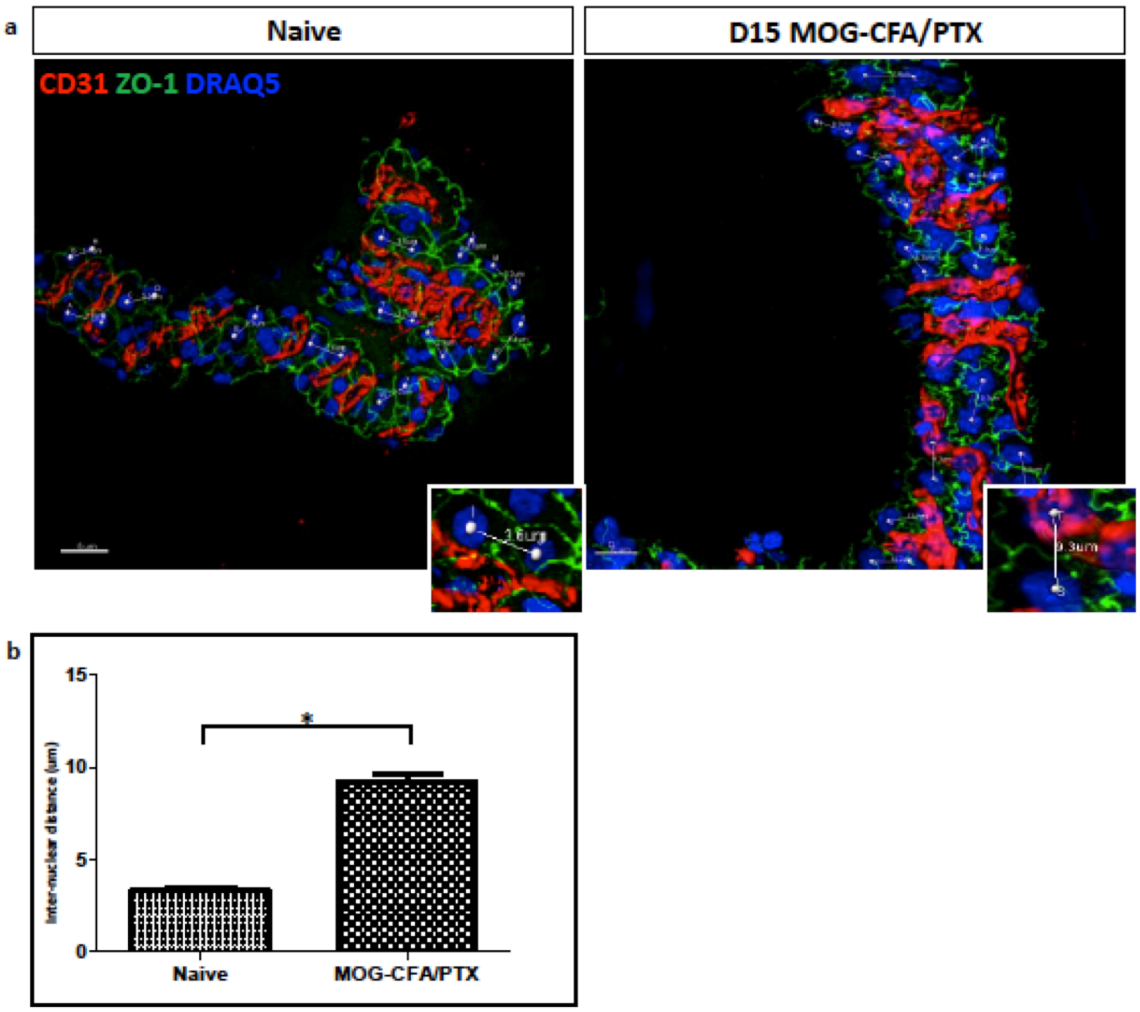

Supplemental Fig. 1 Measurement of inter-nuclei distances between CP choroidal epithelial cells. (a) Representative sections of the CP from naïve and MOG-CFA/PTX-treated mice at D15. Scale bars represent 5µm (naïve) and 10µm (MOG-CFA/PTX). Capillaries were immunostained for CD31 (red) and isosurface rendered. Choroidal epithelial cells were stained with DRAQ5 (blue) to highlight nuclei, and immunostained for ZO-1 (green). Inter-nuclei distances were calculated by placing a measurement point in the center of each epithelial cell nucleus and measuring the distance between adjacent points, as highlighted in the inserts and described in Materials and Methods. Note that the distance bars connecting the adjacent center points are in all three planes; this, together with the different scales, makes some longer distance bars in the MOG-CFA/PTX sample 'appear' artificially smaller than shorter distance bars in the naïve sample. (b) A significant increase in inter-nuclei distances between CP epithelial cells was found in MOG-CFA/PTX-treated (EAE) mice compared to naïve mice, *$p<0.001$.

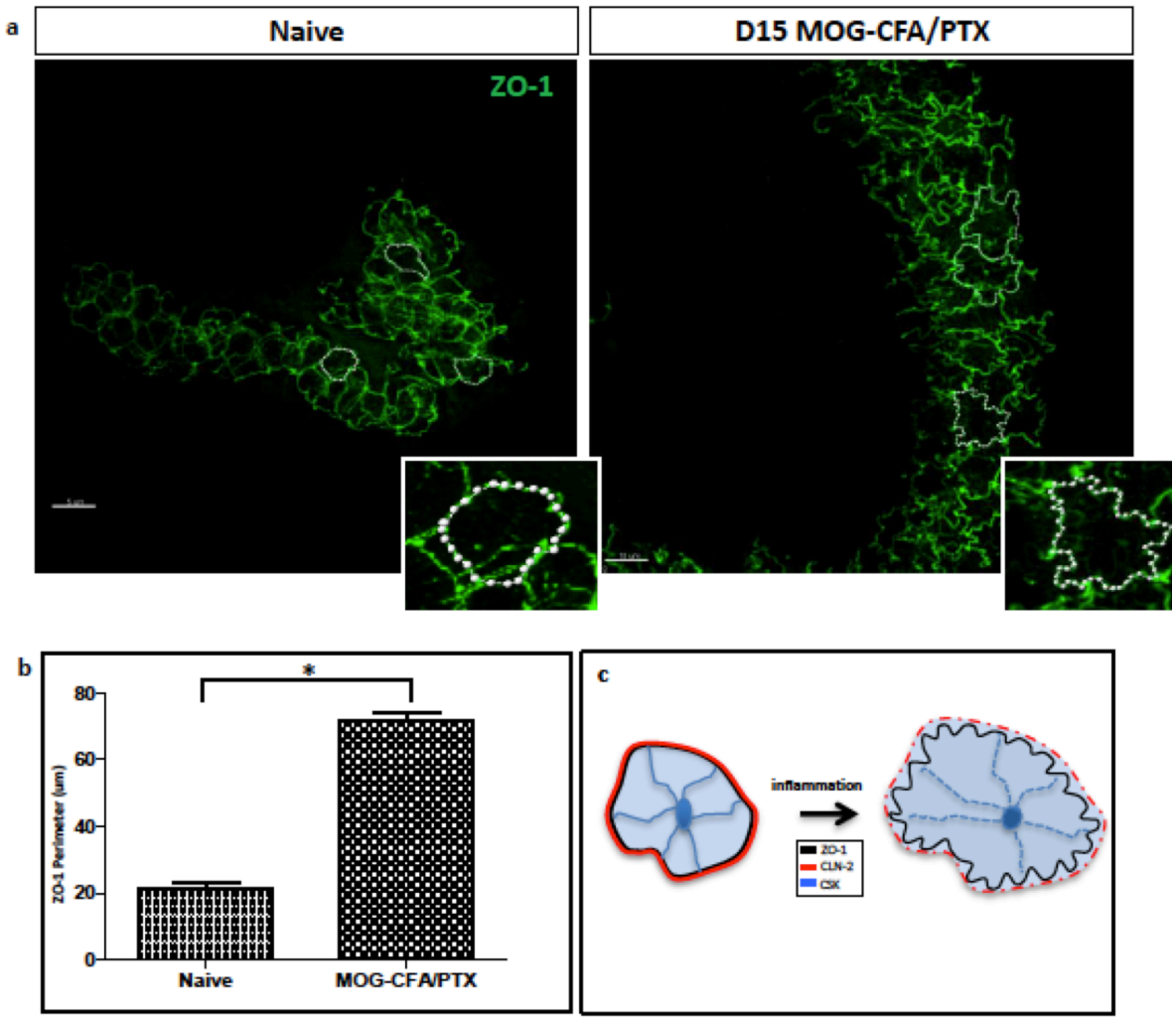

Supplemental Fig. 2 Measurement of the perimeter of ZO-1 staining in choroidal epithelial cells. (a) Representative sections of the CP from naïve and MOG-CFA/PTX-treated mice at D15. Scale bars represent 5µm (naïve) and 10µm (MOG-CFA/PTX). Choroidal epithelial cells were immunostained for ZO-1 (green). Measurement points were placed along epithelial ZO-1 staining to recreate the ZO-1 staining boundary as described in Materials and Methods. The sum of the all the distances between adjacent points provided an estimate of the perimeter of ZO-1 staining. (b) A significant increase in ZO-1 perimeter was found between naïve and MOG-CFA/PTX-treated (EAE) mice, consistent with cellular enlargement, *$p<0.001$. (c) Schematic showing effects of inflammation on choroidal epithelial cell TJ proteins, ZO-1 and CLN-2, in association with disruption of the cytoskeleton (CSK). An increase in epithelial cell size is concomitant with visible distortion of ZO-1, and fragmentation of CLN-2, immunostaining patterns.

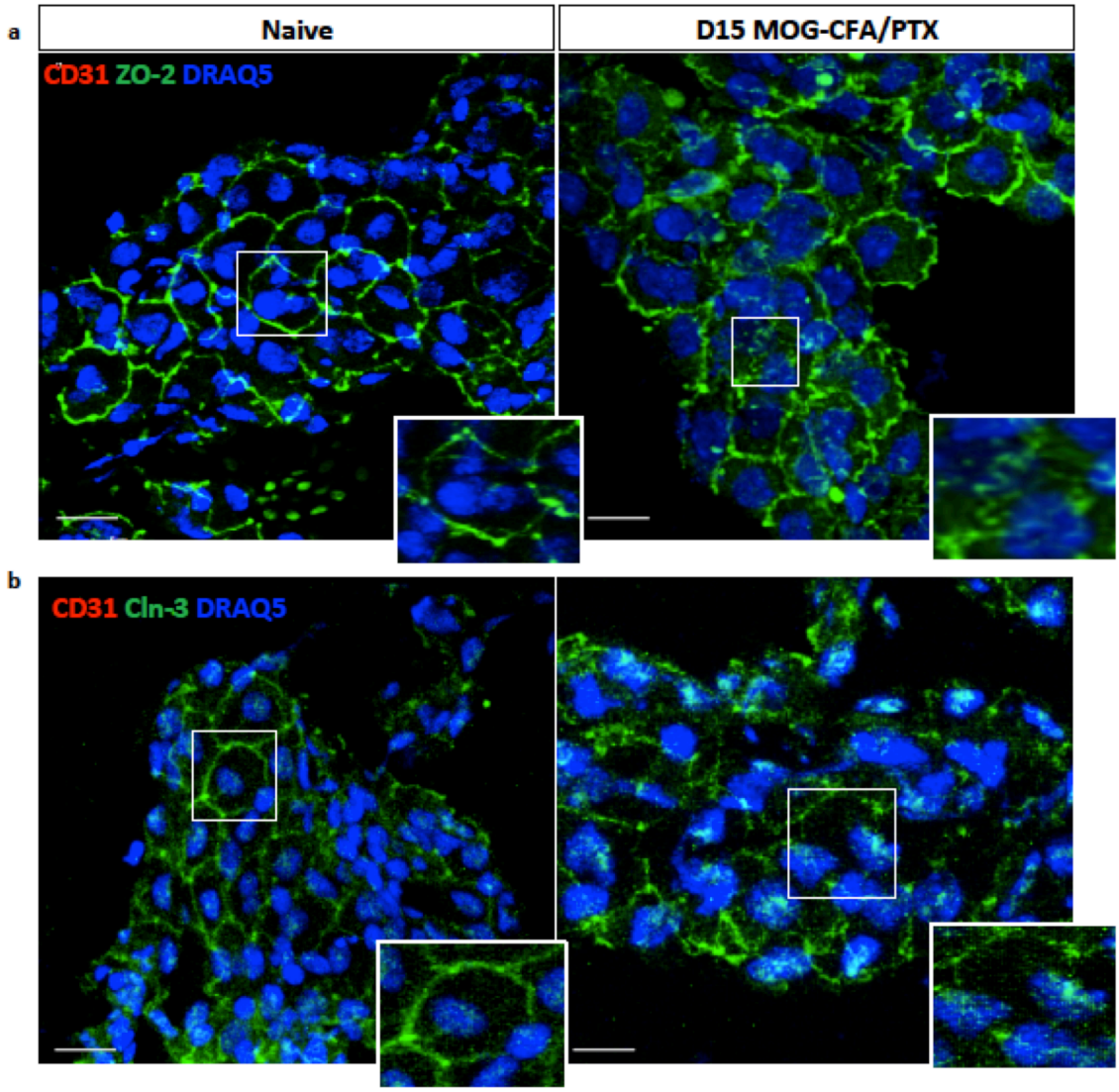

Supplemental Figure 3. ZO-2 and CLN-3 distribution in the choroid plexus during evolving EAE. (a) Representative sections of the CP from naïve and MOG-CFA/PTX-treated mice at D15. Choroidal epithelial cells were immunostained for ZO-1 (green) and epithelial nuclei were stained with DRAQ5 (blue). Insets highlight the smooth TJ staining in naïve CP, which begins to rearrange into a crenulated pattern by D15. (b) Choroidal epithelial cells were immunostained for CLN-3 (green) and epithelial nuclei were stained with DRAQ5 (blue). Insets highlight the smooth TJ staining in naïve CP, which drastically decreases by D15.

Chapter III: Spinal cord in evolving EAE

Spatiotemporal resolution of spinal meningeal and parenchymal inflammation during experimental autoimmune encephalomyelitis

1. Abstract

Experimental Autoimmune Encephalomyelitis (EAE), animal model suggestive of neuroinflammatory events similar to that of Multiple Sclerosis, has a very typical course of disease. The inflammation is known to predominantly localize to the spinal cord with disease pathology known to begin from the caudal most end of the cord, as indicated by the clinical exacerbations following EAE induction in C57BL6 mice. EAE induced mice regress from showing no clinical signs to partial limp tail followed by a paralyzed tail. The paralysis gradually moves towards the hind limbs, followed by the forelimbs and finally to a moribund state at the peak of the disease. However, how the patterns of inflammation propagate within and along the length of the cord is relatively unknown. Lesser known still is the extent and pattern of meningeal inflammation within the cord, which reportedly has been associated with the pathology within the spinal cord parenchyma including axonal loss and increasingly recognized co-relation to the clinical evolution of the disease. This report provides a detailed immunohistochemical analysis of the patterns of inflammation including the waves of immune cells along the cord throughout the course of the disease. Results indicate that meningeal inflammation precedes parenchymal inflammation at all levels of the spinal cord, but does not develop equally or simultaneously throughout the SAS, beginning at the caudal end and working its way to the rostral extreme of the spinal cord. These differences in inflammation patterns within the sections of the spinal cord was further illustrated by immune-LCM assisted selective capture and immune gene profiling of the meningeal and parenchymal vessels within the cervical

and lumbar sections of the spinal cord. Each of these segments, meningeal and parenchymal vessels within the cervical and lumbar regions showed a varied pattern in expression of significantly regulated immune genes along the course disease progression.

2. Introduction

As mentioned in earlier chapter II, multiple sclerosis (MS) and its surrogate animal model, experimental autoimmune encephalomyelitis (EAE), are widely considered chronic, immune-mediated, demyelinating diseases of the central nervous system CNS, with CD4+ T cells most commonly accused of being the major suspects (1-5, 91, 92). Dysfunction of the blood-brain barrier (BBB) - the specialized microvascular endothelium that normally restricts passage of soluble and cellular elements between the CNS and circulation, and accompanying leukocyte infiltration of the CNS parenchyma are noted hallmarks of both diseases (6, 7, 93). Such leukocyte infiltrates in the CNS have long begged the question: How do the earliest myelin-reactive T cells initially breach the formidable BBB of the uninflamed brain?

The "two-wave" model of neuroinflammation offers some possibilities (8, 9), highlighting a previously unappreciated role for the choroid plexus (CP). A specialized out-pocketing of the roofs of the third, fourth, and lateral ventricles, the CP is comprised of two distinct tissue layers: a highly vascularized core of "leaky" fenestrated capillaries with resident perivascular macrophages and dendritic cells entwined in a stromal matrix, encapsulated by a "tight" layer of epithelial cells (94, 95). Because of this arrangement of apparently permeable capillaries closely opposed to a relatively impermeable epithelium, CP is the designated part of the blood-cerebrospinal fluid barrier (BCSFB)(23, 68). The CP has further long been recognized as the major site of production of cerebrospinal fluid (CSF), within which it hangs suspended(19, 35). However, more recent studies have also identified this structure as the locale where pioneer

T cells first gain a foothold in CNS territory (22, 27, 96). It is thought that following extravasation across the CP capillaries and choroidal epithelium into the CSF, T cells are gathered up by bulk CSF flow, and exit the fourth ventricle via the lateral foramina of Lushka and medial foramen of Megendie. They then travel within the CSF stream to the subarachnoid space (SAS) between the arachnoid and pial meningeal membranes covering the brain and spinal cord. Once in the SAS, T cells can forge immune synapses with resident dendritic cells as part of normal immune surveillance, thus concluding the "first wave" of neuroinflammation. The flare of cytokines resulting from these T cell: dendritic cell interactions, in turn, activates endothelial surfaces of nearby microvessels within the SAS, fostering adhesion and extravasation of leukocytes circulating in the bloodstream. Subsequent interactions between these invading leukocytes and other dendritic cells in the SAS and Virchow-Robbins space (with which the SAS is continuous) are thought to follow, ultimately propagating a "second wave" of non-specific leukocyte infiltration along the surface-penetrating microvessels that enter the CNS parenchyma. In this manner, the two-wave model consists of a neuroinflammatory "impulse" that originates in the SAS (first wave) and then is transmitted to the parenchyma (second wave).

While the animal model EAE has provided vast opportunity to gauge the significant role of meningeal inflammation in MS and other neuroinflammatory conditions (97), it obliges still other questions. Why does conventional EAE result primarily in spinal cord inflammation with a trajectory of ascending paralysis(5, 98-100)? Does the most caudal region of the spinal cord parenchyma display the first signs of inflammation? If so, is this because meningeal inflammation begins first at the caudal region as well? Or, might it be that meningeal inflammation is equally florid throughout the spinal cord from disease onset, but the

neuroinflammatory impulse is first conducted to the caudal parenchyma from which it then spreads rostrally?

To address these questions, studies were carried out to document when and where the first signs of inflammation appear in both the meninges and parenchyma along the entire spinal axis. Specifically, high-resolution 3-dimensional (3-D) confocal microscopy was performed to visualize, in detail, the development of leukocyte infiltration at distinct regions of the spinal cord. In addition, holistic examination of the entire spinal cord by "virtual slides" was also conducted using fluorescence microscopy to reveal the direction and relative magnitude of the propagation of inflammatory intensity along the length of the same spinal cord. To further determine whether a difference in inflammatory gene expression by meningeal and parenchymal microvessels along the spinal axis reflects the course of ascending paralysis in EAE, laser capture microdissection (LCM) coupled with gene expression profiling was performed.

Results indicate that meningeal inflammation precedes parenchymal inflammation at all levels of the spinal cord, but does not develop equally or simultaneously throughout the SAS. Instead, meningeal inflammation is initially most obvious in the caudal SAS, from which it then proceeds to the directly underlying parenchyma, paralleling the first signs of clinical disease in the tail and hind limbs. Meningeal inflammation then extends in the caudal-to-rostral direction, followed by a similar, but delayed, trajectory of parenchymal inflammation. LCM further allowed selective profiling of immune genes within the meningeal and parenchymal vessels of the different regions of the spinal cord in its extremes: cervical and lumbar spinal cord.

3. Materials and methods

3.1 Animals

Female C57BL/6 mice, age 8–10 weeks were obtained from Charles River Laboratories, Inc.

(Wilmington, MA). A total of n = 3 animals/group were used for each treatment and time-point assessed. All animal experimental procedures were performed following Animal Care and Use Guidelines of the University of Connecticut Health Center (Animal Welfare Assurance # A3471-01), and approved under protocol # 100937-0917.

3.2 EAE induction

EAE was induced in mice by active immunization with MOG_{35-55} peptide (MEVGWYRSPFSRVVHLYRNGK), of murine origin (W. M. Keck Biotechnology Resource Center, Yale University), as described [21], following Animal Care and Use Guidelines of the University of Connecticut Health Center (Animal Welfare Assurance # A3471-01). Briefly, on day 0 (D0), mice were injected subcutaneously with 300 μg of MOG peptide in complete Freund's adjuvant (DIFCO, BD , Sparks MD) into the right and left flank, 100 μl per site. On D0 and D2 mice were also injected intraperitoneally (i.p.) with 500 ng pertussis toxin (List Laboratories, Campbell CA) in PBS. Another group of age-matched mice was left untreated (referred to as "naïve" mice), and represented "normal" tissue. Mice typically showed development of acute clinical symptoms at ~ D12, followed by ascending paralysis and chronic disease (44). Animals were killed at D0 (naïve), D9 and D15 post-injection. Animals were monitored daily for clinical disease severity and scored as follows: 0 = normal; 1 = tail limpness; 2 = limp tail and weakness of hind legs; 3 = limp tail and complete paralysis of hind legs; 4 = limp tail, complete hind leg and partial front leg paralysis. The time-points selected for both histological and gene expression a

3.3 Tissue preparation and sectioning for 3D imaging

Mice were anesthetized by i.p. injection of Ketamine (80 mg/kg) and Xylazine (10mg/kg) in PBS. Animals were then transcardially perfused first with Heparin-PBS (10 usp/ml) to

eliminate vascular blood content, and then with fixation buffer (2% paraformaldehyde in 0.1 M phosphate buffer) as described previously [20]. Spinal columns were harvested and the vertebrae removed via laminectomy (41). Spinal cords were then embedded in OCT cryomatrix compound (Thermo Fisher Scientific, Waltham, MA) for cryosectioning. Cryosections of 60μm thickness were obtained using a Microm HM 505M cryostat (Mikron Instruments; Oakland, NJ) maintained at -25°C, and deposited onto poly-L-lysine-coated slides for 3D confocal imaging.

3.4 Tissue preparation and sectioning whole spinal cord scan imaging

Spinal cords were harvested after identical perfusion fixation to that used for 3D imaging, except that laminectomy was not performed. Instead, whole spinal cord with intact vertebrae were embedded in OCT cryomatrix compound prior to sectioning. It was important to maintain the vertebrae to preserve the integrity of the meninges lying underneath. Due to the brittleness of the vertebrae, individual 7 μm-thick sections were captured on to an adhesive tape (Cryofilm type IIC, Section-Lab, Japan) and rolled for a smooth, intact cut. Adhesive tape strips were then glued (sections facing up) onto glass sides using an optical adhesive (Norland products, Cranbury, NJ) under UV light for 10 min. The glass slides with the sections were then used for whole spinal cord scan imaging.

3.5 Immunostaining and Image acquisition for 3D analysis and whole image scan

Sections (both for 3D analysis and whole image scans) were permeabilized with 1% Triton X-100 in PBS for 30 min, and non-specific binding blocked by incubation with Power block® for 10 min in Ultrapure (GIBCO) distilled water (41). The spinal cord vessels were stained with rat anti-mouse CD31 antibody (BD Pharmingen) at 1:160 dilution, followed by incubation with

goat anti-rat Alexa Fluor® 555 antibody (Life Technologies) at 1:250 dilution. Epithelial cells were stained with monoclonal pan-cytokeratin-FITC antibody (Sigma) at 1:160 dilution. DRAQ5 (Biostatus Ltd., Leicestershire, UK) was used to stain nuclei at 1:1000 dilution. Alexa Fluor® 647 anti-mouse CD45 (Biolegend) at 1:160 dilution was used to stain leukocytes. Sections were mounted in Mowiol (Sigma-Aldrich). Confocal z-stacks (multi-track scan) were acquired using a Zeiss LSM 510 Meta equipped with a Zeiss Fluar 40X/1.30, 63X Plan-neofluar/1.25 and 100X Plan-apochromatic/1.4 oil immersion objective lens. Thereafter, z-stacks were imported into Bitplane Imaris® suite version 7.1 x64 software (Bitplane Inc., South Windsor, CT), as described previously (41). Whole scan spinal cord images were acquired using a Zeiss Axioscan.Z1 at 10X and images imported into Ziess microscope software Zen (Thornwood, NY, USA) for analysis.

3.6 Tissue preparation and immunostaining for LCM

Immunohistochemistry-guided LCM was performed as recently detailed (42, 96). Naïve animals were euthanized by CO_2 inhalation. Spinal cords were immediately removed, cleaned off of extra tissue and dissected into cervical (C1-C8) and lumbar (L1-L5) sections with the vertebrae intact. The spinal cord segments were then snap-frozen in dry ice-cooled 2-methylbutane (Acros; Geel, Belgium), and embedded in cryomatrix compound (Thermo Fisher Scientific, Waltham, MA) for cryosectioning. Longitudinal sections (7μm) were cut on a Microm HM 505 M cryostat (Mikron Instruments; Oakland, NJ) and affixed to uncoated, pre-cleaned glass slides (Fisher Scientific, Pittsburgh, PA). The spinal cord vessels were stained using a substrate combination, nitro-blue tetrazolium chloride/5-bromo-4-chloro-3'-indolyphosphate p-toluidine salt (Vector Labs, Burlingame, CA), to detect the endogenous alkaline phosphatase activity in endothelial cells.

3.7 Laser Capture Microdissection (LCM) and cDNA synthesis

A PixCell IIe laser capture microscope (Life Technologies, Foster City, CA) was used to retrieve the meningeal and parenchymal vessels. Obtained LCM tissue was solubilized in Cell Lysate Buffer (Signosis; Sunnyvale, CA). Cell Lysate Buffer® extracts were treated with Turbo DNase and inactivation reagent (Ambion; Austin, TX) according to the manufacturer's instructions. Samples were then reverse transcribed using the SuperScript III (Invitrogen) standard protocol with random hexamers (Roche; Indianapolis, IN).

3.8 Pre-amplication of cDNA and qRT-PCR

Pre-amplification was carried out for array analysis out using TaqMan® PreAmp Master Mix and a PreAmp Pool containing all the primers for detection by the Mouse Immune Panel TaqMan® Low density Array (TLDA; Life Technologies Corp., Foster City, CA) as previously described (42). This panel contains 93 immune-related genes plus three housekeeping control genes. Pre-amplification was carried out with an initial hold at 95°C for 10 min, followed by 14 cycles at 95°C for 15 sec and 60°C for 4 min. Relative cDNA levels were quantified by qRT-PCR using an an ABI 7900HT Fast Real-Time PCR System (Life Technologies Corp, and normalized to housekeeping gene GAPDH as described previously (34). Expression of genes relative to GAPDH was then represented as percent expression of GAPDH. Custom TaqMan^{W} primers/probes were used for the Mouse Immune Panel TLDA.

3.9 Statistical Analysis

All statistical analyses were performed using GraphPad Prism 5 (GraphPad, La Jolla, CA). For all sets of comparisons (meningeal vs parenchymal vessels in cervical and lumbar regions, and

cervical vs lumbar regions within meniges and parenchyma) individual genes from the two sets being compared were first subjected to Shapiro-Wilk normality test. Genes that passes the normality test were then compared for significance using paired, 2-tailed T-test, or Mann-Whitney U test was used for genes that did not pass the normality test. Results were considered significant at $P \leq 0.05$.

4. Results

4.1 Regional sections of spinal cord show varying levels of leukocyte infiltration during EAE

Fig. 9a highlights the extent of leukocytes in the respective meningeal and parenchymal compartments of the spinal cord during EAE, as revealed by CD45 staining, is dependent on time and segmental level. At D6, several days before clinical disease is typically manifest, CD45 staining is barely detectable in the meninges of the cervical spinal cord, and undetectable within the parenchyma at this time. Similarly, meningeal and parenchymal leukocyte infiltration of the lumbar spinal cord is sparse as well. Just prior to commencement of clinical disease at D9, the cervical spinal cord reveals limited leukocyte infiltration of the meninges but as yet no readily discernible leukocytes in the parenchyma. The lumbar spinal cord also demonstrates scant leukocytes in both the meninges and parenchyma at this time. By day 15, during the acute phase of clinical EAE disease, the cervical spinal cord displays extensive meningeal leukocytes, while the underlying parenchyma just shows signs of incipient leukocyte infiltration. Meningeal leukocyte infiltration within the lumbar cord is even more florid at this time, and appearance of leukocytes in the parenchyma, while apparently less than that of the overlying meninges, is still vast and far more pervasive than that seen at the cervical level. Fig. 9b confirms the differential extent of leukocyte infiltration in the meningeal and parenchymal compartments at the cervical

and lumbar levels of the spinal cord at D15. Nuclear staining shows there is much denser perivascular cellularity in the lumbar versus cervical meninges, as well as in the lumbar parenchyma compared to the cervical parenchyma. Additionally, perivascular cellularity is greater in the meninges versus the parenchyma at both levels of the spinal cord. The differential cellularity within the respective meningeal and parenchymal compartments at the cervical and lumbar levels of the spinal cord during the progression of EAE is depicted in Suppl. Fig. 4.

4.2 Whole spinal cord image scans reveal an ascending wave of leukocyte infiltration

To acquire better appreciation of the segmental distribution of leukocytes along a single spinal cord at different time-points of EAE, whole spinal cords with intact vertebrae and preserved underlying meninges were analyzed. Fig. 10 shows the immunostaining patterns of several marker proteins in the spinal cord of a naïve mouse, as a reference. Notably, CD45 staining is restricted to the vertebral column, most likely representing leukocytes of the spinal marrow (Kenyon et al., 1997). Absent from the naïve cord is any clear leukocyte infiltration of the spinal meninges or parenchyma. The method of sectioning and attachment of a longitudinal section of whole spinal cord to adhesive film is depicted in Suppl. Fig. 5. Leukocyte distribution patterns along the entirety of spinal cords from animals at the acute (D15) and chronic (D23) stages of EAE are seen in Fig. 11a. At D15, CD45 staining is apparent in the lateral meninges of the lumbar and thoracic levels of the cord, and in the dorso-medial sulcus where the penetrating meninges bisect the spinal parenchyma into the dorsal white matter columns and grey matter horns. Some CD45 staining of the lumbar parenchyma is also seen at this time. By D23, a wave of CD45 staining appears to proceed up the cord and is concentrated at the thoracic level in and around the dorso-medial sulcus. This wave appears more obvious in the intensity charts shown in

Fig. 11b. In the spinal cord of a naïve mouse CD45 staining is confined to the vertebral column – likely reflecting hematopoietic activity of spinal bone marrow (Shah and Hanrahan, 2011) – with no discernible signs of leukocyte infiltration into spinal tissue. At D15 EAE, leukocyte infiltration is overt in the meninges (including the dorso-medial sulcus) of the lumbar region with comparatively sparse CD45 staining seen in the upper levels of the cord. By D23, intensity of CD45 staining of the lateral meninges of the lumbar region is even more florid and manifest diffusely in the parenchyma as well. Severely heightened staining in the dorso-medial sulcus at the thoracic level is also observed at this later stage. The clear distinction in degree of cellularity in the spinal meninges versus parenchyma, and between cervical and lumbar levels, is seen at higher magnification in Fig. 12, along with what appears to be meningeal leukocyte clusters at D15. Fig. 13 shows the disparity in regional parenchymal cellularity becomes even more pronounced by D23, as the most caudal spinal cord becomes suffused with nuclear and CD45 staining, while increased cellularity in the meninges has progressed to the cervical level.

4.3 Varying patterns in immune profiling of meningeal and parenchymal vessels of the cervical and lumbar spinal cord.

Further analysis of differences between the cervical and lumbar regions of the spinal cord within the meningeal and parenchymal vessels was done using LCM. Site-specific isolation of these vessels coupled with TLDA arrays allowed probing of immune genes including adhesion molecules, cytokines, chemokines, statins, interleukins, T cell activation markers, co-stimulatory molecules, transcription factors and apoptotic markers. As the disease progressed from a naïve state to clinical acute EAE at D15, varying patterns of immune gene expressions was seen. Pro-inflammatory gene expression in the naïve spinal cord was very minimal and not significantly

different in between either the meningeal and parenchymal sections or cervical and lumbar regions of the spinal cord. Fig. 14 highlights the genes that were significantly different in these regions in D9 of evolving EAE. Comparisons were made between two distinct sets. 1. Meningeal versus parenchymal vessels separately within first, the cervical region followed by the lumbar region (Fig. 14a-b): Fig 14a depicts cervical region has significant differences in expression of Ptgs2, CCR2, STAT1, VEGFa, Col4a5, Cd68 and Ski 2 between the meningeal and parenchymal vessels. In Fig 14b lumbar region shows significant differences in Ski, STAT1. VEGFa, STAT3, Socs2, Ece1, Edn1, Bax between the meningeal and parenchymal vessels. 2. Cervical versus lumbar regions separately within the meninges and then the parenchyma (Fig. 14c-d): Fig 14c highlights significant differences between the meninges of cervical and lumbar regions observed for Socs2, Ski, CCR2, IL18, STAT1, VEGFa, Bax, CD8a, Csf1, H2-Ea. Fig 14d shows that cervical and lumbar regions have significant differences in CD28, Cxcr3, CD3e, Bcl2, Il2ra, CCR2 and Col4a5. Similarly, the same set of comparisons was carried out for D15 EAE spinal cord in Fig. 15(a-d). Fig. 15a shows the differences between meningeal and parenchymal vessels in the cervical region in CD38, CD86, Socs2, TGFβ1, STAT1, CD68, Il18 and Gzmb while lumbar region shows differences in VEGFa, VCAM1, Csf1, Ikbkb, Ski, Stat3, CCL2, Edn1 and CCR2 as depicted in Fig 15b. As shown in Fig 15c, meninges between the cervical and lumbar regions differed significantly in expression of Socs2, CD80, Stat1 and CD38 while meninges in the parenchyma showed significant differences in NOS2, Nfkb2,Tgfb1, Smad3, VCAM1, Ptprc, STAT3, Col4a5 and Cxcl1 as shown in Fig. 15d.

5. Discussion

Results from this study reinforce and advance awareness that the meninges are sites of significant immune activity and feature prominently in the development of neuroinflammation in MS (101) and its animal model, EAE(10, 13, 102, 103). Specifically, our findings provide new histological evidence of a progressive, spinal meningeal inflammation that proceeds in the caudal-to-rostral direction during development of EAE. A similar trajectory of parenchymal inflammation was also observed, but delayed compared to that of the meninges at all levels of the spinal cord. This scenario is consistent with inflammation being propagated from meninges to parenchyma (8, 9). The possibility remains, however, that once parenchymal inflammation takes hold in the caudal spinal cord, it can then spread rostrally through both parenchymal and meningeal channels.

Whole spinal cord intensity scans most clearly exposed what appears to be an ascending pulsatile wave of leukocyte infiltration in both the meningeal and parenchymal compartments of the spinal cord during EAE progression. While particular sensitivity of the lumbar (L5) region of the spinal cord to autoimmune inflammation has been resolved by ultrahigh-field MRI (104) and reported to be mediated by regional neural stimulation (105, 106), this is the first report we are aware of that documents preferred sites of meningeal involvement during evolving EAE. Moreover, whole spinal cord intensity charts reflect a conspicuous ascending wave of leukocyte infiltration in the meninges, which precedes an underlying parenchymal infiltration that advances in the same direction during EAE progression. The order of these similar, advancing patterns of meningeal inflammation and parenchymal inflammation is consistent with the interpretation that the former helps drive the latter.

Immune gene profiling of selectively isolated meningeal and parenchymal vessels by immune LCM further correlated the differences in the inflammatory gene patterns between the sections of the spinal cord. The distinctly different set of genes expressed by the meningeal vessels in the lumbar versus the cervical region, depict the possible variations in immune regulation depending on the level of the spinal cord. As evidenced by the individual regional spinal cord and whole scan images, accumulation of CD45 positive cells were first visible within the meninges of the lumbar spinal cord by D15, and minimally present during D9. This could correlate with the majority of significantly different genes (Socs2, Ski, CCR2, IL18, Stat1, Vegfa, Bax and Csf1) highly expressed in the meninges of the lumbar region when compared to the cervical region during D9 (Fig 14c). Although immune cell accumulations are not very evident during D9, the differential expression could provide factors increasing the susceptibility of this region to be inflamed first at a later stage in D15. Comparisons also show that meningeal vessels have significantly higher expressed genes-Ski, Stat1, VEGFa, Stat3, Socs2 and Bax than parenchymal vessels at this time point. This could point toward genes such as VEGFa, STAT1 and Ski possibly aiding in the earliest inflammation first noted within the meninges of the lumbar spinal cord evidenced by clusters of CD45. Parenchymal vessel inflammation is minimal at this point as evidenced by the spinal cord images. Differential set of genes is significantly expressed during this time in the parenchymal vessels of the lumbar region versus cervical region and in comparison with the meningeal vessels of both within the cervical and lumbar regions. CCR2 seems to be highly expressed in the parenchymal vessels of the cervical region, more so that the meningeal expression.

Figures 9, 11 and 12 show the florid meningeal inflammation all along the cord including immune cell accumulations seen infiltrating into the sub-pial parenchyma within the lumbar

region. Immune profiling of D15 EAE meningeal and parenchymal vessels highlights gene differences that co-relate with this pattern of inflammation as shown in Fig. 15. Only a limited number of genes, minimally expressed (Socs2, CD80, Stat1, CD38) are significantly higher in the meninges of the lumbar regions compared to the cervical region. Whereas, the parenchyma demonstrates significant differences between the cervical and lumbar regions, with STAT3, Ptprc, Nos2, Nfkb2, Tgfb1 and Smad3 highly expressed in the lumbar region. Also to be noted, is the entirely different set of genes expressed by the parenchymal vessels within the cervical and lumbar regions that prove that each region is unique in its expression of immune genes. Interestingly, both CCL2 and CCR2 are significantly higher in the meningeal vessels of the lumbar region at D15, relating to the evidenced immuno-modulatory effects of CCL2 (44, 107, 108). These results point towards the possibility that each region of the spinal cord is unique in its immune gene expression pattern, which could be the result of its location and differential regulation.

Once the immune cells enter the SAS and are triggered to release inflammatory cytokines, by nature of the anatomy of meningeal vessels lying within the CSF filled SAS (109), inflammation within these vessels could be swift and rampant as reported by Kivisakk et al. by detection of meningeal T cell infiltration through out the CNS(11). Parenchymal vascular inflammation of the underlying white matter tracks that succeeds SAS inflammation however, could be subject to segmental vulnerability. Intimate and convoluted arrangement of meninges within the cauda equina (hair-like endings of the lumbar spinal cord) could uniquely allow inflammatory signals to be readily relayed from SAS meningeal vessels to parenchymal vessels in the lumbar segment. In support, reports by Arima et al. show that autoreactive T cells access the CNS parenchyma via the fifth lumbar spinal cord, this region being defined by an

upregulated CCL20, CCL2 and IL6 (105), important players in inflammation in EAE. Hence, the parenchymal vessels in the lumbar region compared to cervical region showed different immune profile with earlier signs of inflammation by up-regulating their immune profile. We noticed heightened immune response within the meningeal compared to parenchymal vessels during earlier stages (D9), followed by inflammation in the parenchymal vessels in the later stages (D15) beginning from the lumbar segment.

In summary, results obtained from imaging and further validated by immune profiling of meningeal and parenchymal vessels from cervical and lumbar regions give a sense of directed progression of immune cells accumulation and inflammation during evolving neuroinflammation summarized in a schematic (Fig. 18). The sequence of events in developing EAE begin with CD45 cells accumulating within the CP and crossing through the BCSFB into the CSF flowing within the SAS (96) typically around D6 to D9 with the clinical score ranges from 0-0.5. This is followed by the accumulation of infiltrating immune cells seen within the meninges, more distinct within the lumbar region due to these cells penetrating the pial membrane and accumulating within the parenchyma as well, typically evidenced around D15, where EAE induced animals display a clinical score ranging from 0.5-2. By D23, the animals display symptoms of peak disease with a score from 2-3 with increased accumulations of infiltrating immune cells seen within the cervical meninges and added infiltration into the underlying parenchyma. Results from this report highlight the role of meningeal inflammation in initiating the disease course leading to propagation of disease pathology. Reports have shown similar instances that support the idea that the meninges are a gateway for immune cell access into the CNS corresponding with clinical exacerbations in EAE (102). This brings into light the importance of therapies possibly targeted directly to the meninges that might prove more

effective with controlling disease progression. Drug delivered regionally within the meninges of a section of the spinal cord, would be able to modulate the disease and contain the inflammation before it propagates to other regions of the spinal cord. In addition, meningeal targeted therapies would allow drug delivery without the Blood Brain Barrier (BBB) permeability concerns or the need for a systemic immunosuppression as seen with the current FDA approved drugs for MS treatment, hence allowing for novel therapeutic interventions.

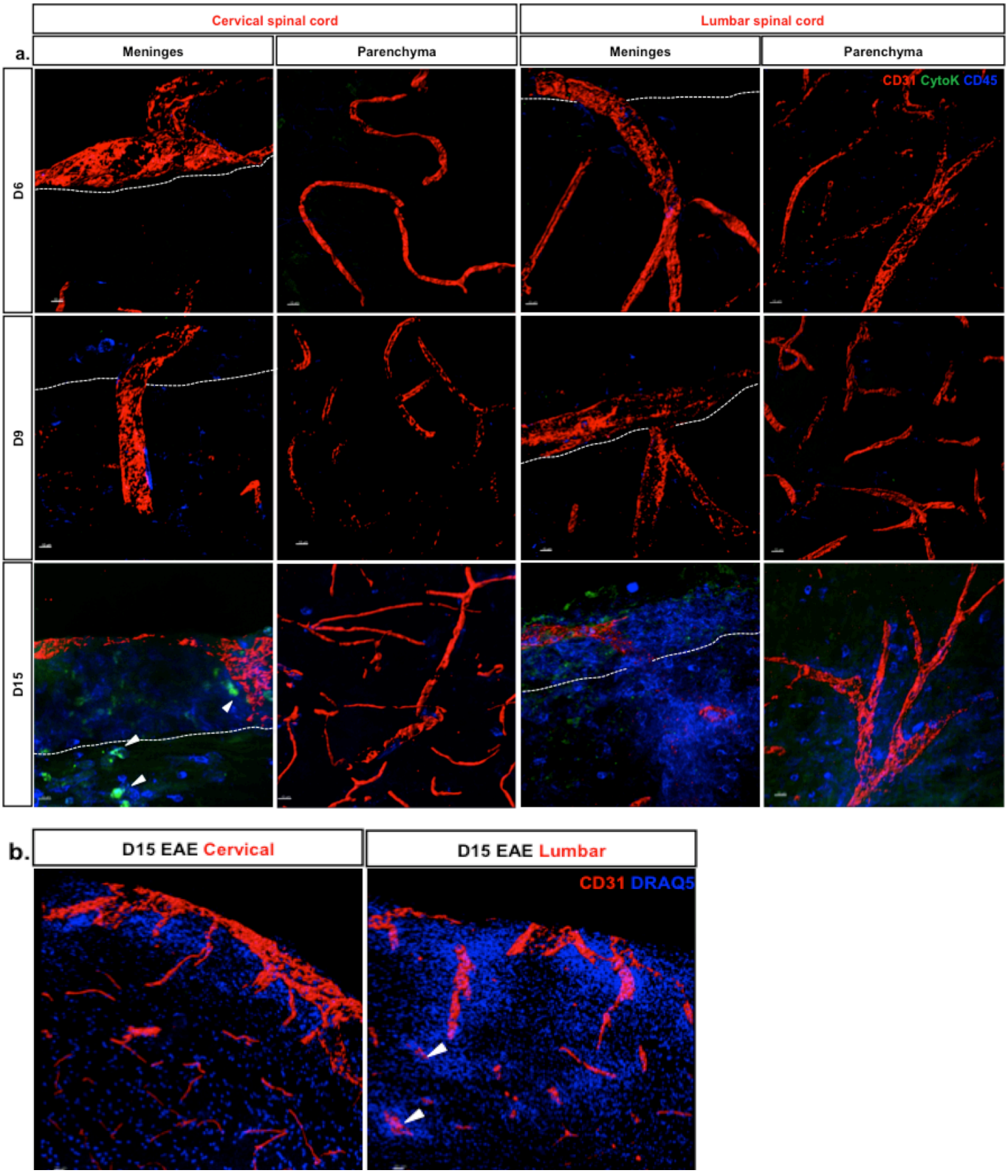

Figure 9: **Spinal cord regions (cervical and lumbar) showing leukocyte extravasation within the meninges and parenchyma during evolving experimental autoimmune encephalomyelitis (EAE). (a)** Representative sections of spinal cord regions were collected at days 6, 9, 15 (D6, D9, D15) from mice affter EAE induction. Vessels are immunostained for CD31 (red) and isosurface rendered to highlight the meningeal vessels penetrating into the parenchyma; leukocytes are immunostained for CD45 (blue) and CytoK (green) was used to immunostain for any cells of epithelial nature. White arrows in D15 cervical spinal cord meninges show the cytokeratin positive CD45 cells accumulated within the meninges and infiltrating into the parenchyma across the pial membrane. **(b)** Cervical and lumbar regions showing meningeal and parenchymal cellularity collected on D15 at 20x magnification with nuclei stained for DRAQ5 highlighting differences in cellularity between cervical and lumbar sections. White arrowheads show increase in cell accumulations around deeper parenchymal vessels.

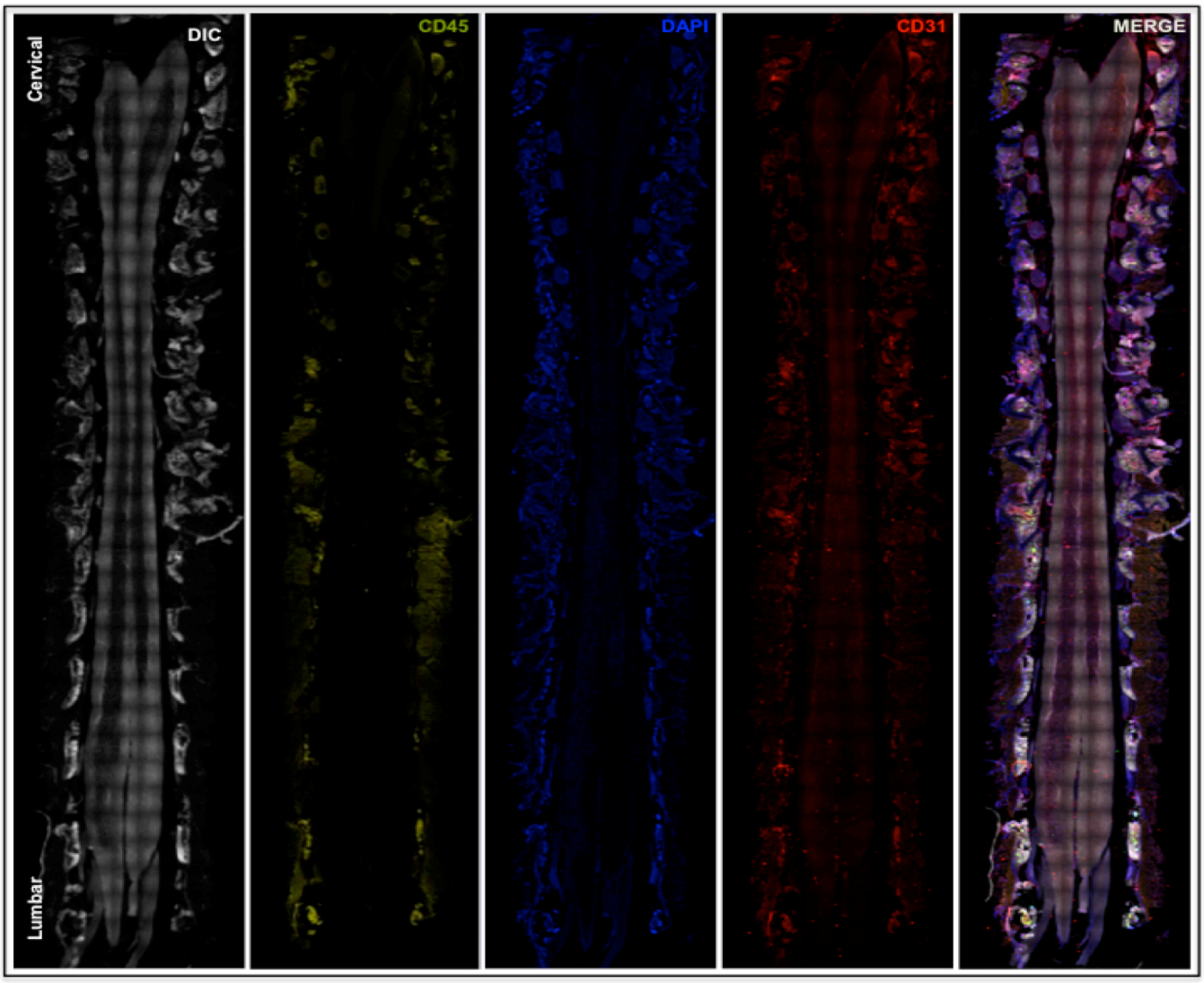

Figure 10: Whole spinal cord image scans in different channels. Representative sections of whole spinal cords collected on day 0 (Naïve) mice are shown. **DIC** shows the differential interphase contrast, **CytoK** was used to immunostain for epithelial cells, **CD45** for leukocytes**, DAPI** for cellularity, **CD31** for vessels and **Merge** for all the channels together. Same pattern of scans was carried for the timepoints in the study-D9,D15 and D23.

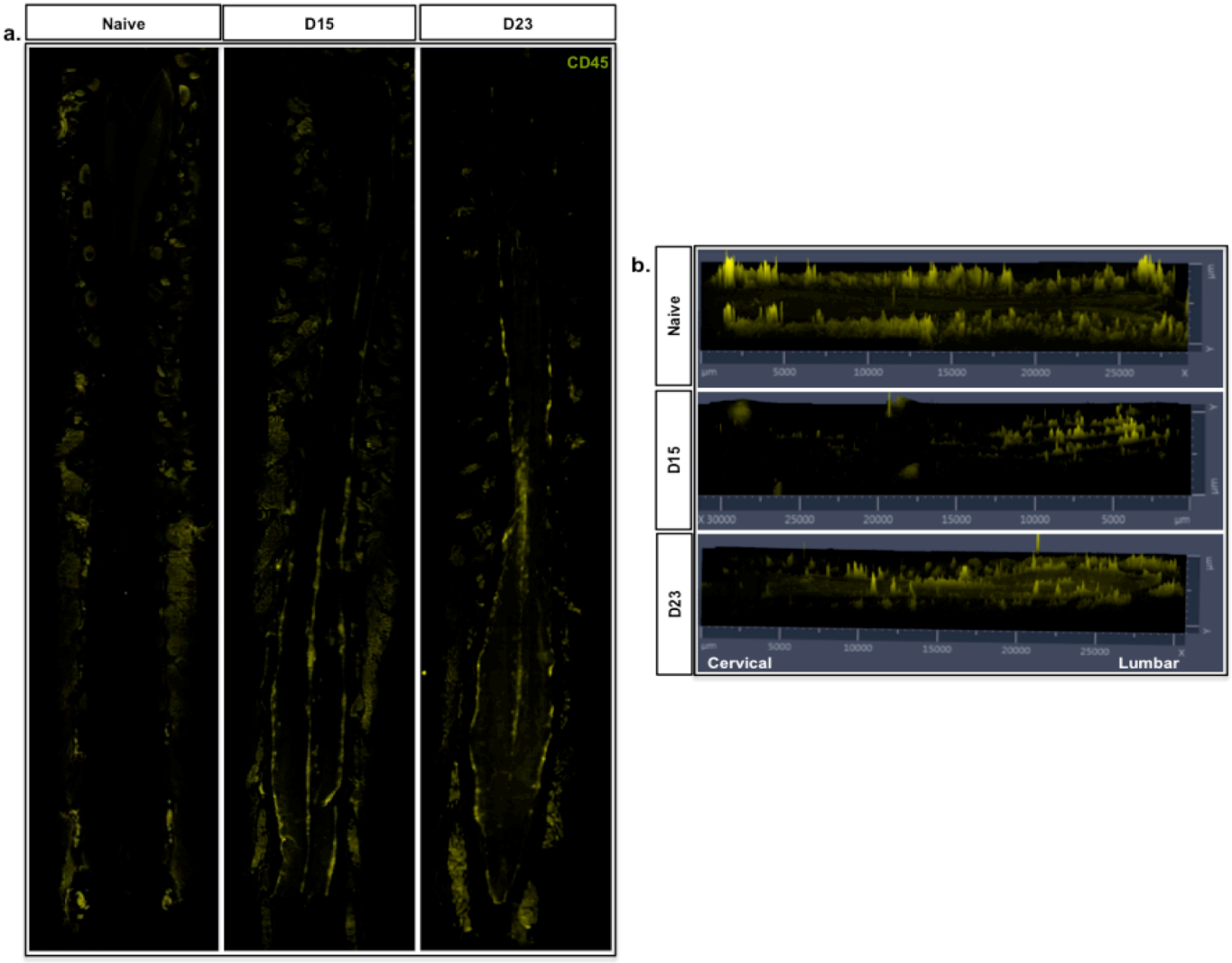

Figure 11: Changes in leukocyte distribution patterns within the meninges and parenchyma along the spinal cord during evolving experimental autoimmune encephalomyelitis (EAE). (a) Representative sections of whole spinal cords were collected on day 0 (Naïve) 15 and 23 (D15 and D23) from mice after EAE induction. Sections were immunostained for CD45 to highlight the distribution patterns during developing stages of disease. **(b)** Quantitative distribution of CD45 shown in intensity plots.

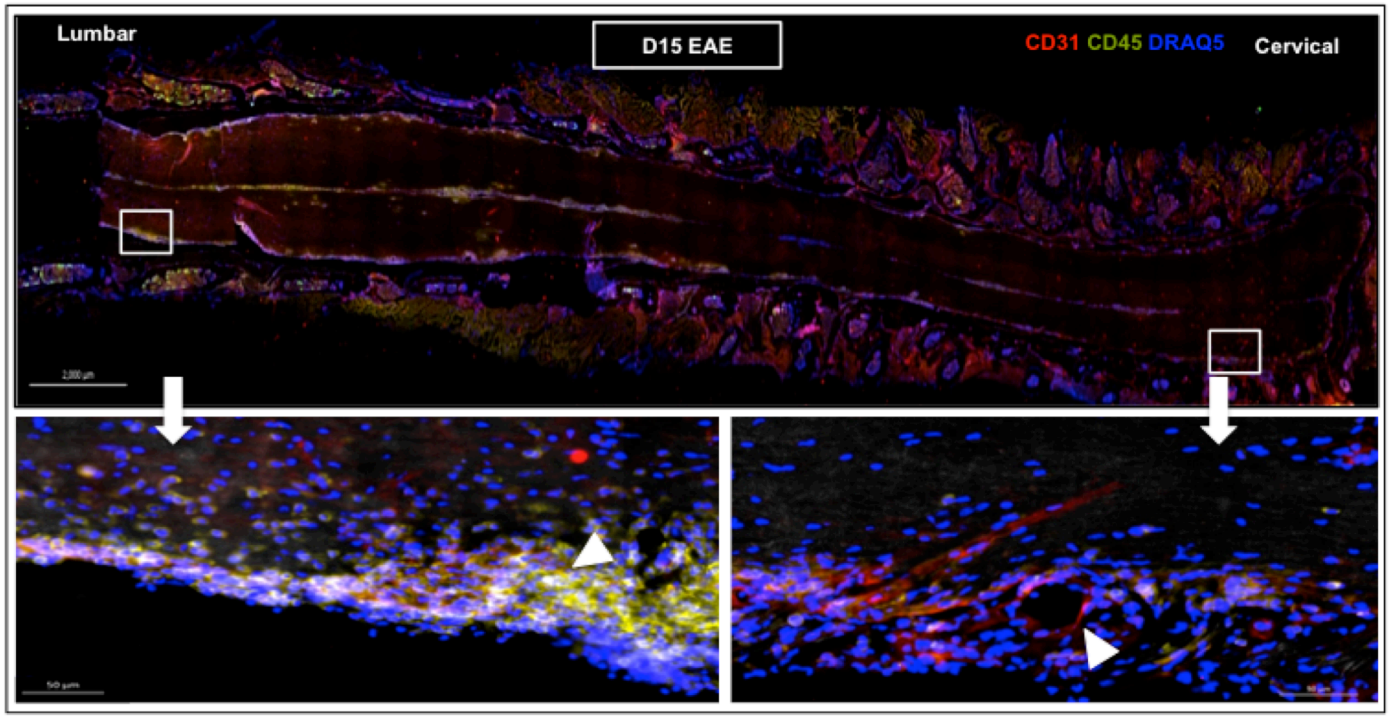

Figure 12: Whole spinal cord showing leukocyte extravasation within the meninges during D15 EAE. **(a)**Representative section of spinal cord collected on day 15 (D15) showing CD45 +ve leukocyte infiltration within the meninges along the entire spinal cord during evolving EAE. **(b)**and **(c)** Insets from the cervical and lumbar regions of the spinal cord showing CD45 cells within the meninges and parenchyma highlighted with brackets. White arrowhead in **(b)** showing a meningeal vessel and in **(c)** showing clusters of CD45 cells accumulating within the meninges of the lumbar spinal cord.

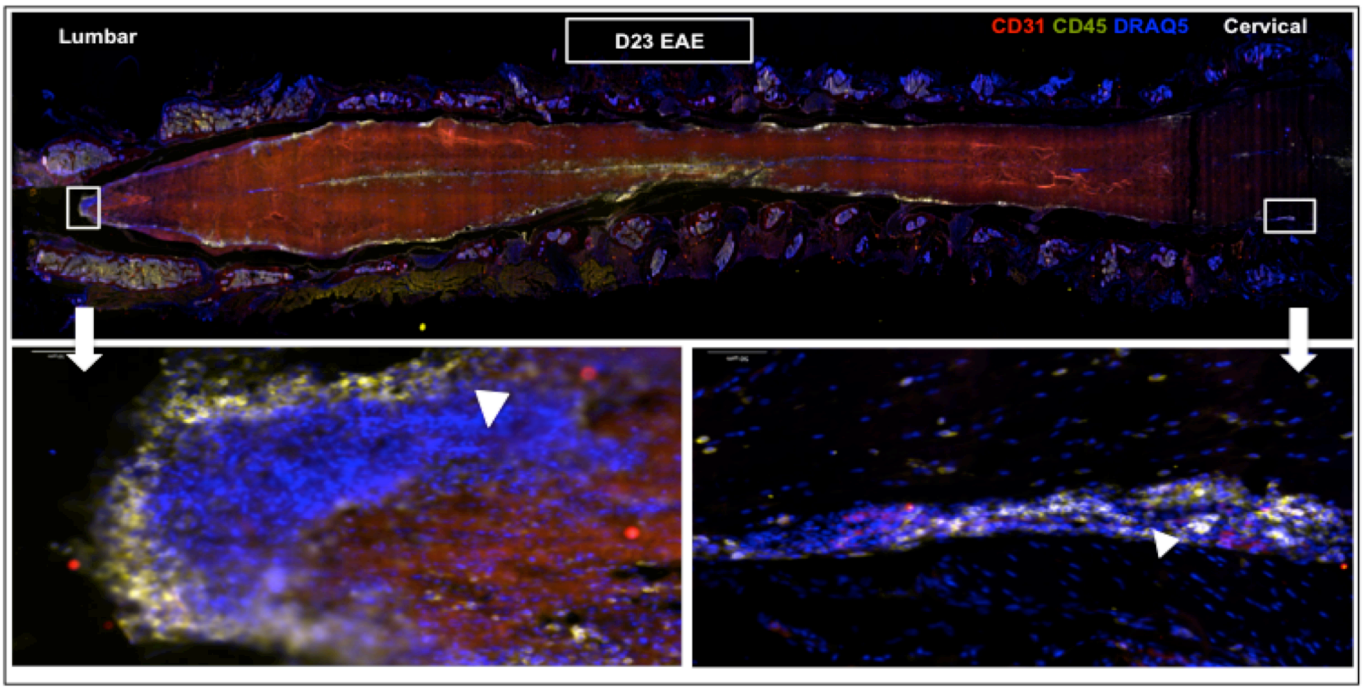

Figure 13: Whole spinal cord showing leukocyte extravasation within the meninges during D23 EAE. **(a)**Representative section of spinal cord collected on day 23 (D23) showing CD45 +ve leukocyte infiltration within the meninges and parenchyma along the entire spinal cord during evolving EAE. **(b)**and **(c)** Insets from the cervical and lumbar regions of the spinal cord showing CD45 cells within the meninges and parenchyma.

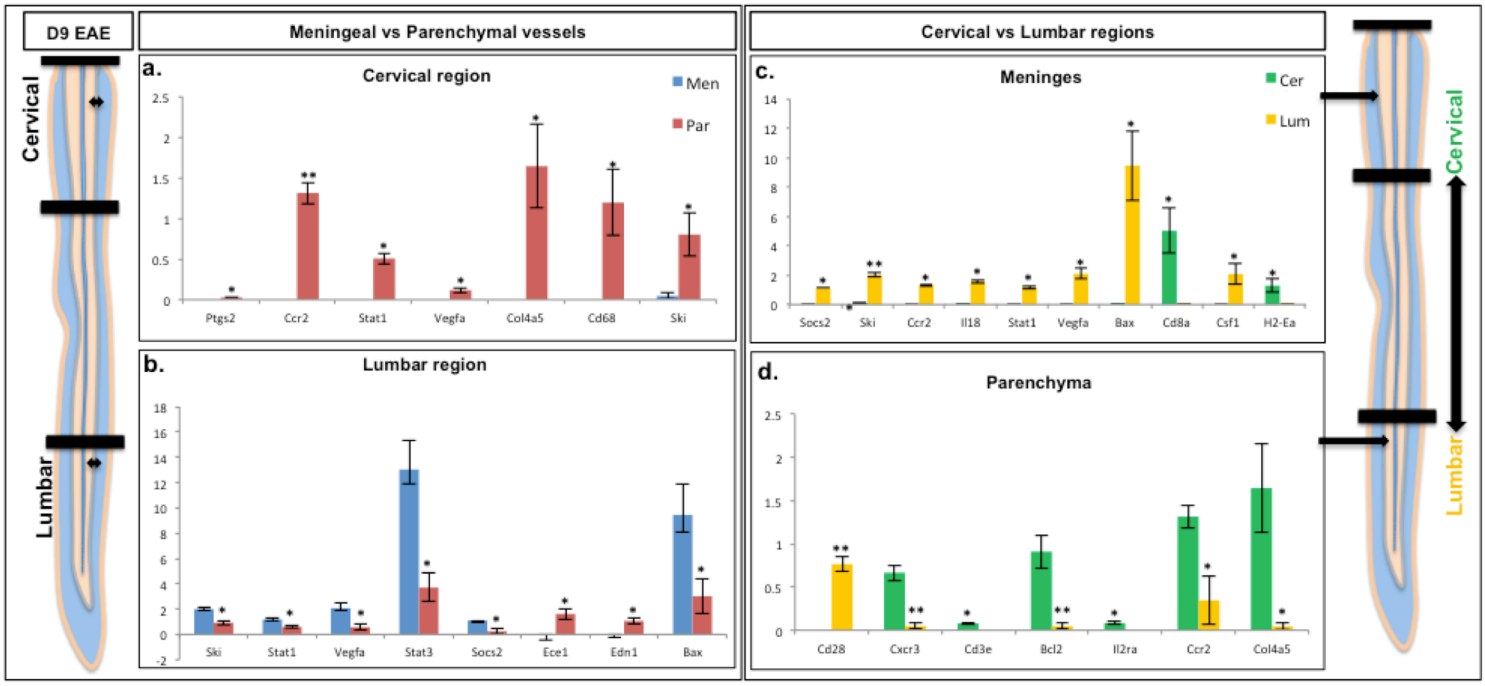

Figure 14: Differential expression of immune genes within spinal cord regions during D9 EAE. (a), (b) Comparison between meningeal and parenchymal vessels within the Cervical and Lumbar regions in their immune gene expression profile during D9 of evolving EAE. **(c), (d)** Comparison between Cervical and Lumbar regions within meningeal and parenchymal vessels in their immune gene expression profile.

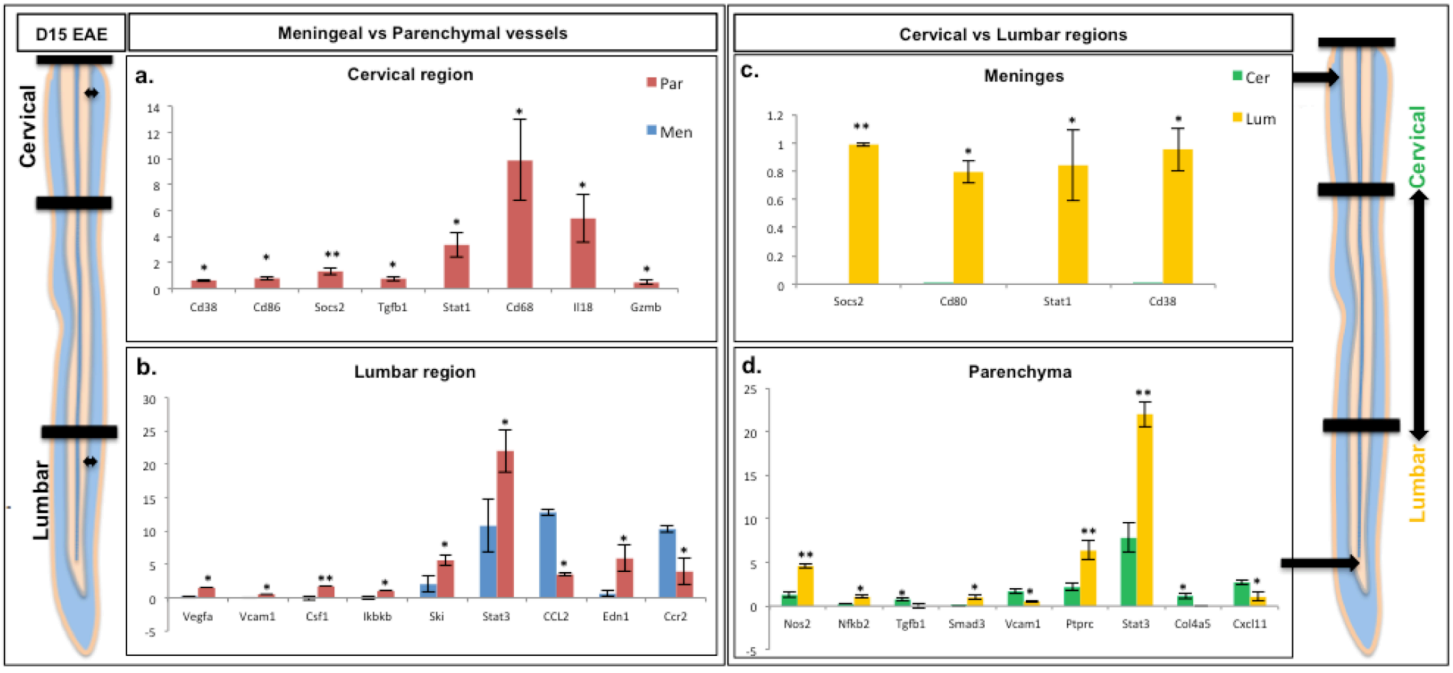

Figure 15: Differential expression of immune genes within spinal cord regions during D9 EAE. (a), (b) Comparison between meningeal and parenchymal vessels within the Cervical and Lumbar regions in their immune gene expression profile during D15 of evolving EAE. **(c), (d)** Comparison between Cervical and Lumbar regions within meningeal and parenchymal vessels in their immune gene expression profile.

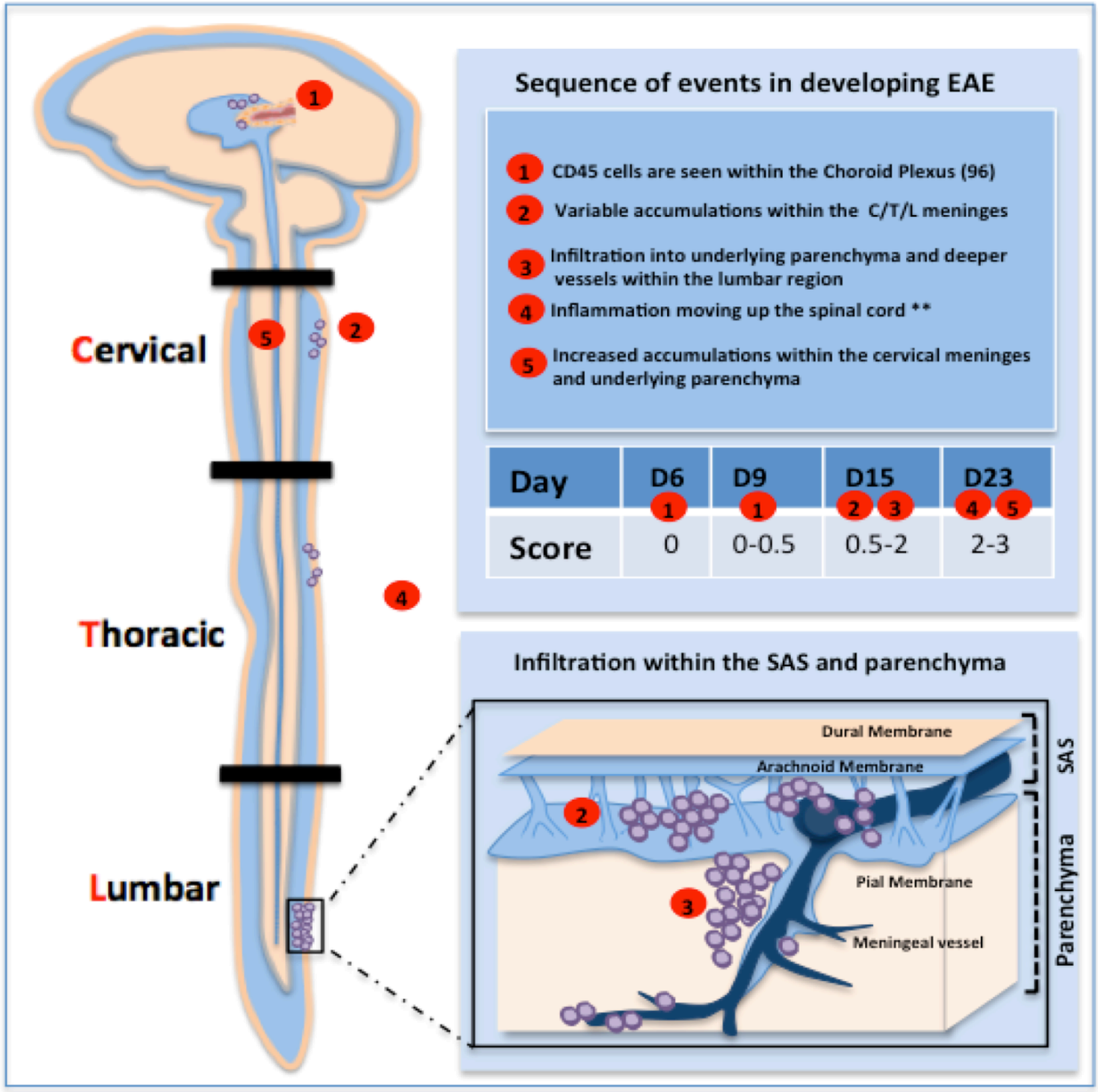

Figure 16: Schematic showing the directed progression of inflammation during evolving neuroinflammation in EAE. Inflammation begins with the accumulation of leukocytes in the Choroid Plexus, followed by entry into the CSF and regional accumulation within different regions of the spinal cord. Immune cells are first seen within the meningeal spaces of the subarachnoid space then with the progression of the disease, into the parenchymal spaces. The events in disease progression from D6 through D23 have been shown in correlation with corresponding scores in the table within the schematic.

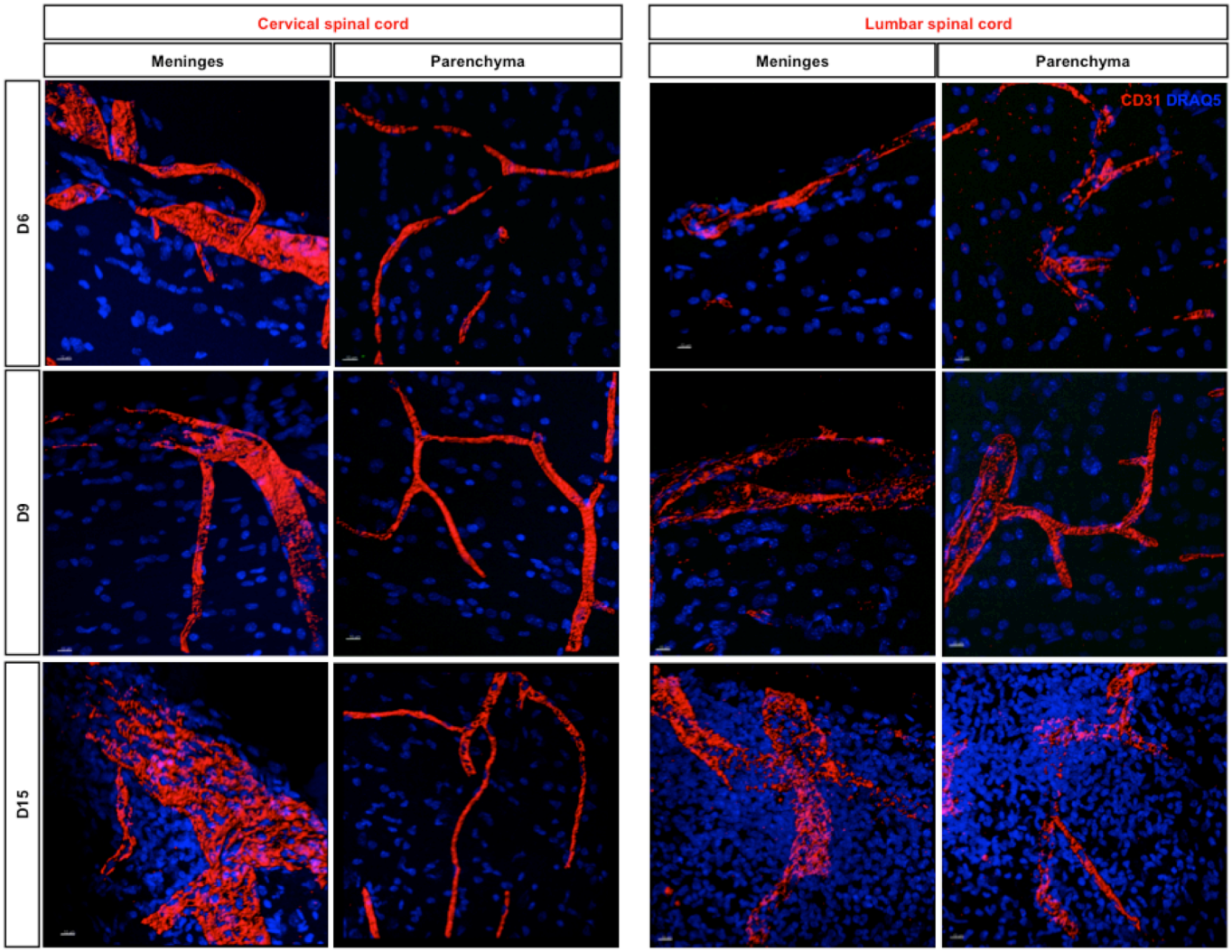

Supplemental figure 4: **Spinal cord regions (cervical and lumbar) showing cellularity within the meninges and parenchyma during evolving experimental autoimmune encephalomyelitis (EAE). (a)**Representative sections of spinal cord regions were collected on days 6, 9, 15 (D6,D9,D15) from mice affter EAE induction with myelin oligodendrocyte glycoprotein(MOG) at 63X magnification. Vessels are immunostained for CD31(red) and isosurface rendered to highlight the meningeal vessels penetrating into the parenchyma and DRAQ5 (blue) stains for cell nuclei.

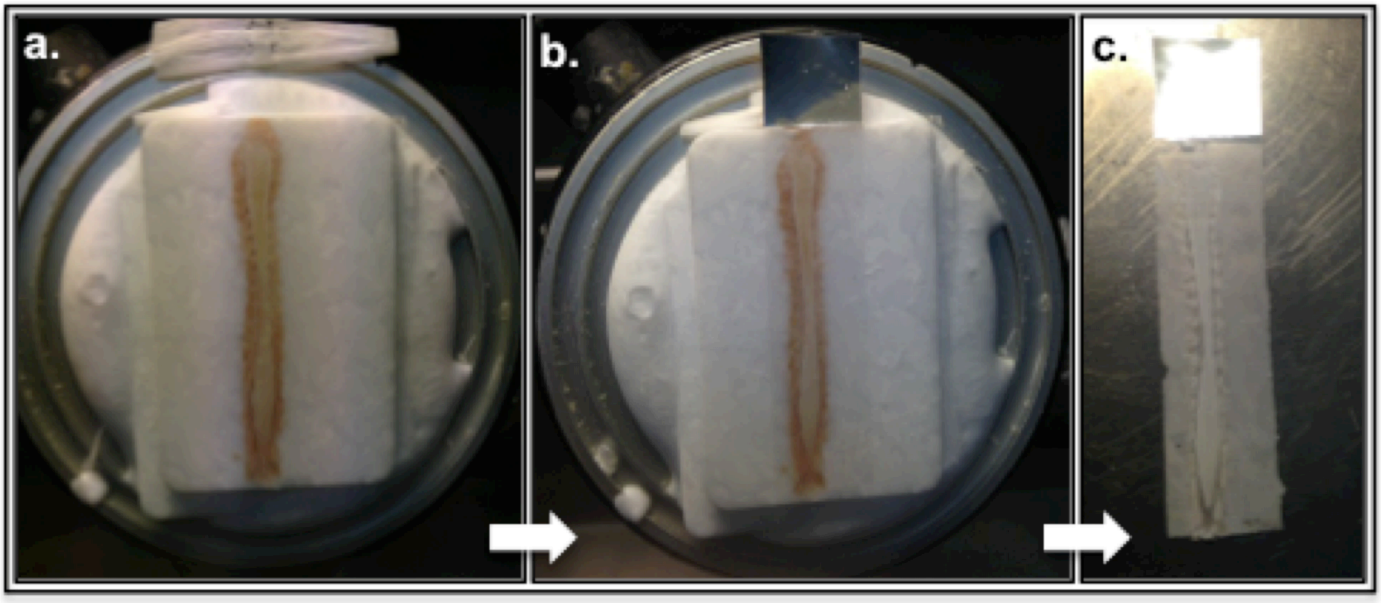

Supplemental figure 5. Spinal cord sectioning for whole spinal cord image scans. (a) Whole spinal columns were embedded in OCT and sectioned to expose the spinal cord. **(b)**An adhesive tape was then applied on top of the section and rolled in place. **(c)** Adhesive tape post sectioning containing the entire spinal cord with surrounding vertebrae remaining intact.

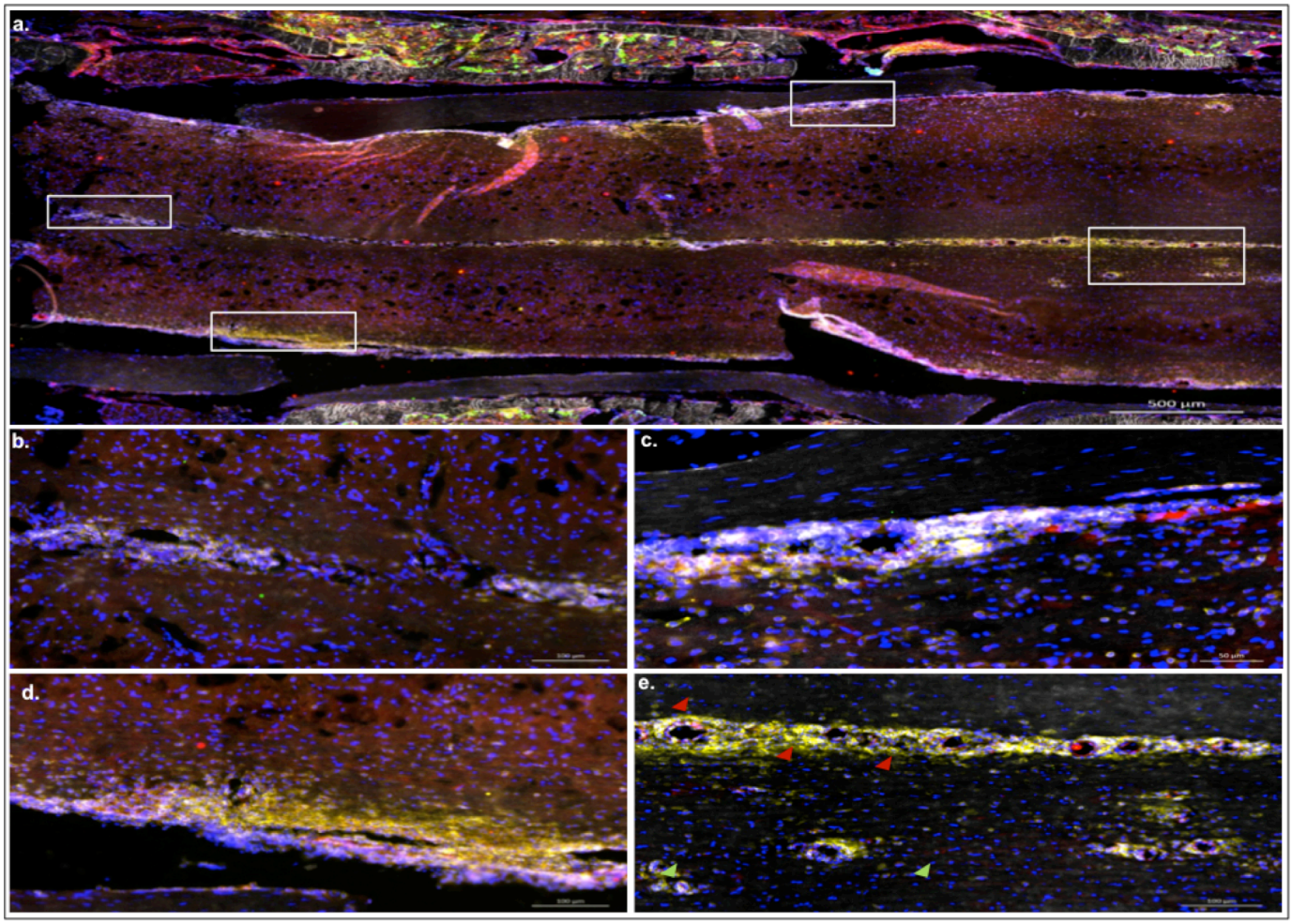

Supplemental figure 6. Inflammation within the lumbar spinal cord region during D15 EAE. **(a)** Representative section of lumbar spinal cord collected on day 15 (D15) showing CD45 +ve leukocyte infiltration within the meninges evolving EAE. Insets **(b)-(e),** from left to right, focus on regional CD45 clusters. **(b)** and **(e)** showing the spinal fissure being populated with CD45 cells. **(e)** Green arrowheads show meningeal vessels within the fissure and red arrowheads show parenchymal vessels being inundated with infiltrating leukocytes. **(c)** and **(d)** show meningeal accumulations of CD45 cells during disease.

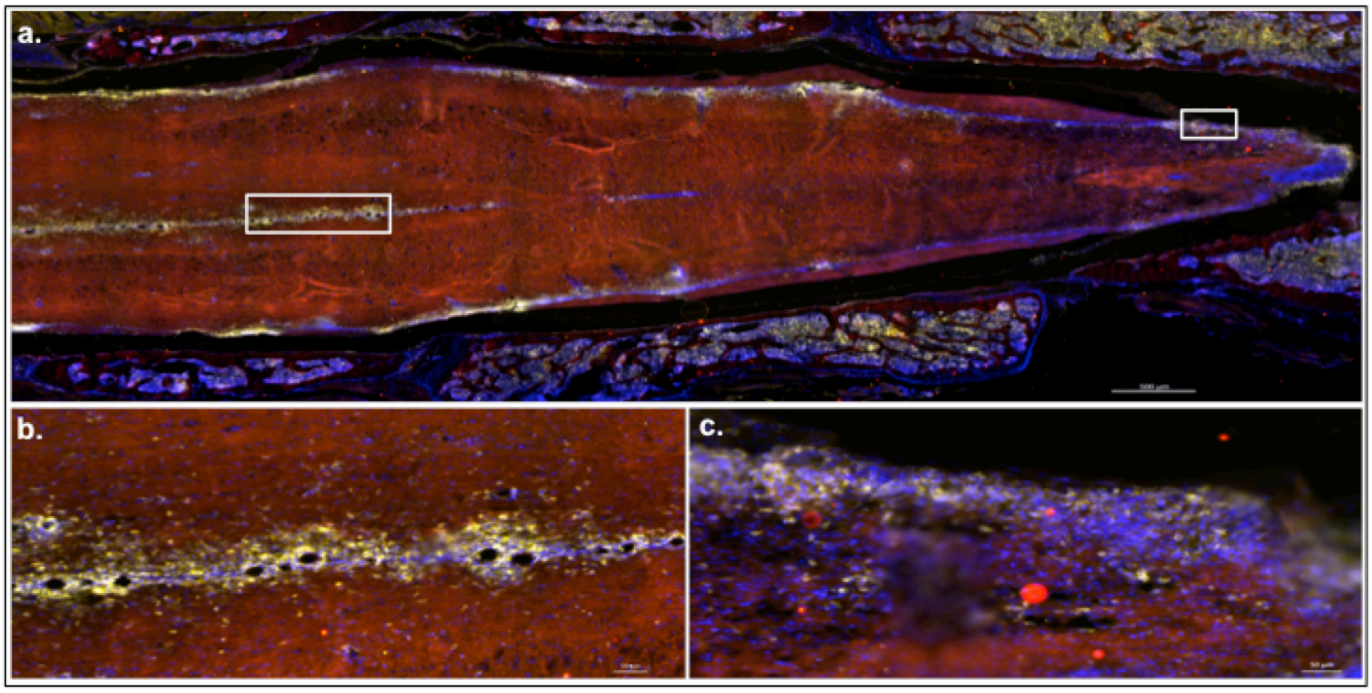

Supplemental figure 7. Inflammation within the lumbar spinal cord region during D23 EAE. **(a)** Representative section of lumbar spinal cord collected on day 23 (D23) showing CD45 +ve leukocyte infiltration within the meninges evolving EAE. Insets **(b)-(d),** from left to right, focus on regional CD45 clusters. **(b)** and **(e)** showing the spinal fissure being populated with CD45 cells. **(e)** Green arrowheads show meningeal vessels within the fissure and red arrowheads show parenchymal vessels being inundated with infiltrating leukocytes. **(c)** and **(d)** show meningeal accumulations of CD45 cells during disease.

Chapter IV: CCL2 sources in evolving EAE

Resolution of central nervous system astrocytic and endothelial sources of CCL2 gene expression during evolving neuroinflammation

1. Abstract

The chemokine CCL2 is a critical mediator of neuroinflammation in diseases such as multiple sclerosis (MS) and its animal model, experimental autoimmune encephalomyelitis (EAE). CCL2 drives mononuclear cell infiltration into the central nervous system (CNS), alters expression and distribution of microvascular endothelial tight junction proteins, and disrupts the blood-brain and blood-spinal cord barriers. Immunohistochemistry has consistently revealed astrocytes to be a source of this chemokine during neuroinflammation, while providing less uniform evidence that CNS endothelial cells may express CCL2 as well. Moreover, the relative contributions of these cell types to the CNS pool of CCL2 during MS/EAE are unclear and require further investigation. CCL2 gene expression was determined by qRT-PCR in different populations of CNS cells at different times following EAE induced by immunization with MOG_{35-55} peptide and adjuvants, or after injection with adjuvants alone. CNS cells types were isolated by two different protocols: bulk isolation to yield crude microvascular and parenchymal fractions (containing astrocytes, other glia, and neurons), or laser capture microdissection (LCM) to more precisely acquire microvascular endothelial cells, astrocytes or other parenchymal cells. Both CNS microvessel and parenchymal populations isolated by crude bulk isolation showed up-regulation of CCL2 mRNA following MOG immunization or injection of adjuvants alone. More exact dissection by LCM revealed microvascular endothelial cells and astrocytes to be the specific sources of CCL2 gene induction following MOG immunization, while only astrocytes

showed elevated CCL2 mRNA in response to just adjuvants. Astrocytes displayed the greatest degree of stimulation of CCL2 gene expression following EAE induction. High precision LCM affirmed both microvascular endothelial cells and astrocytes as the major CNS sources of CCL2 gene expression during EAE. Given the high accessibility of the CNS microvascular endothelium, endothelial-derived CCL2 could prove a viable target for therapeutic intervention in neuroinflammatory disease.

4. Background

Numerous human and animal studies have highlighted the chemokine CCL2 (formerly known as MCP-1 (110)) as a critical mediator of the neuroinflammatory disease multiple sclerosis (MS) and its animal model experimental autoimmune encephalomyelitis (EAE)(2, 4, 8). While long recognized for its chemotactic properties in guiding leukocyte migration, CCL2 has also been shown to destabilize tight junctions of microvascular endothelial cells that comprise the blood-brain and blood-spinal cord barriers (71, 111-113). This multifunctional status underscores CCL2's value as a potential therapeutic target. However, for therapeutic measures to be most effective the sources of CCL2 in the central nervous system (CNS) have to be defined and the timing of CCL2 expression during neuroinflammation elaborated. While astrocytes are widely recognized in reviews as a major CNS source of CCL2 during MS and EAE, BMEC have received only limited acknowledgement as expressing this chemokine (108, 114, 115). The scarce recognition of BMEC as a critical CCL2 source *in situ* may in part stem from the routine use of conventional immunohistochemistry to confirm expression, as this technique may not be sufficiently sensitive to reliably detect perhaps smaller, vesicular quanta of endothelial CCL2 (116). The use of adjuvants to induce EAE, e.g., Complete Freund's Adjuvant (CFA) and pertussis toxin (PTX), can affect CCL2 expression in some endothelial cell types (42, 117), and

might further contribute to ambiguity of BMEC-derived CCL2 during neuroinflammatory disease. Previous reports have not examined the adjuvant issue. The status of BMEC CCL2 gene expression in neuroinflammation thus remains equivocal.

Herein, we report use of two highly sensitive, qRT-PCR-based approaches to clarify the relative contributions of the parenchymal and vascular compartments to CNS CCL2 gene expression during evolution of EAE induced by immunization with myelin oligodendrocyte glycoprotein (MOG) peptide$_{35-55}$ along with adjuvants. One approach used a crude separation of CNS parenchymal and microvessel fractions, based on a common preparative method from homogenized CNS tissue. The other employed the laser capture microdissection (LCM), to more precisely retrieve separate BMEC, astrocyte and other parenchymal cell types. Additionally, we assessed CCL2 expression levels following MOG immunization as well as after injection of these adjuvants alone, to highlight the effects due to MOG immunoreactivity.

3. Material and Methods

3.1 Animals

Female C57BL/6 mice, age 8–10 weeks were obtained from Charles River Laboratories, Inc. (Wilmington, MA) and were euthanized by CO_2 inhalation, following Animal Care and Use Guidelines of the University of Connecticut Health Center (Animal Welfare Assurance # A3471-01). All the experimental procedures conducted have been approved under the protocol #100346-1214.

3.2 EAE induction

Mice were immunized with MOG$_{35-55}$ peptide (MEVGWYRSPFSRVVHLYRNGK; W. M. Keck Biotechnology Resource Center, Yale University) as detailed previously (42). Briefly, on day 0 (D0), female mice 7-9 weeks of age were injected subcutaneously with 300 μg of MOG peptide

in Complete Freund's adjuvant (CFA) (DIFCO, Detroit, MI, USA) containing 1mg/ml Mycobacterium tuberculosis. Mice were also injected intraperitoneally with 200 ng pertussis toxin (List Laboratories, Campbell CA, USA) in phosphate buffered saline (PBS) on D0 and D2 following MOG immunization. Mean clinical scores were calculated from animals monitored for clinical disease severity and scored as 0 =normal; 1 = tail limpness; 2 = limp tail and weak- ness of hind legs; 3=limp tail and complete paralysis of hind legs; 4 = limp tail, complete hind leg and partial front leg paralysis; and 5 = death. The time-points selected for analysis, D9, D15 and D23, represent early EAE (score 0-0.5), acute EAE (score 2-2.5) and chronic EAE (score 2.5-3.5), respectively.

3.3 Bulk isolation of parenchymal and microvessel fractions

Bulk isolations were prepared from each naïve, control and EAE group at all the time-points assessed. Separate parenchymal and microvessel fractions were obtained in bulk from freshly dissected brain and spinal cord using a modification of previously described methods (118). After removal of meninges and large blood vessels, ½ of the brain and spinal cord tissue was homogenized in ice cold PBS using a 7 mL Dounce tissue grinder (Kimble/Kontes,Vineland, NJ, USA). Brain and spinal cord tissue were combined for bulk isolation of parenchymal and microvessel fractions, in keeping with other reports detailing CNS CCL2 expression during EAE (119-121). The remaining spinal cord tissue was snap-frozen in dry ice-cooled 2-methylbutane (Acros; Geel, Belgium), and stored at 80°C until used for LCM. The homogenate was centrifuged at 400 x g for 15 min, and the resulting pellet resuspended in 18% (w/v) dextran (mw_r 60,000 – 90,000) and centrifuged at 4,500x g for 10 min to sediment the crude "microvessel" fraction. The dextran supernatant and floating layer of myelinated axons were collected together to generate the crude "parenchymal" fraction and diluted in PBS; microvessels

were resuspended in PBS and both fractions were washed twice by sedimentation at 720 x g for 10 min and rinsing in PBS. Microvessels were washed of blood cells by filtering through a 40 μm cell strainer (Becton Dickinson Labware, Franklin Lakes, IN, USA) and eluting with PBS. This procedure eliminated a significant fraction of the smaller capillaries, which passed through in the filtrate, while retaining the vast portion of larger venules on the filter (122). The filter-bound-microvessels were then solubilized with lysis buffer from the RNeasy Mini kit (QIAGEN, Valencia, CA).

3.4 Laser Capture Microdissection (LCM) of parenchyma, astrocytes and BMEC

Frozen spinal cords were embedded in cryomatrix compound (Thermo Fisher Scientific, Waltham, MA), and 7μm-thick frozen sections obtained. Immunohistochemstry-guided LCM was performed using a PixCell IIe laser capture microscope (Life Technologies Inc., Foster City, CA), as previously described by this laboratory (123). Significantly, this LCM approach has been shown to yield highly purified populations of microvascular endothelial cells and astrocytes, respectively. Tissue was captured from within the dorsolateral columns along the entire length of the spinal cord, as pathology in this EAE model proceeds up the CNS axis in a caudal-to-rostral direction (124), with lesions prominent in the spinal white matter. Briefly, anti-CD31 was used to label endothelial cells, along with alkaline phosphatase detection employing NBT-BCIP as chromogenic substrate. The endothelial cells of venules (10 – 50 μm in diameter) were specifically acquired (33) as these microvascular tributaries are the preferred sites of leukocyte extravasation (125), and were thus reasoned to express the highest CCL2 expression. This further allowed for a more equitable comparison with the bulk-isolated microvessels, which were enriched in venules. Anti-GFAP immunofluorescence was carried out to identify astrocytes in the same tissue sections. Areas of "other" parenchymal cells selected for LCM were those

that did not stain with CD31 or GFAP, and thus contained neurons, oligodendrocytes and/or microglia. LCM tissue was solubilized in Cell Lysis Buffer® (Signosis; Sunnyvale, CA).

3.5 RNA isolation, cDNA synthesis and qRT-PCR

Total RNA was isolated from bulk microvessel and parenchymal fractions using the RNeasy Mini kit (QIAGEN), and treated with Turbo DNAse (Ambion, Austin, TX, USA). cDNA was generated using SuperScript III (Invitrogen, Carlsbad, CA, USA) and relative CCL2 RNA level determined by qRT-PCR using SYBR green (AB Applied Biosystems, Foster City, CA, USA) as described previously (44). LCM tissue was subjected to DNAse treatment using Turbo DNAse followed by reverse transcription, using SuperScript III. LCM-derived cDNA was then pre-amplified using TaqMan PreAmp Master Mix and a PreAmp Pool containing all primers for detection by the Mouse Immune Panel TaqMan Low density Array (TLDA; Life Technologies Corp., Foster City, CA) and probed for CCL2 by qRT-PCR using a single-plex gene expression assay (42). An ABI 7900HT Fast Real-Time PCR System (Life Technologies Corp.) was used to detect amplicon amount for both bulk and LCM preparations. RPL-19 was used as a reference for relative CCL2 gene expression for bulk isolation as detailed previously (44) and GAPDH for LCM preparation (42), both genes having been shown to be largely invariant during EAE. Relative quantitation was performed using the 2-[Δ][Δ]Ct method of Fleige et al (126). Results were analyzed using a one-way non-parametric Kruskal-Wallis test followed by Dunn's post-test analysis using GraphPad Prism 5 (GraphPad, La Jolla, CA). Results were considered significant at $P \leq 0.05$.

4. Results and Discussion

CCL2 expression levels were first evaluated in separate parenchymal and microvessel fractions prepared by bulk isolation from brain and spinal cord tissue of either MOG-CFA/PTX-treated

(EAE) or CFA/PTX-treated (Control) mice. Analysis was performed at different days after initial injection, which represented onset (D9), peak (D16) and chronic (D23) phases of clinical EAE disease (Fig. 18). As determined by qRT-PCR, relative expression of CCL2 by microvessels was significantly higher in both treatment groups (CFA/PTX and MOG-CFA/PTX) compared to naïve animals at D9 and D16, with a return to naïve level by D23 (Fig.18A, C). The parenchymal fraction showed a similar trend of significantly increased CCL2 expression in both treatment groups compared to naïve animals at D9 and D16 (Fig. 18B, D).

Next, we performed a time-course analysis with CNS tissue that was more precisely dissected into endothelial cells (CD31), astrocytes (GFAP) and "other" parenchymal cells (selected areas devoid of CD31 and GFAP immunostaining) by LCM. As was the case with bulk preparation of microvessels, endothelial cells showed elevated CCL2 expression in MOG-CFA/PTX-treated mice at D16 compared to naïve mice (Fig. 19D). However, corresponding endothelial samples from CFA/PTX-treated mice did not show a similar increase (Fig. 19A). Astrocytes exhibited significantly elevated CCL2 expression at both D9 and D16 in the MOG-CFA/PTX-treated group (Fig. 19E), and a significant increase at D9 in the CFA/PTX-treated cohort (Fig. 19B). In contrast to that observed with the bulk parenchymal preparations, other parenchymal cells isolated by LCM failed to display an increase in CCL2 expression either in MOG-CFA/PTX-treated (Fig. 19F) or CFA/PTX-treated (Fig. 19C) mice compared to naïve mice at any time-point.

These findings underscore several points. Expression of CCL2 is significantly induced in both astrocyte and endothelial cell populations in the MOG-induced EAE paradigm. The fact that CCL2 mRNA level appeared higher in endothelial cells than in astrocytes in naïve mice may reflect the capture of some circulating leukocytes along with endothelial cells, as the mice were

not perfused prior to LCM. Interestingly, while CFA/PTX injection resulted in elevated CCL2 expression in isolated microvessels, it did not do so in LCM-acquired endothelial cells. This suggests that sources other than endothelial cells contributed to the altered CCL2 mRNA level in the bulk microvessel fraction. As astrocytes lie in close proximity to endothelial cells within the neurovascular unit (NVU) (127, 128) and can contaminate microvessel preparations (129, 130), *a priori* these particular glial cells may be a significant source of CCL2 mRNA detected in bulk-isolated microvessels. This caveat reinforces LCM as a critical technology to more effectively resolve sources of gene expression *in situ*.

Our LCM results further suggest astrocytes are the preeminent parenchymal sources of induced CCL2 gene expression during EAE, since the other parenchymal cells acquired by this technique showed no significant stimulation of CCL2 mRNA. As increased immunostaining of CCL2 in microglia has been reported in EAE (131), this may represent up-regulation at the protein rather than the RNA level. It may also be that the percentage contribution of microglia in the other parenchymal cells acquired by LCM, was not high enough to show overall elevation of CCL2 gene expression in these samples from diseased mice. CCL2 mRNA detected in other parenchymal cells from naïve mice could possibly reflect a low level of constitutive CCL2 expression by neurons as well (132).

Lastly, CFA/PTX alone can stimulate CCL2 expression in astrocytes (Fig. 19B), possibly providing a priming function for supernumerary stimulation due to MOG effects (Fig. 19E). This is consistent with reports that peripheral inflammation induced by CFA or Mycobacterium resulted in CNS glial activation (133, 134). Previous results from this laboratory indicated CFA/PTX injection also up-regulated expression of CCL2 by choroid plexus capillary endothelial cells. Thus, it is imperative that any measure of gene expression following the

typical MOG immunization protocol be compared to effects seen after injection of CFA/PTX alone, to discern what gene changes are associated specifically with MOG-induced pathogenesis.

These results reinforce the CNS microvascular endothelium as a significant source of CCL2 [9, 10, 12], as well as spotlight LCM as a critical tool for the selective enrichment of vascular or other CNS cell types for gene expression studies (33, 42, 123). Moreover, given the microvascular endothelium is highly accessible from the circulation – as compared to the astrocyte population, which lies behind the BBB and BSCB – endothelial-derived CCL2 may be a "druggable" target in neuroinflammatory disease (44, 135).

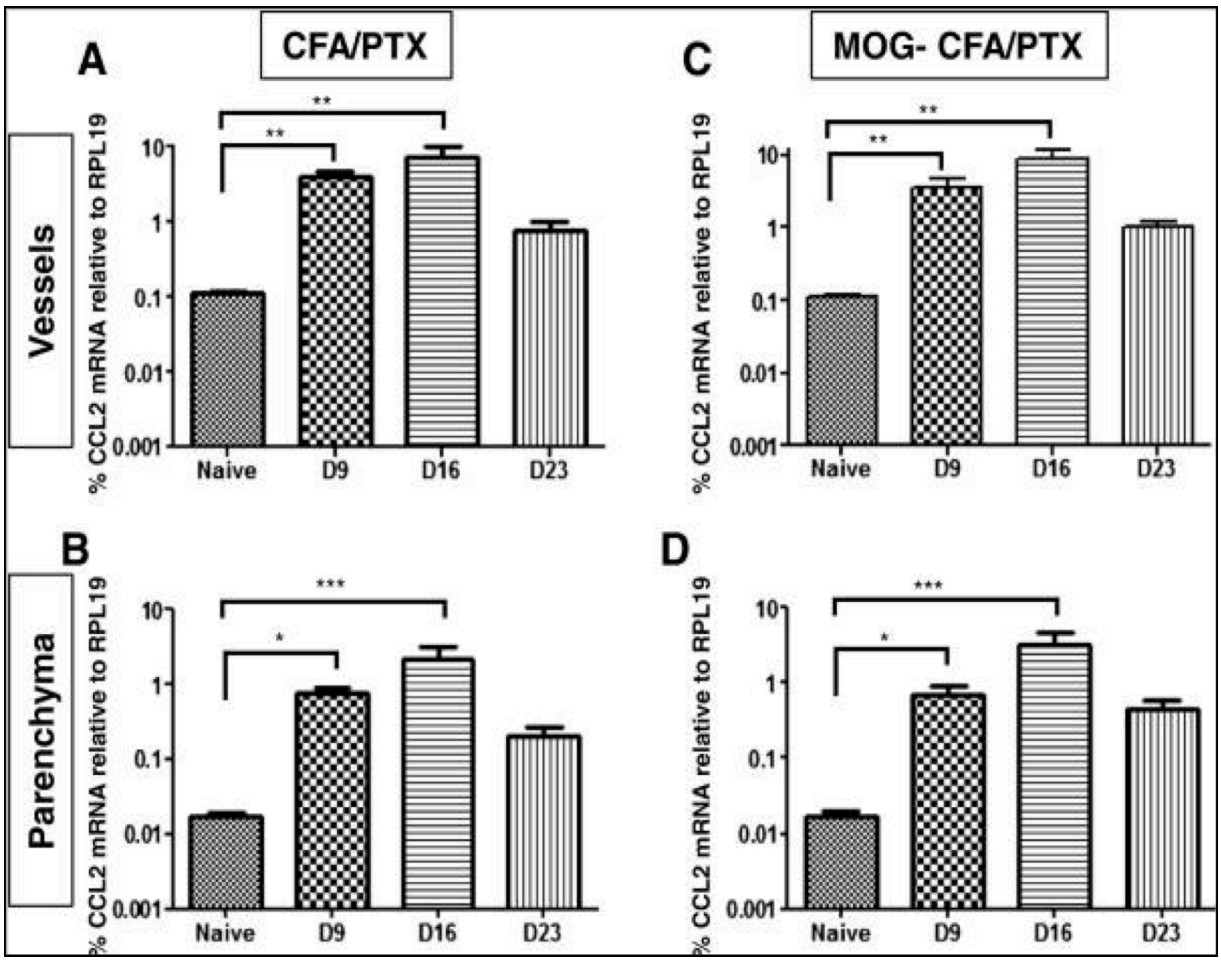

Figure 18: CCL2 gene expression in CNS microvessel and parenchymal fractions obtained by bulk preparation. Separate, crude microvessel (A, C) and parenchymal (B, D) fractions were prepared by bulk isolation from combined brain and spinal cord tissue of mice injected with CFA/PTX (A, B) or immunized with MOG-CFA/PTX (C, D). Analyses were performed at D9, D16 and D23 following beginning of either injection regime, and relative CCL2 mRNA levels are plotted on a log scale. Comparisons were made to naïve mice. * $P \leq 0.05$; ** $P \leq 0.01$; and *** $P \leq 0.001$. Data has been presented as mean +/- SEM. For each experiment, bulk isolations were performed from three individual mice from each naïve, control (CFA/PTX) and EAE (MOG-CFA/PTX) group, and experiments were conducted twice.

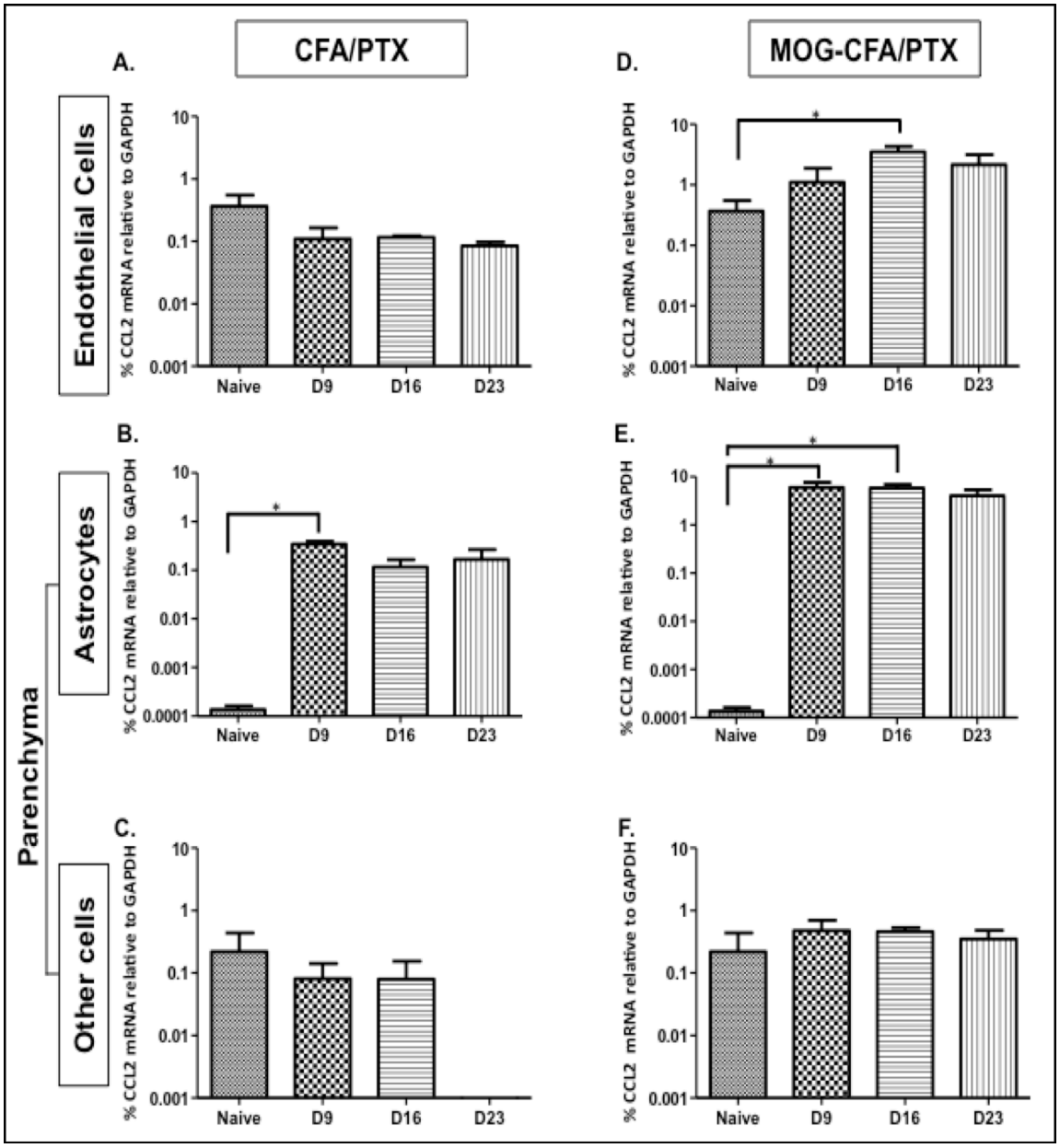

Figure 19: CCL2 gene expression in CNS microvascular endothelial cells, astrocytes and other parenchymal cells isolated by LCM. Endothelial cells (A, D), astrocytes (B, E), and other parenchymal cells (C, F) were separately acquired by LCM from spinal cord tissue of mice injected with CFA/PTX (A-C) or immunized with MOG-CFA/PTX (D-F). Analyses were performed at D9, D16 and D23 following either injection regime, and relative CCL2 mRNA levels are plotted on a log scale. Comparisons were made to naïve mice. *P≤0.05; **P≤0.01; and ***P≤0.001. Data has been presented as mean +/- SEM. For each experiment, LCM was performed on tissue from three individual mice from each naïve, control (CFA/PTX) and EAE (MOG-CFA/PTX) group.

CHAPTER V: Conclusion

CP has been established as one of the alternate routes for immune cell entry during EAE/MS (15, 18) but the changes within CP anatomy that allow this access to the leukocytes was still unknown. Prior to this work, CP barrier integrity had not been evaluated in MS/EAE to the extent of the details as provided by this report. As important was the need to find evidences leading to possible changes in permeability of CP that could aid in leukocyte extravasation. Tight junction breakdown is co-relative with barrier alterations, since the complexity of TJ between adjacent cells constitutes the physical presence of a barrier. There has been very limited work addressing the status of TJ within BCSFB. Few preliminary reports were available before this work and they had been more suggestive than conclusive. Wohlburg et al. noted altered localization of CP TJ proteins claudins 1,2 and 11, occludin and ZO-1 during EAE (24). These reports are more qualitative and did not address progressive changes in TJs through developing stages of disease. Changes in CP TJs following peripheral inflammation have also been reported by Marque et al. (20) and Mitchell et al. (136), providing further evidence that CP TJs are thus subject to alterations in an inflammatory scenario.

Other reports provide indirect links to possibly altered integrity of CP during disease. Severe cerebrospinal venal insufficiency (CCSVI); an abnormality in blood drainage in the brain and spinal cord associated with MS (137), has been linked to altered CSF dynamics (138) which could be due to a disrupted BCSFB. Invitro evidence shows BCSFB alterations in trans epithelial electrical resistance and increase of para cellular flux after TNF stimulation, a potent inflammatory cytokine, which is markedly increased during inflammation (139). These reports point toward changes in BCSFB integrity and permeability during inflammation. We proposed to

quantify these changes using novel 3D quantification technique previously standardized by the lab (41).

Previous reports with the proposed claudins in CP have provided suggestive evidence that they are altered during disease (24, 25). Quantification of TJs in naïve, control and EAE groups painted a similar picture of stable expression in the naïve group, slightly altered levels in the control groups (CFA/PTX alone without the MOG peptide may not have significant effects on TJ regulation), with EAE mice showing the most altered values due to barrier changes and breakdown in disease. The quantification protocol of the TJs was previously used in the lab with experience in IMARIS based applications and has standardized the procedures (41). However, given that the CP epithelial cells are a lot more tortuous (19) than the parenchymal vessels where the quantification method was previously standardized. This opened new challenges in imaging as well as quantification allowing us to add novel modules and techniques into addressing the quantification of tight junctions, permeability of the barrier and leukocyte extravasation.

TJ protein dynamics such as linkage with cytoskeleton and the interactions between the dimers of TJ complex could be subject to changes during the process of disease (140-142). However, imaging molecular changes at this level is beyond the scope of the type of imaging and quantification carried out within this report. Nevertheless effects of such structural alterations can be linked to increase in trans epithelial transport (143) and hence, to changes in permeability, which we have assessed and quantified in our study as well. 3D quantification of IgG diffusion across the CP had never been done before and quantification advances in other systems have only been in 2D (144).

Inflammation of the meninges, another established route of immune cell entry into the SAS has been shown to precede that of the underlying parenchyma, which leads to lesions causing neuroinflammation in EAE/MS (145, 146). This suggests an important role of this compartment in the development of neuroinflammation within the CNS. More recent evidences point out that inflammatory cells are localized around the meningeal venules within this specialized SAS compartment (10, 11, 27). However, it is not clear as to why the SAS meningeal venules are inflamed earlier than the parenchymal vasculature or why does the inflammation progresses from the SAS into the parenchyma. Constitutive expression of P-selectin (required for initial attachment of leukocytes with the vascular endothelial cell) in meningeal vasculature but absent within the resting parenchymal vessels is a possible direction suggesting differential expression of immune genes in different types of vasculature (13, 147). Kivisakk et al. reports suggestive differential expressions of E-selectin and adhesion molecules such as ICAM and VCAM as well (13). Moreover, our reports show that extensive arrays of genes that are important contributors in inflammation are differentially expressed within these vascular locales. This study probed into an array of adhesion molecules, cytokines, chemokines, statins, interleukins, T cell activation markers, co-stimulatory molecules, transcription factors and apoptotic markers investigating their possible differential regulation between meningeal and parenchymal vessels.

Differential expression pattern of immune genes in meningeal and parenchymal venules as shown by this study provide supportive evidence to explain why some regions of the spinal cord are more prone to lesions in EAE. Reports of ascending paralysis have long been around (148) but the reasons for this ascension from lumbar to cervical segment of the cord has remained unexplained. A detailed segmental analysis of immune profiling of both these vessel

types was done, the technique perfected by the group and shown in varied LCM applications (30, 31, 33) in addition to recent reports on coupling it with TLDA analysis (42, 149).

Reports included in this work investigated how the tight junctions between the epithelial cells of BCSFB changed during disease. We assessed the status of junctional integrity and permeability of CP choroidal epithelium at different timepoints during developing EAE using immunostaining, 3D imaging and quantification. We then continued to study the effects of EAE within the meningeal venules that reside in the SAS and the underlying parenchymal venules via regulation of inflammatory genes within these vessels. This allowed a unique opportunity to study the differential inflammation patterns between the venules of the two regions- meninges and parenchyma and the possibility of relay of inflammatory signals between the cervical, thoracic and lumbar spinal cord segments. We were able to characterize and compare the inflammatory gene expression patterns between meningeal and underlying parenchymal venules from three distinct spinal cord segments (lumbar, thoracic and cervical) at different timepoints during developing EAE using immune-LCM coupled to TLDA array analysis.

Studies within this report helped fill in the gaps that are crucial to understanding the initial sequence of events that trigger inflammation and spread of immune cascade as the disease progresses. With an unknown etiology, the main trigger behind MS remains enigmatic. It is probable that more than one factor, a culmination of genetics and environmental players are accountable for the susceptibility of this disease. The field has progressed in terms of identifying the alternate routes other than the BBB that usher in immune cells, which could eventually lead to the breakdown of the BBB, the known hallmark of this neurodegenerative disease. However, the sequence of events that makes the alternate routes-CP and SAS susceptible in the first place has largely been unknown. As puzzling are the events that guide inflammation from these initial

sites to inner parenchyma where the BBB resides. This project aimed to cover these critical questions, answers to which provide a fundamental basis in identifying possible therapeutic avenues within the earliest events of the disease, perhaps the most sensitive to drug interventions as well.

This project assessed TLDA gene analysis of 93 immune genes through EAE progression: from earliest pre-clinical to late chronic disease phase. Results have provided us with an array of information on gene regulation from onset through progression of inflammation, highlighting the genes significantly regulated at different stages of inflammation in different regions of the spinal cord. This data provides us with valuable early and late disease stage biomarkers that could be further co-related with disease pathology. This is important because an ideal biomarker would be an early and accurate indicator of immunological activity and would co-relate with key endpoints in MS patients such as relapse activity, disability and disease progression and possibly early detection. Although this concept is in its incipient pre-clinical stage, further confirming experiments with these markers, could help us screen MS patients and relate them with the stage of the disease they might be in, as well as foresee the possible progression of their inflammation or relapses. With this valuable information of disease stages, we could design targeted anti-inflammatory therapies against co-relating genes in developing inflammation, and successfully impede the looming relapses.

The current measure of disease for MS patients are MRI images of brain and spinal cord lesions, which are essentially end stage results of disease progression. Genetic biomarkers can provide a much-needed shift in gauging the disease, possibly finding it as early as possible, earlier than the manifestation of inflammation resulting in lesions as captured by imaging diagnostics. This late stage is far along the damaging inflammatory cascade for effective

prophylactics leaving room only for therapies targeted to symptomatic relief, as is the case with current FDA approved treatments for MS patients. These treatments could also possibly be paired with new targets of inflammation identified by the study, which would provide a multi-directional approach to treating MS. In another light, the current treatments have a holistic immune-suppressive effect subjecting patients to novel infections they were protected against with an otherwise functional immune system. This study could highlight inflammatory markers related to a particular subset of immune pool, allowing targeted suppression instead of an entire immune pool ablation.

An extension to the CP work, future in-vitro experiments can be carried out to confirm changes in TJs using BCSFB culture mediums. Reports have provided convincing epithelial culture systems with BCSFB properties (150-152) that can be manipulated with inflammatory cytokines and transcription factors to study TJ changes due to inflammation. CP TJs have been assessed with whole tissue extracts as well (25, 136). This system of tissue isolation however defies our purpose of resolving the changes in the choroidal epithelium within the complex layers of the CP (i.e. the inner capillary endothelial layer surrounded by a stroma and outlined by the outermost epithelial layer). None-the-less, this approach can provide overall changes or effects of inflammatory markers on the CP as a whole.

A probable alternative to LCM of meningeal and parenchymal vessels could be vessel isolation from the extracted spinal cord, for which the lab has previous reports with vessel isolation protocols (118, 122, 153). However, those isolations were using brain tissue providing more material to work with, while spinal cord vessel extraction has proved to be more problematic in terms of yield. Working with smaller segments of spinal cord as needed for the purpose of this study, would provide lesser material to work with. Vessel isolation from

extracted meninges of these individual sections of spinal cord segments can prove further problematic in terms of isolation as well as the amount of material that can be extracted from these thin sheets of meninges from small sections. A proper and successful extraction would however provide an invaluable method to understand the gene expression within these unique sections as well as provide an opportunity to co-relate and validate our LCM- gene expression analysis.

Also as a possible future direction from this project, potential therapeutic targets could be narrowed down from the pool of regulated genes changed in inflammation to the most potent regulators, by successive invitro analysis that can analyze the extent of inflammatory roles played by individual up regulated markers. Invitro analysis can be carried out in similar vascular in-vitro systems including but not limited to murine BMECs (Brain Microvascular Endothielial Cells), both on primary and commercially available cell lines and moving translating it further with Primary Human Brain Microvascular Endothelial Cells (ACBRI 376). This will provide a sharper focus in identifying a potential effective biomarker of inflammatory stages. We could also potentially be looking at a novel route of drug delivery. Our results reveal that inflammation primarily begins in the meningeal vessels compared to the parenchymal vessels, so targeted drug delivery into the meningeal compartment, directly into the CSF via intrathecal delivery could prove to be more beneficial rather than an intravenous or subcutaneous method of drug delivery, although this route does pose the risk of being more invasive. Hence future directions to the continuation of this concept of biomarkers will make strides in understanding MS pathology and regulation providing possible avenues for therapeutic interventions.

List of abbreviations:

BBB: Blood Brain Barrier

BCSFB: Blood Cerebrospinal Fluid Barrier

CFA: Complete Freund's Adjuvant

CLN- Claudin

CSF: Cerebrospinal Fluid

CNS: Central Nervous System

Col4a5: Collagen type IV alpha 5.

CP: Choroid Plexus

EAE: Experimental Autoimmune Encephalomyelitis

Ece 1: Endothelin Converting Enzyme 1

Edn1: Endothelin 1

H2-Ea: Histocompatibility 2 class II antigen E alpha

LCM: Laser Capture Microdissection

MCP: Monocyte Chemoattractant Protein

MOG: Myelin Oligodendrocyte Glycoprotein

MS: Multiple Sclerosis

NOS2- Nitric Oxide Synthase 2

PTX: Pertussis Toxin

SAS: Sub Arachnoid Space

SKI-2: Super Killer-2

SOCS-2- Supressor Of Cytokine Signaling-2

STAT 1: Signal Transducers and Activators of Transcription-1

TJ: Tight Junctions

TGFβ: Transforming Growth Factor β

VEGF: Vascular Endothelial Growth Factor

VCAM: Vascular Cell Adhesion Molecule

ZO: Zonula Occludens

REFERENCES

1. Aktas O, Kieseier B, Hartung HP. Neuroprotection, regeneration and immunomodulation: broadening the therapeutic repertoire in multiple sclerosis. Trends in neurosciences. 2010;33(3):140-52. doi: 10.1016/j.tins.2009.12.002. PubMed PMID: 20045200.
2. Barnett MH, Parratt JD, Pollard JD, Prineas JW. MS: is it one disease? International MS journal / MS Forum. 2009;16(2):57-65. PubMed PMID: 19671369.
3. Bennett JL, Stuve O. Update on inflammation, neurodegeneration, and immunoregulation in multiple sclerosis: therapeutic implications. Clinical neuropharmacology. 2009;32(3):121-32. doi: 10.1097/WNF.0b013e3181880359. PubMed PMID: 19483479.
4. Herz J, Zipp F, Siffrin V. Neurodegeneration in autoimmune CNS inflammation. Experimental neurology. 2010;225(1):9-17. doi: 10.1016/j.expneurol.2009.11.019. PubMed PMID: 19961850.
5. Stromnes IM, Goverman JM. Active induction of experimental allergic encephalomyelitis. Nature protocols. 2006;1(4):1810-9. doi: 10.1038/nprot.2006.285. PubMed PMID: 17487163.
6. Engelhardt B, Sorokin L. The blood-brain and the blood-cerebrospinal fluid barriers: function and dysfunction. Semin Immunopathol. 2009;31(4):497-511. doi: 10.1007/s00281-009-0177-0. PubMed PMID: 19779720.
7. Bennett J, Basivireddy J, Kollar A, Biron KE, Reickmann P, Jefferies WA, et al. Blood-brain barrier disruption and enhanced vascular permeability in the multiple sclerosis model EAE. Journal of neuroimmunology. 2010;229(1-2):180-91. doi: 10.1016/j.jneuroim.2010.08.011. PubMed PMID: 20832870.
8. Ransohoff RM. Immunology: In the beginning. Nature. 2009;462(7269):41-2. doi: 10.1038/462041a. PubMed PMID: 19890316.
9. Axtell RC, Steinman L. Gaining entry to an uninflamed brain. Nature immunology. 2009;10(5):453-5. doi: 10.1038/ni0509-453. PubMed PMID: 19381137.
10. Shin T, Kojima T, Tanuma N, Ishihara Y, Matsumoto Y. The subarachnoid space as a site for precursor T cell proliferation and effector T cell selection in experimental autoimmune encephalomyelitis. Journal of neuroimmunology. 1995;56(2):171-8. Epub 1995/02/01. PubMed PMID: 7860712.
11. Kivisakk P, Imitola J, Rasmussen S, Elyaman W, Zhu B, Ransohoff RM, et al. Localizing central nervous system immune surveillance: meningeal antigen-presenting cells activate T cells during experimental autoimmune encephalomyelitis. Annals of neurology. 2009;65(4):457-69. Epub 2008/05/23. doi: 10.1002/ana.21379. PubMed PMID: 18496841; PubMed Central PMCID: PMC3305810.
12. Brown DA, Sawchenko PE. Time course and distribution of inflammatory and neurodegenerative events suggest structural bases for the pathogenesis of experimental autoimmune encephalomyelitis. The Journal of comparative neurology. 2007;502(2):236-60. Epub 2007/03/10. doi: 10.1002/cne.21307. PubMed PMID: 17348011.
13. Kivisakk P, Mahad DJ, Callahan MK, Trebst C, Tucky B, Wei T, et al. Human cerebrospinal fluid central memory CD4+ T cells: evidence for trafficking through choroid plexus and meninges via P-selectin. Proceedings of the National Academy of Sciences of the United States of America. 2003;100(14):8389-94. Epub 2003/06/28. doi: 10.1073/pnas.1433000100. PubMed PMID: 12829791; PubMed Central PMCID: PMC166239.

14. Brown PD, Davies SL, Speake T, Millar ID. Molecular mechanisms of cerebrospinal fluid production. Neuroscience. 2004;129(4):957-70. doi: 10.1016/j.neuroscience.2004.07.003. PubMed PMID: 15561411; PubMed Central PMCID: PMC1890044.
15. Wolburg H, Paulus W. Choroid plexus: biology and pathology. Acta neuropathologica. 2010;119(1):75-88. doi: 10.1007/s00401-009-0627-8. PubMed PMID: 20033190.
16. Vercellino M, Votta B, Condello C, Piacentino C, Romagnolo A, Merola A, et al. Involvement of the choroid plexus in multiple sclerosis autoimmune inflammation: a neuropathological study. Journal of neuroimmunology. 2008;199(1-2):133-41. doi: 10.1016/j.jneuroim.2008.04.035. PubMed PMID: 18539342.
17. Kleine TO, Benes L. Immune surveillance of the human central nervous system (CNS): different migration pathways of immune cells through the blood-brain barrier and blood-cerebrospinal fluid barrier in healthy persons. Cytometry Part A : the journal of the International Society for Analytical Cytology. 2006;69(3):147-51. doi: 10.1002/cyto.a.20225. PubMed PMID: 16479603.
18. Engelhardt B, Wolburg-Buchholz K, Wolburg H. Involvement of the choroid plexus in central nervous system inflammation. Microscopy research and technique. 2001;52(1):112-29. doi: 10.1002/1097-0029(20010101)52:1<112::AID-JEMT13>3.0.CO;2-5. PubMed PMID: 11135454.
19. Dohrmann GJ. The choroid plexus: a historical review. Brain research. 1970;18(2):197-218. PubMed PMID: 4929003.
20. Marques F, Sousa JC, Coppola G, Falcao AM, Rodrigues AJ, Geschwind DH, et al. Kinetic profile of the transcriptome changes induced in the choroid plexus by peripheral inflammation. Journal of cerebral blood flow and metabolism : official journal of the International Society of Cerebral Blood Flow and Metabolism. 2009;29(5):921-32. doi: 10.1038/jcbfm.2009.15. PubMed PMID: 19240744.
21. Skipor J, Thiery JC. The choroid plexus--cerebrospinal fluid system: undervaluated pathway of neuroendocrine signaling into the brain. Acta neurobiologiae experimentalis. 2008;68(3):414-28. PubMed PMID: 18668165.
22. Reboldi A, Coisne C, Baumjohann D, Benvenuto F, Bottinelli D, Lira S, et al. C-C chemokine receptor 6-regulated entry of TH-17 cells into the CNS through the choroid plexus is required for the initiation of EAE. Nature immunology. 2009;10(5):514-23. Epub 2009/03/24. doi: 10.1038/ni.1716. PubMed PMID: 19305396.
23. Redzic ZB, Segal MB. The structure of the choroid plexus and the physiology of the choroid plexus epithelium. Advanced drug delivery reviews. 2004;56(12):1695-716. doi: 10.1016/j.addr.2004.07.005. PubMed PMID: 15381330.
24. Wolburg H, Wolburg-Buchholz K, Liebner S, Engelhardt B. Claudin-1, claudin-2 and claudin-11 are present in tight junctions of choroid plexus epithelium of the mouse. Neuroscience letters. 2001;307(2):77-80. PubMed PMID: 11427304.
25. Kratzer I, Vasiljevic A, Rey C, Fevre-Montange M, Saunders N, Strazielle N, et al. Complexity and developmental changes in the expression pattern of claudins at the blood-CSF barrier. Histochemistry and cell biology. 2012;138(6):861-79. doi: 10.1007/s00418-012-1001-9. PubMed PMID: 22886143; PubMed Central PMCID: PMC3483103.
26. Goverman J. Autoimmune T cell responses in the central nervous system. Nature reviews Immunology. 2009;9(6):393-407. doi: 10.1038/nri2550. PubMed PMID: 19444307; PubMed Central PMCID: PMC2813731.

27. Bartholomaus I, Kawakami N, Odoardi F, Schlager C, Miljkovic D, Ellwart JW, et al. Effector T cell interactions with meningeal vascular structures in nascent autoimmune CNS lesions. Nature. 2009;462(7269):94-8. doi: 10.1038/nature08478. PubMed PMID: 19829296.
28. Prendergast CT, Anderton SM. Immune cell entry to central nervous system--current understanding and prospective therapeutic targets. Endocrine, metabolic & immune disorders drug targets. 2009;9(4):315-27. PubMed PMID: 20028334.
29. Engelhardt B, Ransohoff RM. Capture, crawl, cross: the T cell code to breach the blood-brain barriers. Trends in immunology. 2012. Epub 2012/08/29. doi: 10.1016/j.it.2012.07.004. PubMed PMID: 22926201.
30. Kinnecom K, Pachter JS. Selective capture of endothelial and perivascular cells from brain microvessels using laser capture microdissection. Brain research Brain research protocols. 2005;16(1-3):1-9. Epub 2005/09/20. doi: 10.1016/j.brainresprot.2005.08.002. PubMed PMID: 16168706.
31. Macdonald JA, Murugesan N, Pachter JS. Validation of immuno-laser capture microdissection coupled with quantitative RT-PCR to probe blood-brain barrier gene expression in situ. Journal of neuroscience methods. 2008;174(2):219-26. Epub 2008/08/12. doi: 10.1016/j.jneumeth.2008.07.009. PubMed PMID: 18692089.
32. Murugesan N, Macdonald JA, Lu Q, Wu SL, Hancock WS, Pachter JS. Analysis of mouse brain microvascular endothelium using laser capture microdissection coupled with proteomics. Methods Mol Biol. 2011;686:297-311. Epub 2010/11/18. doi: 10.1007/978-1-60761-938-3_14. PubMed PMID: 21082378.
33. Macdonald JA, Murugesan N, Pachter JS. Endothelial cell heterogeneity of blood-brain barrier gene expression along the cerebral microvasculature. Journal of neuroscience research. 2010;88(7):1457-74. doi: 10.1002/jnr.22316. PubMed PMID: 20025060.
34. Murugesan N, Demarest TG, Madri JA, Pachter JS. Brain regional angiogenic potential at the neurovascular unit during normal aging. Neurobiology of aging. 2012;33(5):1004 e1-16. Epub 2011/10/25. doi: 10.1016/j.neurobiolaging.2011.09.022. PubMed PMID: 22019053; PubMed Central PMCID: PMC3266473.
35. Cserr HF. Physiology of the choroid plexus. Physiological reviews. 1971;51(2):273-311. PubMed PMID: 4930496.
36. Damkier HH, Brown PD, Praetorius J. Cerebrospinal fluid secretion by the choroid plexus. Physiological reviews. 2013;93(4):1847-92. doi: 10.1152/physrev.00004.2013. PubMed PMID: 24137023.
37. Szmydynger-Chodobska J, Pascale CL, Pfeffer AN, Coulter C, Chodobski A. Expression of junctional proteins in choroid plexus epithelial cell lines: a comparative study. Cerebrospinal fluid research. 2007;4:11. doi: 10.1186/1743-8454-4-11. PubMed PMID: 18162136; PubMed Central PMCID: PMC2241822.
38. Fanning AS, Anderson JM. Zonula occludens-1 and -2 are cytosolic scaffolds that regulate the assembly of cellular junctions. Annals of the New York Academy of Sciences. 2009;1165:113-20. doi: 10.1111/j.1749-6632.2009.04440.x. PubMed PMID: 19538295; PubMed Central PMCID: PMC3759978.
39. Tsukita S, Katsuno T, Yamazaki Y, Umeda K, Tamura A, Tsukita S. Roles of ZO-1 and ZO-2 in establishment of the belt-like adherens and tight junctions with paracellular permselective barrier function. Annals of the New York Academy of Sciences. 2009;1165:44-52. doi: 10.1111/j.1749-6632.2009.04056.x. PubMed PMID: 19538286.

40. Spadaro D, Tapia R, Pulimeno P, Citi S. The control of gene expression and cell proliferation by the epithelial apical junctional complex. Essays in biochemistry. 2012;53:83-93. doi: 10.1042/bse0530083. PubMed PMID: 22928510.
41. Paul D, Cowan AE, Ge S, Pachter JS. Novel 3D analysis of Claudin-5 reveals significant endothelial heterogeneity among CNS microvessels. Microvascular research. 2012. doi: 10.1016/j.mvr.2012.12.001. PubMed PMID: 23261753.
42. Murugesan N, Paul D, Lemire Y, Shrestha B, Ge S, Pachter JS. Active induction of experimental autoimmune encephalomyelitis by MOG35-55 peptide immunization is associated with differential responses in separate compartments of the choroid plexus. Fluids and barriers of the CNS. 2012;9(1):15. doi: 10.1186/2045-8118-9-15. PubMed PMID: 22870943; PubMed Central PMCID: PMC3493354.
43. Paul D, Ge S, Lemire Y, Jellison ER, Serwanski DR, Ruddle NH, et al. Cell-selective knockout and 3D confocal image analysis reveals separate roles for astrocyte-and endothelial-derived CCL2 in neuroinflammation. Journal of neuroinflammation. 2014;11(1):10. doi: 10.1186/1742-2094-11-10. PubMed PMID: 24444311.
44. Ge S, Shrestha B, Paul D, Keating C, Cone R, Guglielmotti A, et al. The CCL2 synthesis inhibitor bindarit targets cells of the neurovascular unit, and suppresses experimental autoimmune encephalomyelitis. Journal of neuroinflammation. 2012;9(1):171. Epub 2012/07/14. doi: 10.1186/1742-2094-9-171. PubMed PMID: 22788993.
45. Kooij G, Kopplin K, Blasig R, Stuiver M, Koning N, Goverse G, et al. Disturbed function of the blood-cerebrospinal fluid barrier aggravates neuro-inflammation. Acta neuropathologica. 2013. doi: 10.1007/s00401-013-1227-1. PubMed PMID: 24356983.
46. Brightman MW, Reese TS. Junctions between intimately apposed cell membranes in the vertebrate brain. The Journal of cell biology. 1969;40(3):648-77. PubMed PMID: 5765759; PubMed Central PMCID: PMC2107650.
47. Hilhorat TH, Davis DA, Lloyd BJ, Jr. Two morphologically distinct blood-brain barriers preventing entry of cytochrome c into cerebrospinal fluid. Science. 1973;180(4081):76-8. PubMed PMID: 4347993.
48. van Deurs B. Cell junctions in the endothelia and connective tissue of the rat choroid plexus. The Anatomical record. 1979;195(1):73-94. doi: 10.1002/ar.1091950107. PubMed PMID: 496029.
49. Wakai S, Hirokawa N. Development of blood-cerebrospinal fluid barrier to horseradish peroxidase in the avian choroidal epithelium. Cell and tissue research. 1981;214(2):271-8. PubMed PMID: 7471179.
50. Dziegielewska KM, Hinds LA, Mollgard K, Reynolds ML, Saunders NR. Blood-brain, blood-cerebrospinal fluid and cerebrospinal fluid-brain barriers in a marsupial (Macropus eugenii) during development. The Journal of physiology. 1988;403:367-88. PubMed PMID: 3075668; PubMed Central PMCID: PMC1190718.
51. Watson PM, Anderson JM, Vanltallie CM, Doctrow SR. The tight-junction-specific protein ZO-1 is a component of the human and rat blood-brain barriers. Neuroscience letters. 1991;129(1):6-10. PubMed PMID: 1922971.
52. Gath U, Hakvoort A, Wegener J, Decker S, Galla HJ. Porcine choroid plexus cells in culture: expression of polarized phenotype, maintenance of barrier properties and apical secretion of CSF-components. European journal of cell biology. 1997;74(1):68-78. PubMed PMID: 9309392.

53. Lippoldt A, Liebner S, Andbjer B, Kalbacher H, Wolburg H, Haller H, et al. Organization of choroid plexus epithelial and endothelial cell tight junctions and regulation of claudin-1, -2 and -5 expression by protein kinase C. Neuroreport. 2000;11(7):1427-31. PubMed PMID: 10841351.
54. Ek CJ, Habgood MD, Dziegielewska KM, Saunders NR. Structural characteristics and barrier properties of the choroid plexuses in developing brain of the opossum (Monodelphis Domestica). The Journal of comparative neurology. 2003;460(4):451-64. doi: 10.1002/cne.10661. PubMed PMID: 12717706.
55. Johansson PA, Dziegielewska KM, Ek CJ, Habgood MD, Liddelow SA, Potter AM, et al. Blood-CSF barrier function in the rat embryo. The European journal of neuroscience. 2006;24(1):65-76. doi: 10.1111/j.1460-9568.2006.04904.x. PubMed PMID: 16800861.
56. Lagaraine C, Skipor J, Szczepkowska A, Dufourny L, Thiery JC. Tight junction proteins vary in the choroid plexus of ewes according to photoperiod. Brain research. 2011;1393:44-51. doi: 10.1016/j.brainres.2011.04.009. PubMed PMID: 21529785.
57. Redzic ZB. Studies on the human choroid plexus in vitro. Fluids and barriers of the CNS. 2013;10(1):10. doi: 10.1186/2045-8118-10-10. PubMed PMID: 23391221; PubMed Central PMCID: PMC3573900.
58. Stolp HB, Liddelow SA, Sa-Pereira I, Dziegielewska KM, Saunders NR. Immune responses at brain barriers and implications for brain development and neurological function in later life. Frontiers in integrative neuroscience. 2013;7:61. doi: 10.3389/fnint.2013.00061. PubMed PMID: 23986663; PubMed Central PMCID: PMC3750212.
59. Kratzer I, Liddelow SA, Saunders NR, Dziegielewska KM, Strazielle N, Ghersi-Egea JF. Developmental changes in the transcriptome of the rat choroid plexus in relation to neuroprotection. Fluids and barriers of the CNS. 2013;10(1):25. doi: 10.1186/2045-8118-10-25. PubMed PMID: 23915922; PubMed Central PMCID: PMC3737068.
60. Kam KR, Desai TA. Nano- and microfabrication for overcoming drug delivery challenges. Journal of materials chemistry B, Materials for biology and medicine. 2013;1(14):1878-84. doi: 10.1039/C3TB00048F. PubMed PMID: 23730504; PubMed Central PMCID: PMC3666043.
61. Samak G, Gangwar R, Crosby LM, Desai LP, Wilhelm K, Waters CM, et al. Cyclic stretch disrupts apical junctional complexes in Caco-2 cell monolayers by a JNK-2-, c-Src-, and MLCK-dependent mechanism. American journal of physiology Gastrointestinal and liver physiology. 2014;306(11):G947-58. doi: 10.1152/ajpgi.00396.2013. PubMed PMID: 24722904; PubMed Central PMCID: PMC4042113.
62. Ghabriel MN, Zdziarski IM, Leigh C, Vink R. Changes in the blood-CSF barrier in experimental traumatic brain injury. Acta neurochirurgica Supplement. 2010;106:239-45. doi: 10.1007/978-3-211-98811-4_45. PubMed PMID: 19812957.
63. Brady DC, Alan JK, Madigan JP, Fanning AS, Cox AD. The transforming Rho family GTPase Wrch-1 disrupts epithelial cell tight junctions and epithelial morphogenesis. Molecular and cellular biology. 2009;29(4):1035-49. doi: 10.1128/MCB.00336-08. PubMed PMID: 19064640; PubMed Central PMCID: PMC2643799.
64. Ivanov AI, Parkos CA, Nusrat A. Cytoskeletal regulation of epithelial barrier function during inflammation. The American journal of pathology. 2010;177(2):512-24. doi: 10.2353/ajpath.2010.100168. PubMed PMID: 20581053; PubMed Central PMCID: PMC2913378.

65. Angelow S, Zeni P, Hohn B, Galla HJ. Phorbol ester induced short- and long-term permeabilization of the blood-CSF barrier in vitro. Brain research. 2005;1063(2):168-79. doi: 10.1016/j.brainres.2005.09.058. PubMed PMID: 16271356.
66. Abbott NJ. Dynamics of CNS barriers: evolution, differentiation, and modulation. Cellular and molecular neurobiology. 2005;25(1):5-23. PubMed PMID: 15962506.
67. Williams MJ, Lowrie MB, Bennett JP, Firth JA, Clark P. Cadherin-10 is a novel blood-brain barrier adhesion molecule in human and mouse. Brain research. 2005;1058(1-2):62-72. doi: 10.1016/j.brainres.2005.07.078. PubMed PMID: 16181616.
68. Johanson CE, Stopa EG, McMillan PN. The blood-cerebrospinal fluid barrier: structure and functional significance. Methods Mol Biol. 2011;686:101-31. doi: 10.1007/978-1-60761-938-3_4. PubMed PMID: 21082368.
69. Marques F, Sousa JC, Coppola G, Geschwind DH, Sousa N, Palha JA, et al. The choroid plexus response to a repeated peripheral inflammatory stimulus. BMC neuroscience. 2009;10:135. doi: 10.1186/1471-2202-10-135. PubMed PMID: 19922669; PubMed Central PMCID: PMC2784788.
70. Renkin EM. Cellular and intercellular transport pathways in exchange vessels. The American review of respiratory disease. 1992;146(5 Pt 2):S28-31. doi: 10.1164/ajrccm/146.5_Pt_2.S28. PubMed PMID: 1443902.
71. Song L, Pachter JS. Monocyte chemoattractant protein-1 alters expression of tight junction-associated proteins in brain microvascular endothelial cells. Microvascular research. 2004;67(1):78-89. Epub 2004/01/08. PubMed PMID: 14709405.
72. Stamatovic SM, Shakui P, Keep RF, Moore BB, Kunkel SL, Van Rooijen N, et al. Monocyte chemoattractant protein-1 regulation of blood-brain barrier permeability. Journal of cerebral blood flow and metabolism : official journal of the International Society of Cerebral Blood Flow and Metabolism. 2005;25(5):593-606. doi: 10.1038/sj.jcbfm.9600055. PubMed PMID: 15689955.
73. Song L, Ge S, Pachter JS. Caveolin-1 regulates expression of junction-associated proteins in brain microvascular endothelial cells. Blood. 2007;109(4):1515-23. Epub 2006/10/07. doi: 10.1182/blood-2006-07-034009. PubMed PMID: 17023578; PubMed Central PMCID: PMC1794065.
74. Yao Y, Tsirka SE. Truncation of monocyte chemoattractant protein 1 by plasmin promotes blood-brain barrier disruption. Journal of cell science. 2011;124(Pt 9):1486-95. doi: 10.1242/jcs.082834. PubMed PMID: 21486949; PubMed Central PMCID: PMC3078815.
75. Strecker JK, Minnerup J, Schutte-Nutgen K, Gess B, Schabitz WR, Schilling M. Monocyte chemoattractant protein-1-deficiency results in altered blood-brain barrier breakdown after experimental stroke. Stroke; a journal of cerebral circulation. 2013;44(9):2536-44. doi: 10.1161/STROKEAHA.111.000528. PubMed PMID: 23821228.
76. Baruch K, Schwartz M. CNS-specific T cells shape brain function via the choroid plexus. Brain, behavior, and immunity. 2013. doi: 10.1016/j.bbi.2013.04.002. PubMed PMID: 23597431.
77. Schmitt C, Strazielle N, Ghersi-Egea JF. Brain leukocyte infiltration initiated by peripheral inflammation or experimental autoimmune encephalomyelitis occurs through pathways connected to the CSF-filled compartments of the forebrain and midbrain. Journal of neuroinflammation. 2012;9:187. doi: 10.1186/1742-2094-9-187. PubMed PMID: 22870891; PubMed Central PMCID: PMC3458946.

78. Nataf S, Strazielle N, Hatterer E, Mouchiroud G, Belin MF, Ghersi-Egea JF. Rat choroid plexuses contain myeloid progenitors capable of differentiation toward macrophage or dendritic cell phenotypes. Glia. 2006;54(3):160-71. doi: 10.1002/glia.20373. PubMed PMID: 16817190.
79. Steffen BJ, Breier G, Butcher EC, Schulz M, Engelhardt B. ICAM-1, VCAM-1, and MAdCAM-1 are expressed on choroid plexus epithelium but not endothelium and mediate binding of lymphocytes in vitro. The American journal of pathology. 1996;148(6):1819-38. PubMed PMID: 8669469; PubMed Central PMCID: PMC1861637.
80. Wolburg K, Gerhardt H, Schulz M, Wolburg H, Engelhardt B. Ultrastructural localization of adhesion molecules in the healthy and inflamed choroid plexus of the mouse. Cell and tissue research. 1999;296(2):259-69. PubMed PMID: 10382270.
81. Owens T, Bechmann I, Engelhardt B. Perivascular spaces and the two steps to neuroinflammation. Journal of neuropathology and experimental neurology. 2008;67(12):1113-21. doi: 10.1097/NEN.0b013e31818f9ca8. PubMed PMID: 19018243.
82. Brooks TA, Hawkins BT, Huber JD, Egleton RD, Davis TP. Chronic inflammatory pain leads to increased blood-brain barrier permeability and tight junction protein alterations. American journal of physiology Heart and circulatory physiology. 2005;289(2):H738-43. doi: 10.1152/ajpheart.01288.2004. PubMed PMID: 15792985.
83. Raub TJ. Signal transduction and glial cell modulation of cultured brain microvessel endothelial cell tight junctions. The American journal of physiology. 1996;271(2 Pt 1):C495-503. PubMed PMID: 8769988.
84. Bruckener KE, el Baya A, Galla HJ, Schmidt MA. Permeabilization in a cerebral endothelial barrier model by pertussis toxin involves the PKC effector pathway and is abolished by elevated levels of cAMP. Journal of cell science. 2003;116(Pt 9):1837-46. PubMed PMID: 12665564.
85. Kerfoot SM, Long EM, Hickey MJ, Andonegui G, Lapointe BM, Zanardo RC, et al. TLR4 contributes to disease-inducing mechanisms resulting in central nervous system autoimmune disease. J Immunol. 2004;173(11):7070-7. PubMed PMID: 15557205.
86. Racke MK, Hu W, Lovett-Racke AE. PTX cruiser: driving autoimmunity via TLR4. Trends in immunology. 2005;26(6):289-91. doi: 10.1016/j.it.2005.03.012. PubMed PMID: 15922942.
87. Meeker RB, Bragg DC, Poulton W, Hudson L. Transmigration of macrophages across the choroid plexus epithelium in response to the feline immunodeficiency virus. Cell and tissue research. 2012;347(2):443-55. doi: 10.1007/s00441-011-1301-8. PubMed PMID: 22281685; PubMed Central PMCID: PMC3785230.
88. Goverman J, Brabb T, Paez A, Harrington C, von Dassow P. Initiation and regulation of CNS autoimmunity. Critical reviews in immunology. 1997;17(5-6):469-80. PubMed PMID: 9419434.
89. Dragunow M. Meningeal and choroid plexus cells--novel drug targets for CNS disorders. Brain research. 2013;1501:32-55. doi: 10.1016/j.brainres.2013.01.013. PubMed PMID: 23328079.
90. Gonzalez AM, Leadbeater WE, Burg M, Sims K, Terasaki T, Johanson CE, et al. Targeting choroid plexus epithelia and ventricular ependyma for drug delivery to the central nervous system. BMC neuroscience. 2011;12:4. doi: 10.1186/1471-2202-12-4. PubMed PMID: 21214926; PubMed Central PMCID: PMC3025905.

91. Naegele M, Martin R. The good and the bad of neuroinflammation in multiple sclerosis. Handbook of clinical neurology. 2014;122:59-87. doi: 10.1016/B978-0-444-52001-2.00003-0. PubMed PMID: 24507513.
92. Broux B, Stinissen P, Hellings N. Which immune cells matter? The immunopathogenesis of multiple sclerosis. Critical reviews in immunology. 2013;33(4):283-306. PubMed PMID: 23971528.
93. Ortiz GG, Pacheco-Moises FP, Macias-Islas MA, Flores-Alvarado LJ, Mireles-Ramirez MA, Gonzalez-Renovato ED, et al. Role of the blood-brain barrier in multiple sclerosis. Archives of medical research. 2014;45(8):687-97. doi: 10.1016/j.arcmed.2014.11.013. PubMed PMID: 25431839.
94. Meeker RB, Williams K, Killebrew DA, Hudson LC. Cell trafficking through the choroid plexus. Cell adhesion & migration. 2012;6(5):390-6. doi: 10.4161/cam.21054. PubMed PMID: 22902764; PubMed Central PMCID: PMC3496674.
95. Strazielle N, Ghersi-Egea JF. Choroid plexus in the central nervous system: biology and physiopathology. Journal of neuropathology and experimental neurology. 2000;59(7):561-74. PubMed PMID: 10901227.
96. Shrestha B, Paul D, Pachter JS. Alterations in Tight Junction Protein and IgG Permeability Accompany Leukocyte Extravasation Across the Choroid Plexus During Neuroinflammation. Journal of neuropathology and experimental neurology. 2014. doi: 10.1097/NEN.0000000000000127. PubMed PMID: 25289890.
97. Russi AE, Brown MA. The meninges: new therapeutic targets for multiple sclerosis. Translational research : the journal of laboratory and clinical medicine. 2015;165(2):255-69. doi: 10.1016/j.trsl.2014.08.005. PubMed PMID: 25241937.
98. Lee E, Chanamara S, Pleasure D, Soulika AM. IFN-gamma signaling in the central nervous system controls the course of experimental autoimmune encephalomyelitis independently of the localization and composition of inflammatory foci. Journal of neuroinflammation. 2012;9:7. doi: 10.1186/1742-2094-9-7. PubMed PMID: 22248039; PubMed Central PMCID: PMC3293042.
99. Stoolman JS, Duncker PC, Huber AK, Segal BM. Site-specific chemokine expression regulates central nervous system inflammation and determines clinical phenotype in autoimmune encephalomyelitis. J Immunol. 2014;193(2):564-70. doi: 10.4049/jimmunol.1400825. PubMed PMID: 24928987; PubMed Central PMCID: PMC4091641.
100. Gobel K, Bittner S, Ruck T, Budde T, Wischmeyer E, Doring F, et al. Active immunization with proteolipid protein (190-209) induces ascending paralysing experimental autoimmune encephalomyelitis in C3H/HeJ mice. Journal of immunological methods. 2011;367(1-2):27-32. doi: 10.1016/j.jim.2010.12.018. PubMed PMID: 21199659.
101. Howell OW, Schulz-Trieglaff EK, Carassiti D, Gentleman SM, Nicholas R, Roncaroli F, et al. Extensive grey matter pathology in the cerebellum in multiple sclerosis is linked to inflammation in the subarachnoid space. Neuropathology and applied neurobiology. 2014. doi: 10.1111/nan.12199. PubMed PMID: 25421634.
102. Walker-Caulfield ME, Hatfield JK, Brown MA. Dynamic changes in meningeal inflammation correspond to clinical exacerbations in a murine model of relapsing-remitting multiple sclerosis. Journal of neuroimmunology. 2015;278:112-22. doi: 10.1016/j.jneuroim.2014.12.009. PubMed PMID: 25595260.
103. Matsumoto Y, Abe S, Tsuchida M, Hirahara H, Abo T, Shin T, et al. Characterization of CD4-CD8- T cell receptor alpha beta + T cells appearing in the subarachnoid space of rats with

autoimmune encephalomyelitis. European journal of immunology. 1996;26(6):1328-34. doi: 10.1002/eji.1830260623. PubMed PMID: 8647213.
104. Mori Y, Murakami M, Arima Y, Zhu D, Terayama Y, Komai Y, et al. Early pathological alterations of lower lumbar cords detected by ultrahigh-field MRI in a mouse multiple sclerosis model. International immunology. 2014;26(2):93-101. doi: 10.1093/intimm/dxt044. PubMed PMID: 24150245.
105. Arima Y, Harada M, Kamimura D, Park JH, Kawano F, Yull FE, et al. Regional neural activation defines a gateway for autoreactive T cells to cross the blood-brain barrier. Cell. 2012;148(3):447-57. doi: 10.1016/j.cell.2012.01.022. PubMed PMID: 22304915.
106. Arima Y, Kamimura D, Sabharwal L, Yamada M, Bando H, Ogura H, et al. Regulation of immune cell infiltration into the CNS by regional neural inputs explained by the gate theory. Mediators of inflammation. 2013;2013:898165. doi: 10.1155/2013/898165. PubMed PMID: 23990699; PubMed Central PMCID: PMC3748732.
107. Wang Y, Cui L, Gonsiorek W, Min SH, Anilkumar G, Rosenblum S, et al. CCR2 and CXCR4 regulate peripheral blood monocyte pharmacodynamics and link to efficacy in experimental autoimmune encephalomyelitis. Journal of inflammation. 2009;6:32. doi: 10.1186/1476-9255-6-32. PubMed PMID: 19906300; PubMed Central PMCID: PMC2777898.
108. Mahad DJ, Ransohoff RM. The role of MCP-1 (CCL2) and CCR2 in multiple sclerosis and experimental autoimmune encephalomyelitis (EAE). Seminars in immunology. 2003;15(1):23-32. PubMed PMID: 12495638.
109. Barshes N, Demopoulos A, Engelhard HH. Anatomy and physiology of the leptomeninges and CSF space. Cancer treatment and research. 2005;125:1-16. PubMed PMID: 16211880.
110. International Union of Immunological Societies/World Health Organization Subcommittee on chemokine n. Chemokine/chemokine receptor nomenclature. Journal of leukocyte biology. 2001;70(3):465-6. PubMed PMID: 11527998.
111. Mantovani A, Sozzani S, Bottazzi B, Peri G, Sciacca FL, Locati M, et al. Monocyte chemotactic protein-1 (MCP-1): signal transduction and involvement in the regulation of macrophage traffic in normal and neoplastic tissues. Adv Exp Med Biol. 1993;351:47-54. Epub 1993/01/01. PubMed PMID: 7942298.
112. Dzenko KA, Andjelkovic AV, Kuziel WA, Pachter JS. The chemokine receptor CCR2 mediates the binding and internalization of monocyte chemoattractant protein-1 along brain microvessels. J Neurosci. 2001;21(23):9214-23. Epub 2001/11/22. PubMed PMID: 11717355.
113. Stamatovic SM, Keep RF, Kunkel SL, Andjelkovic AV. Potential role of MCP-1 in endothelial cell tight junction 'opening': signaling via Rho and Rho kinase. J Cell Sci. 2003;116(Pt 22):4615-28. Epub 2003/10/25. doi: 10.1242/jcs.00755. PubMed PMID: 14576355.
114. Conductier G, Blondeau N, Guyon A, Nahon JL, Rovere C. The role of monocyte chemoattractant protein MCP1/CCL2 in neuroinflammatory diseases. Journal of neuroimmunology. 2010;224(1-2):93-100. doi: 10.1016/j.jneuroim.2010.05.010. PubMed PMID: 20681057.
115. Semple BD, Frugier T, Morganti-Kossmann MC. CCL2 modulates cytokine production in cultured mouse astrocytes. Journal of neuroinflammation. 2010;7:67. doi: 10.1186/1742-2094-7-67. PubMed PMID: 20942978; PubMed Central PMCID: PMC2964657.
116. Shulman Z, Cohen SJ, Roediger B, Kalchenko V, Jain R, Grabovsky V, et al. Transendothelial migration of lymphocytes mediated by intraendothelial vesicle stores rather

than by extracellular chemokine depots. Nature immunology. 2012;13(1):67-76. doi: 10.1038/ni.2173. PubMed PMID: 22138716.
117. Lee MY, Li H, Xiao Y, Zhou Z, Xu A, Vanhoutte PM. Chronic administration of BMS309403 improves endothelial function in apolipoprotein E-deficient mice and in cultured human endothelial cells. British journal of pharmacology. 2011;162(7):1564-76. doi: 10.1111/j.1476-5381.2010.01158.x. PubMed PMID: 21175571; PubMed Central PMCID: PMC3057294.
118. Song L, Pachter JS. Culture of murine brain microvascular endothelial cells that maintain expression and cytoskeletal association of tight junction-associated proteins. In vitro cellular & developmental biology Animal. 2003;39(7):313-20. Epub 2003/11/14. doi: 10.1290/1543-706X(2003)039<0313:COMBME>2.0.CO;2. PubMed PMID: 14613336.
119. Glabinski AR, Tani M, Tuohy VK, Tuthill RJ, Ransohoff RM. Central nervous system chemokine mRNA accumulation follows initial leukocyte entry at the onset of acute murine experimental autoimmune encephalomyelitis. Brain, behavior, and immunity. 1995;9(4):315-30. doi: 10.1006/brbi.1995.1030. PubMed PMID: 8903849.
120. Juedes AE, Hjelmstrom P, Bergman CM, Neild AL, Ruddle NH. Kinetics and cellular origin of cytokines in the central nervous system: insight into mechanisms of myelin oligodendrocyte glycoprotein-induced experimental autoimmune encephalomyelitis. J Immunol. 2000;164(1):419-26. PubMed PMID: 10605038.
121. Zaheer A, Sahu SK, Wu Y, Zaheer A, Haas J, Lee K, et al. Diminished cytokine and chemokine expression in the central nervous system of GMF-deficient mice with experimental autoimmune encephalomyelitis. Brain research. 2007;1144:239-47. doi: 10.1016/j.brainres.2007.01.075. PubMed PMID: 17316572; PubMed Central PMCID: PMC1899479.
122. Ge S, Pachter JS. Isolation and culture of microvascular endothelial cells from murine spinal cord. Journal of neuroimmunology. 2006;177(1-2):209-14. Epub 2006/06/30. doi: 10.1016/j.jneuroim.2006.05.012. PubMed PMID: 16806499.
123. Ge S, Murugesan N, Pachter JS. Astrocyte- and endothelial-targeted CCL2 conditional knockout mice: critical tools for studying the pathogenesis of neuroinflammation. Journal of molecular neuroscience : MN. 2009;39(1-2):269-83. Epub 2009/04/03. doi: 10.1007/s12031-009-9197-4. PubMed PMID: 19340610; PubMed Central PMCID: PMC2903863.
124. Pierson E, Simmons SB, Castelli L, Goverman JM. Mechanisms regulating regional localization of inflammation during CNS autoimmunity. Immunological reviews. 2012;248(1):205-15. doi: 10.1111/j.1600-065X.2012.01126.x. PubMed PMID: 22725963; PubMed Central PMCID: PMC3678350.
125. Nourshargh S, Hordijk PL, Sixt M. Breaching multiple barriers: leukocyte motility through venular walls and the interstitium. Nature reviews Molecular cell biology. 2010;11(5):366-78. doi: 10.1038/nrm2889. PubMed PMID: 20414258.
126. Fleige S, Walf V, Huch S, Prgomet C, Sehm J, Pfaffl MW. Comparison of relative mRNA quantification models and the impact of RNA integrity in quantitative real-time RT-PCR. Biotechnology letters. 2006;28(19):1601-13. doi: 10.1007/s10529-006-9127-2. PubMed PMID: 16900335.
127. Abbott NJ, Patabendige AA, Dolman DE, Yusof SR, Begley DJ. Structure and function of the blood-brain barrier. Neurobiology of disease. 2010;37(1):13-25. doi: 10.1016/j.nbd.2009.07.030. PubMed PMID: 19664713.

128. Ge S, Song L, Pachter JS. Where is the blood-brain barrier ... really? Journal of neuroscience research. 2005;79(4):421-7. Epub 2005/01/07. doi: 10.1002/jnr.20313. PubMed PMID: 15635601.
129. Yousif S, Marie-Claire C, Roux F, Scherrmann JM, Decleves X. Expression of drug transporters at the blood-brain barrier using an optimized isolated rat brain microvessel strategy. Brain research. 2007;1134(1):1-11. doi: 10.1016/j.brainres.2006.11.089. PubMed PMID: 17196184.
130. Beaulieu E, Demeule M, Ghitescu L, Beliveau R. P-glycoprotein is strongly expressed in the luminal membranes of the endothelium of blood vessels in the brain. The Biochemical journal. 1997;326 (Pt 2):539-44. PubMed PMID: 9291129; PubMed Central PMCID: PMC1218702.
131. Dogan RN, Elhofy A, Karpus WJ. Production of CCL2 by central nervous system cells regulates development of murine experimental autoimmune encephalomyelitis through the recruitment of TNF- and iNOS-expressing macrophages and myeloid dendritic cells. J Immunol. 2008;180(11):7376-84. PubMed PMID: 18490737.
132. Banisadr G, Gosselin RD, Mechighel P, Rostene W, Kitabgi P, Melik Parsadaniantz S. Constitutive neuronal expression of CCR2 chemokine receptor and its colocalization with neurotransmitters in normal rat brain: functional effect of MCP-1/CCL2 on calcium mobilization in primary cultured neurons. The Journal of comparative neurology. 2005;492(2):178-92. doi: 10.1002/cne.20729. PubMed PMID: 16196033.
133. Raghavendra V, Tanga FY, DeLeo JA. Complete Freunds adjuvant-induced peripheral inflammation evokes glial activation and proinflammatory cytokine expression in the CNS. The European journal of neuroscience. 2004;20(2):467-73. doi: 10.1111/j.1460-9568.2004.03514.x. PubMed PMID: 15233755.
134. Wu Z, Zhang J, Nakanishi H. Leptomeningeal cells activate microglia and astrocytes to induce IL-10 production by releasing pro-inflammatory cytokines during systemic inflammation. Journal of neuroimmunology. 2005;167(1-2):90-8. doi: 10.1016/j.jneuroim.2005.06.025. PubMed PMID: 16095726.
135. Haqqani AS, Stanimirovic DB. Prioritization of therapeutic targets of inflammation using proteomics, bioinformatics, and in silico cell-cell interactomics. Methods Mol Biol. 2013;1061:345-60. doi: 10.1007/978-1-62703-589-7_21. PubMed PMID: 23963948.
136. Mitchell K, Yang HY, Berk JD, Tran JH, Iadarola MJ. Monocyte chemoattractant protein-1 in the choroid plexus: a potential link between vascular pro-inflammatory mediators and the CNS during peripheral tissue inflammation. Neuroscience. 2009;158(2):885-95. doi: 10.1016/j.neuroscience.2008.10.047. PubMed PMID: 19032979; PubMed Central PMCID: PMC2668531.
137. Zamboni P, Galeotti R, Menegatti E, Malagoni AM, Tacconi G, Dall'Ara S, et al. Chronic cerebrospinal venous insufficiency in patients with multiple sclerosis. Journal of neurology, neurosurgery, and psychiatry. 2009;80(4):392-9. doi: 10.1136/jnnp.2008.157164. PubMed PMID: 19060024; PubMed Central PMCID: PMC2647682.
138. Zamboni P, Menegatti E, Weinstock-Guttman B, Schirda C, Cox JL, Malagoni AM, et al. The severity of chronic cerebrospinal venous insufficiency in patients with multiple sclerosis is related to altered cerebrospinal fluid dynamics. Functional neurology. 2009;24(3):133-8. PubMed PMID: 20018140.
139. Schwerk C, Rybarczyk K, Essmann F, Seibt A, Molleken ML, Zeni P, et al. TNFalpha induces choroid plexus epithelial cell barrier alterations by apoptotic and nonapoptotic

mechanisms. Journal of biomedicine & biotechnology. 2010;2010:307231. doi: 10.1155/2010/307231. PubMed PMID: 20369072; PubMed Central PMCID: PMC2847764.
140. Colegio OR, Van Itallie CM, McCrea HJ, Rahner C, Anderson JM. Claudins create charge-selective channels in the paracellular pathway between epithelial cells. American journal of physiology Cell physiology. 2002;283(1):C142-7. doi: 10.1152/ajpcell.00038.2002. PubMed PMID: 12055082.
141. Coyne CB, Gambling TM, Boucher RC, Carson JL, Johnson LG. Role of claudin interactions in airway tight junctional permeability. American journal of physiology Lung cellular and molecular physiology. 2003;285(5):L1166-78. doi: 10.1152/ajplung.00182.2003. PubMed PMID: 12909588.
142. Daugherty BL, Ward C, Smith T, Ritzenthaler JD, Koval M. Regulation of heterotypic claudin compatibility. The Journal of biological chemistry. 2007;282(41):30005-13. doi: 10.1074/jbc.M703547200. PubMed PMID: 17699514.
143. Pfeiffer F, Schafer J, Lyck R, Makrides V, Brunner S, Schaeren-Wiemers N, et al. Claudin-1 induced sealing of blood-brain barrier tight junctions ameliorates chronic experimental autoimmune encephalomyelitis. Acta neuropathologica. 2011;122(5):601-14. doi: 10.1007/s00401-011-0883-2. PubMed PMID: 21983942; PubMed Central PMCID: PMC3207130.
144. Pelegri C, Canudas AM, del Valle J, Casadesus G, Smith MA, Camins A, et al. Increased permeability of blood-brain barrier on the hippocampus of a murine model of senescence. Mechanisms of ageing and development. 2007;128(9):522-8. doi: 10.1016/j.mad.2007.07.002. PubMed PMID: 17697702.
145. Lassmann H, Wisniewski HM. Chronic relapsing EAE. Time course of neurological symptoms and pathology. Acta neuropathologica. 1978;43(1-2):35-42. PubMed PMID: 676685.
146. Waksman BH, Adams RD. A histologic study of the early lesion in experimental allergic encephalomyelitis in the guinea pig and rabbit. The American journal of pathology. 1962;41:135-62. PubMed PMID: 14004485; PubMed Central PMCID: PMC1949599.
147. Barkalow FJ, Goodman MJ, Gerritsen ME, Mayadas TN. Brain endothelium lack one of two pathways of P-selectin-mediated neutrophil adhesion. Blood. 1996;88(12):4585-93. PubMed PMID: 8977250.
148. Simmons RD, Bernard CC, Singer G, Carnegie PR. Experimental autoimmune encephalomyelitis. An anatomically-based explanation of clinical progression in rodents. Journal of neuroimmunology. 1982;3(4):307-18. PubMed PMID: 7174784.
149. Demarest TG, Murugesan N, Shrestha B, Pachter JS. Rapid expression profiling of brain microvascular endothelial cells by immuno-laser capture microdissection coupled to TaqMan((R)) low density array. Journal of neuroscience methods. 2012;206(2):200-4. doi: 10.1016/j.jneumeth.2012.02.023. PubMed PMID: 22425714; PubMed Central PMCID: PMC3327762.
150. Monnot AD, Zheng W. Culture of choroid plexus epithelial cells and in vitro model of blood-CSF barrier. Methods Mol Biol. 2013;945:13-29. doi: 10.1007/978-1-62703-125-7_2. PubMed PMID: 23097098.
151. Zheng W, Zhao Q. Establishment and characterization of an immortalized Z310 choroidal epithelial cell line from murine choroid plexus. Brain research. 2002;958(2):371-80. PubMed PMID: 12470873.

152. Tenenbaum T, Steinmann U, Friedrich C, Berger J, Schwerk C, Schroten H. Culture models to study leukocyte trafficking across the choroid plexus. Fluids and barriers of the CNS. 2013;10(1):1. doi: 10.1186/2045-8118-10-1. PubMed PMID: 23305147.
153. Ge S, Song L, Serwanski DR, Kuziel WA, Pachter JS. Transcellular transport of CCL2 across brain microvascular endothelial cells. Journal of neurochemistry. 2008;104(5):1219-32. Epub 2008/02/22. doi: 10.1111/j.1471-4159.2007.05056.x. PubMed PMID: 18289346.

JOURNAL OF NEUROINFLAMMATION

RESEARCH Open Access

The CCL2 synthesis inhibitor *bindarit* targets cells of the neurovascular unit, and suppresses experimental autoimmune encephalomyelitis

Shujun Ge[1*], Bandana Shrestha[1], Debayon Paul[1], Carolyn Keating[1], Robert Cone[2], Angelo Guglielmotti[3] and Joel S Pachter[1]

Abstract

Background: Production of the chemokine CCL2 by cells of the neurovascular unit (NVU) drives critical aspects of neuroinflammation. Suppression of CCL2 therefore holds promise in treating neuroinflammatory disease. Accordingly, we sought to determine if the compound bindarit, which inhibits CCL2 synthesis, could repress the three NVU sources of CCL2 most commonly reported in neuroinflammation – astrocytes, microglia and brain microvascular endothelial cells (BMEC) – as well as modify the clinical course of neuroinflammatory disease.

Methods: The effect of bindarit on CCL2 expression by cultured murine astrocytes, microglia and BMEC was examined by quantitative reverse transcription polymerase chain reaction (qRT-PCR). Bindarit action on mouse brain and spinal cord *in vivo* was similarly investigated by qRT-PCR following LPS injection in mice. And to further gauge the potential remedial effects of bindarit on neuroinflammatory disease, its impact on the clinical course of experimental autoimmune encephalomyelitis (EAE) in mice was also explored.

Results: Bindarit repressed CCL2 expression by all three cultured cells, and antagonized upregulated expression of CCL2 in both brain and spinal cord *in vivo* following LPS administration. Bindarit also significantly modified the course and severity of clinical EAE, diminished the incidence and onset of disease, and evidenced signs of disease reversal.

Conclusion: Bindarit was effective in suppressing CCL2 expression by cultured NVU cells as well as brain and spinal cord tissue *in vivo*. It further modulated the course of clinical EAE in both preventative and therapeutic ways. Collectively, these results suggest that bindarit might prove an effective treatment for neuroinflammatory disease.

Keywords: CCL2, Neuroinflammation, Blood–brain barrier, Neurovascular unit, Brain microvascular endothelial cells, Astrocytes, Microglia

Background

The chemokine CCL2 (formerly called MCP-1) is a critical mediator of neuroinflammation in a myriad of diseases states, including multiple sclerosis (MS) and its animal model experimental autoimmune encephalomyelitis (EAE) [1], HIV-1 encephalitis [2], Guillain-Barré Syndrome [3], Alzheimer's disease [4], ischemia [5], neurotrauma [6], epilepsy [7], neurogenic hypertension [8] and alcoholism [9]. While its precise mechanisms of action remain to be elaborated, among CCL2's widely recognized effects are disruption of the blood–brain barrier (BBB) [10-12] and stimulated migration of mononuclear leukocytes into the central nervous system (CNS) [13-17].

These actions and pathogenic role, along with the fact that constitutive expression of CCL2 in the healthy central nervous system is severely limited [18], render CCL2 an ideal target for therapeutic intervention in neuroinflammatory disease [17,19,20]. Indeed, there is already strong suggestion that pharmacological suppression of CCL2 expression [21,22], oligomerization [23,24] or binding to its cognate receptor, CCR2 [25,26], can

* Correspondence: Ge@uchc.edu
[1]Department of Cell Biology, Blood–brain Barrier Laboratory, 263 Farmington Ave., Farmington, CT 06030, USA
Full list of author information is available at the end of the article

mitigate aspects of EAE. Pharmacologic blockade of CCL2 binding to glycosaminoglycans (GAGs) has also been reported to antagonize an autoimmune inflammatory condition of the neural retina, experimental autoimmune uveitis [27].

While highly effective in moderating neuroinflammation experimentally, many pharmacological agents that abrogate CCL2 expression and/or activity have nevertheless failed clinically. This disappointing performance in clinical trials might stem, in part, from overly broad suppression of microglia and astrocytes, a potential caveat that could curtail beneficial action of these cells in resolving neuroinflammation [28,29], as well as redundancy of chemokine binding sites and targets [30,31]. An alternative approach that more selectively targets CCL2 synthesis might therefore hold therapeutic promise in the treatment of human neuroinflammatory disease.

An attractive candidate in this regard is the well-char acterized compound 2-((1-benzyl-indazol-3-yl) methoxy)-2-methyl propionic acid (bindarit) [32]. A small, synthetic indazolic derivative that preferentially inhibits transcription of the monocyte chemoattractant subfamily of CC chemokines (MCP-1/CCL2, MCP-2/CCL8 and MCP-3/CCL7) [33], bindarit has shown clinical efficacy in a broad array of experimental inflammatory, autoimmune and vascular disorders involving peripheral organ beds [34-38], as well as success in recent clinical trials for diabetic nephropathy [39] and lupus nephritis [40]. Such efficacy has been associated with bindarit's ability to interfere with monocyte recruitment, which is also a critical feature in neuroinflammatory disease [13-17].

Given this clinical history of bindarit suppressing various examples of peripheral inflammation, we investigated its effect on expression of CCL2 in culture by the three cell types that represent the most frequently reported CNS sources of this chemokine during neuroinflammation: astrocytes, microglia and brain microvascular endothelial cells (BMEC). These cells serve as integral components of the neurovascular unit (NVU) [41] and, via their expression of CCL2, can impact the BBB and course of neuroinflammatory disease [42,43]. As a complement to these culture studies, the ability of bindarit to suppress LPS induction of CNS CCL2 expression *in vivo* was well determined. And to gauge bindarit's potential clinical efficacy, its effect on EAE, a prototypical neuroinflammatory disease [44,45], was also examined. Results indicate bindarit significantly suppressed CCL2 gene expression in culture, as well as blunted lipopolysaccharide (LPS)-induced expression of CCL2 in the CNS. It also inhibited various facets of clinical EAE, and showed signs of promoting disease recovery. Collectively, these data suggest that bindarit might offer promise, either alone or in conjunction with other therapies, in the treatment of human neuroinflammatory disease.

Methods

Reagents

All reagents and antibodies were purchased from Sigma-Aldrich (St. Louis, MO, USA), unless specified otherwise. Bindarit was synthesized by and obtained from Angelini (Angelini Research Center-ACRAF, Italy). MOG peptide$_{35-55}$ was synthesized by the WM Keck Biotechnology Resource Center at Yale University, New Haven, CT, USA.

Preparation of bindarit

For experiments with cultured cells, a stock solution of 100 mM bindarit was prepared in dimethyl sulfoxide (DMSO), and dilutions (50, 100, 300 and 500 μM) of the DMSO stock were made in culture medium. For *in vivo* experiments, bindarit was prepared as a suspension in 0.5% methylcellulose (MTC) at a concentration of 20 mg/ml as previously described [37].

Mice

C57BL/6 mice were obtained from the Charles River Laboratories, Inc. (Wilmington, MA, USA). All animal studies were performed, and CO_2-mediated euthanasia carried-out, according to the Animal Care and Guidelines of the University of Connecticut Health Center (Animal Welfare Assurance #A3471-01).

Isolation and culture of mouse astrocytes and microglia

Brain tissue obtained from mice at postnatal days 2 to 3 was used as the source of astrocytes and microglia. After decapitation, brains were removed immediately and separate astrocyte and microglial cultures prepared following a modified version of the protocol described by Ge and Pachter [46]. Cerebral cortices were first cut into small pieces (approximately 1 mm), and the minced tissue incubated in dissecting medium (Hank's Balanced Salt Solution, from Gibco/BRL, Rockville, MD, USA), containing 0.5% glucose, 0.7% sucrose, 20 mM: hydroxyethyl piperazineethanesulfonic acid (Hepes) (pH 7.4) with 0.03% trypsin at 37 °C for 20 to 30 minutes. The tissue extract was then centrifuged at 1000 × g for 5 minutes and the resulting pellet washed and resuspended in astrocyte culture medium (Earl's Modified Eagle Medium, from Gibco/BRL) containing 10% fetal bovine serum, 10% horse serum, 2 mM glutamine, 20 mM D-glucose, 4 mM sodium bicarbonate, 100 μg/ml penicillin and 100 μg/ml streptomycin. The tissue was mildly triturated to produce a single cell suspension, and the dissociated cells plated onto tissue culture flasks (T-75 cm^2) coated with polylysine (BD Biosciences, Bedford, MA, USA). Cultures were maintained up to 1 week in plating medium in a humidified atmosphere (5% CO_2) at 37 °C. After this time, cultures were shaken at 200 rpm for 2 hr at 4 °C, and supernatants containing dislodged microglia collected.

Supernatant material was then centrifuged at 1000 × g for 5 minutes to pellet microglia. Microglia were then resuspended in microglia culture medium (Dulbecco's modified Eagle Medium, from Gibco-BRL) supplemented with 10% heat-inactivated fetal calf serum, 100 μg/ml penicillin and 100 μg/ml streptomycin) and cultured in a 24-well plate. Following removal of microglia from the initial mixed glial cultures, the latter were shaken for an additional 18 hr at 37 °C to remove residual neurons. The enriched astrocyte population that remained was further depopulated of remaining microglia by treatment with L-leucine methyl ester (LME) [47]. LME was dissolved in astrocyte culture medium, and the solution adjusted to pH 7.4 and filtered prior to adding to cultures to achieve a final concentration of 50 mM. After 90 minutes of LME treatment, astrocyte-enriched cultures were washed thoroughly and re-incubated with fresh astrocyte culture medium. Cell purity was determined by immunocytochemistry using a monoclonal anti-human glial fibrillary acid protein (GFAP) antibody, and cultures assessed to be ≥ 98% astrocytes (GFAP+).

Isolation and culture of mouse brain microvascular endothelial cells

BMEC were isolated as previously detailed by this laboratory [10,48]. Primary cultures were typically grown for approximately five days prior to sub-culturing for experiments. At that time, purity was gauged to be ≥ 98% BMEC, according to dil-acetylated LDL uptake [48]. BMEC also exhibited common endothelial characteristics, e.g. CD31 and vWF immunostaining, plus displayed expression of the tight junction-associated proteins ZO-1 and occluding, found enriched at the BBB.

Treatment of cultured cells

To examine effects of bindarit on basal CCL2 expression, cultured microglia and BMEC were incubated with different concentrations of bindarit for 4 hr or exposed to 300 μM bindarit for different time. To gauge effects of bindarit on LPS-stimulated CCL2 expression, astrocytes and microglia were pretreated with 300 μM bindarit for 1 hr; then cells were incubated with ± 100 ng/ml LPS (*Escherichia coli* Serotype 026:B6) for 4 or 20 hr in the continued presence of bindarit. After treatments, cells were extracted for RNA purification.

Separation of brain microvessels and parenchyma

Distinct brain microvessel and parenchymal fractions were obtained using a modification of the method to prepare BMEC [10,48]. In brief, after removal of the brain from the cranium, the meninges and big vessels were discarded, and the whole brain diced into approximately 1 mm pieces. Brain tissue was then homogenized with a 7 mL Dounce tissue grinder (Kimble/Kontes, Vineland, NJ, USA) in PBS. The homogenate was then transferred to a 15 ml conical tube and centrifuged at 400 × g for 15 minutes in an Eppendorf Model 5804R centrifuge/A-4-44 rotor. The resulting pellet was resuspended in 18% dextran (v/v, molecular weight 60 000 to 90 000; USB Corporation, Cleveland, OH, USA) and centrifuged at 4,500 × g for 15 minutes to pellet the crude microvessel fraction. The dextran supernatant and floating layer of myelinated axons were separated from the crude microvessel pellet, then diluted 1:2 with PBS and centrifuged at 720 × g for 10 minutes to sediment the parenchymal fraction. Both microvessel and parenchymal fractions were washed twice with PBS to eliminate traces of dextran. Microvessels were further washed free of blood cells by filtering through a 40 μm cell strainer (Becton Dickinson Labware, Franklin Lakes, IN, USA) and eluting with PBS. Eluted microvessels were pelleted by centrifugation at 16,000 × g in a table-top microcentrifuge.

Treatment of animals

To determine effects of bindarit on LPS-stimulated CCL2 expression in brain and spinal cord, C57BL/6 female mice were given intraperitoneal (i.p.) injection of bindarit (200 mg/kg) or methylcellulose vehicle, once a day, for 4 consecutive days. At 30 minutes following the last bindarit injection, mice were given i.p. injection of LPS (5 mg/kg; *Escherichia coli* Serotype 026:B6). Then, 4 hr after LPS injection, mice were euthanized and brain and spinal cord dissected for CCL2 mRNA and protein analysis.

For active induction of EAE, C57BL/6 female mice were immunized with MOG_{35-55} peptide (MEVGWYRSPFSRVVHLYRNGK) of rat origin, by a modification of the method previously described [49]. Briefly, on day 0 female mice 7 to 9 weeks of age were injected subcutaneously with 150 μg of MOG peptide and 300 μg of *Mycobacterium tuberculosis* (DIFCO, Detroit, MI, USA) in complete Freund's adjuvant (CFA) (DIFCO) into the right and left flank, 100 μl per site. Mice were also injected i.p. with 200 ng pertussis toxin (List Laboratories, Campbell CA, USA) in PBS on days 0 and 2 following the first immunization. Animals were monitored and scored daily for clinical disease severity according to the following scale: 0 = normal; 1 = tail limpness; 2 = limp tail and weakness of hind legs; 3 = limp tail and complete paralysis of hind legs; 4 = limp tail, complete hind leg and partial front leg paralysis; and 5 = death. Several disease parameters were calculated as described [49]. The mean day of onset was calculated by averaging the time when clinical symptoms, that is, a clinical score ≥ 1, were first observed for two consecutive days in each mouse. The mean maximum clinical score was calculated by averaging the highest score for each mouse. The disease index was calculated by

adding the daily average clinical scores in each group, dividing by the mean day of onset, and multiplying by 100. In the case that an animal showed no disease, the day of onset was arbitrarily counted as one day after the last day of the experiment (for example, day 22). And the disease incidence was the fraction of mice experiencing EAE.

To investigate the effects of bindarit on both the clinical course of EAE and CCL2 level during disease, mice were given daily i.p. injection of bindarit (or vehicle MTC) at 200 mg/kg for three consecutive days, beginning the day before MOG immunization (day −1), then injections every other day till day 20. This schedule was designed to mitigate, as much as possible, trauma associated with daily injections at times of peak neurologic disease and physical compromise.

RNA purification from cell cultures

Total RNA was extracted from cell cultures using the RNeasy kit according to the manufacturer's instructions. RNA was treated with Turbo DNAse (Ambion, Austin, TX, USA) according to the protocol provided by the manufacturer. RNA yield and purity were determined by spectrophotometry absorption at 260 and 280 nm.

RNA purification from CNS tissue

RNA and protein were differentially extracted from the same mouse brain and spinal cord samples using the AllPrep RNA/Protein kit (QIAGEN, Valencia, CA) following the manufacturer's instructions. RNA was treated with Turbo DNAse (Ambion, Austin, TX, USA) according to the protocol provided by the manufacturer. RNA yield and purity were determined by spectrophotometry absorption at 260 and 280 nm. Protein level was determined using the Micro BCA protein assay kit (Pierce, Rockford, IL, USA), using bovine serum albumin as a standard.

Reverse transcription

cDNA was synthesized from the total RNA using a SuperScript III (Invitrogen, Carlsbad, CA, USA) First-strand synthesis system for RT-PCR with a standard protocol. The resulting cDNA was stored at −80 °C until used for further analysis.

CCL2 RNA determination by quantitative RT-PCR

Measurements of cDNA levels were performed by quantitative (q) RT-PCR using an ABI PRISM 7500 Sequence Detection System Version 1.3, and SYBR green (AB Applied Biosystems, Foster sity, CA, USA) fluorescence was used to quantify relative amplicon amount. Separate controls included a no template-control and no reverse transcriptase-control, and standard curves were constructed for all primers used. Cycle time (Ct) values for all samples were normalized to RPL-19, the housekeeping gene encoding the 60 S ribosmal protein L19. Specifically, relative amplicon quantification was performed using the formula: $(1 + \mathrm{Eref})\mathrm{Ct}(\mathrm{ref})/(1 + \mathrm{Etarget})\mathrm{Ct}(\mathrm{target})\tilde{n}\ 100\%$, with ref: RPL19; target: CCL2; E: primer pair efficiency; and Ct: threshold cycle.

For all cell culture studies and *in vivo* LPS studies, relative CCL2 gene expression values (after normalization to RPL19) were expressed as percentage of control. For EAE studies, relative CCL2 gene expression values were designated as percentage of RPL-19 expression, as control CCL2 level (time-point 0) was undetectable. The primer sequences used in this study were as following: for mouse CCL2, 5′- GGC TCA GCC AGA TGC AGT TAA-3′ (forward) and 5′- CCA GCC TAC TCA TTG GGA TCA −3′ (reverse); for RPL-19, 5′- CGC TGC GGG AAA AAG AAG-3′ (forward) and 5′- CTG ATC TGC TGA CGG GAG TTG −3′ (reverse).

CCL2 protein determination

The level of CCL2 was measured with mouse JE/CCL2 commercial enzyme-linked immunoassay kit (BioSource International Inc., Camarillo, CA) according to the manufacturer's instructions.

Statistical analysis

Statistical significance of differences between mean values of bindarit-treated cultures and control cultures was analyzed using a paired two-tailed *t*-test, while comparisons of bindarit treatment on LPS-treated mice were performed using a two-tailed *t*-test for independent samples. For analysis of bindarit effects on clinical EAE, a *chi*-squared (χ^2) test was used for comparisons of disease incidence; a Mann–Whitney *U*-test was used for comparisons of disease index; and a two-tailed *t*-test for independent samples was used for comparison of disease onset. A $P\text{-value} < 0.05$ was considered significant in all cases.

Results

Bindarit differentially suppresses CCL2 expression by cultured CNS cells

The effects of bindarit on cultured glial and BMEC were investigated first (Figures 1, 2, 3). Figure 1 shows that cultured microglia demonstrated both a dose and time dependency of bindarit effect on CCL2 mRNA level. Suppression of basal CCL2 mRNA was seen beginning with the lowest dose of 50 μM for 4 hr, amounting to nearly 75% reduction. Increasing the dose to 300 and 500 μM resulted in still further diminution of CCL2 mRNA to approximately 10% and 5%, respectively, of control level. Treatment with bindarit at 300 μM for as little as 2 hr resulted in near 60% reduction in CCL2 mRNA level, and treatment for longer times at this

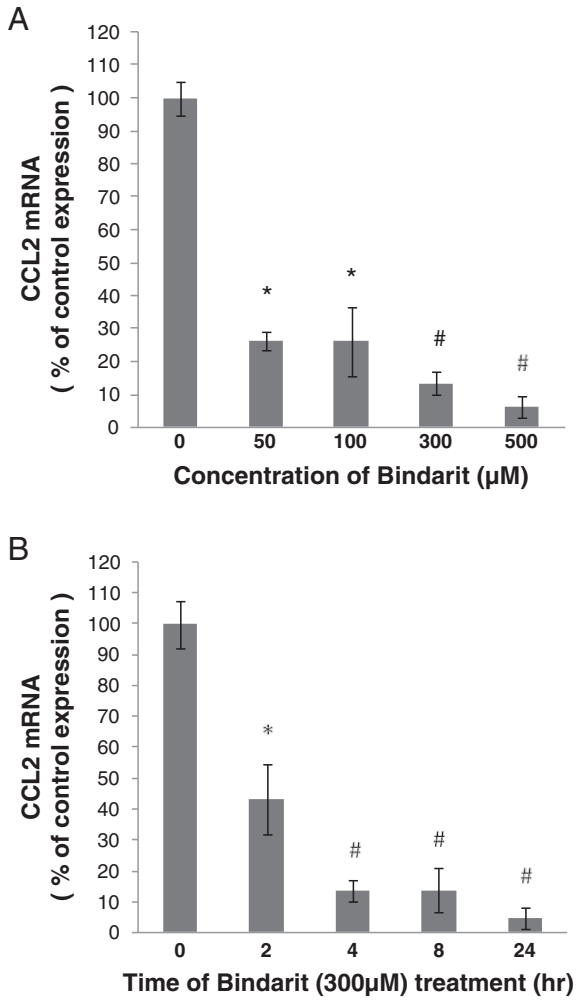

Figure 1 Bindarit effects on CCL2 mRNA in cultured microglia. Microglia, prepared from C57BL/6 mouse brain, were incubated with bindarit at the indicated concentrations for 4 hr **(A)**, or exposed to 300 μM bindarit for the indicated times **(B)**. Control cultures received only vehicle. Relative CCL2 RNA levels were determined by qRT-PCR, and effects of bindarit treatment reported as % change compared to control cultures. $^{*}P < 0.05$; $^{\#}P < 0.01$ (compared to control at 0 concentration or 0 time of bindarit).

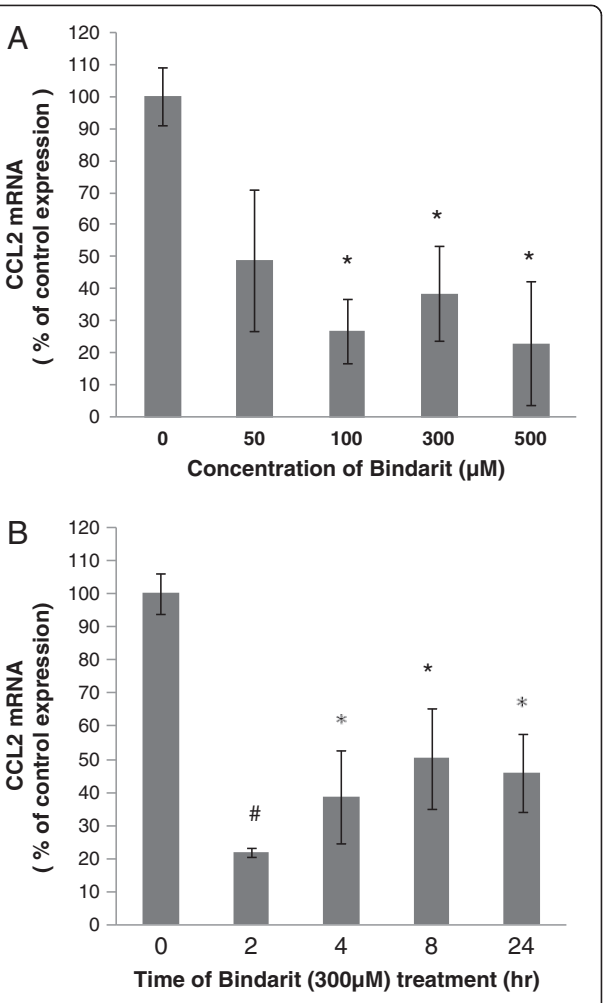

Figure 2 Bindarit effects on CCL2 mRNA in cultured BMEC. Brain microvascular endothelial cells (BMEC), prepared from C57BL/6 mouse brain, were incubated with bindarit at the indicated concentrations for 4 hr **(A)**, or exposed to 300 μM bindarit for the indicated times **(B)**. Control cultures received only vehicle. Relative CCL2 RNA levels were determined by qRT-PCR, and effects of bindarit treatment reported as % change compared to control cultures. $^{*}P < 0.05$; $^{\#}P < 0.01$ (compared to control at 0 concentration or 0 time of bindarit).

concentration resulted in suppression of CCL2 mRNA to ≥ 90% of control level.

BMEC demonstrated a similar qualitative response in basal CCL2 mRNA to increasing bindarit concentration, but suppression was not as severe as seen with microglia (Figure 2). Significant reduction was not observed until 100 μM, and the maximal suppression achieved was about 20% that of control. The time course of bindarit action on BMEC also differed. Maximal suppression by 300 μM bindarit was achieved at the earliest time-point of 2 hr, reaching a level of approximately 20% of that of the control. Longer time-points, however, appeared to result in a lesser effect. It is important to reemphasize that, in the normal CNS, CCL2 expression is barely detectable. This would suggest that both cultured microglia and BMEC, possibly removed from a normally suppressive microenvironment, are in a somewhat activated state.

This situation appears different for astrocytes. In this case, bindarit's effects on constitutive CCL2 gene expression could not be accurately assessed, as level of this chemokine's mRNA in murine culture of these cells is very low. Astrocyte cultures were thus stimulated with LPS for different lengths of time to greatly induce CCL2 mRNA, and the effect of bindarit on this CCL2 induction was assayed (Figure 3A). Stimulation with 100 ng/ml LPS for both 4 hr and 20 hr

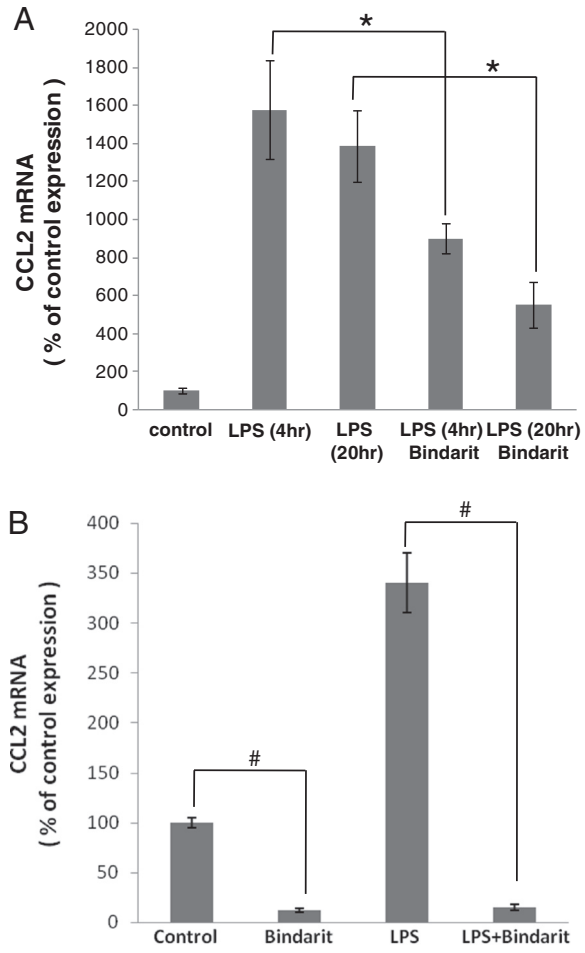

Figure 3 Bindarit effects on LPS-stimulated CCL2 mRNA in cultured astrocytes and microglia. Separate cultures of astrocytes **(A)** and microglia **(B)**, prepared from C57BL/6 mouse brain, were pre-treated with 300 μM bindarit for 1 hr, then incubated with ± 100 ng/ml lipopolysaccharide (LPS) in the continued presence of bindarit. Astrocytes cultures were exposed to LPS for the indicated times to stimulate CCL2 expression. Microglial cultures were only exposed to LPS for 4 hr, as these highly express CCL2 even under basal conditions. Control cultures received only vehicle. Relative CCL2 RNA levels were determined by qRT-PCR, and effects of bindarit treatment reported as % change compared to control cultures. Brackets designate comparison between the two respective groups. $^{*}P < 0.05$; $^{\#}P < 0.01$.

produced similar elevations in CCL2 gene expression, and bindarit treatment at 300 μM similarly suppressed, by 40 to 60%, the induction of CCL2 mRNA at both time-points.

In light of bindarit's success at mitigating induction of CCL2 in astrocytes, we next assayed whether it was similarly effective in preventing induction in LPS-stimulated microglia. Figure 3B shows that this was in fact the case, bindarit completely suppressing the induction and reducing CCL2 mRNA level to 15% of the control (basal) value.

Bindarit blocks LPS-induced CCL2 expression in brain and spinal cord

It was next investigated whether bindarit could suppress LPS-induced CCL2 expression in the CNS *in vivo* (Figure 4). In the normal, resting state, CNS CCL2 mRNA level is barely detectable in C57BL/6 mice [50], but is elevated 50- to 100-fold shortly after peripheral LPS injection [51]. Pretreatment with bindarit was nevertheless able to effectively block this induction both in the brain and spinal cord, by 92% and 86%, respectively. In addition to abrogating LPS-induction of CCL2 mRNA in the CNS, bindarit was also effective at reducing CCL2 protein level in both brain and spinal cord, though not to the same extent as mRNA.

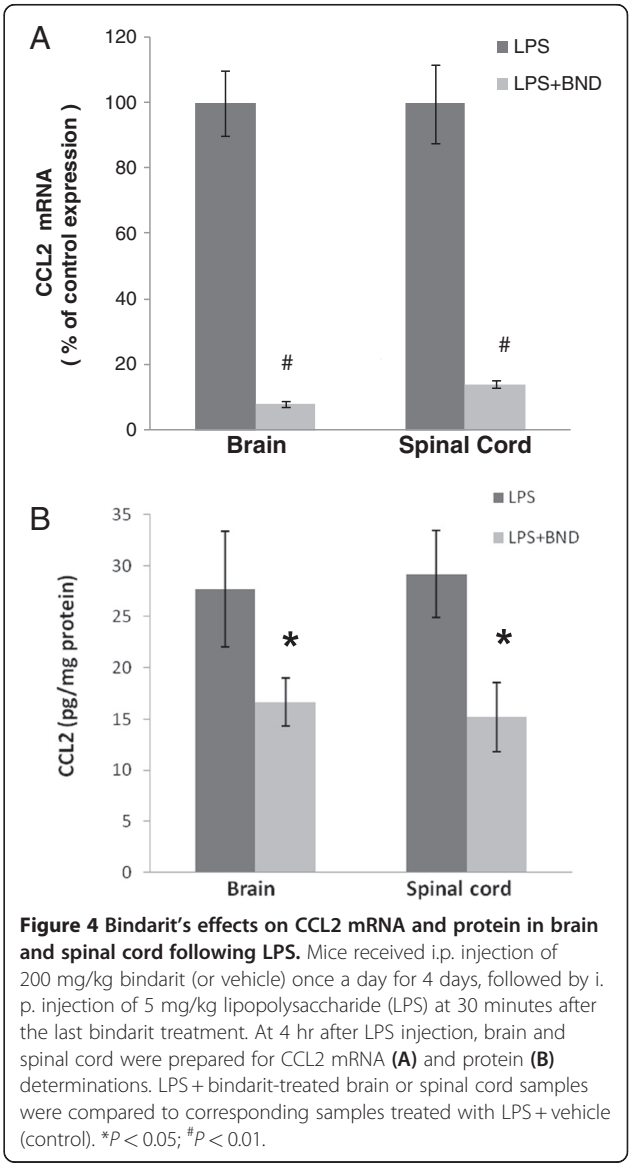

Figure 4 Bindarit's effects on CCL2 mRNA and protein in brain and spinal cord following LPS. Mice received i.p. injection of 200 mg/kg bindarit (or vehicle) once a day for 4 days, followed by i.p. injection of 5 mg/kg lipopolysaccharide (LPS) at 30 minutes after the last bindarit treatment. At 4 hr after LPS injection, brain and spinal cord were prepared for CCL2 mRNA **(A)** and protein **(B)** determinations. LPS + bindarit-treated brain or spinal cord samples were compared to corresponding samples treated with LPS + vehicle (control). $^{*}P < 0.05$; $^{\#}P < 0.01$.

Bindarit therapeutically modifies clinical EAE

The ability of bindarit to modify clinical EAE was examined next. Figure 5 shows that, with a bindarit schedule of daily injections for the first three days, and beginning at day −1, then injections every other day till day 20, bindarit yielded several therapeutic effects. By the criterion that disease is manifest when a clinical score of at least 1 is demonstrated for at least two consecutive days [49], bindarit delayed onset of EAE. Specifically, control mice developed acute disease beginning at day 8, while bindarit-treated mice did not show evidence of clinical disease until days 14 to 15. A second therapeutic effect observed was reduced disease progression and severity. Control mice showed rapid progression of EAE, proceeding towards a maximum mean clinical score of approximately 2.1 to 2.2 by day 9. Bindarit-treated mice evidenced slower progression, and only reached a maximum mean clinical score of 1.5. A third therapeutic effect was apparent reversal of disease course. After experiencing rapid onset, control mice showed a plateau in disease score typical of this monophasic MOG-induced EAE [52,53]. However, in marked distinction, bindarit-treated mice demonstrated a consistent downward trend in disease score following their delayed and attenuated peak in clinical presentation. A summary of the effects of bindarit treatment on clinical EAE is presented in Table 1.

We next sought to examine how bindarit modifies CCL2 expression in the brain during EAE. First, the temporal expression of CCL2 was determined only in MOG-immunized mice not receiving any bindarit, to gauge the window of opportunity during which bindarit might act. As seen in Figure 6, CCL2 RNA is barely detectable at the time of immunization. Its expression then accelerates beginning around day 9, is significantly

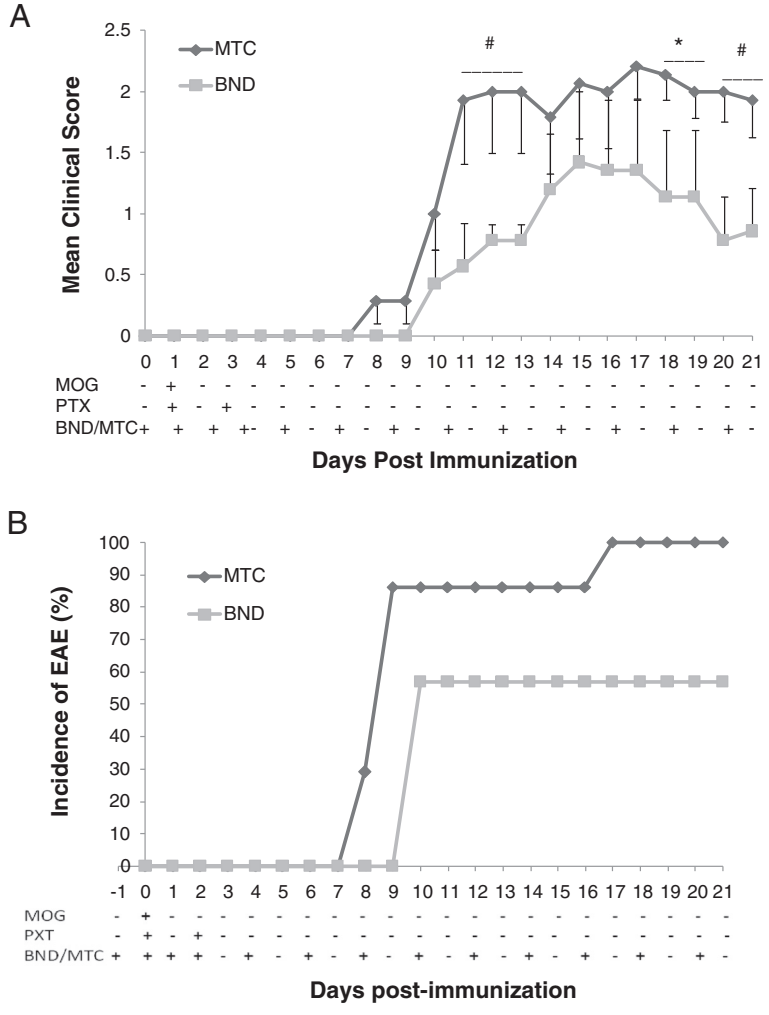

Figure 5 Bindarit effects on clinical experimental autoimmune encephalomyelitis (EAE). Mice were subject to EAE by active immunization with MOG peptide, beginning on day 0, as detailed in Methods. Bindarit (or vehicle) was injected i.p. at 200 mg/kg according to the schedule indicated, beginning at day −1 (one day before MOG immunization). Mean clinical score **(A)** and % incidence of EAE **(B)** were determined. EAE was diagnosed when animals demonstrated a clinical score ≥ 1 for two consecutive days.

Table 1 Summary of bindarit effects on clinical experimental autoimmune encephalomyelitis (EAE) parameters

Group	Sick/total, number	Mean day of onset[a]	Mean max clinical score	Mean disease index[b]
MTC	14/14	11.42 ± 1.76	2.43 ±0.47	163.7 ± 20.53
BND	8/14	16.85 ± 2.17	1.52 ± 0.88	99.3 ± 10.21
P-value	-	<0.005	<0.001	<0.01

Mean presented ± SD.
[a]Day of onset established when clinical score ≥ for two consecutive days.
[b]Disease index calculated at day 21.

elevated by day 14, rapidly declines at day 17, and reaches near basal level by day 21. Because bindarit has been shown to most effectively suppress stimulated, rather than basal, CCL2 expression [33,54], bindarit effects on CCL2 were analyzed selectively during this peak interval. Additionally, brain tissue was resolved into microvascular and parenchymal fractions to further identify targeted cell types. This resolution was deemed important, as both microvessels (BMEC) and parenchymal neural cells (astrocytes and microglia) have been reported as sources of CCL2 during EAE [55-58], though microvessels only contribute < 1% to brain volume [59]. It was thus reasoned that parenchymal effects could overshadow possible bindarit-induced changes in microvascular CCL2 expression if only whole-brain levels were evaluated. Figure 7 reveals that bindarit significantly reduced peak CCL2 expression during EAE in both microvascular and parenchymal fractions, in agreement with what was found in our culture studies. Also, bindarit did not affect CCL2 expression outside the peak window, reinforcing that its action appears restricted to activated cells within and outside the CNS [33,54].

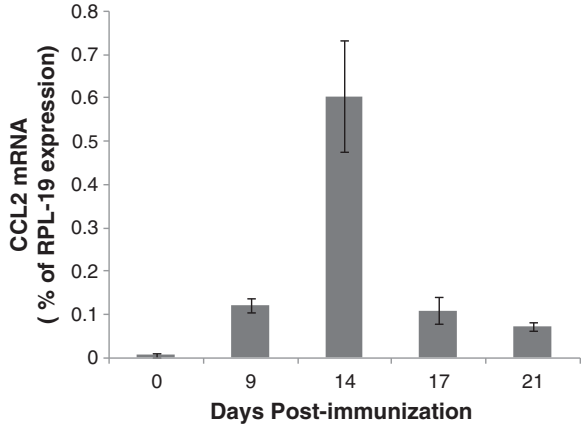

Figure 6 CCL2 expression profile during experimental autoimmune encephalomyelitis (EAE). Mice were immunized with MOG peptide to induce EAE. At the indicated days post-immunization, mice were sacrificed and CCL2 mRNA levels determined in the whole brain. CCL2 expression is seen to rapidly rise and fall between days 9 to 21, showing the highest level at day 14.

Discussion

Given the success of the CCL2 synthesis inhibitor bindarit in ameliorating several animal disease models and human clinical conditions associated with peripheral inflammatory disease, initial studies were conducted to examine its effects on elements critical to neuroinflammatory disease. Focusing on the three main cell types responsible for CCL2 expression during neuroinflammation, experiments revealed bindarit significantly suppressed CCL2 in cultured BMEC, microglia and astrocytes. Bindarit was further shown to be effective *in vivo* in two neuroinflammatory paradigms: 1) it blocked LPS induction of CCL2 in both brain and spinal cord; and 2) it therapeutically modified the course of EAE while suppressing CCL2 expression in both brain microvascular and parenchymal compartments.

As to the effects on the seminal sources of CCL2, it was critical to determine whether each was susceptible to bindarit, as the specific cellular pool(s) responsible for CCL2's pathogenic actions during neuroninflammatory disease remain unclear [51]. While all three cell types responded with significant reduction in CCL2 mRNA, microglia were the most sensitive - experiencing > 90% diminution in this chemokine's expression. This high sensitivity to bindarit holds particular significance, as microglia are widely considered the primary immune effector cells in the CNS [60-63], and their expression of CCL2 has been linked to monocyte recruitment into the CNS [64,65]. As CCL2 can also direct recruitment and proliferation of microglia [66-68], as well as activation of these cells [68], microglial expression of CCL2 can potentially support a self-sustaining cycle of neuroinflammation. Bindarit action, however, might effectively abrogate such a scenario.

That bindarit also suppressed CCL2 mRNA in BMEC is noteworthy. As these cells form the first line of defense in the BBB [69], their expression of CCL2 might strongly influence incipient steps of neuroinflammation [70]. Indeed, elevated CCL2 expression by BMEC has been reported in MS [71] and EAE [55,56], as well as in autoimmune inflammation of the peripheral nervous system [3]. Furthermore, intravenously administered anti-CCL2 antibody blocked heightened leukocyte adhesion to pial venular endothelium *in vivo* in mice suffering acute

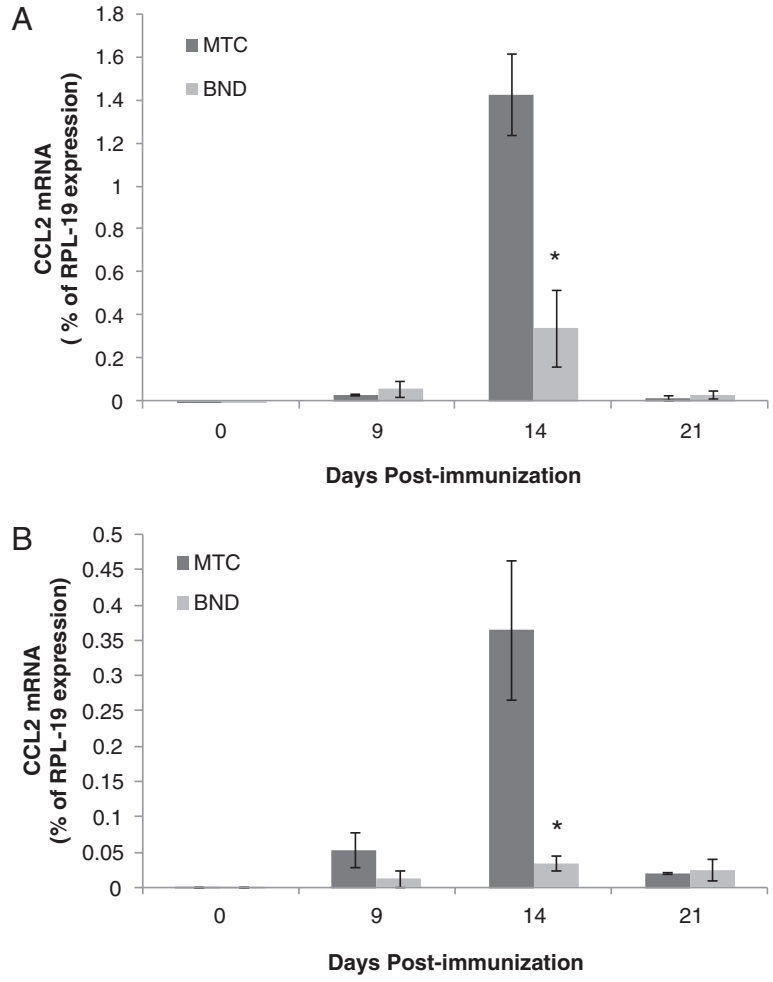

Figure 7 Effects of bindarit on CCL2 expression in central nervous system (CNS) fractions during experimental autoimmune encephalomyelitis (EAE). Mice were immunized with MOG peptide to induce EAE, and were injected with bindarit (or MTC vehicle) as in Figure 5. At the indicated days post-immunization, mice were sacrificed and CCL2 mRNA levels determined in microvascular **(A)** and parenchymal **(B)** fractions. Bindarit treated groups were compared to vehicle treated groups. $^{*}P < 0.01$.

EAE [72], as well as prevented recurring clinical episodes in a chronic relapsing EAE model [73], possibly by antagonizing CCL2 at the luminal endothelial surface. Supporting this possibility, CCL2 harbors in its C-terminal α-helix a binding site for GAGs typically found on the luminal endothelial surface [74], and has been shown to bind to the luminal surface of cultured endothelial cells and then trigger firm adhesion followed by transmigration of mononuclear leukocytes [75,76]. Binding of CCL2 released from BMEC in culture has most recently been shown to switch from the luminal to the abluminal surface following cytokine-induced activation [77], possibly reflecting the changing roles of this chemokine pool from first promoting leukocyte adhesion to later directing extravasation into the parenchyma. Thus, by targeting the BMEC reservoir of CCL2 during disease, bindarit might be able to blunt neuroinflammation at different stages.

Bindarit action on CCL2 expression by cultured astrocytes had to be studied in the context of LPS stimulation, as these cells exhibit barely detectable CCL2 mRNA in culture or *in situ* in the naïve state [50,51]. Yet despite significant induction, astrocyte CCL2 mRNA was reduced by half or more following bindarit exposure. As astrocytes constitute the most abundant glial cell population in the CNS [78], suppression of their CCL2 production by bindarit *in vivo* might well exert profound influence on pathologic events.

That bindarit could indeed act *in vivo* to effectively suppress neuroinflammation was evident in both the LPS and EAE paradigms. Injection of bindarit dramatically reduced LPS-stimulated expression of CCL2 in both brain and spinal cord, dropping mRNA levels to near 10% of vehicle-injected control values, while cutting protein levels approximately by half. In this case, the efficacy of bindarit in suppressing brain CCL2 may have

been aided by the fact that LPS can severely disrupt the BBB [79,80], and thereby possibly facilitate bindarit entry into the CNS parenchyma. As CCL2 can also disrupt tight junctions leading to elevated BBB permeability [10-12], CCL2 generated early after LPS injection may have contributed to its subsequent suppression by further enabling bindarit CNS access.

The effects of bindarit on clinical EAE suggest that bindarit exerted both preventative and therapeutic actions. Preventative action is indicated by the considerable delay in disease onset in the bindarit-treated group, as well as the reduced incidence and severity of disease displayed by these mice. Possible therapeutic action is conveyed by the steady decline in disease severity following diminished peak clinical score. Such decline was in marked contrast to the typical plateau in clinical score exhibited by EAE mice given vehicle. These results are qualitatively similar to those recently reported by Laborde *et al.* [81] who, employing a regimen of twice daily oral dosage of a novel heteroaroylphenylurea antagonist of CCL2 function, also described delayed disease onset and resolution of EAE symptoms. In the case of bindarit, however, clinical symptoms seemed to steadily remit following attenuated peak disease, and a reduced incidence was also noted. Both studies nevertheless highlight the prospect that selective targeting of CCL2 activity might prevent EAE, as well as reverse its course.

The effect of bindarit on clinical EAE was accompanied by significant reduction of CCL2 mRNA in both brain microvessel and parenchymal fractions, consistent with bindarit's mechanism of action being inhibition of CCL2 transcription [33]. Reinforcing this point, global knockout of the CCL2 gene has been shown to similarly delay EAE onset, and reduce both disease incidence and severity, effects that have been attributed to absence of CCL2 expression within the CNS compartment [81,82]. This, along with demonstration that CCL2-deficient mice also exhibit reduced neuroinflammatory responses to peripheral LPS injection [83,84], underscores CCL2's non-redundant role in neuroinflammatory disease and accentuates its value as a therapeutic target. Results with bindarit and EAE may further suggest that both microvascular and parenchymal sources of CCL2 contribute to pathogenesis. If this is so, it could further imply bindarit would not have to penetrate the BBB in order to reach at least one of its targets, BMEC. In contrast to the acute situation with LPS, which acts directly on the endothelium, it is reasoned that the BBB was more intact in EAE mice receiving bindarit, as mean disease score only reached approximately 1.5. Thus, a likely scenario is that bindarit also sufficiently crossed the BBB to suppress the astrocyte and/or microglial response as well. This lends promise that bindarit can access the CNS parenchyma during the early stages of neuroinflammatory disease, when BBB breakdown is not yet manifested.

Conclusions

In summary, the CCL2 synthesis inhibitor bindarit, previously shown to be highly effective in myriad experimental disease models as well as human conditions having inflammatory involvement [34-40], was observed to significantly reduce steady state and LPS-induced CCL2 expression in cultured microglia, BMEC and astrocytes, as well as LPS-stimulated CCL2 mRNA and protein levels in CNS tissue *in situ*. Bindarit was further effective in delaying, preventing and attenuating clinical EAE, and evidenced signs of possibly reversing disease course while also suppressing elevation of CCL2 in brain microvascular and parenchymal compartments. Collectively, these data are consistent with the widely proposed critical role for CCL2 in neuroinflammation [18-20], and suggest bindarit, by targeting cells of the NVU [41], might have therapeutic success in the treatment of MS and/or other human neuroinflammatory diseases.

Abbreviations

BBB: Blood–brain barrier; BMEC: Brain microvascular endothelial cells; CFA: Complete Freund's adjuvant; CNS: Central nervous system; Ct: Cycle time; DMSO: Dimethyl sulfoxide; EAE: Experimental autoimmune encephalomyelitis; GAG: Glycosaminoglycan; GFAP: Glial fibrillary acid protein; Hepes: Hydroxyethyl piperazineethanesulfonic acid; i.p.: Intraperitoneal; LME: L-leucine methyl ester; LPS: Lipopolysaccharide; MTC: Methylcellulose; MS: Multiple sclerosis; NVU: Neurovascular unit; PBS: Phosphate buffered saline; PCR: Polymerase chain reaction; RT: Reverse transcription.

Competing interests

The author(s) declare that they have no competing interests.

Acknowledgements

This work was supported in part by grant R0-1-MH061525 from the National Institutes of Health, and grants PP-1215 and RG-4503A4/1 from the National Multiple Sclerosis Society to JSP. CK was supported by a summer intern fellowship from the University of Connecticut Health Center.

Author details

[1]Department of Cell Biology, Blood–brain Barrier Laboratory, 263 Farmington Ave., Farmington, CT 06030, USA. [2]Department of Immunology, University of Connecticut Health Center, 263 Farmington Ave., Farmington, CT 06030, USA. [3]Angelini R&D, Angelini Research Center, S. Palomba-Pomezia, Rome 00040, Italy.

Authors' contribution

SG, BS, DP and CK performed all the experiments. SG assisted with design of the experiments and data analysis, prepared the figures, and participated in drafting the manuscript. AG and RC assisted with the data analysis. JP designed the experiments and wrote the manuscript. All authors read and approved the final manuscript.

Received: 23 March 2012 Accepted: 12 July 2012
Published: 12 July 2012

References

1. Mahad DJ, Ransohoff RM: **The role of (MCP-1) CCL2 and CCR2 in multiple sclerosis and experimental autoimmune encephalomyelitis (EAE).** *Sem Immunol* 2003, **15**:23–32.

2. Eugenin EA, Osieki K, Lopez L, Goldstein H, Calderon TM, Bruce-Keller AJ, Huaser KF: **CCL2/monocyte chemoattractant protein-1 mediates and enhances transmigration of human immunodeficiency virus (HIV)-infected leukocytes across the blood–brain barrier: a potential mechanism of HIV-CNS invasion and NeuroAIDS.** *J Neurosci* 2006, **26:**1098–1106.
3. Fujioka T, Purev E, Rostami A: **Chemokine mRNA expression in the cauda equina of Lewis rats with experimental allergic neuritis.** *J Neuroimmunol* 1999, **97:**51–59.
4. Hickman SE, El Khoury J: **Mechanisms of mononuclear phagocyte recruitment in Alzheimer's disease.** *CNS Neurol Disord Drug Targets* 2010, **9:**168–173.
5. Chen Y, Hallenbeck JM, Ruetzler C, Bol D, Thomas K, Berman NE, Vogel SN: **Overexpression of monocyte chemoattractant protein-1 in the brain exacerbates ischemic brain injury and is associated with recruitment of inflammatory cells.** *J Cereb Blood Flow Metab* 2003, **23:**748–755.
6. Rancan M, Otto VI, Hans VH, Gerlach I, Jork R, Trentz O, Kossman T, Morganti-Kossman MC: **Upregulation of ICAM-1 and MCP-1, but not MIP-1 and sensorimotor deficit in response to traumatic axonal injury in rats.** *J Neurosci Res* 2001, **63:**438–446.
7. Foresti M, Arisi GM, Katki K, Montanez A, Sanchez RM, Shapiro LA: **Chemokine CCL2 and its receptor CCR2 are increased in the hippocampus following pilocarpine-induced status epilepticus.** *J Neuroinflamm* 2009, **6:**40–50.
8. Waki H, Gouraud SS, Maeda M, Paton JF: **Specific inflammatory condition in nucleus solitarii of the SHR: novel insight for neurogenic hypertension.** *Auton Neurosci* 2008, **142:**25–31.
9. Sullivan EV, Zahr NM: **Neuroinflammation as a neurotoxic mechanism in alcoholism: commentary on "increased MCP-1 and microglia in various regions of human alcoholic brain.** *Exp Neurol* 2008, **213:**10–17.
10. Song L, Pachter JS: **Monocyte chemoattractant protein-1 alters expression of tight junction-associated proteins in brain microvascular endothelial cells.** *Microvasc Res* 2004, **67:**78–89.
11. Stamatovic SM, Keep RF, Kunkel SL, Andjelkovic AV: **Potential role of MCP-1 in endothelial cell tight junction 'opening': signaling via Rho and Rho kinase.** *J Cell Sci* 2003, **116:**4615–4628.
12. Yao Y, Tsirka SE: **Truncation of monocyte chemoattractant protein-1 by plasmin promotes blood–brain barrier disruption.** *J Cell Sci* 2011, **124:**1486–1495.
13. Fuentes ME, Durham SK, Swerdel MR, Lewin AC, Barton DS, Megill JR, Bravo R, Lira SA: **Controlled recruitment of monocytes and macrophages to specific organs through transgenic expression of monocyte chemoattractant protein-1.** *J Immunol* 1995, **155:**5769–5776.
14. Huang D, Tani M, Han Y, He TT, Weaver J, Charo IF, Tuohy VK, Rollins BJ, Ransohoff RM: **Pertussis toxin-induced reversible encephalopathy dependent on monocyte chemoattractant protein-1 overexpression in mice.** *J Neurosci* 2002, **22:**10633–10642.
15. Babcock AA, Kuziel WA, Rivest S, Owens T: **Chemokine expression by glial cells directs leukocytes to sites of axonal injury in the CNS.** *J Neurosci* 2003, **23:**7922–7930.
16. Toft-Hansen H, Buist R, Sun XJ, Schellenberg A, Peeling J, Owens T: **Metalloproteinases control brain inflammation by pertussis toxin in mice overexpressing the chemokine CCL2 in the central nervous system.** *J Immunol* 2006, **177:**7242–7249.
17. Yadav A, Saini V, Avora S: **MCP-1: chemoattractant with a role beyond immunity: a review.** *Clin Chim Acta* 2010, **411:**1570–1579.
18. Dawson J, Miltz W, Mir AK, Weissner C: **Targeting monocyte chemoattractant protein-1 signalling in disease.** *Expert Opin Ther Targets* 2003, **7:**35–48.
19. Izikon L, Klein RS, Luster AD, Weiner HL: **Targeting monocyte recruitment in CNS autoimmune disease.** *Clin Immnunol* 2002, **103:**125–131.
20. Semple BD, Kossman T, Morganti-Kossman MC: **Role of chemokines in CNS health and pathology: a focus on the CCL2/CCR2 and CXCL8/CCR2 networks.** *J Cereb Blood Flow Metab* 2010, **30:**459–473.
21. Karpus WJ, Reynolds N, Behanna HA, Van Eldik LJ, Watterson DM: **Inhibition of experimental autoimmune encephalomyelitis by a novel small molecular weight proinflammatory cytokine suppressing drug.** *J Neuroimmunol* 2008, **203:**73–78.
22. Guo X, Nakamura K, Kohyama K, Harada C, Behanna HA, Watterson DM, Matsumoto Y, Harada T: **Inhibition of glial activation ameliorates the severity of experimental autoimmune encephalomyelitis.** *Neurosci Res* 2007, **59:**457–466.
23. Handel TM, Johnson Z, Rodrigues DH, dos Santos AC, Cirillo R, Muzio V, Riva S, Mack M, Deruaz M, Borlat F, Vitte P-A, Wells TNC, Teixera MM, Proudfoot AEI: **An engineered monomer of CCL2 has antiinflammatory properties emphasizing the importance of oligomerization for chemokine activity in vivo.** *J Leuk Biol* 2008, **84:**1101–1108.
24. Brini E, Ruffini F, Bergamin A, Brambilla E, Dati G, Greco B, Cirillo R, Proudfoot AEI, Comi G, Furlan R, Zaratin P, Martino G: **Administration of a monomeric CCL2 variant to EAE mice inhibits inflammatory cell recruitment and protects from demyelination and axonal loss.** *J Neuroimmunol* 2009, **209:**33–39.
25. Brodmerkel CM, Huber R, Covington M, Diamond S, Hall L, Collins R, Leffet L, Gallagher K, Feldman P, Collier P, Stow M, Gu X, Baribund F, Shin N, Thomas B, Burn T, Hollis G, Yeleswaram S, Solomon K, Friedman S, Wang A, Xue CB, Newton RC, Scherle P, Vaddi K: **Discovery and pharmacological characterization of a novel rodent-active CCR2 antagonist, INCB334.** *J Immunol* 2005, **175:**5370–5378.
26. Wang Y, Cui L, Gonsiorek W, Min S-H, Anilkumar G, Rosenblum S, Kozlowski J, Lundell D, Fine JS, Grant EP: **CCR2 and CXCR4 regulate peripheral blood monocyte pharmacodynamics and link to efficacy in experimental autoimmune encephalomyelitis.** *J Neuroinflamm.* 2009, **6:**32–46.
27. Piccinini AM, Kneble K, Rek A, Wildner G, Diedrichs-Mohring M, Kungle AJ: **Rationally evolving MCP-1/CCL2 into a decoy protein with potent anti-inflammatory activity in vivo.** *J Biol Chem* 2010, **285:**8782–8792.
28. Gay F: **Activated microglia in primary progressive MS lesions: defenders or aggressors?** *Int Ms* 2007, **14:**78–83.
29. Sanders P, De Kayser J: **Janus faces of microglia in multiple sclerosis.** *Brain Res Rev* 2007, **54:**274–285.
30. Ghandi NS, Mancera RL: **The structure of glycosaminoglycans and their interactions with proteins.** *Chem Biol Des* 2008, **72:**455–482.
31. Horuk R: **Chemokine receptor antagonists: overcoming developmental hurdles.** *Nat Rev Drug Disc* 2009, **8:**23–33.
32. Cioli V, Ciarniello MG, Guglielmotti A, Luparini MR, Durando L, Martinelli B, Catanese B, Fava L, Silvestrini B: **A new possible protein antidenaturant agent, bindarit, reduces secondary phase adjuvant arthritis in rats.** *J Rheumatol* 1992, **19:**1735–1742.
33. Mirolo M, Fabbri M, Sironi M, Vecchi A, Guglielmotti A, Mangano G, Biondi G, Locati M, Mantovani A: **Impact of the anti-inflammatory agent bindarit on the chemokinome: selective inhibition of the monocyte chemoattractant proteins.** *Eur Cytokine Netw* 2008, **19:**119–122.
34. Bhatia M, Ramath RD, Chevali L, Guglielmotti A: **Treatment with bindarit, a blocker of MCP-1 synthesis, protects mice against acute pancreatitis.** *Am J Physiol Gastrointest Liver Physiol* 2005, **288:**G1259–G1265.
35. Guglielmotti A, D'Onofrio E, Coletta I, Aquilini L, Milanese C, Pinza M: **Amelioration of rat adjuvant arthritis by therapeutic treatment with bindarit, an inhibitor of MCP-1 and TNF-alpha production.** *Inflamm Res* 2002, **51:**252–258.
36. Guglielmotti A, Aquilini L, D'Onofrio F, Rosignoli MT, Milanese C, Pinza M: **Bindarit prolongs survival and reduces renal damage in NZB/W lupus mice.** *Clini Exp Rheumatol* 1998, **16:**149–154.
37. Grassia G, Maddaluno M, Guglielmotti A, Mangano G, Biondi G, Maffia P, Ialenti A: **The anti-inflammatory agent bindarit inhibits neointima formation in both rats and hyperlipodaemic mice.** *Cardiovasc Res* 2009, **84:**485–493.
38. Lin J, Zhu X, Chade A, Jordan KL, Lavi R, Daghini E, Gibson ME, Guglielmotti A, Lerman A, Lerman LO: **Monocyte chemoattractant proteins mediate microvascular dysfunction in swine renovascular hypertension.** *Arterioscler Thromb Vasc Biol* 2009, **29:**1810–1816.
39. Ruggenenti P: **Effects of MCP-1 inhibition by bindarit therapy in type 2 diabetes subjects with micro- or macro-albuminuria.** *J Am Soc Nephrol* 2009, **21:**44A [Abstract].
40. Ble A, Mosca M, Di Loreto G, Guglielmotti A, Biondi G, Bombardieri S, Remuzzi G, Ruggenenti P: **Antiproteinuric effect of chemokine cc-motif ligand 2 inhibition in subjects with acute proliferative lupus nephritis.** *Am J Nephrol* 2011, **34:**367–372.
41. Vangilder RL, Rosen CL, Barr TL, Huber JD: **Targeting the neurovascular unit for treatment of neurological disorders.** *Pharmacol Ther* 2011, **139:**239–247.
42. Mahad D, Callaghan MK, Williams KA, Ubogu EE, Kivisakk P, Tucky B, Kidd G, Kingsbury GA, Change A, Fox RJ, Mack M, Sniderman MB, Ravid R, Staugaitis SM, Stins MF, Ransohoff RM: **Modulating CCR2 and CCL2 at the blood–brain barrier: relevance for multiple sclerosis pathogenesis.** *Brain* 2006, **129:**212–223.

43. Conductier G, Blondeau N, Guyon A, Nahon JL, Rovere C: **The role of monocyte chemoattractant protein MCP-/CCL2 in neuroinflammatory diseases.** *J Neuroimmunol* 2010, **224:**93–100.
44. Baxter AG: **The origin and application of experimental autoimmune encephalomyelitis.** *Nat Rev Immunol* 2007, **7:**904–912.
45. Krishnamoorthy G, Wekerle H: **EAE: an immunologist's magic eye.** *Eur J Immunol* 2009, **39:**2031–2035.
46. Ge S, Pachter JS: **Caveolin-1 knockdown by small interfering RNA suppresses responses to the chemokine monocyte chemoattractant protein-1 by human astrocytes.** *J Biol Chem* 2004, **2004**(279):6688–6695.
47. Hamby ME, Uliasz TF, Hewett SJ, Hewett JA: **Characterization of an improved procedure for the removal of microglia from confluent monolayers of primary astrocytes.** *J Neurosci Methods* 2006, **150:**128–137.
48. Song L, Pachter JS: **Culture of murine brain microvascular endothelial cells that maintain expression and cytoskeletal association of tight junction-associated proteins.** *In Vitro Cell Devel Biol* 2003, **39:**313–320.
49. Suen WE, Bergman CM, Hjelstrom P, Ruddle NH: **A critical role for lymphotoxin in experimental allergic encephalomyelitis.** *J Exp Med* 1997, **1865:**1233–1240.
50. Juedes AE, Hjlemstrom P, Bergman CM, Neild L, Ruddle NH: **Kinetics and cellular origin of cytokines in the central nervous system: Insight into mechanisms of myelin oligodendrocyte glycoprotein-induced experimental autoimmune encephalomyelitis.** *J Immunol* 2000, **164:**410–426.
51. Ge S, Murugesan N, Pachter JS: **Astrocyte- and Endothelial-Targeted CCL2 Conditional Knockout Mice: Critical Tools for Studying the Pathogenesis of Neuroinflammation.** *J Mol Neurosci* 2009, **39:**269–283.
52. Stromnes I, Goverman J: **Active induction of experimental allergic encephalomyelitis.** *Nat Protoc* 2006, **1:**1810–1819.
53. Jones MV, Nguyen TT, Beboy CA, Griffin JW, Whartenby KA, Kerr DA, Calabresi PA: **Behavioral and pathological outcomes in MOG 35–55 experimental autoimmune encephalomyelitis.** *J Neuroimmunol* 2008, **199:**83–93.
54. Mora E, Guglielmotti A, Biondi G, Sassone-Corsi P: **Bindarit: an anti-inflammatory small molecule that modulates the NFkB pathway.** *Cell Cycle* 2012, **11:**159–169.
55. Berman JW, Guida MP, Warren J, Amat J, Brosnan CF: **Localization of monocyte chemoattractant protein-1 expression in the central nervous system in experimental autoimmune encephalomyelitis and trauma in the rat.** *J Immunol* 1996, **156:**3017–3023.
56. Adamus G, Machnicki M, Amundson D, Adlard K, Offner H: **Similar pattern of CCL2 expression in spinal cords and eyes of Lewis rats with experimental autoimmune encephalomyelitis. Associated uveitis.** *J Neurosci Res* 1997, **50:**531–538.
57. Basso AS, Frenkel D, Quintana FJ, Costa-Pinto FA, Petrovic-Stojkovic S, Puckett L, Monsonegro A, Bar-Shir A, Engel Y, Gozin M, Weiner HL: **Reversal of axonal loss and disability in a mouse model of progressive multiple sclerosis.** *J Clin Invest* 2008, **118:**1532–1543.
58. Tokuhara N, Namiki K, Uesigi M, Miyamoto C, Ohgoh M, Ido K, Yoshinaga T, Yamauchi T, Kuromitsu J, Kimura S, Miyamoto N, Kasuya Y: **N-type calcium channel in the pathogenesis of experimental autoimmune encephalomyelitis.** *J Biol Chem* 2010, **285:**33294–33306.
59. Yi J, Boado RJ, Pardridge WM: **Blood–brain barrier genomics.** *J Cereb Blood Flow Metab* 2001, **21:**61–68.
60. Carson MJ: **Microglia as liaisons between the immune and central nervous systems: functional implications for multiple sclerosis.** *Glia* 2002, **40:**218–231.
61. Milner R, Campbell IL: **The extracellular matrix and cytokines regulate microglial integrin expression and activation.** *J Immunol* 2003, **170:**3850–3858.
62. Kim SU, de Vellis J: **Microglia in health and disease.** *J Neurosci Res* 2005, **81:**302–313.
63. Lehnardt S: **Innate immunity and neuroinflammation in the CNS: the role of microglia in Toll-like receptor-mediated neuronal injury.** *Glia* 2010, **58:**253–283.
64. D'Mello C, Le T, Swain MG: **Cerebral microglia recruit monocytes into the brain in response to tumor necrosis factor alpha signaling during peripheral inflammation.** *J Neurosci* 2009, **2009:**2089–2912.
65. Yao H, Yang Y, Kim KJ, Bethel-Brown C, Gong N, Funa K, Gendelman HE, Su TP, Wang JQ, Buch S: **Molecular mechanisms involving sigma receptor-mediated induction of MCP-1: implication for increased monocyte transmigration.** *Blood* 2010, **115:**4951–4962.
66. Deng YY, Lu J, Ling EA, Kaur C: **Monocyte chemoattractant protein-1 (MCP-1) produced via NF-kappaB signaling pathway mediates migration of amoeboid microglia in the periventricular white matter in hypoxic neonatal rats.** *Glia* 2009, **57:**604–621.
67. Hinojosa AE, Garcia-Bueno B, Leza JC, Madrigal JL: **CCL2/MCP-1 modulation of microglial activation and proliferation.** *J Neuroinflamm.* 2011, **8:**77–86.
68. Thacker MA, Thacker MA, Clark AK, Bishop T, Grist J, Yip PK, Moon LD, Thompson SW, Marchand F, McMahon SB: **CCL2 is key player of microglial activation in neuropathic pain states.** *Eur J Pain* 2009, **13:**263–272.
69. Zeevi N, Pachter J, McCullough LD, Wolfson L, Kuchel GA: **The blood–brain barrier: geriatric relevance of a critical brain-body interface.** *J Am Geriatr Soc* 2010, **58:**1749–1757.
70. Greenwood J, Heasman SJ, Alvaraez JI, Prat A, Lyck R, Engelhardt B: **Review: leukocyte-endothelial cell crosstalk at the blood–brain barrier: a prerequisite for successful immune cell entry to the brain.** *Neuropathol Appl Neurobiol* 2011, **37:**24–39.
71. Subileau EA, Rezaie P, Davies HA, Colyer FM, Greenwood J, Male DK, Romero IA: **Expression of chemokines and their receptors by human brain endothelium: implications for multiple sclerosis.** *J Neuropathol Exp Neurol* 2009, **68:**227–240.
72. dos Santos AC, Barsante MM, Arantes RME, Bernard CCA, Teixera MM, Carvalho-Tavares J: **CCL2 and CCL5 mediate leukocyte adhesion in experimental autoimmune encephalomyelitis – an intravital microscopy study.** *J Neuroimmunol* 2005, **162:**122–129.
73. Kennedy KJ, Streiter RM, Kunkel SL, Lukacs NW, Karpus WJ: **Acute and relapsing autoimmune encephalomyelitis are regulated by differential expression of the CC chemokines macrophage inflammatory protein-1α and monocyte chemoattractant protein-1.** *J Neuroimmunol* 1998, **92:**98–108.
74. Chakravarty L, Rogers L, Quach T, Breckenridge S, Kolattukudy PE: **Lysine 58 and histidine 66 at the C-terminal alpha helix of monocyte chemoattractant protein-1 are essential for glycosaminoglycan binding.** *J Biol Chem* 1998, **273:**29641–29647.
75. Gerzten RE, Garcia-Zapeda EA, Lim Y-C, Yoshida M, Ding H, Gimbrone MA, Luster AD, Luscinskas FW, Rosenzweig A: **MCP-1 and IL-8 trigger firm adhesion of monocytes to vascular endothelium under flow conditions.** *Nature* 1999, **398:**718–723.
76. Hardy LA, Booth TA, Lau EK, Handel TM, Ali S, Kirby JA: **Examination of CCL2 partitioning and presentation during transendothelial migration.** *Lab Invest* 2004, **84:**81–90.
77. Chui R, Dorovini-Zis K: **Regulation of CCl2 and CCL3 expression in human brain endothelial cells by cytokines and lipopolysaccharide.** *J Neuroinflamm.* 2010, **7:**1–12.
78. Farina C, Aloisi F, Meinl E: **Astrocytes are active players in cerebral innate immunity.** *Trends Immunol* 2007, **28:**138–145.
79. Banks WA, Erickson MA: **The blood–brain barrier and immune function and dysfunction.** *Neurobiol Dis* 2010, **37:**26–32.
80. Aid S, Silva AC, Candelario-Jalil E, Choi SH, Rosenberg GA, Bosetti F: **Cyclooxygenase-1 and −2 differentially modulate lipopolysaccharide-induced blood–brain barrier disruption through matrix metalloproteinase activity.** *J Cereb Blood Flow Metab* 2010, **30:**370–380.
81. Laborde E, Macsata RW, Meng F, Peterson BT, Robinson L, Schow SR, Simon RJ, Xu H, Baba K, Inagaki H, Ishiwata Y, Jomori T, Matsumoto Y, Miyachi A, Nakamura T, Okamoto M, Handel TM, Bernard CCA: **Discovery, optimization, and pharmacological characterization of novel heteroaryoylphenylureas antagonists of C-C ligand 2 function.** *J Med Chem* 2011, **54:**1667–1681.
82. Huang DR, Wang J, Kivisakk P, Rollins BJ, Ransohoff RM: **Absence of monocyte chemoattractant protein 1 in mice leads to decreased local macrophage recruitment and antigen-specific T helper cell type 1 immune response in experimental autoimmune encephalomyelitis.** *J Exp Med* 2001, **193:**713–726.
83. Dogan RN, Elhofy A, Karpus WJ: **Production of CCL2 by central nervous system cells regulates development of murine experimental**

autoimmune encephalomyelitis through the recruitment of TNF- and INOS-expressing macrophages and myeloid dendritic cells. *J Immunol* 2008, **180**:7376–7384.

84. Thompson WL, Karpus WJ, Van Eldick LJ: **MCP-1-deficient mice show reduced neuroinflammatory responses and increased peripheral inflammatory responses to peripheral endotoxin insult.** *J Neuroinflammation* 2008, **15**:5–35.

doi:10.1186/1742-2094-9-171
Cite this article as: Ge *et al.*: The CCL2 synthesis inhibitor *bindarit* targets cells of the neurovascular unit, and suppresses experimental autoimmune encephalomyelitis. *Journal of Neuroinflammation* 2012 **9**:171.

Journal of Neuroscience Methods 206 (2012) 200–204

Contents lists available at SciVerse ScienceDirect

Journal of Neuroscience Methods

journal homepage: www.elsevier.com/locate/jneumeth

Basic Neuroscience
Short communication

Rapid expression profiling of brain microvascular endothelial cells by immuno-laser capture microdissection coupled to TaqMan® Low Density Array

Tyler G. Demarest, Nivetha Murugesan, Bandana Shrestha, Joel S. Pachter*

Blood-Brain Barrier Laboratory, Department of Cell Biology, University of Connecticut Health Center, 263 Farmington Ave., Farmington, CT 06030, United States

ARTICLE INFO

Article history:
Received 23 January 2012
Received in revised form 21 February 2012
Accepted 27 February 2012

Keywords:
Laser capture microdissection
Brain microvascular endothelial cells
Gene expression profiling
Microarray
TLDA

ABSTRACT

Immuno-laser capture microdissection (immuno-LCM) enables highly selective retrieval of designated cell populations from their *in situ* locations in complex tissue like the brain. However, the amount of tissue acquired by immuno-LCM is extremely limited, and the RNA purification, amplification and labeling steps necessary for expression analysis by hybridization microarray are tedious and time consuming. This report therefore describes a protocol in which these RNA steps are eliminated altogether, yet allows for global gene profiling. Specifically, immuno-LCM tissue was solubilized and the extract directly subjected to reverse transcription to generate cDNA. Pre-amplification of cDNA was performed next, and then relative expression of 96 different immune-related genes simultaneously determined by quantitative real-time PCR using a microfluidic card TaqMan® Low Density Array (TLDA). This protocol was highly reproducible and extremely sensitive, demonstrating high correlation of raw Ct values among both technical and biological replicate samples when using only 1/32 of total pre-amplified cDNA obtained from as little as 500 LCM 'shots.' As this abridged protocol takes only approximately 7 h from LCM tissue acquisition to analysis by TLDA, it can prove a very effective tool for both screening and validation purposes when investigating gene regulation in health and disease of the nervous system and other tissues.

1. Introduction

The endothelium shows considerable phenotypic and molecular diversity along the CNS vascular tree (Ge et al., 2005). *Segmental heterogeneity* exists between the endothelium of parenchymal microvessels (*e.g.*, arterioles, capillaries and venules) and surface macrovessels (*e.g.*, arteries and veins), and even between the endothelium of the respective microvascular tributaries. There is also *regional heterogeneity* between the endothelium of similar type vessel segments within different CNS regions.

Endothelial heterogeneity poses challenges to studying CNS vascular gene expression. Whole brain and/or spinal cord homogenates suffer from pooling different vascular segments from different CNS regions, providing at best a mosaic of endothelial subtypes. This can lead to significant misinterpretation of vascular function. A means to enrich for specific endothelial populations, coupled to a platform to quantitatively analyze gene expression efficiently, is needed to accurately assess the CNS endothelium in health and disease.

Laser capture microdissection (LCM) enables selective isolation of cells from microscopic samples of tissue (Espina et al., 2007) – and presents opportunity to exploit CNS endothelial heterogeneity in depth. This laboratory showed that, when guided by combined immunohistochemistry/immunofluorescence and coupled to SYBR® Green-based, quantitative real-time PCR (qrt-PCR), *immuno-LCM* allowed analysis of endothelial gene expression in separate populations of CNS arterioles, capillaries and venules (Macdonald et al., 2010).

Coupling gene expression to LCM has nonetheless been encumbered by the rigors of isolating intact RNA from mere fractions of cells and, thus, largely limited to analyzing only a few genes at a time. Moreover, isolating RNA on such a small scale from multiple samples can become unmanageable in time and cost. A method that would avoid time-consuming and inefficient RNA isolation, yet allow for more extensive gene profiling, would thus be advantageous.

Here we describe a novel protocol, whereby brain microvascular endothelial cell (BMEC) tissue retrieved by LCM is lysed and directly reverse-transcribed, then subject to pre-amplification of cDNA, and analyzed by TaqMan® Low Density Array (TLDA) for simultaneous assessment of 96 different genes. Significantly, the high sensitivity of this approach enables analysis of a modest amount of LCM tissue

* Corresponding author. Tel.: +1 860 679 3698.
E-mail address: pachter@nso1.uchc.edu (J.S. Pachter).

0165-0270/$ – see front matter © 2012 Elsevier B.V. All rights reserved.
doi:10.1016/j.jneumeth.2012.02.023

that can be quickly acquired, allowing *in situ* gene profiling on this global scale to be completed in approximately 7.0 h from beginning to end.

2. Materials and methods

Specific aspects of immuno-LCM, including examples of immunostained tissue, discussion of tissue preservation and confirmation of endothelial purity, have been elaborated in previous reports from this laboratory (Kinnecom and Pachter, 2005; Macdonald et al., 2008), and not reiterated here. Where appropriate, approximate times are indicated below next to individual steps in the immuno-LCM/TLDA protocol, to allow comparison to other procedures used for global gene profiling.

2.1. Animals

Female C57 BL/6 mice, age 8–10 weeks and obtained from Charles River Laboratories, Inc. (Wilmington, MA), were used to minimize microvascular heterogeneity due to genetic variability, sex, and age (Macdonald et al., 2008). Animals were euthanized by CO_2 inhalation, following Animal Care and Use Guidelines of the University of Connecticut Health Center (Animal Welfare Assurance # A3471-01).

2.2. Induction of experimental autoimmune encephalomyelitis (EAE)

EAE was induced in mice by active immunization with $MOG_{35–55}$ peptide (MEVGWYRSPFSRVVHLYRNGK), of murine origin (W.M. Keck Biotechnology Resource Center, Yale University), as described (Juedes et al., 2000). Mice were observed daily and scored on a scale of 0–4 with gradations of 0.5 for intermediate scores: 0, no clinical signs; 1, loss of tail tone; 2, wobbly gait; 3, hind limb paralysis; and 4 hind and fore limb paralysis. LCM tissue was acquired at day 16 post-immunization (score ~2.0).

2.3. Tissue preparation and sectioning

Following euthanasia, the brain was removed, snap-frozen in dry ice-cooled 2-methylbutane (Acros; Geel, Belgium) and processed for cryosectioning (Macdonald et al., 2008). Coronal sections (7 μm thick) of cerebellum were cut between Bregma −6.56 mm and −7.32 mm, adhered to glass slides, and stored at −80 °C until immuno-LCM.

2.4. Fixation and immunostaining of sections for identification of microvessels [30 min]

To obtain sufficient material for comparing two samples by LCM/qrt-PCR analysis, two slides, each containing two consecutive brain sections, were fixed, stained, and dehydrated simultaneously. Two sections provided sufficient material for each sample. Pairing samples this way enabled both samples to experience the same environmental conditions for the same time (Macdonald et al., 2008). Double immunostaining of BMEC and astrocyte populations, by combined immunohistochemistry and immunofluorescence, respectively, was carried out as detailed (Macdonald et al., 2008).

2.5. Dehydration [8.0 min]

After immunostaining, sections were dehydrated in the following solutions, made by diluting 100% EtOH (Pharmco-AAPER; Brookfield, CT) with DEPC treated water: 75% EtOH for 10 s, 95% EtOH for 30 s, 100% EtOH for 60 s, 100% EtOH for 90 s, xylene (Fisher Scientific; Pittsburgh, PA) for 2 min and a final xylene for 3 min.

2.6. LCM [20–30 min]

The Arcturus PixCell IIe microscope (Life Technologies; Bedford, MA) was used to retrieve BMEC according to the LCM conditions described (Kinnecom and Pachter, 2005; Macdonald et al., 2008). In brief, the LCM parameters utilized were as follows: 7.5 μm spot size; 72 mW power; and 0.950 ms pulse duration. BMEC were captured exclusively from capillaries (~ 5–9 μm diameter) within the designated cerebellar boundaries. As LCM can only be performed on one slide at a time, one of the two simultaneously stained slides was left at room temperature until action on the first slide was completed. Tissue samples were captured onto HS® caps (Life Technologies Corp.) by a designated number of 'shots' (*i.e.*, laser pulses), with one cap used per sample. An equal number of LCM shots was necessary to standardize the amount of input RNA, and was previously shown to provide a highly reproducible amount of tissue equivalent (Macdonald et al., 2008).

Because LCM acquires material from tissue sections, only "fractions" of cells are obtained with each LCM shot. However, the following sample calculation may be used to estimate the number of endothelial cells captured in an LCM session: Assuming the typical endothelial cell is 10–15 μm deep × 25–50 μm long (Simionescu and Simnionescu, 1977), then in 7 μm-thick sections each capillary endothelial profile cut in longitudinal section would represent 0.47–0.7 cells in thickness. Using a 7.5 μm diameter laser spot size, the number of capillary endothelial cells cut lengthwise would be 0.15–0.3. Hence, the number of endothelial cells captured/shot = 0.07–0.21 cells; 500 shots would thus represent 35–105 cells, and 1000 shots represent 70–210 cells.

2.7. Tissue extraction [15 min]

Once LCM was completed, tissue was solubilized in Cell Lysate Buffer® (Signosis; Sunnyvale, CA) for direct reverse transcription. Cell Lysate Buffer®, pre-heated to 75 °C, was added and the resulting lysate heated at 75 °C for an additional 15 min. Samples of both extracts were immediately frozen at −80 °C.

2.8. DNase treatment and cDNA synthesis [2 h]

Cell Lysate Buffer® extracts were treated with Turbo DNase (Ambion; Austin, TX) according to the manufacturer's instructions. Specifically, Turbo DNase buffer and DNase were added and samples incubated at 37 °C for 30 min. Next, DNAse inactivation reagent was added for 2 min at room temperature. Samples were then reverse transcribed using the SuperScript III (Invitrogen) standard protocol with random hexamers (Roche; Indianapolis, IN), and employing an extension temperature of 42 °C – optimal for random hexamers – for 60 min. cDNA was stored at −20 °C until used for analysis.

2.9. cDNA pre-amplification [1 h 40 min]

Pre-amplification was carried out using TaqMan® PreAmp Master Mix and a custom PreAmp Pool containing all the primers for detection by TaqMan® Gene Expression Assays. Relative amplification was validated using single gene (single-plex) probes for CCL2, VCAM1 and GAPDH prior to analysis by TaqMan® Low Density Array (TLDA) Microfluidic Cards. Both 10 and 14 cycles of pre-amplification were evaluated initially, with an initial hold at 95 °C for 10 min, followed by 10/14 cycles at 95 °C for 15 s and 60 °C for 4 min. For TLDA analysis, 14 cycles of pre-amplification were used.

2.10. qrt-PCR [2 h]

Relative cDNA levels were quantified by qrt-PCR using an ABI PRISM 7500 Sequence Detection System Version 2.3, and custom TaqMan® MGB probes. For single-plex assays, separate controls included no template or no reverse transcriptase, and standard curves were constructed for all primers used. Custom TaqMan® primers/probes were used for both single-plex qrt-PCR and the Mouse Immune Panel TLDA (Life Technologies Corp.). TLDA analysis was conducted as per the manufacturer's protocol, with 100 μl sample volumes containing a 1/32 or 1/4 dilution of pre-amplified cDNA added to each port of the microfluidic card.

2.11. Statistical analysis

Data from single-plex reactions were analyzed in SDS 2.3 and Microsoft Excel 2007, while that from TLDA plates were imported to the SDS 2.3 companion software RQ Manager and exported to Microsoft Excel 2007 for calculations. Linear regression analysis was conducted and a Pearson product-moment correlation (Pearson *r*) determined using GraphPad Prism 5.0. Pearson *r* was calculated from paired Ct values reflecting expression of each of the 96 genes represented in the Immune Panel TLDA. A Spearman-Rho rank order correlation (Spearman *r*) was calculated to determine if these 96 gene expression values were comparable in rank order between samples.

3. Results

Because of the extremely low level of RNA from LCM samples, the first step was to determine if cDNA generated directly from LCM tissue extracted in Cell Lysate Buffer® – without RNA purification – could be amplified using a commercially available pre-amplification kit prior to quantification by qrt-PCR. A sampling of three genes represented on the Mouse Immune-TLDA (GAPDH, VCAM-1 and CCL2) was individually analyzed in single-plex format. These genes were selected as they exhibit high (GAPDH), moderate (VCAM-1), and relatively low expression (CCL2) by BMEC during acute EAE, the animal model for the neuroinflammatory disease multiple sclerosis (MS) (Furlan et al., 2009) – and thus provide a wide spectrum by which to judge efficacy of the pre-amplification. Fig. 1 demonstrates a 14-cycle pre-amplification significantly lowered Ct values for all three genes. Both GAPDH and VCAM-1 had their Ct values similarly lowered by 12 cycles, while Ct value of CCL2 decreased by 10.2 cycles, thus indicating the relative abundance of amplicons was generally preserved through pre-amplification. The apparent lesser amplification of CCL2 signal may have resulted from expression of this gene being lower than that which was reliably detectable in the non-amplified sample.

It was next determined if pre-amplified BMEC cDNA, generated from Cell Lysate Buffer extracts® without RNA isolation, could be coupled to the Immune Panel TLDA for simultaneous analysis of 96 genes related to inflammation/autoimmunity. This specific TLDA was selected as it contains a cadre of genes thought to be involved in MS/EAE.

Two different dilutions of the pre-amplified cDNA were assayed to cover a broad range of gene expression and test the limits of sensitivity. Fig. 2(a) and (b) depicts linear regression analyses of raw Ct values for the genes represented in the TLDA, contrasting values obtained from 1/4 and 1/32 dilutions of pre-amplified cDNA samples generated from 500 or 1000 LCM shots. Notably, raw Ct values – as apposed to values normalized to a reference gene – reflect the absolute values of input RNA for qrt-PCR and, thus, reveal an accurate picture of the reproducibility of the immuno-LCM/TLDA approach (Chen et al., 2009).

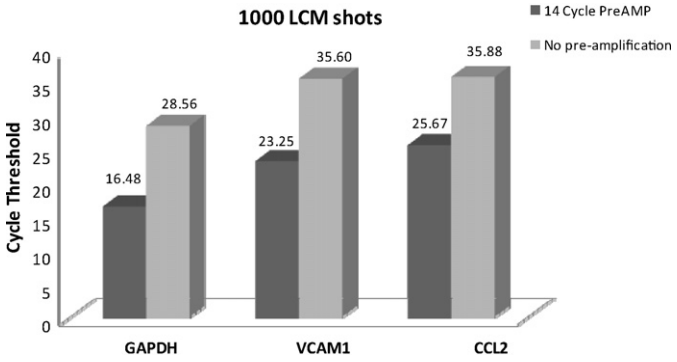

Fig. 1. Pre-amplification of cDNA from Cell Lysate Buffer® proportionally enhances LCM/qrt-PCR of BMEC. At day 16 following $MOG_{35–55}$ peptide immunization to induce EAE (disease score ~2.0), mouse cerebellar tissue was processed for immuno-LCM, and BMEC captured by 1000 LCM shots then extracted with Cell Lysate Buffer®. BMEC extract then underwent reverse transcription reaction without prior RNA isolation, and equal aliquots of the resulting cDNA were either not pre-amplified or subject to 14 cycles of pre-amplification prior to single-plex qrt-PCR detection with TaqMan® probes/primers for the genes GAPDH, VCAM1 and CCL2. Each qrt-PCR reaction was run in duplicate (technical replicates), and the mean Ct values for each gene are depicted. Pre-amplification of 14 cycles with extract from 1000 shots of LCM-derived BMEC yielded the following mean ΔCt [cDNA – pre-AMP] values: GAPDH (12.087), VCAM1 (12.34), and CCL2 (10.21). Inherent lower expression of CCL2 may explain the lesser-detected amplification of this gene.

Raw Ct values considered "undetermined" by the software, or at a level ≥40 cycles, were excluded from analysis. In the case of 1000 LCM shots, 14 genes were so excluded, while only 6 genes were omitted from the 500 LCM shot sample. Both 1000 and 500 LCM shot samples yielded Pearson *r* values of >0.95, signifying extremely high linear correlation between technical replicates. These technical replicates originated from the same tissue sections and resultant cDNA pools, their only difference being they represented either 1/4 or 1/32 dilutions of pre-amplified cDNA applied to the TLDA. The high Pearson *r* thus highlights that diluting cDNA samples over an eightfold range did not distort the relationship between amplicon measurements of the different genes. Such technical replicates showed a high Spearman *r* value as well, denoting that raw Ct scores for each gene maintained their rank position relative to all other genes in the TLDA when 1/4 and 1/32 dilutions of pre-amplified cDNA were compared.

Immuno-LCM/TLDA further demonstrated both a high Pearson *r* (0.95) and Spearman *r* (0.93) among raw Ct values obtained from "biological" replicates (Fig. 2(c)). To obtain biological replicates, 500 LCM shots were performed on separate brain sections of the same animal, and a 1/32 dilution of pre-amplified cDNA derived from these respective sections was used in each case. As such, these biological replicates were subject to potential technical variability as well. Brain tissue from different animals was intentionally not compared here, as the immunization protocol itself could produce varying disease states in individual mice, and the objective was to isolate any variability due solely to analysis of random BMEC populations. Despite undergoing a multitude of separate acquisition and processing steps, however, biologic replicates also demonstrated high fidelity. Specifically, linear regression yielded a line with a slope of 1.03 ± 0.038 (SD) and Y and X intercepts of near zero – reflecting that raw scores of any specific gene were virtually identical in the biological replicates. These results collectively demonstrate – for the first time – high efficiency and reproducibility of linking immuno-LCM to TLDA format without need of tedious RNA isolation and amplification steps.

4. Discussion

Coupling LCM to genomic profiling platforms has greatly expanded the capacity to probe gene expression within the most

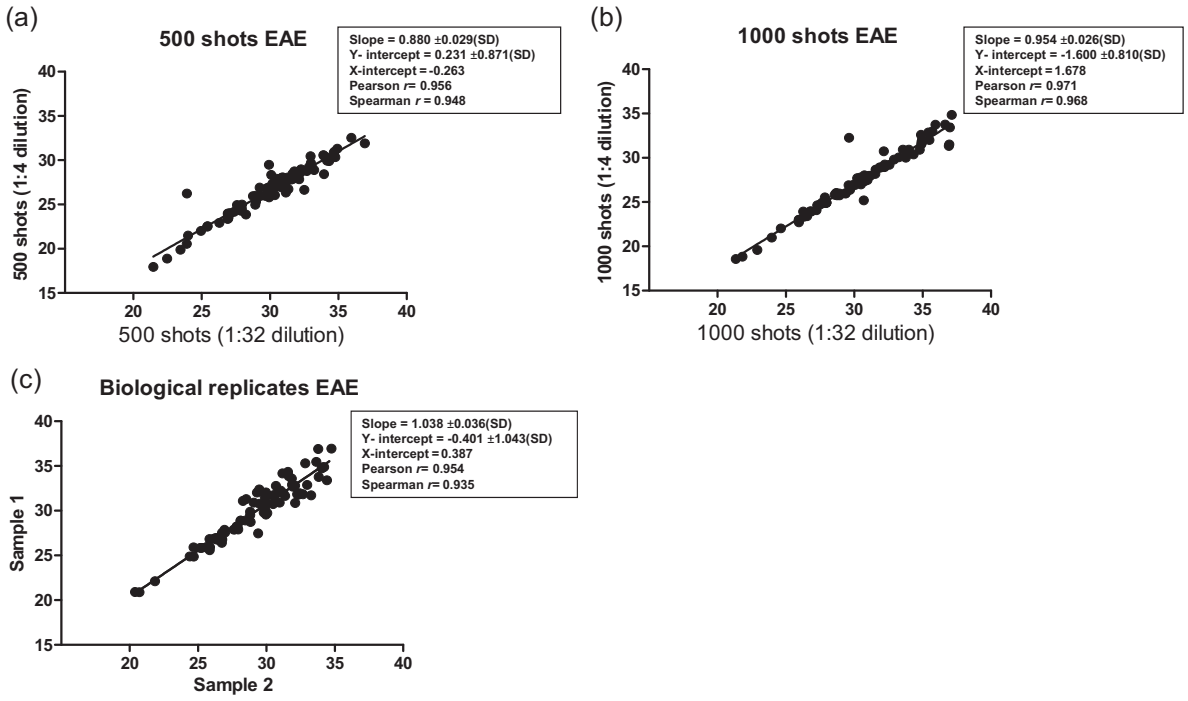

Fig. 2. Expression profiling of BMEC by immuno-LCM/TLDA with no RNA purification shows high reproducibility. Immuno-LCM of BMEC was carried out on separate EAE cerebellar sections, and captured tissue extracted with Cell Lysate Buffer® then processed through reverse transcription and cDNA pre-amplification, as in Fig. 1. To gauge sensitivity and exclusively highlight technical reproducibility, different dilutions (1/4 or 1/32) of pre-amplified cDNA derived from 500 (a) or 1000 (b) LCM shots were analyzed by qrt-PCR using the Immune Panel TLDA, and linear regression performed on the two corresponding raw Ct values obtained for each gene at the respective dilutions. To highlight overall reproducibility, while accounting for all potential variation due to both biological and technical components, the results of 500 LCM shots from two different tissue sections were compared (c), and linear regression performed on the two corresponding raw Ct values obtained for each gene from the respective sections.

discrete CNS domains *in situ*. Linking LCM to hybridization-based microarrays, in particular, has enabled transcriptional profiling of tens of thousands of genes from select cell groups in CNS tissue samples (Rossner et al., 2006). Nevertheless, this particular combinatorial approach is labor intensive, expensive, and presents difficulties with quantification and statistical evaluation.

Much of this labor stems from RNA isolation and downstream amplification steps needed to generate sufficient labeled complementary RNA (cRNA) for detection (usually >1 μg). These steps can become unmanageable when dealing with multiple samples. Thus, proceeding directly from solubilization of LCM tissue to reverse transcription and then cDNA pre-amplification, would save considerable time and effort when comparing a number of variables (*e.g.*, stages of disease progression or different drug dosages). Concerns have also been raised regarding bias in the RNA amplification process (Li et al., 2005). Furthermore, while the wide breadth of genes that can be analyzed with hybridization-based microarrays may be advantageous in certain applications (*e.g.*, whole-cell transcriptome analysis), it may not be warranted in others. A limited analysis may be more desirable when investigating a specific biological process or tissue property. As qrt-PCR is often used to confirm results of hybridization arrays – which frequently illuminate no more than a few hundred significantly variable genes – coupling LCM to a qrt-PCR-based array format without RNA purification would also prove an efficient validation or screening tool.

Given these considerations, this report described a simplified and expeditious approach whereby immuno-LCM of BMEC was followed by tissue solubilization and direct reverse transcription (in the absence of RNA purification), pre-amplification of the resulting cDNA, and then simultaneous qrt-PCR analysis of 96 *immune-related* genes by TLDA. Because RNA was not isolated in this study, equal number of LCM shots served as basis for sample comparisons. Previous work from this laboratory showed utilizing equal numbers of LCM shots was an effective means to standardize RNA input (Macdonald et al., 2008), this approach yielding no statistically significant variance in relative gene expression values between technical or biological replicates as detected by single-plex qrt-PCR. The number of shots in the present study was capped at 1000 to minimize the time between immunostaining and processing of RNA for analysis, as restricting this period to <30 min has been shown to be critical for reliable qrt-PCR detection (Macdonald et al., 2008). Notably, 500 LCM shots was able to be performed in <20 min, and yielded a higher number of detectable genes than did 1000 LCM shots (90 genes *vs.* 82 genes, respectively) – perhaps reflecting loss of RNA with increased LCM time. Both 500 and 1000 LCM shots nevertheless showed high reproducibility in technical and biological replicates among 96 different genes assayed simultaneously by TLDA – even in the absence of RNA purification. These results support the findings of Keays et al. (2005), who coupled LCM to single-plex qrt-PCR without purifying RNA. But, to the best of our knowledge, this is the first report to describe linkage of LCM to microarray while bypassing RNA purification and employing cDNA pre-amplification.

While there have been more than 100 published reports of LCM/microarray analysis, the array format used has near exclusively been genomic DNA chip hybridization – necessitating RNA purification and amplification. Most recently, Balogh et al. (2007) described coupling LCM of hemotoxylin/eosin-stained tissue to the Immune Panel TLDA used in this study. However, they utilized a four-step RNA amplification process: first purifying RNA, then amplifying it based on dT-T7 and switch T7 primers followed by *in vitro* transcription, and finally purifying the synthetic RNA population. The present study averted these steps entirely. It is further significant that high reproducibility of immuno-LCM/TLDA was demonstrated with raw Ct scores – not gene expression values normalized to a housekeeping gene.

The validity of the immuno-LCM/TLDA approach was underscored by the distribution of raw Ct scores obtained – from the

low 20s to upper 30s – reflecting the variable expression patterns of genes during evolving EAE. Moreover, preliminary comparison between naïve and EAE mice revealed several significant differences. Among these were elevated expression of STAT6 and CCR4 (data not shown), both of which have been shown to be up-regulated in EAE (Zaheer et al., 2007; Forde et al., 2011).

In summary, the immuno-LCM/TLDA approach described offers a relatively quick, reliable and inexpensive means to globally profile gene expression patterns of select cell groups *in situ*. Given the significant cellular heterogeneity within the nervous system, immuno-LCM/TLDA holds high promise for elaborating gene regulatory mechanisms in the neurobiology of health and disease, and could provide a highly efficient clinical diagnostic tool for neuropathologists (McShea et al., 2006).

Acknowledgments

This work was supported by grants R0-1-MH061525 from the National Institutes of Health, RG-4503A4/1 from the National Multiple Sclerosis Society, and 2010-0913 from the Connecticut Department of Public Health to J.S.P., and American Heart Association predoctoral fellowship award 0815733D to N.M. Special thanks are owed to Alan Carpino, Rachele Kardon and Paula Miccinesi of Life Technologies Corp. for helpful discussions.

References

Balogh GH, Russo IH, Spittle C, Heulings R, Russo J. Immune – surveillance and programmed cell death-related genes are significantly overexpressed in the normal breast epithelium of postmenopausal parous women. Int J Oncol 2007;31:303–12.

Chen Y, Gelfond JAL, McManus LM, Shireman PK. Reproducibility of quantitative RT-PCR array in miRNA expression profiling and comparison with microarray analysis. BMC Genomics 2009;10:407–16.

Espina V, Heiby M, Pierobon M, Liotta L. Laser capture microdissection technology. Expert Rev Mol Diagn 2007;7:647–57.

Forde EA, Dogan R-N, Karpus WJ. CCR4 contributes to the pathogenesis of experimental autoimmune encephalomyelitis by regulating inflammatory macrophage function. J Neuroimmunol 2011;236:17–26.

Furlan R, Cuomo C, Martino G. Animal models of multiple sclerosis. Methods Mol Biol 2009;549:157–73.

Ge S, Song Li, Pachter JS. Where is the blood-brain barrier . . . really? J Neurosci Res 2005;74:421–7.

Juedes AE, Hjelstrom P, Bergman CM, Neild AL, Ruddle NH. Kinetics and cellular origin of cytokines in the central nervous system: insight into mechanisms of myelin oligodendrocyte glycoprotein-induced experimental encephalomyelitis. J Immunol 2000;164:419–26.

Keays KM, Owens GP, Ritchie AM, Gilden DH, Burgoon MP. Laser capture microdissection and single-cell RT-PCR without RNA purification. J Immunol Methods 2005;302:90–8.

Kinnecom K, Pachter JS. Selective capture of endothelial cells and perivascular cells from brain microvessels by laser capture microdissection. Brain Res Protoc 2005;16:1–9.

Li L, Roden J, Shapiro BE, Wold BJ, Bhatia S, Forman SJ, et al. Reproducibility, fidelity, and discriminant validity of mRNA amplification for microarray analysis from primary hematopoietic cells. J Mol Diagn 2005;7:48–56.

Macdonald JA, Murugesan N, Pachter JS. Validation of immunolaser capture microdissection coupled with quantitative RT-PCR to probe blood-brain barrier gene expression in situ. J Neurosci Methods 2008;174:219–26.

Macdonald J, Murugesan N, Pachter JS. Endothelial cell heterogeneity of blood-brain barrier gene expression along the cerebral microvasculature. J Neurosci Res 2010;88:1457–74.

McShea A, Marlatt MW, Lee HG, Tarkowsky SM, Smit M, Smith MA. The application of microarray technology to neuropathology: cutting edge tool with clinical diagnostics potential or too much information? J Neuropathol Exp Neurol 2006;65:1031–9.

Rossner MJ, Hirrlinger J, Wichert SP, Boehm C, Newrzella D, Hiemsch H, et al. Global transcriptome analysis of genetically identified neurons in the adult cortex. J Neurosci 2006;26:9956–66.

Simionescu N, Simnionescu M. The cardiovascular system. In: Weiss L, editor. Histology cell and tissue biology. 5th ed. New York: Elsevier Biomedical; 1977. p. 371–433.

Zaheer S, Wu Y, Bassett J, Yang B, Zaheer A. Glia maturation factor regulation of STAT expression: a novel mechanism in experimental autoimmune encephalomyelitis. Neurochem Res 2007;32:2123–31.

FLUIDS AND BARRIERS
OF THE CNS

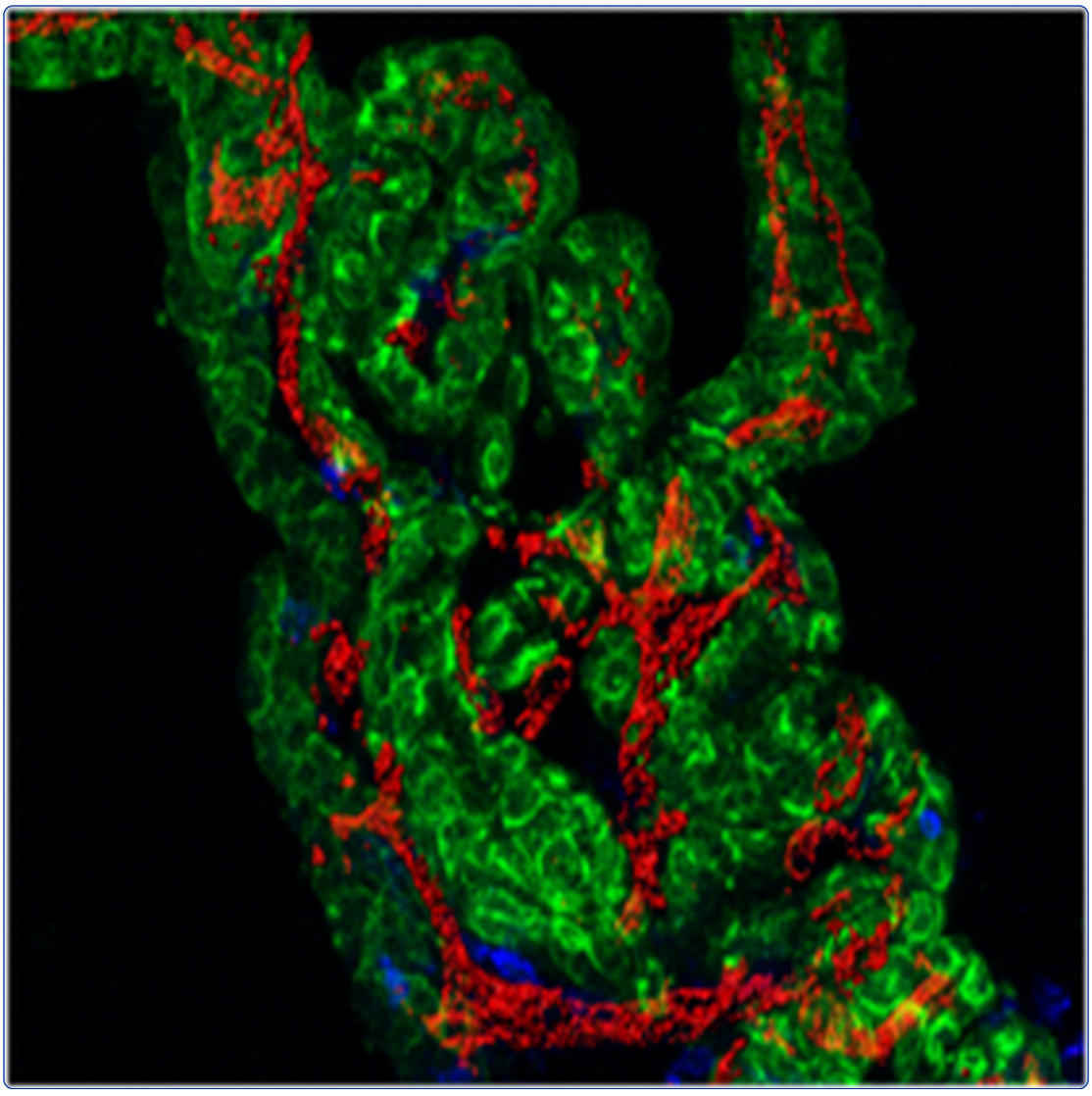

Active induction of experimental autoimmune encephalomyelitis by MOG_{35-55} peptide immunization is associated with differential responses in separate compartments of the choroid plexus

Murugesan *et al.*

BioMed Central

Murugesan *et al. Fluids and Barriers of the CNS* 2012, **9**:15
http://www.fluidsbarrierscns.com/content/9/1/15

FLUIDS AND BARRIERS OF THE CNS

RESEARCH Open Access

Active induction of experimental autoimmune encephalomyelitis by MOG_{35-55} peptide immunization is associated with differential responses in separate compartments of the choroid plexus

Nivetha Murugesan, Debayon Paul, Yen Lemire, Bandana Shrestha, Shujun Ge and Joel S Pachter*

Abstract

Background: There is increasing awareness that, aside from producing cerebrospinal fluid, the choroid plexus (CP) might be a key regulator of immune activity in the central nervous system (CNS) during neuroinflammation. Specifically, the CP has recently been posited to control entry of sentinel T cells into the uninflamed CNS during the early stages of neuroinflammatory diseases, like multiple sclerosis (MS) and its animal model experimental autoimmune encephalomyelitis (EAE). As the CP is compartmentalized into a stromal core containing fenestrated capillaries devoid of typical blood–brain barrier properties, surrounded by a tight junction-expressing choroidal epithelium, each of these compartments might mount unique responses that instigate the neuroinflammatory process.

Methods: To discern responses of the respective CP stromal capillary and choroidal epithelial tissues during evolving neuroinflammation, we investigated morphology and *in situ* expression of 93 immune-related genes during early stages of EAE induced by immunization with myelin oligodendrocyte glycoprotein peptide (MOG_{35-55}). Specifically, 3-D immunofluorescent imaging was employed to gauge morphological changes, and laser capture microdissection was coupled to an *Immune Panel* TaqMan Low Density Array to detail alterations in gene expression patterns at these separate CP sites on days 9 and 15 post-immunization (p.i.). To resolve CP effects due to autoimmunity against MOG peptide, from those due to complete Freund's adjuvant (CFA) and pertussis toxin (PTX) included in the immunization, analysis was performed on MOG-CFA/PTX-treated, CFA/PTX-treated, and naïve cohorts.

Results: The CP became swollen and displayed significant molecular changes in response to MOG-CFA/PTX immunization. Both stromal capillary and choroidal epithelial tissues mounted vigorous, yet different, changes in expression of numerous genes over the time course analyzed - including those encoding adhesion molecules, cytokines, chemokines, statins, interleukins, T cell activation markers, costimulatory molecules, cyclooxygenase, pro-inflammatory transcription factors and pro-apoptotic markers. Moreover, CFA/PTX-treatment, alone, resulted in extensive, though less robust, alterations in both CP compartments.

(Continued on next page)

* Correspondence: Pachter@nso1.uchc.edu
Blood–brain Barrier Laboratory, Department of Cell Biology, University of Connecticut Health Center, 263 Farmington Ave, Farmington, CT 06030, USA

(Continued from previous page)

Conclusions: MOG-CFA/PTX immunization significantly affects CP morphology and stimulates distinct expression patterns of immune-related genes in CP stromal capillary and epithelial tissues during evolving EAE. CFA/PTX treatment, alone, causes widespread gene alterations that could prime the CP to unlock the CNS to T cell infiltration during neuroinflammatory disease.

Keywords: Laser capture microdissection (LCM), Choroid plexus, EAE, Pertussis toxin, Neuroinflammation

Introduction

Though the choroid plexus (CP) is commonly recognized as the production site of cerebrospinal fluid (CSF) [1-3], it has relatively recently gained attention as a critical player in central nervous system (CNS) inflammation [4-6]. Specifically, the CP has been suggested as the site of entry into the uninflamed CNS of pioneer T cells searching for their cognate antigens during immunosurveillance and in the early stages of neuroinflammatory diseases such as multiple sclerosis (MS) and its animal model experimental autoimmune encephalomyelitis (EAE) [7,8]. Current theory holds that, after crossing the CP into the CSF, pioneer T cells travel to the subarachnoid space (SAS), where antigen-presenting cells reactivate them. In turn, reactivation is thought to set off a burst of cytokines and other mediators that inflames meningeal and parenchymal venules to initiate disease [9-11].

The anatomy of the CP appears well suited to orchestrating the initial steps of CNS inflammation. It projects from the roofs of all four ventricles into the CSF, and is composed of two distinct tissue layers: a highly vascularized stroma encapsulated by a "tight" layer of epithelial cells [12]. Unlike the parenchymal capillaries forming the restrictive blood–brain barrier (BBB), CP stromal capillaries are fenestrated and contain pentilaminar junctions whose outer leaflets are not fused [13] – properties that render the CP capillary population highly permeable to macromolecules [14]. This juxtaposition of "leaky" capillaries and tight epithelium constitutes the blood-cerebrospinal fluid barrier (BSCFB) [15,16], an arrangement construed as enabling blood-born leukocytes to extravasate into an uninflamed brain during the incipient stages of MS and EAE [17,18]. Supporting this process, expression of chemokine CCL20 by choroidal epithelial cells is thought to chemotactically draw T cells – bearing the cognate receptor CCR6 – from the CP stroma, across the epithelium and into the CSF [8].

In situ hybridization and immuno-electron microscopy of the CP has further revealed expression of adhesion molecules, VCAM-1 and ICAM-1, by choroidal epithelial cells of the healthy CP, and additionally of MAdCAM-1 by these same cells during EAE [19,20]. Also, transcriptome analysis of the whole adult CP has highlighted expression of immune mediators in both healthy mice [21] and those subject to peripheral inflammation [22], reinforcing the view this organ is a critical conduit linking immune/inflammatory activities between the periphery and CNS. But the extremely close apposition of the different CP layers has posed a significant challenge to studying the depth of their respective contributions to inflammatory processes. In fact, no immune function has yet been ascribed to the CP capillary endothelium, leaving completely unresolved the factors that drive T cell emigration into the stroma. And gene regulatory events surrounding transmigration of T cells across the choroidal epithelium further remain unsettled.

To elaborate the sequence of events in the CP that set the stage for CNS inflammation during EAE induced by active immunization with MOG_{35-55} peptide, we used laser capture microdissection (LCM) coupled to qrt-PCR-based microarray [23] to establish the time course of expression of a panorama of immune mediators in the separate stromal (including capillaries) and choroid epithelial layers. Morphological changes in the CP associated with MOG immunization were also examined by quantitative 3-D image analysis following confocal microscopy. Results reveal substantial changes in CP gene expression and morphology occurred in response to vspecific aspects of the MOG immunization process. These results could hold relevance for how combinations of environmental factors trigger neuroinflammatory disease.

Materials and methods

Animals

Female C57BL/6 mice, age 8–10 weeks and obtained from Charles River Laboratories, Inc. (Wilmington, MA), were used to minimize microvascular heterogeneity due to genetic variability, sex, and age [24]. Animals were euthanized by CO_2 inhalation, following Animal Care and Use Guidelines of the University of Connecticut Health Center (Animal Welfare Assurance # A3471-01). A total of n = 3 animals/group were used for each treatment and time-point assessed.

Induction of experimental autoimmune encephalomyelitis (EAE)

EAE was induced in mice by active immunization with MOG_{35-55} peptide (MEVGWYRSPFSRVVHLYRNGK), of murine origin (W. M. Keck Biotechnology Resource

Center, Yale University), as described [25]; following Animal Care and Use Guidelines of the University of Connecticut Health Center (Animal Welfare Assurance # A3471-01). Briefly, on day 0, one group of female mice 7–9 weeks of age was injected subcutaneously with 300 μg of MOG peptide in complete Freund's adjuvant (CFA, DIFCO) into the right and left flank, 100 μl per site. These mice were also injected i.p. with 500 ng pertussis toxin (PTX, List Laboratories, Campbell CA) in PBS on days 0 and 2 following the first immunization (referred to as the MOG-CFA/PTX group). The second group of age-matched mice received CFA alone and PTX (500 ng) injections on day 0 and a second injection of 500 ng PTX alone on day 2 (referred to as the CFA/PTX group). The third group of naïve age-matched female mice was left untreated. Animals were monitored and scored daily for clinical disease severity according to the following scale: 0 = normal; 1 = tail limpness; 2 = limp tail and weakness of hind legs; 3 = limp tail and complete paralysis hind legs; 4 = limp tail, complete hind leg and partial front leg paralysis; and 5 = death. LCM tissue was acquired at day 9 (score 0) and day 15 (score ~ 2.0) post-immunizations.

Tissue preparation for Immuno-LCM

Brains were snap-frozen in dry ice-cooled 2-methylbutane (Acros; Geel, Belgium), and stored at −80°C. Frozen brain was embedded in cryomatrix compound (Thermo Fisher Scientific, Waltham, MA) prior to sectioning. Coronal sections (7 μm) were cut on a Microm HM 505 M cryostat (Mikron Instruments; Oakland, NJ) and affixed to uncoated, pre-cleaned glass slides (Fisher Scientific, Pittsburgh, PA) and stored in a slide box at −80°C. Tissue was processed for LCM within a week of sectioning.

Immunostaining for Immuno-LCM

Immunostaining was performed as detailed [24,26,27], with minor modifications. Briefly, sections were fixed in 75% ethanol, on ice, for 3 min prior to staining. The CP stromal capillaries were stained using alkaline phosphatase substrate NBT (nitro-blue tetrazolium chloride)/BCIP (5-bromo-4-chloro-3'-indolyphosphate p-toluidine salt), (Vector Labs, Burlingame, CA) for 3–5 minutes in 100 Mm Tris–HCl (pH 9.5) to detect endogenous alkaline phosphatase activity in the endothelial cells. In this case, endothelial cells were intentionally not immunostained by anti-CD31/ABC alkaline phosphatase [24,27], as it resulted in extensive deposition of chromogenic precipitate, which made the stromal capillaries difficult to resolve from the choroidal epithelial layer. The choroidal epithelial cells were immunostained with monoclonal pan-cytokeratin-FITC antibody (Sigma) for 10 minutes (diluted 1:10 in 1X PBS + 0.5% Tween-20). RNAsin® RNAse inhibitor (Promega, Madison, WI) was added to all staining reagents. Immediately after immunostaining, sections were dehydrated through graded alcohol and xylenes as described [24].

Laser capture microdissection (LCM)

A PixCell IIe laser capture microscope (ABI, Foster City, CA) was used to separately procure CP stromal capillary and CP choroidal epithelial tissues, as previously described for brain parenchymal vessels [24,27,28]. We refer specifically to CP stromal capillary tissue, instead of pure capillary endothelium, as it was not possible to completely resolve vascular from matrix elements (including extravasating leukocytes) within the dense CP stroma. Likewise, the choroidal epithelial tissue may contain some epiplexus cells, and so is not described as pure epithelium. Only choroid plexus material from within the fourth ventricle and lateral recess of the fourth ventricle was retrieved.

Tissue extraction

LCM-retrieved tissue was solubilized in Cell Lysate Buffer® (Signosis; Sunnyvale, CA) for direct reverse transcription. Cell Lysate Buffer®, pre-heated to 75°C, was added and the resulting lysate heated at 75°C for an additional 15 min. Samples were immediately frozen at −80°C.

DNase treatment and cDNA synthesis

Cell Lysate Buffer® extracts were treated with Turbo DNase (Ambion; Austin, TX) according to the manufacturer's instructions. Specifically, Turbo DNase buffer and DNase were added and samples incubated at 37°C for 30 min. Next, DNAse inactivation reagent was added for 2 min at room temperature. Samples were then reverse transcribed using the SuperScript III (Invitrogen) standard protocol with random hexamers (Roche; Indianapolis, IN), and employing an extension temperature of 42°C – optimal for random hexamers – for 60 min. Resulting cDNA was stored at −20°C until used for analysis.

cDNA Pre-Amplification

Pre-amplification was carried for array analysis out using TaqMan® PreAmp Master Mix and a PreAmp Pool containing all the primers for detection by the Mouse Immune Panel TaqMan® Low density Array (TLDA; Life Technologies Corp., Foster City, CA) [23]. This panel conatins 93 immune-related genes plus three housekeeping control genes (see Additional file 1: *Mouse Immune Panel TLDA*). Pre-amplification was carried out with an initial hold at 95°C for 10 min, followed by 14 cycles at 95°C for 15 sec and 60°C for 4 min.

qrt-PCR

Relative cDNA levels were quantified by qrt-PCR using an ABI PRISM 7500 Sequence Detection System Version 2.3, and reported compared to housekeeping gene GAPDH. Relative quantitation to GAPDH was performed using the standard $2^{-\delta Ct}$ method of Pfaffl [29], where $\delta Ct = Ct$ target threshold cycle – Ct reference (GAPDH) threshold cycle. Expression of genes relative to GAPDH was then represented as percent expression of GAPDH. To assure consistency in relating gene expression patterns to a housekeeping gene, GAPDH and two other housekeeping genes, β-actin and 18 S ribosomal RNA, were evaluated for constant expression across treatments. Additionally, gene expression values for a handful of randomly selected immune-related genes were also determined relative to β-actin and 18 S ribosomal RNA (see Additional file 2: *Housekeeping control genes*). Custom TaqMan® primers/probes were used for the Mouse Immune Panel TLDA. TLDA analysis was conducted as per the manufacturer's protocol, with 100 μl sample volumes containing a 1/32 dilution of pre-amplified cDNA added to each port of the microfluidic card [23]. For *qrt-PCR* analysis of CD31 and Cytokeratin 8, 'singleplex' assays were used as neither of these genes are represented in the mouse Immune Panel TLDA.

Immunostaining for confocal microscopy

Frozen cryosections (60 μm) were fixed with 4% paraformaldehyde, permeabilized with 1% Triton X-100 (in PBS) and incubated with Powerblock® for 10 min. Purified rat anti-mouse CD31 antibody (BD Pharmingen; 1:150 dilution in 10% NBS in 1X PBS + 0.5% TW-20) was used to stain the CP capillary network followed by incubation with goat anti-rat Alexa-555 secondary antibody (1:200). Pan-cytokeratin-FITC 1: 150 dilution, (Sigma) was used to stain the CP epithelium. Next, Alexa-647 anti-mouse CD45 antibody (1:160 dilution) was used to stain leukocytes.

Confocal microscopy

Images were acquired on a Zeiss LSM 510 Meta laser scanning confocal microscope, and optical slices (at 2-μm intervals) obtained using a 40x objective. Acquired z-stacks were background-subtracted, and 3-D isosurface rendering performed using Bitplane IMARIS suite version 7.1 x 64 software (Bitplane Inc. Saint Paul, MN). Each z-stack was thresholded and the "filament tracker" module used to generate a 3-D traced outline of immunostained vessels in order to determine the diameter range of the CD31-immunostained capillary network within the choroid plexus across different treatments.

Statistical analysis

Relative gene expression values are given as mean ± SEM. Student's two-tailed test (Microsoft Excel 2003, Redmond, WA) was employed to assess statistical significance in gene expression values between MOG-CFA/PTX and CFA/PTX samples from the CP capillary stroma and CP epithelium groups, separately for the two different time points assessed. Results were considered significant at a $p \leq 0.05$. Additionally, two-way ANOVA followed by post-hoc Bonferroni analysis was performed using GraphPad Prism 5 (GraphPad, La Jolla, CA) to determine *interactive effects* between immunization treatment and time of analysis post-immunization, and assessed for each CP compartment.

Results

Anatomy of the CP is altered in response to MOG-immunization

First, the anatomy of the CP was investigated using confocal microscopy followed by 3-D isosurface rendering. The close apposition of stromal capillary and choroidal epithelial layers in the CP is depicted in Figure 1. The 3-D analysis highlights the tortuosity of the capillary plexus. At day 15 post immunization (p.i.) with PTX and MOG_{35-55} peptide in CFA to induce EAE (MOG-CFA/PTX group), or with PTX and CFA alone (CFA/PTX group), which does not produce disease in this paradigm, the capillary plexus can be seen to locally 'swell' in certain regions (Figure 1). Specifically, the range in diameter of capillaries in the MOG-CFA/PTX and CFA/PTX groups was 1.24 to 11.39 μm and 1.86 to 10.84 μm respectively, as compared to that found in naïve (1.24 to 6.22 μm) mice. In contrast to that seen within CP capillaries, the morphology of the choroidal epithelial layer remained relatively constant following immunization.

LCM enables resolution of CP stromal capillaries from the choroidal epithelium

Studies were next carried out to confirm the ability of LCM to resolve the stromal capillary and choroidal epithelial layers. Figure 2A shows an example of the highly selective retrieval of both tissues from naïve and EAE brain specimens. Microscopic analysis indicates no appearance of fluorescently-stained choroidal epithelial tissue in the LCM-captured capillaries and, conversely, no alkaline phosphatase-stained capillary tissue in the retrieved epithelial samples. Figure 2B further highlights the purity in qrt-PCR detection of LCM tissue from the respective CP compartments. Using equivalent amounts of input LCM tissue (1000 laser 'shots') from both CP compartments, the endothelial marker CD31 was significantly enriched in the CP capillary tissue, while the epithelial marker cytokeratin 8 was observed in CP epithelial tissue alone. The extremely low level of CD31

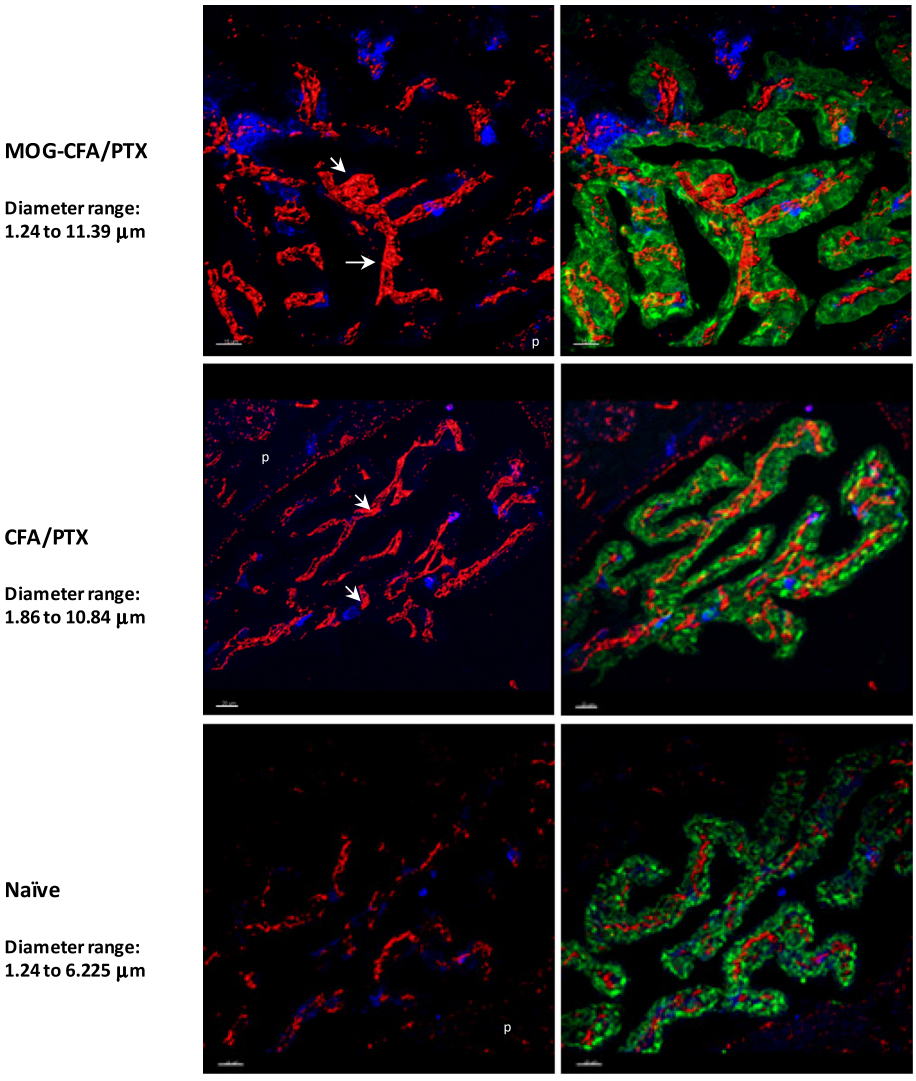

Figure 1 Morphological analysis of CP compartments following immunization. CP epithelium was stained with polyclonal antibody to pan-cytokeratin (FITC, green), and CP stromal capillaries were immunostained with monoclonal anti-CD31 antibody (red). A CD45 antibody was used to stain for any leukocytes present within the CP (blue). Confocal microscopy z-stack images of thick (60 µm) frozen sections of the CP were acquired, and three dimensional rendering was performed using Imaris image analysis software. Shown are rendered images of the CP from all three treatment conditions (MOG-CFA/PTX day 15 p.i., CFA-PTX day 15 p.i. and Naïve), revealing swelling of the stromal capillaries (arrows) following both immunization protocols. The left side shows leukocyte and capillary staining, emphasizing the distended capillary diameters. The right side is a composite of leukocyte, capillary, and epithelial staining. Mean capillary diameter ranges for each group were determined using the Filament tracer module in Imaris. The choroidal epithelium appears unaltered by immunization. 'p' indicates brain parenchymal region. Scale: 20 µm.

mRNA detected in CP epithelial tissue may reflect the few monocytes and/or dendritic cells circulating through this area in the steady-state mouse brain [29,30]. There is thus high confidence that LCM effectively separates CP stromal capillary from choroidal epithelial layers with high purity.

Expression of immune-related genes by stromal CP capillary tissue following immunization

The next series of experiments coupled LCM to TLDA qrt-PCR arrays to further characterize expression patterns of a panorama of 93 immune-related genes in the separate CP compartments at different stages of the neuroinflammatory response to immunization. Expression of these genes relative to housekeeping gene GAPDH (GAPDH was unaffected across treatments; Additional file 2: *Housekeeping control genes*), was determined in three groups of mice: MOG-CFA/PTX, CFA/PTX and naïve at two time points: day 9 and 15 p.i. Contrasting these three treatment groups enabled effects of the adjuvants CFA and PTX to be distinguished from the autoimmune response to MOG. Furthermore,

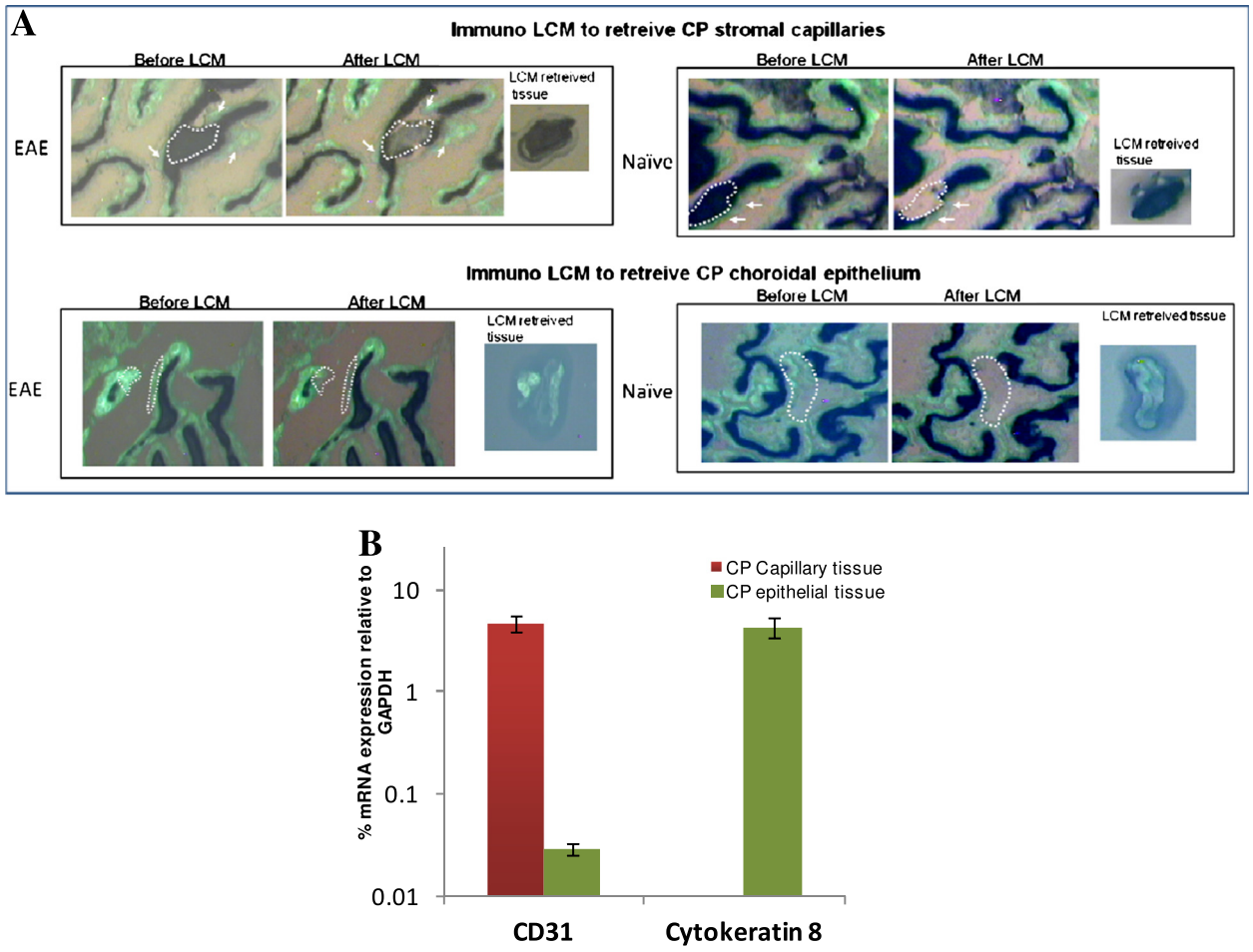

Figure 2 Immuno-LCM allows retrieval of tissue from specific CP compartments. A) Evidence of histological purity. Immunofluorescence was performed using FITC-conjugated pan-cytokeratin antibody to highlight the CP epithelium (green), while immunohistochemistry using alkaline phosphatase detection with NBT/BCIP as substrate was carried-out to label the endothelium of CP stromal capillaries (dark brown). LCM was performed on a Pixcell IIe LCM unit. Images both BEFORE and AFTER LCM, as well as LCM retrieved tissue deposited on the cap, are shown to highlight selective retrieval of CP stromal capillary (top row) and CP choroidal epithelial tissues (bottom row). **B)** Evidence of purity by qrt-PCR. Levels of CD31, an endothelial marker, and Cytokeratin-8, an epithelial marker, were probed to determine the purity of the CP capillary and CP epithelial tissues, respectively, retrieved by LCM.

examining effects at day 9 p.i. (prior to any evidence of clinical disease) and day 15 p.i. (after disease onset), highlighted the progression of gene changes that may be linked with developing pathology.

At *day 9 p.i.* (EAE clinical score 0), numerous gene changes were already evident in the CP stromal capillary tissue, despite the lack of onset of any clinical disease signs. Specifically, both MOG-CFA/PTX- and CFA/PTX-immunized mice showed up-regulated expression in 49 of the genes in the panel compared to naïve animals, (Table 1), with there being no statistically significant differences between the two immunized groups. Some prominent inflammatory genes that were equivalently elevated at this time point included: CCL2, CCL5, CXCL10, Sele (E-selectin), Selp (P-selectin), IL1b, Stat1 and Fasl all of which were modulated more than 10 fold higher than naïve levels. It would thus appear that, at this early stage before clinical EAE symptoms are present, the gene responses in the CP stromal capillary tissue following MOG immunization may stem largely from adjuvants CFA and/or PTX.

By *day 15 p.i.* (EAE clinical score 1.5-2.0), however, the MOG-CFA/PTX-immunized group surpassed the CFA/PTX group in up-regulation of several genes, highlighting what might specifically be the autoimmune response of the CP vascular stroma. These genes included B2m, C3, CCL19, CCL5, CD4, Gzmb, Ptgs2, Ptprc (CD45), Smad3, Stat4, and CD40l – which were selectively augmented in the CP stromal capillary tissue of the MOG-CFA/PTX group (Figure 3). The fold changes in these genes following immunization (Figure 3, bottom) indicate their super-stimulation by MOG-CFA/PTX

Table 1 Genes similarly up-regulated in CP stromal capillary tissue from both MOG-CFA/PTX- and CFA-PTX-immunized mice at day 9 p.i

Genes modulated similarly in stromal CP capillary of MOG-CFA/PTX mice at day 9 p.i	
Gene name	**Gene name**
B2m‡	Il15*
Bcl2l1	Il18*
C3**‡	Il1b**
Ccl19‡	Il7
Ccl2**	Lrp2
Ccl5**‡	Nfkb1*
Ccr2**	Nfkb2
Cd34**	Ptgs*‡
Cd80	Sele**
Cd86*	Selp**
Cd8a	Amad3‡
Col4a5	Socs2
Csf1*	Stat1**
Cxcl10**	Stat3
Cxcr3*	Stat4‡
Ece1	Stat6
Edn1	Tbx21
Fas	Tfrc*
Fn1	Tgfb1
Gzmb‡	Cd40
Hmox1	Fasl**
Hprt1	Vcam1
Icos	Vegfa
Ifng**	

genes with * ≥ 5 and ** ≥ 10 fold increase in expression in comparison to Naïve animals.

Relative mRNA expression values of 93 immune-related genes were determined by immuno-LCM/TLDA in CP stromal capillary tissue from immunized and naïve mice at day 9 p.i. At this early time-point, all 49 immunization-induced genes were similarly stimulated in both MOG-CFA/PTX- and CFA-PTX-immunized mice compared to naïve animals, and only these are listed. ‡ denotes genes that show specific upregulation later on with disease progression on day 15.

treatment. The lymphoid chemokine CCL19, expressed by venules in brain and spinal cord in mice afflicted with EAE [31], was elevated nearly 80-fold in the MOG-CFA/PTX immunized mice at this time-point. And CCL5, another chemokine shown to play an important role in EAE [32], was elevated 146-fold higher than naïve levels. Expression of Ptgs2 (COX2), suppression of which has been associated with resistance to EAE [33,34], was near similarly elevated – having increased 96-fold higher than that in naïve cohorts. Slightly less elevated was Stat4, a transcription factor whose absence has been shown to inhibit EAE [35], which was increased > 40-fold in the MOG immunized group. It is further noteworthy that expression of Ptprc (CD45), the common leukocyte marker, stimulated 219-fold higher, possibly reflecting increased leukocyte extravasation across the stromal capillaries at this later time-point. Consistent with this interpretation is that message for CD40l (CD154), a protein primarily expressed on activated T cells [36], was detected within the CP stromal capillary tissue only following MOG-CFA/PTX immunization.

Notably, the CFA/PTX group indicated some dampening of immune regulation by this time, as certain genes e.g., Smad3 and Gzmb, dropped back to levels matching those of naïve mice, after initially displaying an elevation at day 9. Genes that trended towards elevated expression following MOG-CFA/PTX treatment (but with p values slightly > 0.05) are displayed in Additional file 3: *Genes that trended towards elevated expression in MOG-CFA/PTX- immunized CP stromal capillary tissue compared to CFA-PTX-immunized mice, at day 15 p.i*, while those that were similarly up-regulated in CP stromal capillary tissue of MOG-CFA/PTX- and CFA/PTX-immunized mice compared to naïve mice at day 15 are listed in Additional file 4: *Genes similarly up-regulated in CP stromal capillary tissue from both MOG-CFA/PTX- and CFA-PTX-immunized mice at day 15 p.i.* Genes that were undetected in the CP capillary tissue in all treated and naïve mice at both time-points were the following: CCR4, CD19, CD3e, CSF3, Ctla4, Cyp1a2, Cyp7a1, H2-Ea, IL12b, IL13, IL3, IL4, IL5, IL6, IL9, and Lta.

Expression of immune-related genes by CP choroidal epithelium following immunization

Immunization also produced a change in expression of numerous immune-related genes within the CP choroidal epithelium. Moreover, these changes differed from those observed in the capillary stroma, emphasizing the differential immune sensitivities of the two tissues.

At *day 9 p.i.,* the CP choroidal epithelium of only MOG-CFA/PTX-immunized mice displayed increased expression of any immune-related genes compared to that of naïve cohorts. Specifically, the following eight immune-related genes were up-regulated: B2m, CCL19, CCL2, CCR2, CD8a, CXCL10, Sele, and Selp (Figure 4A). B2m (beta 2 microglobulin), a biomarker for certain peripheral inflammatory conditions [37] was increased 2.2-fold in MOG-treated versus naïve mice. The chemokine CCL2 has been demonstrated to play a critical, non-redundant role in directing mononuclear leukocyte extravasation into the CNS during EAE [32,38,39], and was stimulated > 24-fold higher in the CP choroidal epithelial tissue of MOG-CFA/PTX-treated mice compared to that in naïve cohorts. CXCL10 and CCL19 were 28-and 14-fold higher than naïve values, respectively. Sele (E-selectin) and Selp (P-selectin), CCL19 and CD8a further showed pronounced

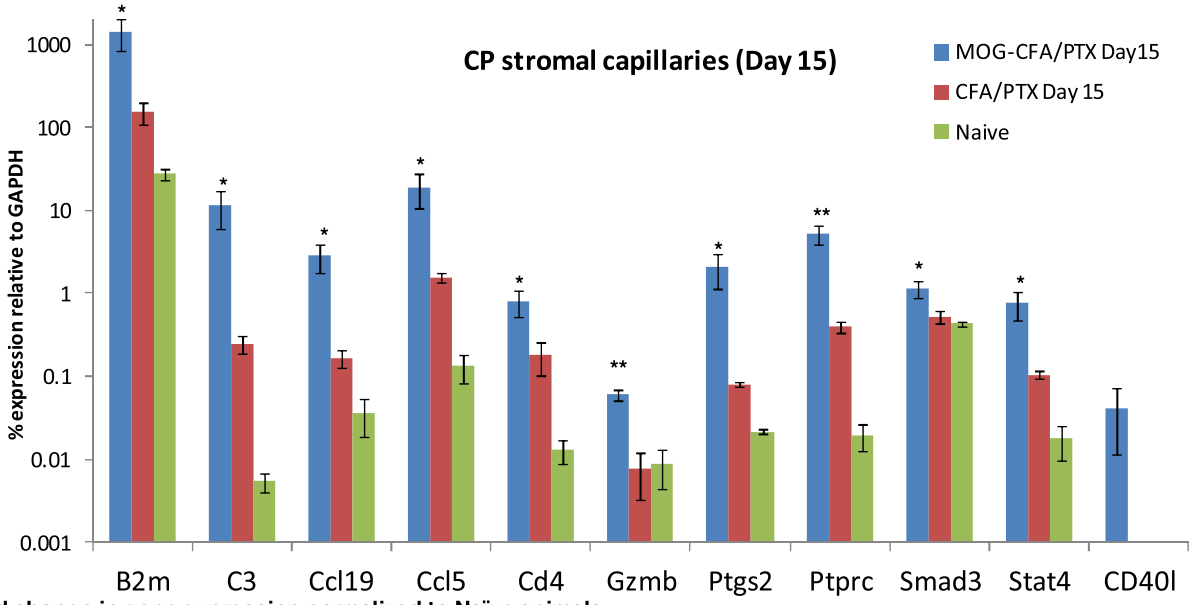

Fold change in gene expression normalized to Naïve animals

	B2m	C3	Ccl19	Ccl5	Cd4	Gzmb	Ptgs2	Ptprc	Smad3	Stat4	CD40l
MOG-CFA/PTX	51.65 ± 15.03	2133 ±704.4	79.59 ±20.6	146.29 ±45.84	62.11 ±15.96	6.81 ±0.82	96.67 ±31.54	219.59 ±74.5	2.71 ±0.45	43.94 ±6.26	∞
CFA/PTX	5.52 ±1.69	45.81 ±10.4	4.77 ±1.16	12.06 ±1.59	14.19 ±6.3	0.85 ±0.49	3.74 ±0.25	20.13 ±3.03	1.23 ±0.22	5.96 ±0.65	-

Figure 3 Genes super-induced in CP stromal capillary tissue from MOG-CFA/PTX-immunized mice at day 15 p.i. Relative mRNA expression values were determined by immuno-LCM/TLDA in CP stromal capillary tissue from MOG-CFA/PTX-immunized, CFA-PTX-immunized, and naïve mice at day 15 p.i. Those genes that were more stimulated; i.e., 'super-induced', in MOG-CFA/PTX- versus CFA-PTX-immunized mice at day 15 p.i. (compared to naïve mice) are graphed. The bar graphs depict those specific genes showing statistically significant differences in relative expression values (*p* values indicated by asterisks) between MOG-CFA/PTX and CFA/PTX experimental groups. RNA values are presented as mean percent expression relative to GAPDH (± SEM) in log scale. * and ** represent comparisons made between MOG-CFA/PTX and CFA-PTX- treatment groups, * $p < 0.05$, ** $p < 0.005$, Student's *t*-test, n = 3 animals/group. Fold changes in gene expression normalized to naïve animals are tabulated below the graph. Fold changes of those genes that were up-regulated after immunizations but undetectable in naïve are denoted as '∞'.

stimulation specifically following MOG immunization, being undetectable in the epithelium of both CFA/PTX and naïve cohorts. In what appears to reflect the differential sensitivities of the two CP tissues, CFA/PTX immunization clearly 'activated' the stromal CP capillary tissue on day 9 p.i. at both the anatomical and molecular levels (Figure 1 and Table 1), but produced no detectable changes in the CP epithelium at this time.

By *day 15 p.i.,* genes B2m and CXCL10 displayed further increases in expression in the CP choroidal epithelium of MOG-CFA/PTX mice compared to that seen in this cohort at day 9 (Figure 4B), showing > 19-fold and > 800-fold higher levels, respectively, compared to naïve mice. Expression levels of yet additional genes in MOG-treated mice also became elevated by this time; these included Bax, Bcl2l1, C3, CD68, Gusb, H2-Eb1 and Ski (Figure 4B). Moreover, genes CCL19, CCL2, CCR2, CD8a, Sele and Selp, which had previously shown up-regulation only in the MOG-CFA/PTX group at day 9, became similarly induced in the CFA/PTX group at this later time-point. Genes that trended towards elevated expression following MOG-CFA/PTX treatment for both time points (but with *p* values slightly >0.05) are displayed in Additional file 5 and Additional file 6: *Genes that trended towards elevated expression in MOG-CFA/PTX immunized CP epithelium tissue compared to CFA-PTX-immunized mice, at day 9/15p.i.,* while those that were similarly up-regulated in CP choroidal epithelial tissue of MOG-CFA/PTX- and CFA/PTX-immunized mice compared to naïve mice for both time points are listed in Additional file 7 and Additional file 8: *Genes similarly up-regulated in CP epithelium from both MOG-CFA/PTX- and CFA-PTX-immunized mice at day 9/15 p.i.* Those few genes that were in the CP epithelial tissue in both immunized groups and naïve mice included IL3, IL4, IL5, IL6, Lta.

Interaction between immunization treatment and time

In order to gain further appreciation of the extent to which time impacted the effect of specific type immunization on the expression patterns of immune-related genes, two-way ANOVA was performed to

deduce *interactive effects* between immunization treatment (e.g., MOG-CFA/PTX, CFA/PTX or naïve) and time post-immunization. For example, the expression of CCL19 in CP stromal capillary tissue following MOG-CFA/PTX immunization was time-dependent ($p < 0.05$ for positive interaction). Two-way ANOVA was done on all genes that displayed statistically significant modulation after immunization in at least one of the CP

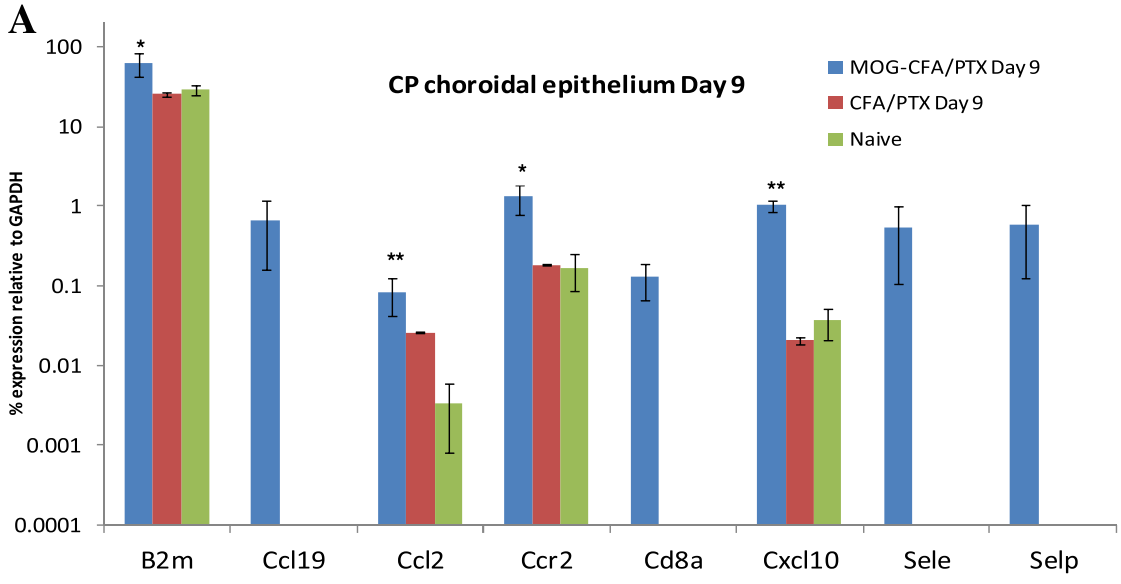

Fold change in gene expression normalized to Naïve animals

MOG-CFA/PTX	2.2 ± 0.98	∞	24.71 ± 12.37	7.85 ± 3.09	∞	28.23 ± 4.71	∞	∞
CFA/PTX	0.88 ± 0.06	-	7.63 ± 0.10	1.09 ± 0.03	-	0.57 ± 0.06	-	-

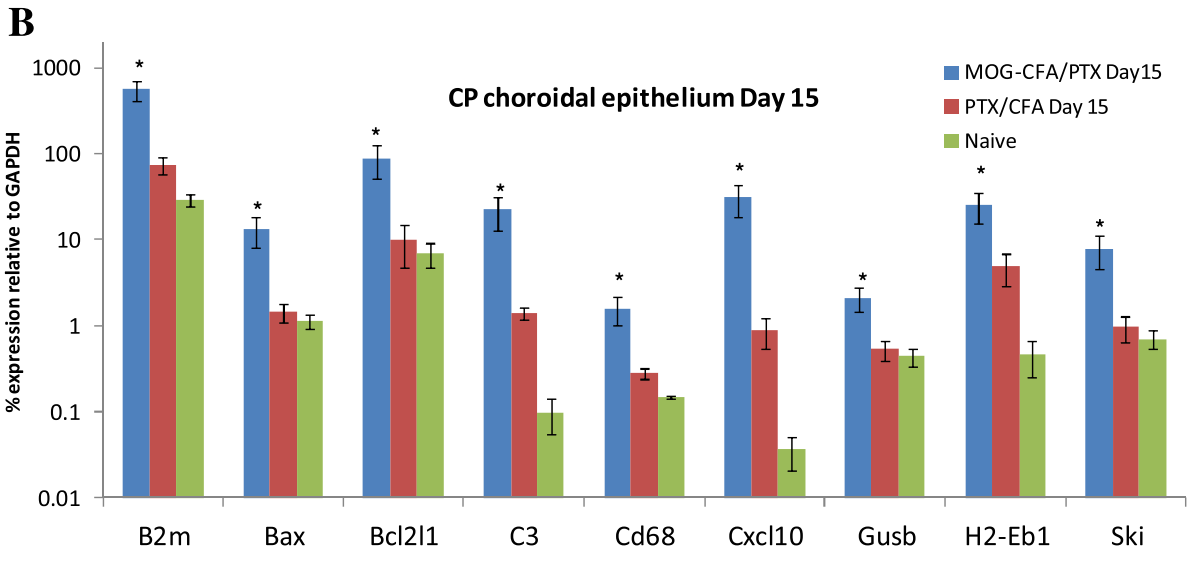

Fold change in gene expression normalized to Naïve animals

MOG-CFA/PTX	19.39 ± 4.24	11.825 ± 3.69	12.74 ± 4.38	228.37 ± 79.27	10.62 ± 3.20	861.39 ± 291.07	4.74 ± 1.17	54.39 ± 16.48	11.08 ± 3.82
CFA/PTX	2.53 ± 0.54	1.3 ± 0.32	1.45 ± 0.75	14.31 ± 2.28	1.89 ± 0.26	24.73 ± 9.70	1.2 ± 0.31	10.58 ± 4.22	1.37 ± 0.46

Figure 4 (See legend on next page.)

(See figure on previous page.)

Figure 4 Genes super-induced in CP choroidal epithelial tissue from MOG-CFA/PTX-immunized mice at days 9 and 15 p.i. Relative mRNA expression values of 93 immune-related genes were determined by immuno-LCM/TLDA in CP choroidal epithelial tissue from MOG-CFA/PTX-immunized, CFA-PTX-immunized, and naïve mice at two time-points. Those genes that were more stimulated in MOG-CFA/PTX- versus CFA-PTX-immunized mice at day 9 (Figure 4**A**) and day 15 p.i (Figure 4**B**) (compared to naïve mice) are graphed. The bar graphs depict those specific genes showing statistically significant differences in relative expression values (*p* values indicated by asterisks) between MOG-CFA/PTX and CFA/PTX experimental groups. RNA values are presented as mean percent expression relative to GAPDH (± SEM) in log scale. * and ** represent comparisons made between MOG-CFA/PTX and CFA-PTX- treatment groups, * $p < 0.05$, ** $p < 0.005$, Student's *t*-test, n = 3 animals/group. Fold changes in gene expression normalized to naïve animals are tabulated below the corresponding graphs. Fold changes of those genes that were up-regulated after immunizations but undetectable in naïve are denoted as '∞'.

compartments (as shown in Figures 3 and 4A, B) in either of the time-points analyzed (twenty-three genes in total). Interactive effects differed depending on the CP compartment, further highlighting the unique responses of the two CP tissues analyzed. Specifically, two-way ANOVA of CP stromal capillary tissue revealed the following twelve genes displayed *positive interaction* between immunization treatment and time post-immunization: B2m, C3, CCL19, CCL5, CD4, Gzmb, Ptgs2, Ptprc, Stat4, CCR2, CD68, Gusb (Figure 5). CP choroidal epithelial tissue, on the other hand, demonstrated *positive interaction* for another collective of genes: B2m, Bax, C3, CXCL10 (Figure 5).

Figure 6 qualitatively summarizes the differential responses of the CP capillary and CP choroidal epithelial tissues, respectively, to MOG-CFA/PTX immunization versus CFA/PTX immunization, contrasting adjuvant versus autoimmune effects on immune-related gene regulation over the two time-points analyzed.

Discussion

Due to increasing awareness of the CP as fundamental to the development of CNS inflammation [4-6], immuno-LCM coupled to qrt-PCR array was used to separately acquire CP stromal capillary and choroidal epithelial tissues and assess their respective patterns of expression *in situ* of a wide panorama of immune-related genes. Gene patterns were evaluated during pre-clinical and early clinical stages of EAE to appreciate the switches in gene expression that accompany evolving disease.

It is clear that the CP responds vigorously to MOG immunization at both the anatomical and molecular levels. Interestingly, immunization with CFA and PTX alone produced striking effects. Swelling of the capillary plexus occurred to nearly the same extent with injection of just these agents, as with PTX and MOG in CFA. PTX is an ancillary adjuvant commonly employed to elicit EAE, as well as several other experimental autoimmune diseases [40-44]. And while its mechanism of action in this regard has generally been attributed to increasing vascular permeability [45-47] – most notably that of the BBB [48-51] – additional hypotheses have been put forth [52-55]. However, to the best of our knowledge, this is the first report to turn attention to the CP as a possible target of PTX. It is of further interest to point out that the distension of CP capillaries noted here study bears similarity to that seen following systemic neutralization of VEGF and TGFβ [56]. In the latter case, CP capillary swelling was accompanied by loss of fenestrae from endothelial cells and appearance of multiple caveolae, transport vesicles that transcytose a variety of cargo [57] – including chemokines [58] – and are often associated with heightened vascular permeability and inflammation [59,60]. Engelhardt et al. [4] had also described ultrastructural changes of the CP during EAE (along with CFA and PTX as adjuvants), but noted these were mostly restricted to the CP choroidal epithelium. Moreover, as comparison in this latter study was just between healthy mice and those afflicted with EAE, it is unclear whether the observed epithelial response was autoimmune in nature and/or due to adjuvant action.

Our results suggest that injection of PTX and/or CFA, alone, might trigger an immune response in the CP capillaries that helps "set the stage" for CNS inflammation [61]. The CP capillaries might be uniquely responsive in this regard, as CFA/PTX treatment evoked an early response (day 9 p.i.) in the CP stromal capillary tissue, while the choroidal epithelium experienced neither overt morphological nor gene expression changes at this time. If, as speculated during MS/EAE, Th17 cells first transit through the CP, and then travel in the CSF to reach their cognate antigens in the SAS, then the CP capillaries must somehow initially be rendered capable of supporting T cell extravasation. In the EAE paradigm used here, PTX and/or CFA might provide the stimulus to evoke such capability. In this regard, we noted > 10-fold increase in chemokines CCL2, CCL5 and CXCL10 in the CP stromal capillaries of both MOG-CFA/PTX- and CFA/PTX-treated mice at day 9 p.i. Constitutive CCL2 expression within the CP stromal tissue has been reported using *in situ* hybridization analysis, and shown to be induced following peripheral tissue inflammation [62]. The ability of CFA/PTX treatment to stimulate expression of these chemokines could potentially reflect the actions of one or both of these adjuvants to 'prime' the neuroinflammatory process by activating the

2-way ANOVA analysis of the interaction between Treatment and Timepoint		
	CP Stromal Capillaries	CP Epithelium
Gene	*Interaction*	*Interaction*
B2m	p < 0.05	p <0.005
C3	p < 0.05	p < 0.05
CCL19	p < 0.05	x
CCL2	x	x
CCL5	p < 0.05	x
CCR2	p < 0.05	x
CD4	p < 0.05	x
CD40l	x	x
CD68	p < 0.05	x
CD8a	x	x
Gusb	p < 0.05	x
Gzmb	p < 0.0005	x
Ptgs2	p < 0.05	x
Ptprc	p < 0.0005	x
Smad3	p < 0.05	x
Stat4	p < 0.0005	x
CXCL10	x	p < 0.05
Bax	x	p < 0.05
Bcl2l1	x	x
H2-Eb1	x	x
Ski	x	x
Sele	x	x
Selp	x	x

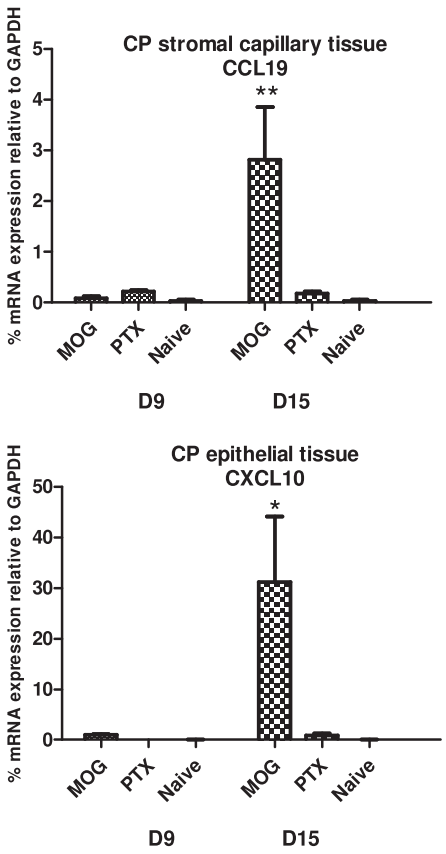

Figure 5 Interaction between immunization treatment and time of analysis post-immunization on expression of immune-related genes within CP stromal capillary and choroidal epithelial compartments. Interactive effects of treatment (MOG-CFA/PTX, CFA-PTX and naïve) and time post-immunization were determined by two-way ANOVA on the 23 immune-related genes that were super-induced following MOG-CFA/PTX immunization in either of the two CP compartments (those genes graphed in Figures 3, 4A and B). Of these 23 genes, 13 genes in the CP stromal capillary and 4 genes in the CP epithelial tissue exhibited significant *positive interaction* between treatment and time post-immunization, and are denoted with their corresponding *p* values. The remaining genes that showed no significant interaction are labeled by (*x*). Time-dependent changes in expression of CCL19 in stromal capillary tissue and CXCL10 in choroidal epithelial tissue are graphed as representative examples * $p < 0.05$, ** $p < 0.005$.

endothelium to elicit initial auto reactive T cell extravasation from the circulation into the stromal compartment. This hypothesis is consistent with the recent observation that administration of PTX to transgenic mice over-expressing CCL2 in the CNS causes disruption of the BBB and promotes leukocyte migration into the brain parenchyma [63].

Notwithstanding the effects of CFA/PTX treatment on CP capillary morphology and gene expression, immunization with MOG-CFA/PTX further induced the expression of additional genes – some or all of which might specifically reflect the autoimmune response and associated development of EAE. While perhaps necessary for disease to develop, the CP conditions set in place by PTX and CFA are insufficient for inducing EAE in wild-type C57BL/6 mice. For disease to occur, supernumerary induction of some genes, and *de novo* induction of others must take place. The findings by Goverman et al. and Brabb et al. [61,64], that injection of PTX alone can "trigger" EAE in TCR-transgenic mice specific for myelin basic protein, by fostering T cell access to the CNS, comports with our results and the view that PTX enables mice to reach the disease threshold. And helping pull this trigger may be additional effects of PTX on T cell behavior. Our observation of increased mRNA for genes CD8a, CD80, CD86, Gzmb (granzyme) and Ptprc (CD45) in the CP capillary stromal tissue of both MOG-CFA/PTX and CFA/PTX cohorts may reflect capture of PTX-activated CD8 T cells in transit across the CP and into the CSF. This interpretation is consistent with the recent finding by Murphey et al. [65], that PTX stimulation of cultured spleen cells results in CD 8 T cell activation via CD80/86 co-stimulation.

As to signals responsible for the extravasation of T cells from the circulation into the CP stroma during MOG-induced EAE, a combination of chemokines may fill this role, as these immune mediators do in guiding

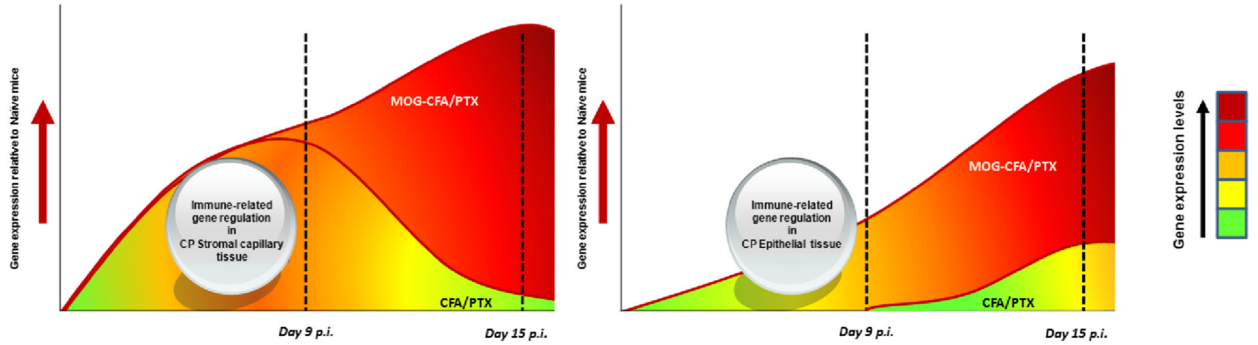

Figure 6 Schematic summary of the induction of immune-related genes in the choroid plexus compartments following MOG-CFA/PTX versus CFA-PTX immunization. Depicted are qualitative 'heat maps' of overall modulation in immune-related gene expression patterns over time, within the separate CP stromal capillary (left) and CP choroidal epithelial (right) tissues after the two type immunization regimens. While CFA/PTX immunization alone induces expression of immune-related genes in both tissues, MOG-CFA/PTX immunization causes supernumerary stimulation above this level. The differences in gene expression between the immunization regimens highlight what might reflect gene changes specifically due to MOG-associated autoimmunity. The effects due solely to CFA/PTX immunization might reveal priming of the immune response that is necessary for the development of EAE.

parenchymal leukocyte infiltration. In particular, CCL5 level was increased significantly in CP stromal capillary tissue at day 15 p.i., which coincides with high CCL5 protein level reported in whole brain extract of EAE mice at a similar time-point, and argued to mediate leukocyte adherence to the CNS microvasculature [32]. And CCL19 – a CCR7 ligand known to play a crucial role in EAE development through IL-23 producing Th17 cells [66] – was likewise up-regulated dramatically in the CP stromal capillaries of MOG immunized mice at day 15 p.i.

With specific regard to those mechanism(s) further driving T cell migration from the CP stroma into the CSF, recent evidence points toward expression of another chemokine - CCL20 - by the CP choroidal epithelium as directing $CCR6^+$ T cells across this layer and into ventricular fluid during MS/EAE [8]. However, as this chemokine:cognate receptor pair was not represented on the commercial TLDA card used in these experiments, confirmation of this pathway was not performed. Aside from CCL20 providing a driving force for T cell migration into CP epithelium, CCL2 might also serve in this capacity, as Chodobska et al. [67] noted the latter chemokine was rapidly stimulated in this tissue *in vivo* and then released into the CSF, following traumatic brain injury. Indeed, the significant increase in CCL2 we observed in the MOG-CFA/PTX CP choroidal epithelium at day 9 p.i. might just reflect such a role for this chemokine in EAE. The cognate receptor for CCL2, CCR2 was also seen to be elevated in the choroidal epithelium at this early time-point. Presently, it is unclear if the high levels of CCR2 mRNA indicate activation of the epithelium, which, in the periphery, has been shown to express CCR2 [68,69], or the accumulation of infiltrating $CCR2^+$ T cells.

In what might suggest multi-level control of leukocyte extravasation into the CSF, still other chemokines were also significantly up-regulated by the CP during EAE – namely CXCL10 and CCL19. As CXCL10 has been reported to be up-regulated in the sub-ventricular zone (SVZ) during EAE, and postulated to stimulate migration of activated T cells into the SVZ [70], its spike in expression by CP choroidal epithelial tissue at day 9 p.i. and more robust elevation by day 15 p.i., might imply this chemokine is obligate for T cell entry into the ventricles. In analogous manner, CCL19 was also elevated at this site at day 9 p.i. In fact, the timing of the CP epithelial spikes in this chemokine during early stages of EAE noted here, coincides well with that reported by Reboldi et al. [8] for initial T cell entry into the uninflamed CNS through the CP. Recently, Marques et al. [22,71] used hybridization-based microarray to assess the global transcriptome of the whole CP following chronic peripheral LPS stimulation. When compared to our study, there were some common and unique findings. Among the common findings, complement protein C3, and chemokines CCL2 and CCL5 were elevated following either *acute* or *chronic* peripheral LPS stimulation, as well as during MOG-induced EAE (complement C3 in both CP capillary tissue and epithelium; CCL2 in CP epithelium; and CCL5 in CP capillary tissue). And Selectin (Sele and Selp) expression was also elevated both following *acute* peripheral LPS stimulation [22], and in the CP epithelium after MOG-induced EAE. These common gene modulations may thus reflect more generic CP inflammatory response genes. As for unique findings, these too involved chemokines. Marques et al. [71] reported stimulation of CCL7 and CXCL1 in the CP following *chronic* LPS stimulation, while we detected stimulation of CCL19 and CXCL10 in the CP epithelium and CCL19 in the CP endothelium during

MOG-induced EAE. *A priori*, up-regulation of these latter two chemokine genes may more distinguish an EAE signature for the respective CP tissue compartments.

Of further note was our observation of a MOG-sensitive increase in expression of B2m at day 15 p.i. in CP stromal capillary tissue, and at both time-points in the choroidal epithelial tissue. Aside from perhaps reinforcing a more ubiquitous role for B2m in inflammation [37], this result complements previous reports of increased B2m mRNA and protein levels in both neuronal and non neuronal cell types during EAE [72,73], a response thought to be due to induction of synaptic plasticity by infiltrating autoreactive immune cells. The sharp induction of complement C3, also noted in both CP compartments of MOG-CFA/PTX mice at the later time point (day 15 p.i), further supports previous studies highlighting C3 deficiency inhibits development of EAE [74].

As to the specific approach used here, i.e., LCM coupled to TLDA, it offered extraordinary opportunity to probe, in extensive detail, the focused immune response within the distinct CP compartments. Earlier reports, using immunohistochemistry and *in situ* hybridization, had shown that the respective CP stromal capillary endothelial cells and the CP choroidal epithelial cells displayed different expression patterns of a small nucleus of adhesion molecules during EAE [4,20]. Specifically, VCAM-1 and ICAM-1 were found to be expressed constitutively by CP choroidal epithelial cells of healthy SJL/N mice, and then further induced following active immunization with spinal cord homogenate. MAdCAM-1 was only seen in these cells after induction of EAE. However, none of these adhesion molecules, nor E- or P-selectin, was detected in CP stromal capillary endothelial cells [75].

We too noted constitutive VCAM-1 expression in the CP choroidal epithelial tissue of healthy naïve mice. Likewise, VCAM-1 trended toward elevation within this CP compartment of MOG-CFA/PTX cohorts at both days 9 and 15 p.i., though it showed no up-regulation in CFA-PTX-immunized mice at either time-point. In further agreement with previous observations [75], our analysis demonstrated induction of E-selectin and P-selectin in the CP choroidal epithelial tissue from MOG-CFA/PTX-immunized mice at day 9. Our results nevertheless displayed some stark differences with earlier reports. Specifically, we also noted a trend of increased VCAM-1 expression by day 15 in CP stromal capillary tissue with MOG immunization, paralleling what has been described in MS brain tissue [6]. And both E- and P-selectin mRNA were also observed to be induced in CP stromal capillary tissue of both MOG-CFA/PTX- and CFA/PTX-immunized mice compared to that of naïve mice at day 9 p.i. E-selectin increased expression in the two immunized groups by >100-fold, while P-selectin was stimulated >10-fold.

A priori, differences in results between these EAE studies could result from several factors, among them being 1) the EAE model employed (e.g., immunization of SJL/6 mice with spinal cord homogenate versus immunization of C57BL/6 mice with MOG_{35-55} peptide), the time of analysis post-immunization (e.g, before or after disease onset), and 3) the sensitivity of the analytic techniques (e.g., *in situ* hybridization versus qrt-PCR). As neither MAdCAM-1 nor ICAM-1 were represented on the TLDA card used in these experiments, confirmation of expression or lack thereof was not possible for these genes.

Most recently, Liddelow et al. [76] employed LCM to collect mouse lateral ventricular CP tissue CP for transcriptome analysis of transporter gene expression during normal development. Here, we extended this application, utilizing LCM to resolve – for the first time – the CP capillary stromal tissue from the CP choroidal tissue, and then separately analyzing each for their unique immune responses to MOG immunization.

Conclusions

Induction of EAE in C57BL/6 mice by active immunization with MOG_{35-55} peptide results in the respective CP stromal capillary and choroidal epithelial compartments each mounting vigorous, yet distinct, immune responses, underscoring the active role of the CP in instigating CNS inflammatory disease. Furthermore, our results make clear that a significant component of the total CP response is due to effects elicited by adjuvants PTX and/or CFA used in the immunization protocol – which might serve to prime the CP to support autoimmune activity necessary for developing MS/EAE. These results are summarized schematically in Figure 6.

Additional files

Additional file 1: Mouse Immune Panel TLDA. The card map for the 96 genes (93 immune-related genes and 3 control genes) on the commercially available mouse Immune panel TLDA is shown, with gene names and corresponding accession numbers.

Additional file 2: Housekeeping control genes. Ct (Threshold cycle) values for the three housekeeping genes – GAPDH, β-Actin and 18 S represented on the mouse Immune-panel TLDA are shown. The housekeeping genes were almost unchanged across treatments (shown in A and B) with < 1 cycle difference between samples. C, Six genes were normalized to each of the three housekeeping gene and expression patterns plotted, indicating identical patterns of expression across housekeeping control gene used.

Additional file 3: Genes that trended towards elevated expression in MOG-CFA/PTX- immunized CP stromal capillary tissue compared to CFA-PTX-immunized mice, at day 15 p.i. Relative mRNA expression values of 93 immune-related genes were determined by immuno-LCM/TLDA in CP stromal capillary tissue from immunized and naïve mice at day 15 p.i. A total of 14 genes trended towards greater induction in the MOG-CFA/PTX group compared to the CFA-PTX group; these genes are listed with their corresponding *p* values. Analysis was by Student's two-tailed *t*-test.

Additional file 4: Genes similarly up-regulated in CP stromal capillary tissue from both MOG-CFA/PTX- and CFA-PTX-immunized mice at day 15 p.i. Relative mRNA expression values of 93 immune-related genes were determined by immuno-LCM/TLDA in CP stromal capillary tissue from immunized and naïve mice at day 15 p.i. At this later time-point, 25 immunization-induced genes were similarly stimulated in both MOG-CFA/PTX- and CFA-PTX-immunized mice compared to naïve animals, and only these are listed.

Additional file 5: Genes that trended towards elevated expression in MOG-CFA/PTX immunized CP epithelium tissue compared to CFA-PTX-immunized mice, at day 9 p.i. Relative mRNA expression values of 93 immune-related genes were determined by immuno-LCM/TLDA in CP epithelium from immunized and naïve mice at day 9 p.i. A total of 15 genes trended towards greater induction in the MOG-CFA/PTX group compared to the CFA-PTX group; these genes are listed with their corresponding *p* values. Analysis was by Student's two-tailed *t*-test.

Additional file 6: Genes that trended towards elevated expression in MOG-CFA/PTX immunized CP epithelium tissue compared to CFA-PTX-immunized mice, at day 15 p.i. Relative mRNA expression values of 93 immune-related genes were determined by immuno-LCM/TLDA in CP epithelium from immunized and naïve mice at day 15 p.i. A total of 19 genes trended towards greater induction in the MOG-CFA/PTX group compared to the CFA-PTX group; these genes are listed with their corresponding *p* values. Analysis was by Student's two-tailed *t*-test.

Additional file 7: Genes similarly up-regulated in CP epithelium from both MOG-CFA/PTX- and CFA-PTX-immunized mice at day 9 p.i. Relative mRNA expression values of 93 immune-related genes were determined by immuno-LCM/TLDA in CP epithelium from immunized and naïve mice at day 9 p.i. At this early time-point, 10 immunization-induced genes were similarly stimulated in both MOG-CFA/PTX- and CFA-PTX-immunized mice compared to naïve animals, and only these are listed.

Additional file 8: Genes similarly up-regulated in CP epithelium from both MOG-CFA/PTX- and CFA-PTX-immunized mice at day 15 p.i. Relative mRNA expression values of 93 immune-related genes were determined by immuno-LCM/TLDA in CP epithelium from immunized and naïve mice at day 15 p.i. At this later time-point, 8 immunization-induced genes were similarly stimulated in both MOG-CFA/PTX- and CFA-PTX-immunized mice compared to naïve animals, and only these are listed.

Competing interests
The authors have no competing interests.

Authors' contributions
N. Murugesan assisted in the design of the experiments, developed the immuno-LCM protocol for evaluating the different CP tissues, performed the immuno-LCM/TLDA analyses of CP tissues and microscopic evaluation of CP structure in response to immunization, and contributed to the writing and editing of the manuscript. D. Paul assisted with the 3-D image analysis of CP structure. B. Shrestha assisted with the immuno-LCM/TLDA analyses. Y. Lemire and S. Ge assisted with the immunizations. J. Pachter designed the experiments, wrote the manuscript and provided oversight for all studies. All authors have read and approved the final version of the manuscript.

Acknowledgements
This work was supported by grant RG 4503A4/1 from the National Multiple Sclerosis Society to J. S. Pachter and S. Ge.

Received: 30 May 2012 Accepted: 30 July 2012
Published: 7 August 2012

References
1. Davson H, Segal MB: **The effects of some inhibitors and accelerators of sodium transport on the turnover of 22Na in the cerebrospinal fluid and the brain.** *J Physiol* 1970, **209:**131–153.
2. Speake T, Whitwell C, Kajita H, Majid A, Brown PD: **Mechanisms of CSF secretion by the choroid plexus.** *Microsc Res Tech* 2001, **52:**49–59.
3. Brown PD, Davies SL, Speake T, Millar ID: **Molecular mechanisms of cerebrospinal fluid production.** *Neuroscience* 2004, **129:**957–970.
4. Engelhardt B, Wolburg-Buchholz K, Wolburg H: **Involvement of the choroid plexus in central nervous system inflammation.** *Microsc Res Tech* 2001, **52:**112–129.
5. Brown DA, Sawchenko PE: **Time course and distribution of inflammatory and neurodegenerative events suggest structural bases for the pathogenesis of experimental autoimmune encephalomyelitis.** *J Comp Neurol* 2007, **502:**236–260.
6. Vercellino M, Votta B, Condello C, Piacentino C, Romagnolo A, Merola A, Capello E, Mancardi GL, Mutani R, Giordana MT, Cavalla P: **Involvement of the choroid plexus in multiple sclerosis autoimmune inflammation: a neuropathological study.** *J Neuroimmunol* 2008, **199:**133–141.
7. Kivisakk P, Mahad DJ, Callahan MK, Trebst C, Tucky B, Wei T, Wu L, Baekkevold ES, Lassmann H, Staugaitis SM, Campbell JJ, Ransohoff RM: **Human cerebrospinal fluid central memory CD4+ T cells: evidence for trafficking through choroid plexus and meninges via P-selectin.** *Proc Natl Acad Sci USA* 2003, **100:**8389–8394.
8. Reboldi A, Coisne C, Baumjohann D, Benvenuto F, Bottinelli D, Lira S, Uccelli A, Lanzavecchia A, Engelhardt B, Sallusto F: **C-C chemokine receptor 6-regulated entry of TH-17 cells into the CNS through the choroid plexus is required for the initiation of EAE.** *Nat Immunol* 2009, **10:**514–523.
9. Kivisakk P, Imitola J, Rasmussen S, Elyaman W, Zhu B, Ransohoff RM, Khoury SJ: **Localizing central nervous system immune surveillance: meningeal antigen-presenting cells activate T cells during experimental autoimmune encephalomyelitis.** *Ann Neurol* 2009, **65:**457–469.
10. Bartholomaus I, Kawakami N, Odoardi F, Schlager C, Miljkovic D, Ellwart JW, Klinkert WE, Flugel-Koch C, Issekutz TB, Wekerle H, Flugel A: **Effector T cell interactions with meningeal vascular structures in nascent autoimmune CNS lesions.** *Nature* 2009, **462:**94–98.
11. Goverman J: **Autoimmune T cell responses in the central nervous system.** *Nat Rev Immunol* 2009, **9:**393–407.
12. Wolburg H, Paulus W: **Choroid plexus: biology and pathology.** *Acta Neuropathol* 2010, **119:**75–88.
13. Brightman M: **Ultrastructural characteristics of adult choroid plexus: Relation to the blood-cerebral spinal fluid barrier to proteins.** In *The Choroid Plexus in Health and Disease*. Edited by Netsky MG, Shuangshoti. VA: University Press of Virginia Charlottesville; 1975:86–112.
14. Hurley JV, Anderson RM, Sexton PT: **The fate of plasma protein which escapes from blood vessels of the choroid plexus of the rat–an electron microscope study.** *J Pathol* 1981, **134:**57–70.
15. Redzic ZB, Segal MB: **The structure of the choroid plexus and the physiology of the choroid plexus epithelium.** *Adv Drug Deliv Rev* 2004, **56:**1695–1716.
16. Johanson CE, Stopa EG, McMillan PN: **The blood-cerebrospinal fluid barrier: structure and functional significance.** *Methods Mol Biol* 2011, **686:**101–131.
17. Axtell RC, Steinman L: **Gaining entry to an uninflamed brain.** *Nat Immunol* 2009, **10:**453–455.
18. Ransohoff RM: **Immunology: In the beginning.** *Nature* 2009, **462:**41–42.
19. Steffen BJ, Breier G, Butcher EC, Schulz M, Engelhardt B: **ICAM-1, VCAM-1, and MAdCAM-1 are expressed on choroid plexus epithelium but not endothelium and mediate binding of lymphocytes in vitro.** *Am J Pathol* 1996, **148:**1819–1838.
20. Wolburg K, Gerhardt H, Schulz M, Wolburg H, Engelhardt B: **Ultrastructural localization of adhesion molecules in the healthy and inflamed choroid plexus of the mouse.** *Cell Tissue Res* 1999, **296:**259–269.
21. Marques F, Sousa JC, Coppola G, Gao F, Puga R, Brentani H, Geschwind DH, Sousa N, Correia-Neves M, Palha JA: **Transcriptome signature of the adult mouse choroid plexus.** *Fluids Barriers CNS* 2011, **8:**10.
22. Marques F, Sousa JC, Coppola G, Falcao AM, Rodrigues AJ, Geschwind DH, Sousa N, Correia-Neves M, Palha JA: **Kinetic profile of the transcriptome changes induced in the choroid plexus by peripheral inflammation.** *J Cereb Blood Flow Metab* 2009, **29:**921–932.
23. Demarest TG, Murugesan N, Shrestha B, Pachter JS: **Rapid expression profiling of brain microvascular endothelial cells by immuno-laser capture microdissection coupled to TaqMan((R)) Low Density Array.** *J Neurosci Methods* 2012, **206:**200–204.
24. Macdonald JA, Murugesan N, Pachter JS: **Validation of immuno-laser capture microdissection coupled with quantitative RT-PCR to probe**

blood–brain barrier gene expression in situ. *J Neurosci Methods* 2008, **174:**219–226.
25. Juedes AE, Hjelmstrom P, Bergman CM, Neild AL, Ruddle NH: **Kinetics and cellular origin of cytokines in the central nervous system: insight into mechanisms of myelin oligodendrocyte glycoprotein-induced experimental autoimmune encephalomyelitis.** *J Immunol* 2000, **164:**419–426.
26. Kinnecom K, Pachter JS: **Selective capture of endothelial and perivascular cells from brain microvessels using laser capture microdissection.** *Brain Res Brain Res Protoc* 2005, **16:**1–9.
27. Macdonald JA, Murugesan N, Pachter JS: **Endothelial cell heterogeneity of blood–brain barrier gene expression along the cerebral microvasculature.** *J Neurosci Res* 2010, **88:**1457–1474.
28. Murugesan N, Macdonald JA, Lu Q, Wu SL, Hancock WS, Pachter JS: **Analysis of mouse brain microvascular endothelium using laser capture microdissection coupled with proteomics.** *Methods Mol Biol* 2011, **686:**297–311.
29. Ma L, Mauro C, Cornish GH, Chai JG, Coe D, Fu H, Patton D, Okkenhaug K, Franzoso G, Dyson J, Nourshargh S, Marelli-Berg FM: **Ig gene-like molecule CD31 plays a nonredundant role in the regulation of T-cell immunity and tolerance.** *Proc Natl Acad Sci U S A* 2010, **107:**19461–19466.
30. Anandasabapathy N, Victora GD, Meredith M, Feder R, Dong B, Kluger C, Yao K, Dustin ML, Nussenzweig MC, Steinman RM, Liu K: **Flt3L controls the development of radiosensitive dendritic cells in the meninges and choroid plexus of the steady-state mouse brain.** *J Exp Med* 2011, **208:**1695–1705.
31. Engelhardt B: **Molecular mechanisms involved in T cell migration across the blood–brain barrier.** *J Neural Transm* 2006, **113:**477–485.
32. dos Santos AC, Barsante MM, Arantes RM, Bernard CC, Teixeira MM, Carvalho-Tavares J: **CCL2 and CCL5 mediate leukocyte adhesion in experimental autoimmune encephalomyelitis–an intravital microscopy study.** *J Neuroimmunol* 2005, **162:**122–129.
33. Moon C, Ahn M, Wie MB, Kim HM, Koh CS, Hong SC, Kim MD, Tanuma N, Matsumoto Y, Shin T: **Phenidone, a dual inhibitor of cyclooxygenases and lipoxygenases, ameliorates rat paralysis in experimental autoimmune encephalomyelitis by suppressing its target enzymes.** *Brain Res* 2005, **1035:**206–210.
34. Perez-Nievas BG, Garcia-Bueno B, Madrigal JL, Leza JC: **Chronic immobilisation stress ameliorates clinical score and neuroinflammation in a MOG-induced EAE in Dark Agouti rats: mechanisms implicated.** *J Neuroinflammation* 2010, **7:**60.
35. Chitnis T, Najafian N, Benou C, Salama AD, Grusby MJ, Sayegh MH, Khoury SJ: **Effect of targeted disruption of STAT4 and STAT6 on the induction of experimental autoimmune encephalomyelitis.** *J Clin Invest* 2001, **108:**739–747.
36. Elgueta R, Benson MJ, de Vries VC, Wasiuk A, Guo Y, Noelle RJ: **Molecular mechanism and function of CD40/CD40L engagement in the immune system.** *Immunol Rev* 2009, **229:**152–172.
37. Bethea M, Forman DT: **Beta 2-microglobulin: its significance and clinical usefulness.** *Ann Clin Lab Sci* 1990, **20:**163–168.
38. Huang DR, Wang J, Kivisakk P, Rollins BJ, Ransohoff RM: **Absence of monocyte chemoattractant protein 1 in mice leads to decreased local macrophage recruitment and antigen-specific T helper cell type 1 immune response in experimental autoimmune encephalomyelitis.** *J Exp Med* 2001, **193:**713–726.
39. Dogan RN, Elhofy A, Karpus WJ: **Production of CCL2 by central nervous system cells regulates development of murine experimental autoimmune encephalomyelitis through the recruitment of TNF- and iNOS-expressing macrophages and myeloid dendritic cells.** *J Immunol* 2008, **180:**7376–7384.
40. Lee JM, Olitsky PK: **Simple method for enhancing development of acute disseminated encephalomyelitis in mice.** *Proc Soc Exp Biol Med* 1955, **89:**263–266.
41. Levine S, Sowinski R: **Experimental allergic encephalomyelitis in inbred and outbred mice.** *J Immunol* 1973, **110:**139–143.
42. Mochizuki M, Charley J, Kuwabara T, Nussenblatt RB, Gery I: **Involvement of the pineal gland in rats with experimental autoimmune uveitis.** *Invest Ophthalmol Vis Sci* 1983, **24:**1333–1338.
43. Tung K, Taguchi O, Tester C: **Testicular and ovarian autoimmune diseases.** In *Autoimmune Disease Models*. Edited by Cohen I, Miller A. San Diego: Academic; 1994:267–290.
44. Caspi RR, Silver PB, Chan CC, Sun B, Agarwal RK, Wells J, Oddo S, Fujino Y, Najafian F, Wilder RL: **Genetic susceptibility to experimental autoimmune uveoretinitis in the rat is associated with an elevated Th1 response.** *J Immunol* 1996, **157:**2668–2675.
45. Garcia JG, Wang P, Liu F, Hershenson MB, Borbiev T, Verin AD: **Pertussis toxin directly activates endothelial cell p42/p44 MAP kinases via a novel signaling pathway.** *Am J Physiol Cell Physiol* 2001, **280:**C1233–C1241.
46. Garcia JG, Wang P, Schaphorst KL, Becker PM, Borbiev T, Liu F, Birukova A, Jacobs K, Bogatcheva N, Verin AD: **Critical involvement of p38 MAP kinase in pertussis toxin-induced cytoskeletal reorganization and lung permeability.** *FASEB J* 2002, **16:**1064–1076.
47. Munoz J: **Action of pertussigen (pertussis toxin) on the host immune system.** In *Pathogenesis and Immunity in Pertussis*. Edited by Wardlaw AC, Partoin R. New York: Wiley; 1988:173–187.
48. Linthicum DS, Munoz JJ, Blaskett A: **Acute experimental autoimmune encephalomyelitis in mice. I. Adjuvant action of Bordetella pertussis is due to vasoactive amine sensitization and increased vascular permeability of the central nervous system.** *Cell Immunol* 1982, **73:**299–310.
49. Yong T, Meininger GA, Linthicum DS: **Enhancement of histamine-induced vascular leakage by pertussis toxin in SJL/J mice but not BALB/c mice.** *J Neuroimmunol* 1993, **45:**47–52.
50. Kugler S, Bocker K, Heusipp G, Greune L, Kim KS, Schmidt MA: **Pertussis toxin transiently affects barrier integrity, organelle organization and transmigration of monocytes in a human brain microvascular endothelial cell barrier model.** *Cell Microbiol* 2007, **9:**619–632.
51. Bruckener KE, el Baya A, Galla HJ, Schmidt MA: **Permeabilization in a cerebral endothelial barrier model by pertussis toxin involves the PKC effector pathway and is abolished by elevated levels of cAMP.** *J Cell Sci* 2003, **116:**1837–1846.
52. Blankenhorn EP, Butterfield RJ, Rigby R, Cort L, Giambrone D, McDermott P, McEntee K, Solowski N, Meeker ND, Zachary JF, Doerge RW, Teuscher C: **Genetic analysis of the influence of pertussis toxin on experimental allergic encephalomyelitis susceptibility: an environmental agent can override genetic checkpoints.** *J Immunol* 2000, **164:**3420–3425.
53. Hofstetter HH, Shive CL, Forsthuber TG: **Pertussis toxin modulates the immune response to neuroantigens injected in incomplete Freund's adjuvant: induction of Th1 cells and experimental autoimmune encephalomyelitis in the presence of high frequencies of Th2 cells.** *J Immunol* 2002, **169:**117–125.
54. Racke MK, Hu W, Lovett-Racke AE: **PTX cruiser: driving autoimmunity via TLR4.** *Trends Immunol* 2005, **26:**289–291.
55. Richard JF, Roy M, Audoy-Remus J, Tremblay P, Vallieres L: **Crawling phagocytes recruited in the brain vasculature after pertussis toxin exposure through IL6, ICAM1 and ITGalphaM.** *Brain Pathol* 2011, **21:**661–671.
56. Maharaj AS, Walshe TE, Saint-Geniez M, Venkatesha S, Maldonado AE, Himes NC, Matharu KS, Karumanchi SA, D'Amore PA: **VEGF and TGF-beta are required for the maintenance of the choroid plexus and ependyma.** *J Exp Med* 2008, **205:**491–501.
57. Frank PG, Pavlides S, Lisanti MP: **Caveolae and transcytosis in endothelial cells: role in atherosclerosis.** *Cell Tissue Res* 2009, **335:**41–47.
58. Ge S, Song L, Serwanski DR, Kuziel WA, Pachter JS: **Transcellular transport of CCL2 across brain microvascular endothelial cells.** *J Neurochem* 2008, **104:**1219–1232.
59. Chidlow JH Jr, Sessa WC: **Caveolae, caveolins, and cavins: complex control of cellular signalling and inflammation.** *Cardiovasc Res* 2010, **86:**219–225.
60. Komarova Y, Malik AB: **Regulation of endothelial permeability via paracellular and transcellular transport pathways.** *Annu Rev Physiol* 2010, **72:**463–493.
61. Brabb T, Goldrath AW, von Dassow P, Paez A, Liggitt HD, Goverman J: **Triggers of autoimmune disease in a murine TCR-transgenic model for multiple sclerosis.** *J Immunol* 1997, **159:**497–507.
62. Mitchell K, Yang HY, Berk JD, Tran JH, Iadarola MJ: **Monocyte chemoattractant protein-1 in the choroid plexus: a potential link between vascular pro-inflammatory mediators and the CNS during peripheral tissue inflammation.** *Neuroscience* 2009, **158:**885–895.
63. Schellenberg AE, Buist R, Del Bigio MR, Khorooshi R, Toft-Hansen H, Owens T, Peeling J: **Blood–brain barrier disruption in CCL2 transgenic**

mice during pertussis toxin-induced brain inflammation. *Fluids Barriers CNS* 2012, **9**:10.
64. Goverman J, Woods A, Larson L, Weiner LP, Hood L, Zaller DM: **Transgenic mice that express a myelin basic protein-specific T cell receptor develop spontaneous autoimmunity.** *Cell* 1993, **72**:551–560.
65. Murphey C, Chang S, Zhang X, Arulanandam B, Forsthuber TG: **Induction of polyclonal CD8+ T cell activation and effector function by Pertussis toxin.** *Cell Immunol* 2011, **267**:50–55.
66. Kuwabara T, Ishikawa F, Yasuda T, Aritomi K, Nakano H, Tanaka Y, Okada Y, Lipp M, Kakiuchi T: **CCR7 ligands are required for development of experimental autoimmune encephalomyelitis through generating IL-23-dependent Th17 cells.** *J Immunol* 2009, **183**:2513–2521.
67. Szmydynger-Chodobska J, Strazielle N, Gandy JR, Keefe TH, Zink BJ, Ghersi-Egea JF, Chodobski A: **Posttraumatic invasion of monocytes across the blood-cerebrospinal fluid barrier.** *J Cereb Blood Flow Metab* 2012, **32**:93–104.
68. Monzon ME, Forteza RM, Casalino-Matsuda SM: **MCP-1/CCR2B-dependent loop upregulates MUC5AC and MUC5B in human airway epithelium.** *Am J Physiol Lung Cell Mol Physiol* 2011, **300**:L204–L215.
69. van der Veen BS, Petersen AH, Belperio JA, Satchell SC, Mathieson PW, Molema G, Heeringa P: **Spatiotemporal expression of chemokines and chemokine receptors in experimental anti-myeloperoxidase antibody-mediated glomerulonephritis.** *Clin Exp Immunol* 2009, **158**:143–153.
70. Muzio L, Cavasinni F, Marinaro C, Bergamaschi A, Bergami A, Porcheri C, Cerri F, Dina G, Quattrini A, Comi G, Furlan R, Martino G: **Cxcl10 enhances blood cells migration in the sub-ventricular zone of mice affected by experimental autoimmune encephalomyelitis.** *Mol Cell Neurosci* 2010, **43**:268–280.
71. Marques F, Sousa JC, Coppola G, Geschwind DH, Sousa N, Palha JA, Correia-Neves M: **The choroid plexus response to a repeated peripheral inflammatory stimulus.** *BMC Neurosci* 2009, **10**:135.
72. Freria CM, Zanon RG, Santos LM, Oliveira AL: **Major histocompatibility complex class I expression and glial reaction influence spinal motoneuron synaptic plasticity during the course of experimental autoimmune encephalomyelitis.** *J Comp Neurol* 2010, **518**:990–1007.
73. Jain MR, Bian S, Liu T, Hu J, Elkabes S, Li H: **Altered proteolytic events in experimental autoimmune encephalomyelitis discovered by iTRAQ shotgun proteomics analysis of spinal cord.** *Proteome Sci* 2009, **7**:25.
74. Szalai AJ, Hu X, Adams JE, Barnum SR: **Complement in experimental autoimmune encephalomyelitis revisited: C3 is required for development of maximal disease.** *Mol Immunol* 2007, **44**:3132–3136.
75. Engelhardt B, Sorokin L: **The blood–brain and the blood-cerebrospinal fluid barriers: function and dysfunction.** *Semin Immunopathol* 2009, **31**:497–511.
76. Liddelow SA, Temple S, Mollgard K, Gehwolf R, Wagner A, Bauer H, Bauer HC, Phoenix TN, Dziegielewska KM, Saunders NR: **Molecular characterisation of transport mechanisms at the developing mouse blood-CSF interface: a transcriptome approach.** *PLoS One* 2012, **7**:e33554.

doi:10.1186/2045-8118-9-15
Cite this article as: Murugesan *et al.*: Active induction of experimental autoimmune encephalomyelitis by MOG_{35-55} peptide immunization is associated with differential responses in separate compartments of the choroid plexus. *Fluids and Barriers of the CNS* 2012 **9**:15.